Structural Engineering Report No. 134

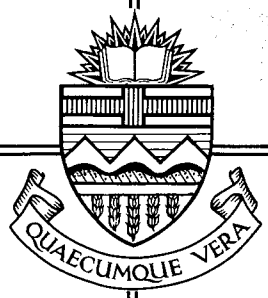

INELASTIC SEISMIC RESPONSE OF PRECAST CONCRETE LARGE PANEL COUPLED SHEAR WALL SYSYTEMS

By
M. REZA KIANOUSH
and
ANDREW SCANLON

MARCH, 1986

RECENT STRUCTURAL ENGINEERING REPORTS

Department of Civil Engineering

University of Alberta

103. *Local Buckling of Thin-Walled Tubular Steel Members* by M.J. Stephens, G.L. Kulak and C.J. Montgomery, February 1982.

104. *Test Methods for Evaluating Mechanical Properties of Waferboard: A Preliminary Study* by M. MacIntosh and J. Longworth, May 1982.

105. *Fatigue Strength of Two Steel Details* by K.A. Baker and G.L. Kulak, October 1982.

106. *Designing Floor Systems for Dynamic Response* by C.M. Matthews, C.J. Montgomery and D.W. Murray, October 1982.

107. *Analysis of Steel Plate Shear Walls* by L. Jane Thorburn, G.L. Kulak, and C.J. Montgomery, May 1983.

108. *Analysis of Shells of Revolution* by N. Hernandez and S.H. Simmonds, August 1983.

109. *Tests of Reinforced Concrete Deep Beams* by D.M. Rogowsky, J.G. MacGregor and S.Y. Ong, September 1983.

110. *Shear Strength of Deep Reinforced Concrete Continuous Beams* by D.M. Rogowsky and J.G. MacGregor, September 1983.

111. *Drilled-In Inserts in Masonry Construction* by M.A. Hatzinikolas, R. Lee, J. Longworth and J. Warwaruk, October 1983.

112. *Ultimate Strength of Timber Beam Columns* by T.M. Olatunji and J. Longworth, November 1983.

113. *Lateral Coal Pressures in a Mass Flow Silo* by A.B.B. Smith and S.H. Simmonds, November 1983.

114. *Experimental Study of Steel Plate Shear Walls* by P.A. Timler and G.L. Kulak, November 1983.

115. *End Connection Effects on the Strength of Concrete Filled HSS Columns* by S.J. Kennedy and J.G. MacGregor, April 1984.

116. *Reinforced Concrete Column Design Program* by C-K. Leung and S.H. Simmonds, April 1984.

117. *Deflections of Two-way Slabs under Construction Loading* by C. Graham and A. Scanlon, August 1984.

118. *Effective Lengths of Laterally Unsupported Steel Beams* by C.D. Schmitke and D.J.L. Kennedy, October 1984.

119. *Flexural and Shear Behaviour of Large Diameter Steel Tubes* by R.W. Bailey and G.L. Kulak, November 1984.

120. *Concrete Masonry Prism Response due to Loads Parallel and Perpendicular to Bed Joints* by R. Lee, J. Longworth and J. Warwaruk.

121. *Standardized Flexible End Plate Connections for Steel Beams* by G.J. Kriviak and D.J.L. Kennedy, December 1984.

122. *The Effects of Restrained Shrinkage on Concrete Slabs* by K.S.S. Tam and A. Scanlon, December 1984.

123. *Prestressed Concrete Beams with Large Rectangular Web Openings* by T. do M.J. Alves and A. Scanlon, December 1984.

124. *Tests on Eccentrically Loaded Fillet Welds* by G.L. Kulak and P.A. Timler, December 1984.

125. *Analysis of Field Measured Deflections Scotia Place Office Tower* by A. Scanlon and E. Ho, December 1984.

126. *Ultimate Behaviour of Continuous Deep Reinforced Concrete Beams* by D.R. Ricketts and J.G. MacGregor, January 1985.

127. *The Interaction of Masonry Veneer and Steel Studs in Curtain Wall Construction* by W.M. McGinley, J. Warwaruk, J. Longworth and M. Hatzinikolas, May 1985.

128. *Evaluation of Existing Bridge Structure by Nondestructive Test Methods* by L. Mikhailovsky and A. Scanlon, May 1985.

129. *Finite Element Modelling of Buried Structures* by D.K. Playdon and S.H. Simmonds, October 1985.

130. *Behaviour and Ultimate Strength of Transversely Loaded Continuous Steel Plates* by K.P. Ratzlaff and D.J.L. Kennedy, November 1985.

131. *Inelastic Lateral Buckling of Steel Beam-Columns* by P.E. Cuk, M.A. Bradford and N.S. Trahair, December 1985.

132. *Design Strengths of Steel Beam-Columns* by N.S. Trahair, December 1985.

133. *Behaviour of Fillet Welds as a Function of the Angle of Loading* by G.S. Miazga and D.J.L. Kennedy, March 1986.

134. *Inelastic Seismic Response of Precast Concrete Large Panel Coupled Shear Wall Systems* by M.R. Kianoush and A. Scanlon, March 1986.

INELASTIC SEISMIC RESPONSE OF PRECAST CONCRETE LARGE PANEL COUPLED SHEAR WALL SYSTEMS

by

Mohammed Reza Kianoush

and

Andrew Scanlon

March 1986

ABSTRACT

Large panel precast wall systems have many economical and technical advantages over monolithic cast-in-place walls. In the past two decades, large panel construction has become a common practice in North America. However, due to the lack of understanding of their behaviour, the use of this type of system in active seismic zones is still questionable.

In large panel systems, horizontal connections are the locations of weakness in terms of strength and stiffness. During a major earthquake, the connections may be subjected to slip and rocking. Previous studies on the behaviour of simple walls have shown that due to the effects of slip and rocking, large panel walls may be subjected to overstressing and concrete crushing which may lead to the loss of structural stability/integrity.

Analytical studies are carried out to investigate the effect of coupling in precast wall systems. Several models are developed and incorporated into the computer program DRAIN-2D. It is assumed that wall panels remain linear-elastic throughout the analysis and that inelastic action is concentrated in the connections and the coupling beams.

The effect of various parameters on the response of a 10-story precast wall system is investigated. It was found that the method of providing vertical continuity across the connections and the level of coupling beam strength have a

significant effect on the response. Coupled walls with post-tensioning bars showed considerable improvement in their response over simple walls. This study suggests that the design of precast wall systems should be based on inelastic dynamic analysis. Internal forces based on the "equivalent static analysis" proposed by the National Building Code of Canada (1985) did not agree well with forces obtained from inelastic dynamic analysis.

ACKNOWLEDGEMENTS

Financial support received from the Natural Science and Engineering Research Council of Canada under operating grant No. A5153 is greatly appreciated. The assistance of Tom Casey in computer related areas is greatly appreciated.

TABLE OF CONTENTS

LIST OF TABLES

LIST OF FIGURES

LIST OF SYMBOLS

$[B], [B]^T$ = matrix relating assumed displacement field parameters to nodal displacement and its transpose

$[C]$ = constitutive matrix

$[C]$ = damping matrix

$[J]$ = Jacobian matrix

$[K]$ = element stiffness matrix corresponding to translational and rotational d.o.f.

$[K]_T$ = element stiffness matrix corresponding to translational d.o.f.

$[M]$ = diagonal mass matrix

$[K_T]$ = tangent stiffness matrix

$[T]$ = transformation matrix

$[T]^T$ = transpose of $[T]$

$\{R\}$ = vector of unbalanced forces

A_s = cross sectional area of diagonal reinforcement

d' = distance from extreme concrete fibre to centroid of reinforcement at beam ends

E = axial tangent modulus per unit thickness of the connection

E_c = elastic modulus of concrete

E_{ij} = normalized cumulative energy disspated

E_o = initial tangent modulus

E_s = elastic modulus of steel

E_s = secant modulus at maximum stress σ_p/ε_p

EA = axial stiffness of beam

EI = flexural stiffness of beam

e_k = energy dissipated in the kth load cycle

$F_{uB}(v_1)$ ... $F_{uB}(v_4)$ = unbalanced forces corresponding to translational d.o.f. v_1 ... v_4

F = foundation factor

F_y = yield load

f'_c = compressive strength of concrete

f_y = yield stress of diagonal reinforcement

G = shear tangent modulus per unit thickness of the connection

G_d = tangent shear moduli of the connection material

G_s = tangent shear moduli of the slip surface

GA = shear stiffness of beam

H_1 = horizontal shear due to lateral loads on wall above

H_2 = horizontal shear in the plane of the floor resulting from diaphragm action

H_3,H_4 = horizontal shear in the plane of the floor resulting from diaphragm action and restraint force due to creep, shrinkage and temperature effects

h = connection height

I = importance factor

I_{gross} = gross moment of inertia of beam

$I_{effective}$ = effective moment of inertia of beam

K = ductility factor

K_S = spring stiffness

k = load cycle

L = connection length

L = length of beam

L_L, L_R = length of plane-stress elements for left panels and right panels respectively

M = transverse bending moment from floor continuity and load eccentricities

M_A, M_B = internal moment generated in wall A or wall B

$(M_{uB})_A$, $(M_{uB})_B$ = unbalanced moments at ends A and B respectively

M_y = yield moment of beam

n = modular ratio, E_S/E_C

P_y = yield load

S = seismic response factor

T = axial force induced in the walls (tension or compression)

T = period of vibration in the nth node

T_u, C_u = maximum tensile and compressive forces respectively

t = connection thickness

t = panel thickness

t_σ = stress at time t

t_ε = compressive strain at time t

u = increment in horizontal displacement field of the entire connection region

u_θ = rotation ductility ratio

u_d = increment in horizontal displacement field within the finite region of the connection

u_s = increment in horizontal displacement field along the slip plane

$u_1, v_1, \ldots u_4, v_4$ = translational degrees of freedom

V = total base shear

v = zonal velocity ratio

v = increment in vertical displacement field of the entire connection region

V_1 = vertical load from wall panel above

V_2 = vertical load from floor loading

V_u = maximum shear force

W = dead load + 25 percent of snow load

α = angle between diagonal bar and horizontal

α = stress ratio σ_1/σ_2, $\sigma_1 > \sigma_2$

α and β = constants to be specified by the program

α_A, α_B = ratios of the slope of the post-yield branch to the slope of the bilinear moment-rotation curves at member ends A and B respectively

ε_i = uniaxial strain in the principal stress direction

Δ_y = yield deflection

θ_{max} = maximum rotation

θ_y = yield rotation

ε_c = maximum compressive strain at maximum stress

level

μ = coefficient of friction

ℓ = distance between centroids of the two walls

ℓ = total length of the coupling beam

σ_y = yield stress of steel

σ_i, ε_i = stress and strain in the principal stress direction

σ_p, ε_p = maximum biaxial compressive stress and corresponding strain

σ_c, ε_c = maximum compressive stress and corresponding strain in the principal direction

ν = Poisson's ratio

λ = proportion of critical damping in the nth node

ρ = reinforcement ratio

ρ_x, ρ_y = reinforcement ratios in x and y directions, respectively

$\Delta\theta_A^e, \Delta\theta_B^e$ = increments of chord rotations due to bending of elastic beam at ends A and B respectively

$\Delta\theta_A^P, \Delta\theta_B^P$ = increments of hinge rotations at ends A and B respectively

θ_A, θ_B = rotations at ends A and B respectively

1. INTRODUCTION

1.1 General

Large panel construction has been used extensively in Europe in the past 50 years. The construction of large panel systems in the past 15 years has been applied in seismic regions such as USSR, Bulgaria, Romania, Japan and elsewhere. As pointed out by Fintel (1977), precast panel buildings have shown good performance during the 1977 Romanian earthquake. Although many high-rise buildings collapsed, precast panel buildings withstood the earthquake with minimum damage. Despite the satisfactory performance of large panel systems in the past, little is known about their seismic behaviour. For the typical precast concrete large panel systems common in North America, the use of this type of system in seismic regions is still questionable.

Large panels are concrete members which are used as either vertical wall panels of one story height or floor and roof panels or planks. Precast wall elements may be reinforced, prestressed or partially prestressed. The use of precast walls has attractive features such as good quality control of the product and speedier construction.

In large panel systems, the "connections" or "joints" are locations of weakness in terms of strength and stiffness compared to wall panels. During a major earthquake, sliding and opening may occur at the connection level which may produce large deformations in the system. This may lead to

distress and degradation in the connection regions which may finally lead to the loss of structural stability/integrity.

Figure 1-1 shows two common types of precast wall systems. Figure 1-1(a) and (b) are a simple wall and a coupled wall respectively. The behaviour of simple walls has been studied analytically by Schricker and Powell (1980), and Llorente and Becker (1981). These studies have shown that during a major earthquake, large deformations may take place in the connection regions which may create problems similar to those described above. In the present study, the behaviour of coupled wall systems is investigated.

1.2 Objective and Scope

The main objective of the present study is to investigate the inelastic dynamic response of precast coupled wall systems. As mentioned earlier, large inelastic action in the connections of simple walls may produce undesirable situations. For this reason, it may be possible to improve the response of precast walls by dissipating a significant portion of the energy in the coupling beams. Since the coupling beams are not the primary gravity load bearing elements, yielding in the beams does not threaten the overall structural stability/integrity.

The scope of the present study is summarized as follows.

1) Determine modeling techniques and develop models for

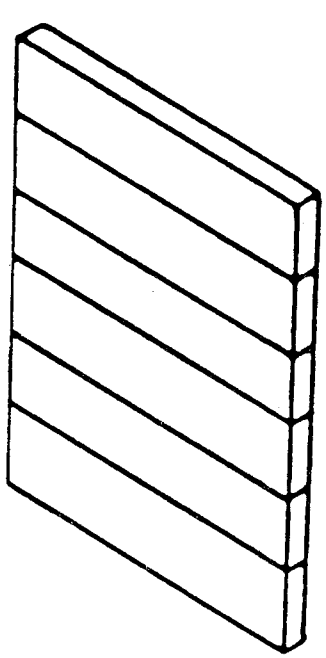

(a) simple wall

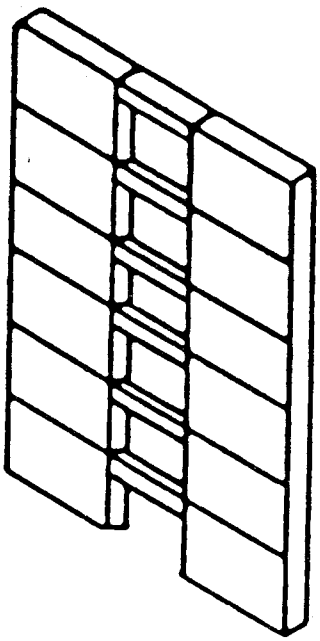

(b) coupled wall

Figure 1-1 Precast Wall Configurations

computer analysis.

2) Incorporate models into a computer program.
3) Investigate the significance of each of the individual models on the response of precast wall systems and verify the models.
4) Select structural parameters and a ground accelerogram for inelastic dynamic analysis.
5) Study the effect of various parameters on the response of precast wall systems.
6) Propose a design procedure based on the results of the parametric study.

1.3 Report Layout

This report is divided into eight chapters. The objective of the study is described in Chapter 1. A review of literature related to precast panel systems and details are described in Chapter 2. The experimental test results reported in the literature concerning the behaviour of precast panel systems are also described in the same chapter.

Chapter 3 presents the modeling technique used for the present study. The finite element modeling of wall panels and connections is discussed. The elastic and inelastic models incorporated into the computer program DRAIN-2D are described. The modeling of coupling beams is discussed and a method used for the compatibility of beam element and plane-stress element is described.

In Chapter 4, the effect of modeling technique on the response of precast wall systems is investigated. The accuracy of modeling techniques and their computer implementations are verified using both static and dynamic analysis.

In Chapter 5, the type of structure and its properties selected for parametric study is described. The response of the structure under three different accelerograms is studied.

Chapter 6 presents the results of a series of parametric studies on the response of precast wall systems. The effect of coupling beam parameters and the method for providing vertical continuity across the connections is the major part of the investigation. The results of the parametric study are discussed in detail.

Chapter 7 is related to the design of precast wall systems. General behaviour of precast wall systems is discussed and the failure modes are identified. A design procedure is recommended based on the results of the parametric study.

Finally, Chapter 8 summarizes the major conclusions reached from the study. Recommendations for further study are also presented in this chapter.

2. BEHAVIOUR OF PRECAST WALL SYSTEMS

2.1 General

This chapter presents a review of literature related to the behaviour of precast panel systems and details. In Sections 2.2 and 2.3, the types of precast wall systems and details that are commonly used in North America are discussed. Problems associated with the behaviour of simple walls are highlighted. Experimental results reported in the literature concerning the behaviour of precast panel connection details and reinforced concrete coupling beams are reviewed. Significant aspects of behaviour are identified to provide a basis for realistic modeling for dynamic analysis.

2.2 Basic Configurations and Details of Wall Systems

The structural wall systems which are used in North America can be divided into two categories of "single panel" and "large panel" construction. In the single panel form of construction, individual panels extend the full height of the structure and only vertical joints are required between the individual panels. Site precast tilt-up construction is an example of single panel construction, as is the use of precast double-tee wall units.

The term "large panel" construction is used to describe a structural system composed of precast wall panels with floors and roofs of precast panels or planks. The wall

panels are usually solid and of one story height. The hollow core precast roof or floor slabs span in one direction. Solid two-way panels are also used for floor and roof construction. In some cases, a cast-in-place topping is provided to work compositely with the precast slab units and continuity reinforcement is embedded in it. Load bearing walls of large panel buildings can be arranged in three different ways.

a) Cross-Wall System: This is the most common system. The load bearing walls are placed in the transverse direction of the building and one way floor and roof slabs span in that direction. Lateral forces in the transverse direction are resisted by these walls. Non load bearing walls are placed parallel to the longitudinal axis of the building and provide resistance to lateral load in the longitudinal direction as shown in Figure 2-1(a).

b) Long-Wall or Spine Wall System: Load bearing walls placed along the longitudinal axis of the building, resist lateral load in that direction. Lateral load in the transverse direction is resisted by non load bearing walls placed in that direction as shown in Figure 2-1(b).

c) Two-Way or Mixed System: In this system, load bearing walls are placed in both longitudinal and transverse directios with floor and roof slabs spanning in both directions as shown in Figure 2.1(c).

Figure 2.2 shows some of the common types of precast wall configurations in use in North America. Figure 2-2(a)

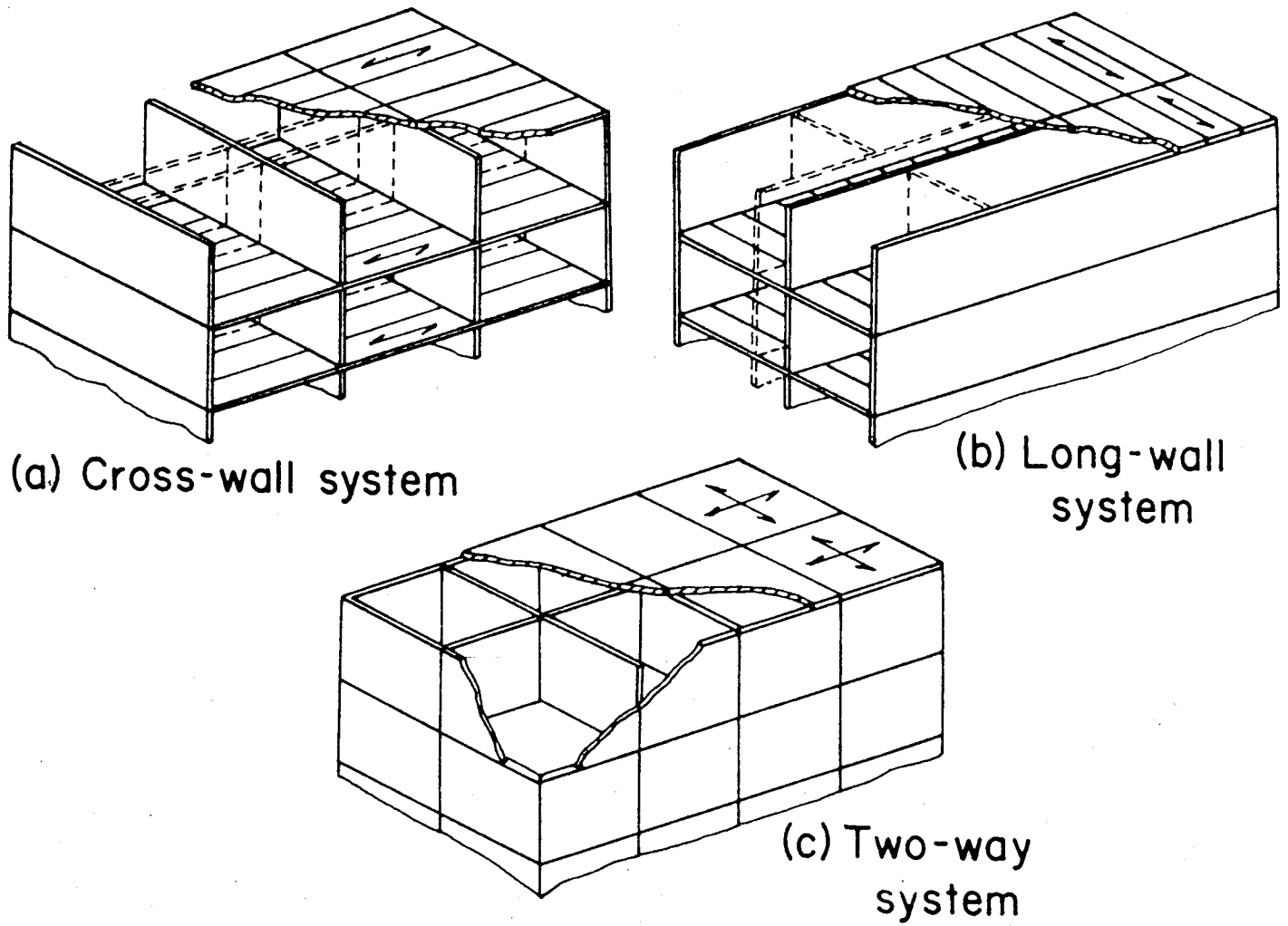

Figure 2-1 Types of Large Panel Systems (Mattock, 1981)
(Dashed lines indicate non-load bearing)

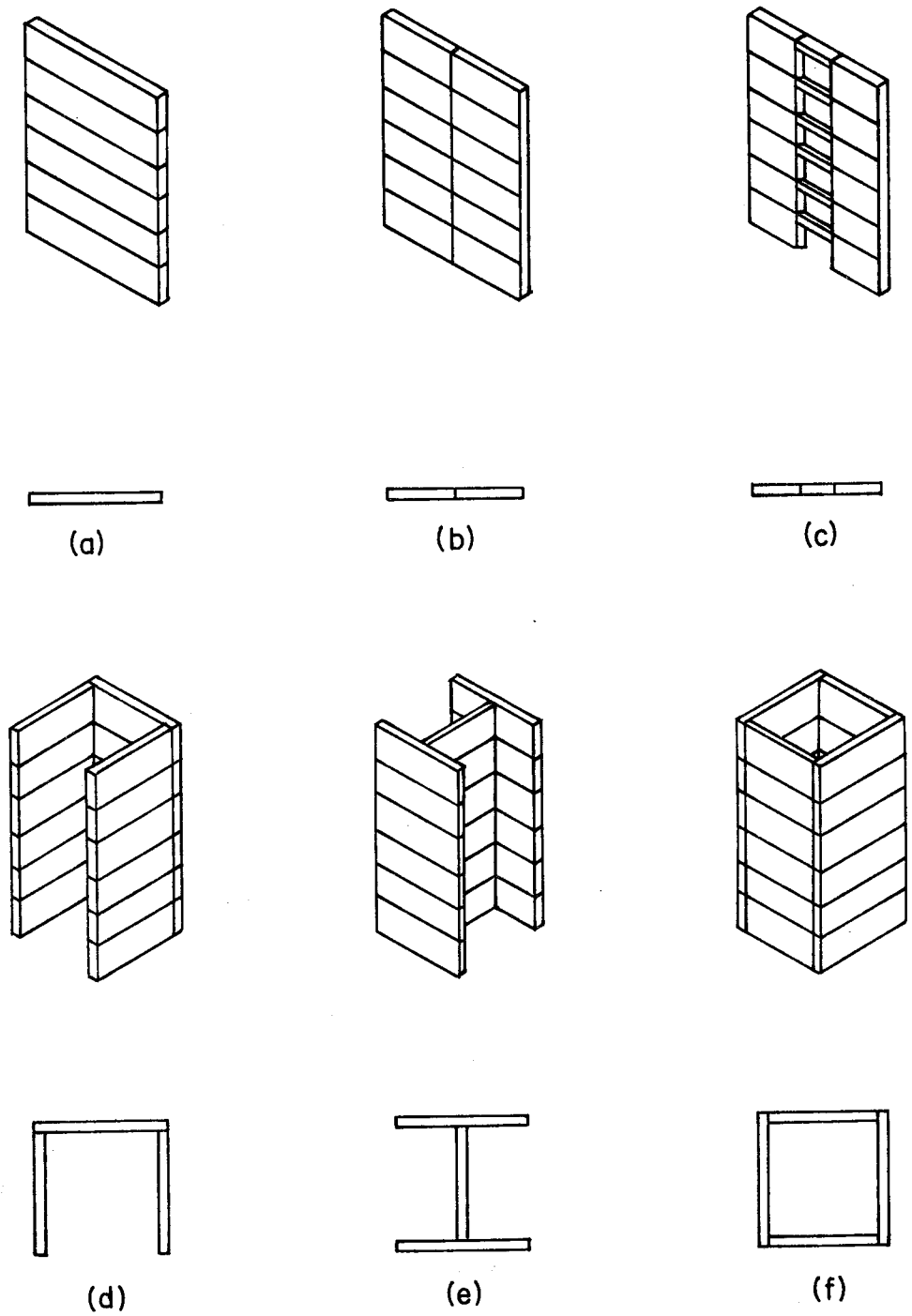

Figure 2-2 Typical Precast Wall Configurations

shows a simple wall which is a vertical stack of story high wall panels and has only horizontal connections. Figure 2-2(b) shows a composite wall which has vertical and horizontal connections. A coupled wall system with coupling beams connecting the two walls together is shown in Figure 2-2(c); this type of system is the subject of the present study. Walls shown in Figures 2-2(a), (b) and (c) can either be cross walls or end walls in apartment buildings. Walls shown in Figure 2-2(d), (e) and (f) are used to enclose service cores, stairs and other building services.

2.3 Connection Details

Detailing of horizontal connections is one of the most difficult problems in design and construction of precast wall panels. There are several connection details which are used in practice in North America. Some of the common details of horizontal connections are shown in Figures 2-3 and 2-4. Figure 2-3 shows the interior wall to floor connections and Figure 2-4 illustrates the exterior wall to floor connections. In these figures, all the reinforcing details except the vertical ties crossing the connections have been omitted for clarity.

In a precast wall system, vertical ties are usually deformed bars of large diameter (25 mm). Vertical continuity of wall panels can be provided in several different ways. Figure 2-3(a) shows a "spliced sleeve" type connection in which bars are grouted in place. This type of

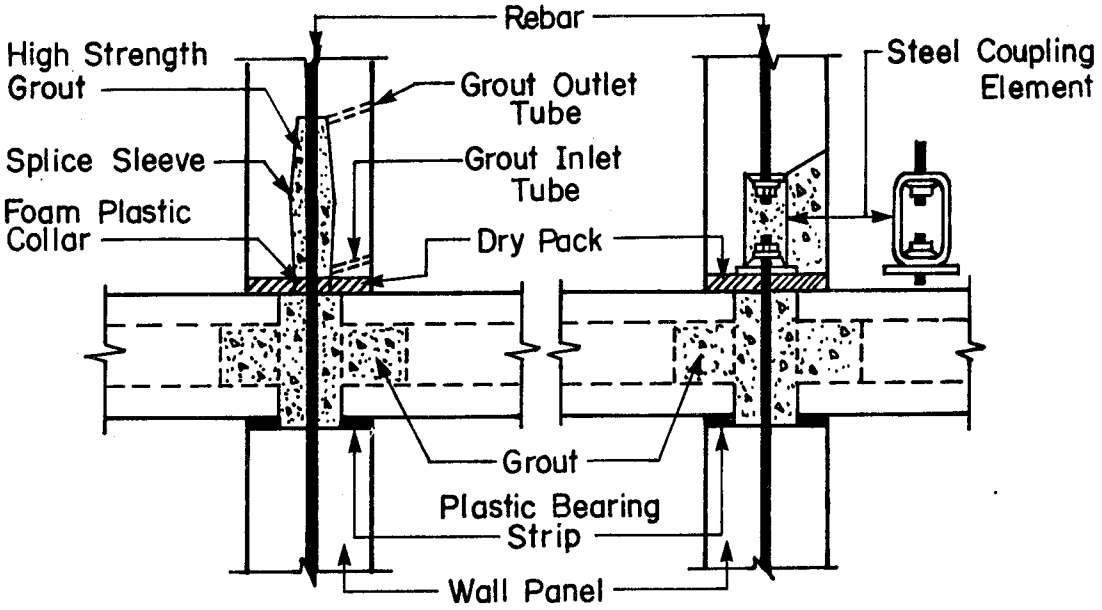

(a) Sleeved Connection

(b) Bolted Coupling

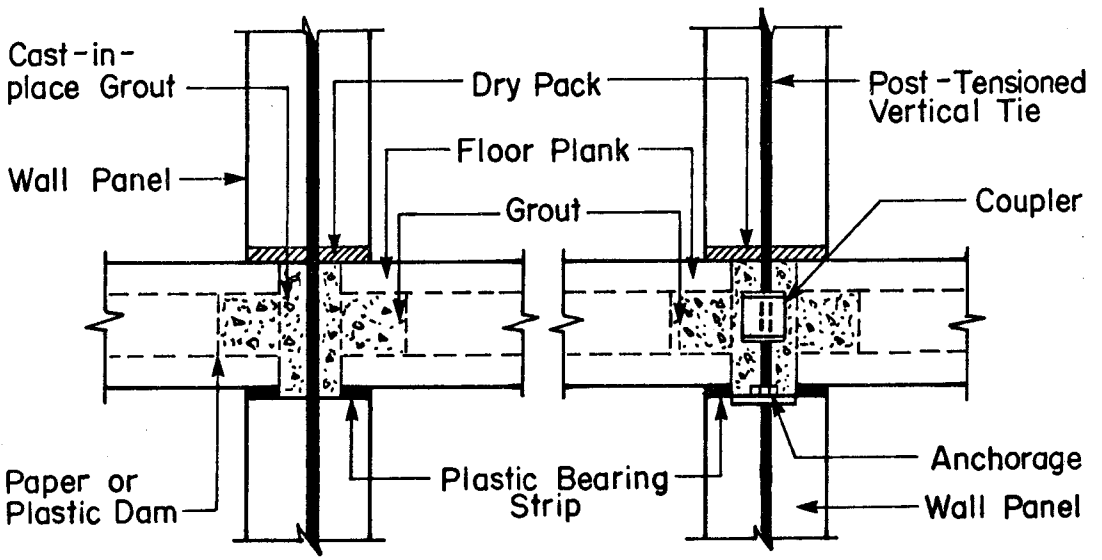

(c) Platform Connection (Reinforcing bar)

(d) Platform Connection (Post-Tensioning bar)

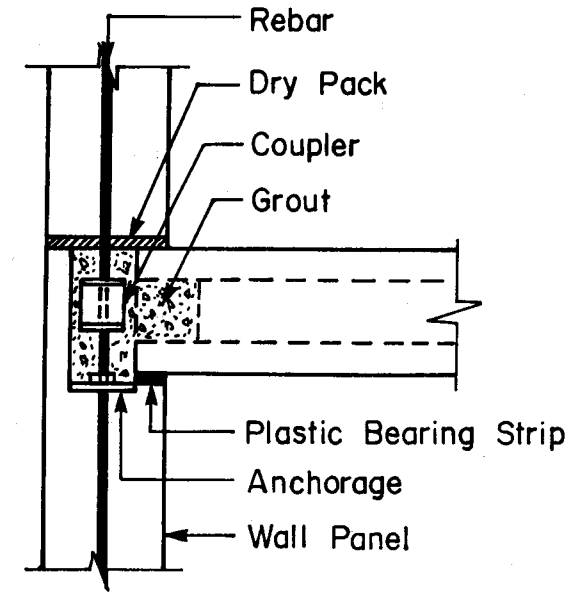

(a) Platform Connection
(Post - Tensioning)

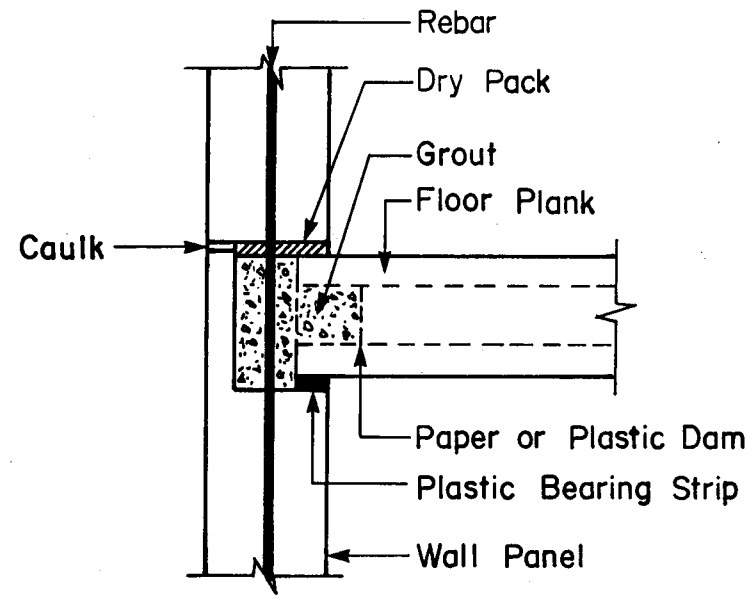

(b) Platform Connection
(Reinforcing)

Figure 2-4 Exterior Wall to Floor Connection

system was originally developed in Japan. Vertical continuity can also be provided with threaded rods or reinforcing bars with a coupling or bolting mechanism as shown in Figure 2-3(b). Reinforcing bars which project from the panels and are welded in the connection region are classified as "platform" type connections. This type of system is shown in Figures 2-3(c) and 2-4(b) and is very common in North America.

The use of post tensioning as vertical continuity is also quite common. Post-tensioning rods usually extend from the foundation up to the roof level. Post-tensioning details are shown in Figures 2-3(d) and 2-4(a). One of the advantages of post-tensioning over reinforcing bars is the avoidance of laps in vertical steel.

In a typical North American type connection, floor slabs are supported on plastic bearing pads. Cast in place grout fills in the space between the wall panels and some portions of hollow core slab with paper or plastic dam inserted in the slab to limit the extent of grout in the slab. Space between the wall panel above the floor slab and the floor panel is usually filled with dry-pack.

Experimental tests carried out by Backler et al. (1973) on the compressive strength of the horizontal connection indicate lower strength and stiffness (about 50% or even less) as compared to monolithic wall panels. Due to the effects of creep and shrinkage, horizontal connections are considered as pre-cracked planes and hence they cannot

develop any tension if no vertical continuity steel is provided. Figure 2-5 shows an interior floor-to-wall connection with the corresponding connection forces. The connection must resist the following forces:

V_1 = vertical load from wall panel above

V_2 = vertical load from floor loading

H_1 = horizontal shear due to lateral loads on wall above

H_2 = horizontal shear in the plane of the floor resulting from diaphragm action

H_3, H_4 = horizontal shear in the plane of the floor resulting from diaphragm action and restraint force due to creep, shrinkage and temperature effects

M = transverse bending moment from floor continuity and load eccentricities.

The vertical connection details can be either "wet" or "dry" as shown in Figure 2-6. "Wet" joint results in a structure with its behaviour similar to the response of monolithic walls while the "dry" joint speeds erection of the construction. Since vertical joints are not the subject of the present study, they will not be discussed further, however more information can be found in references by Pall and Marsh (1979), Pollner et al. (1975), Cholewicki (1971), Muller and Becker (1980), Becker and Muller (1980), and

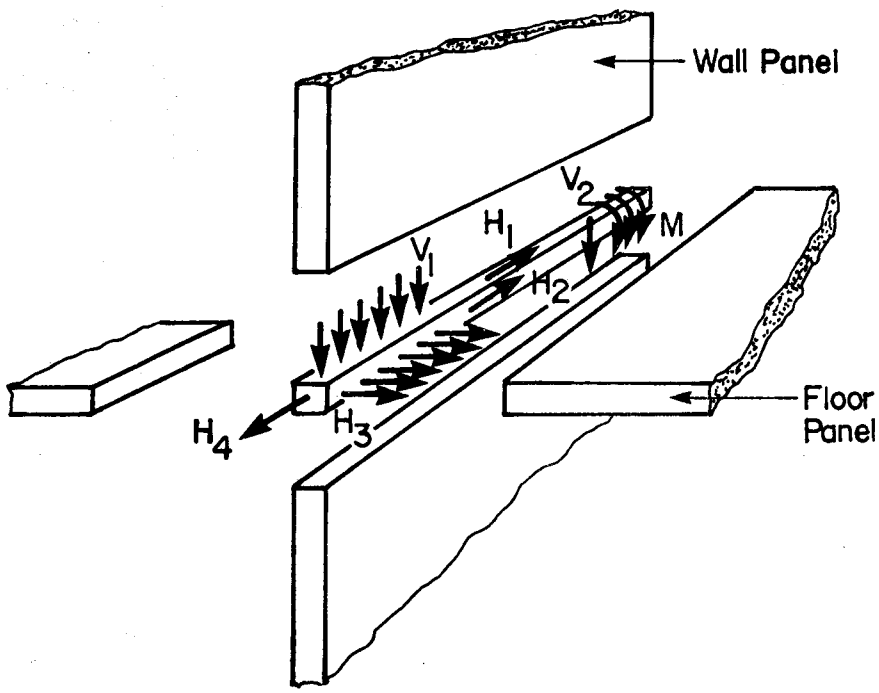

Figure 2-5 Various Forces in the Connection Region

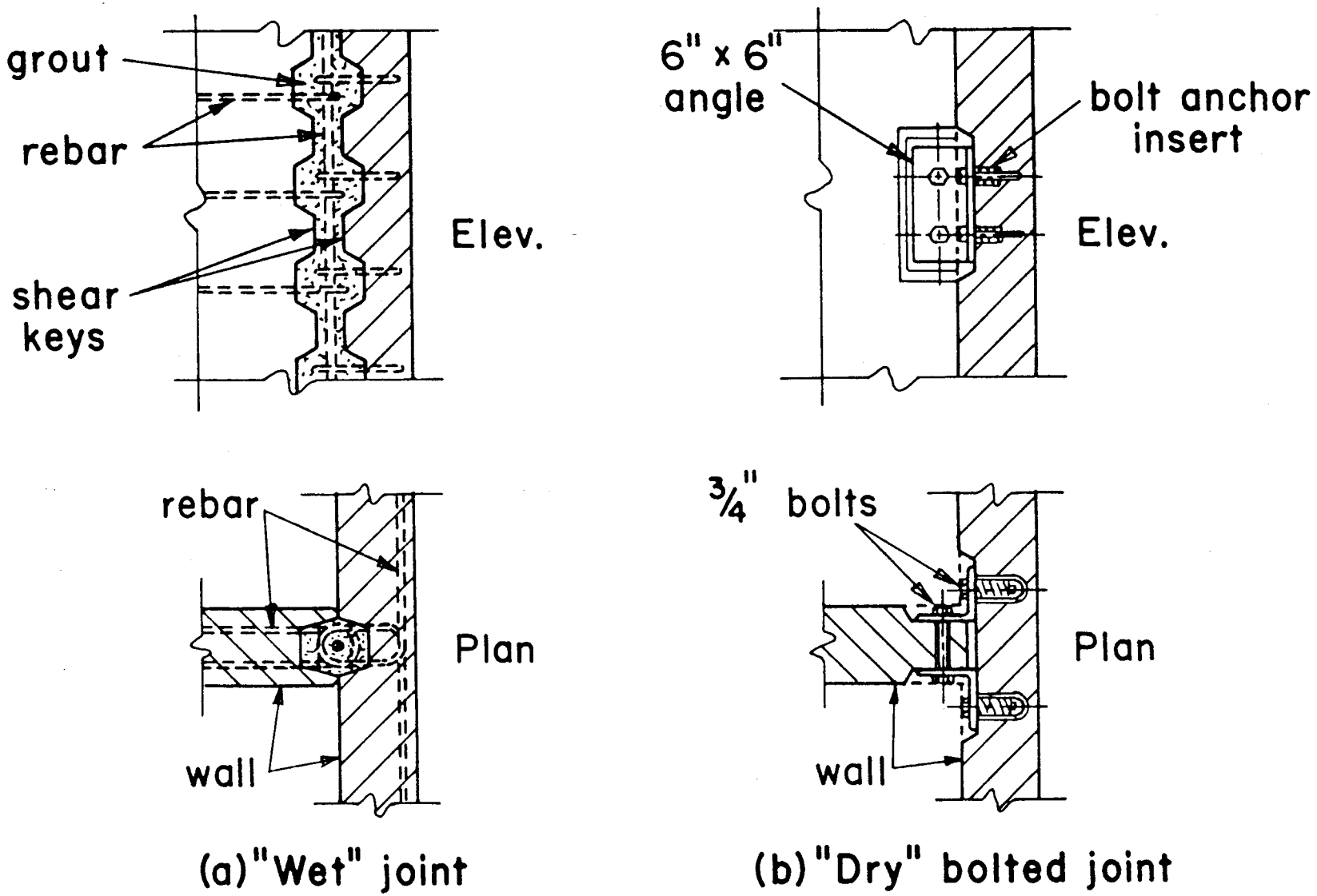

Figure 2-6 Types of Vertical Joints (Mattock, 1981)

Pekau (1981).

2.4 Structural Behaviour of Precast Walls

2.4.1 Behaviour of Simple Walls

Precast wall panels behave quite differently from cast-in-situ monolithic walls. The main difference between a precast wall and the corresponding cast-in-situ wall is the presence of the connections in precast walls. As mentioned earlier, horizontal connections are locations of weakness both in compression and shear in structural walls and hence there is the likelihood that plastic hinges may concentrate in the connection region.

There are two principal mechanisms, namely rocking and shear slip, associated with the connection behaviour as shown in Figure 2-7. Rocking is a term which describes the overturning response of the structure. That is, under external lateral loads, the horizontal connections may open and close which can produce large localized changes in bending. It is suggested by Llorente and Becker (1981) that opening and closing of the horizontal connections occur smoothly and progressively in which plane sections no longer remain plane in the connection regions.

The second mechanism, shear slip, is a term which describes the transfer of shear forces in the horizontal connections through Coulomb friction due to normal stresses and post-tensioning, and through shear friction due to dowel action and clamping action of vertical reinforcement.

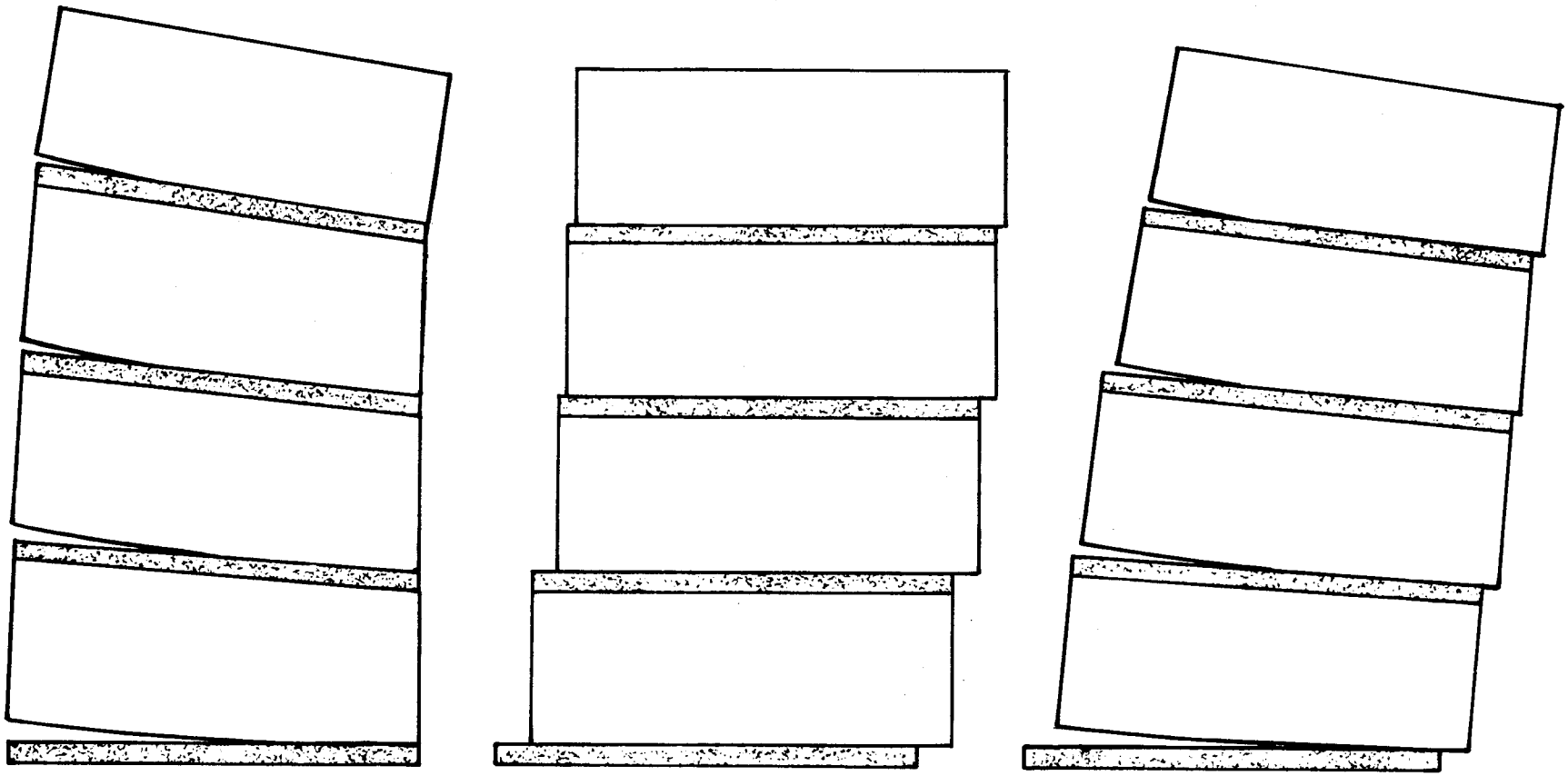

Figure 2-7 Deformed Configurations of a Simple Wall

Because of plain and smooth edges, such connections are susceptible to slip before a plastic hinge forms at the base of the walls.

The seismic response of simple walls has been analytically studied by Llorente and Becker (1981), Schricker and Powell (1980) and Mueller and Becker (1979). Their studies show that joint opening can significantly reduce the forces in the structure by a base isolation mechanism, with little energy dissipated. Their results also indicate that joint opening can cause large crack lengths along the connections which may cause severe stress concentration in the closed portion of the connection. This may lead to severe distress in the wall panel or the connection regions, thus threatening the overall stability of the system. Their results also show that large deformations could also occur due to shear slip which is very effective as a force isolation and energy dissipation mechanism. However they found that shear transfer by Coulomb friction is an unconfined yield mechanism, that is, once the walls start slipping, they move in the same direction and they do not return to their original position.

In view of the above results, they concluded that the horizontal connections between wall panels are not the desirable location for energy dissipation. The inelastic action in the horizontal connections can cause the destruction of the interfaces and may lead the structure to become unserviceable or it may even endanger the integrity

and the stability of the structure. Based on the above discussion a design concept that relies on the inelastic action in the horizontal connection of simple precast walls is questionable and therefore a more desirable location for inelastic action other than the horizontal connections is necessary.

2.4.2 Behaviour of Coupled Walls

Simple walls connected to each other by connecting elements are called coupled walls. The coupling elements in precast wall panels are through either of the following:

1) welded or bolted connections embedded in the walls to be joined,
2) limited slip bolted joints, or
3) coupling beams in which the spaces between the two walls are used as window or door opening.

Use of coupled walls with coupling beams which is the subject of the present study can be due to architectural and/or structural reasons. Coupled walls are used commonly as structural elements both in office buildings and residential buildings. Office buildings generally require open office space with minimum interruptions by vertical members. For this reason, central core exterior column or exterior wall, interior column layouts are generally used. Structural walls in residential buildings provide acoustical privacy and fire separation. Figures 2-8(a) and (b) show common use of coupled walls in office buildings and

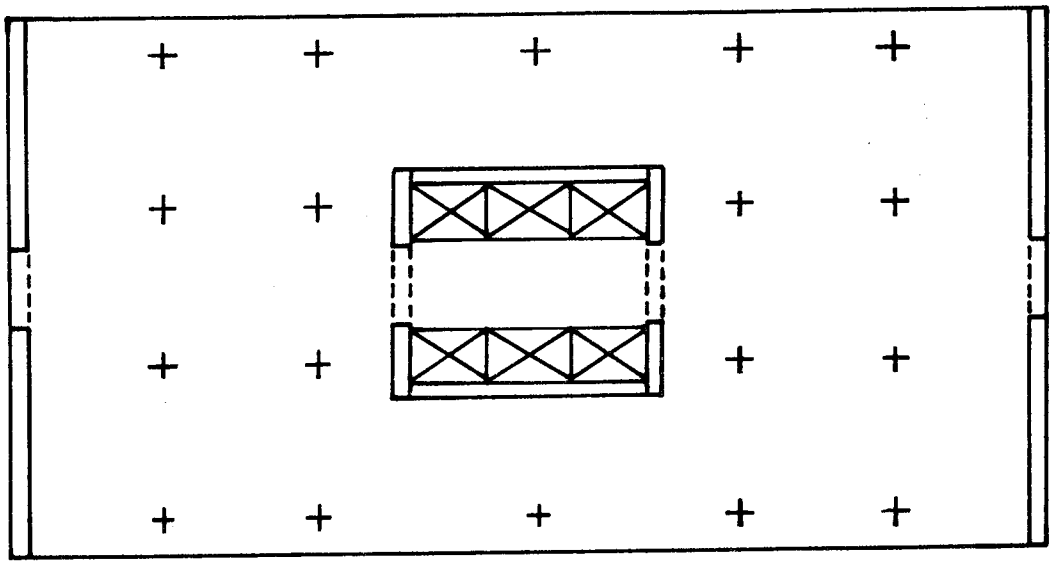

(a) Office Building

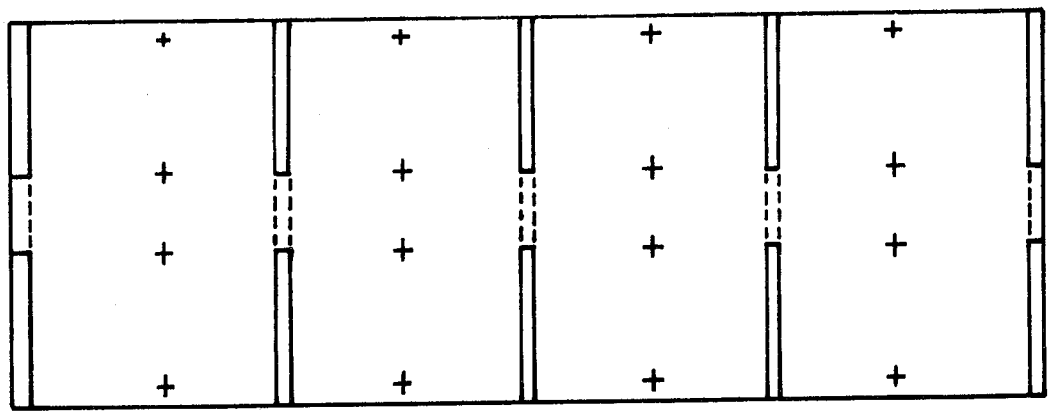

(b) Residential Building

Figure 2-8 Common Use of Coupled Wall Systems

apartment buildings respectively.

As mentioned earlier, horizontal connections are not the desirable locations for dissipating energy. For this reason, the behaviour of coupled walls is studied to investigate the effect of coupling on the response of large panel structures. In this fashion, it may be possible to confine inelastic energy dissipation to coupling beams which are not crucial to the overall stability of the structure. The yielding in the coupling beams may dissipate a significant portion of the input energy while the walls continue to provide overall stiffness and stability to the structure.

In a coupled wall system, the external overturning moment is resisted at any horizontal section by the corresponding equilibrium equation (Figure 2-9)

$$M_n = M_A + M_B + T\,\ell$$

where

M_A, M_B = internal moment generated in wall A or wall B

T = axial force induced in the walls (tension or compression)

ℓ = distance between centroids of the two walls.

The magnitude of these forces depends on the relative stiffnesses and strengths of the coupling beams and the coupled walls, and the number of stories.

Coupling beams in a coupled wall structure can either

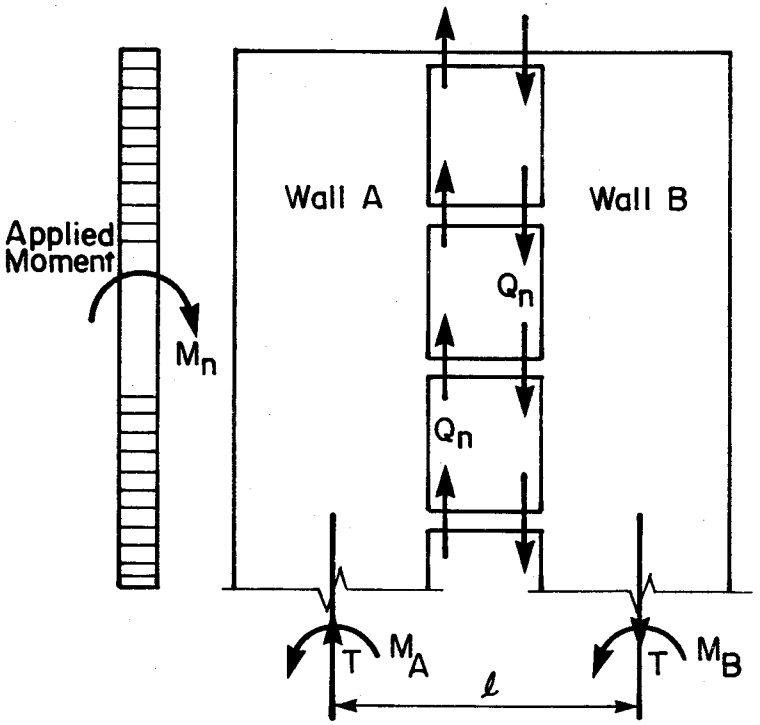

Figure 2-9 Internal and External Forces in a Coupled Wall System

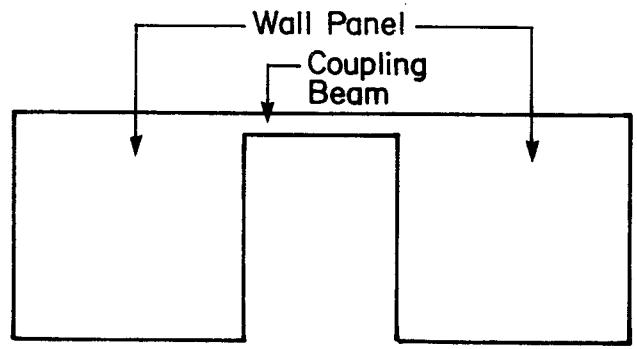

Figure 2-10 Coupling Beam Precast with Wall Panels

be cast-in-place or precast with the wall panels as shown in Figure 2-10. To ensure ductility in a coupled wall system, it has been suggested by Fintel and Ghosh (1981) that the coupling beams be preferably cast-in-place. Vertical continuity in the walls can either be provided with post-tensioning or reinforcing bars. When bars are used, the reinforcement should be uniformly distributed over the cross-section of the wall in order to resist shear forces developed across the connection. Concentrated reinforcement is also necessary at the corners of the walls to resist forces due to overturning. Figure 2-11(a) illustrates the details of vertical mild reinforcement and Figure 2-11(b) shows the details of post-tensioning in a coupled wall system.

2.4.3 Behaviour of Coupling Beams

When coupled walls are displaced laterally, the coupling beams behave in a double curvature configuration as shown in Figure 2-12(a). The assumed moment diagram for such beams is linear with opposite sign at each end as shown in Figure 2-12(b).

There has been considerable experimental research carried out on the behaviour of coupling beams. Most of these experiments have been carried out by Paulay (1971a-b, 1977), Paulay and Binney (1974), Paulay and Santhakumar (1976), and Barney et al. (1978). Test results have indicated that coupling beams with varying depth/length

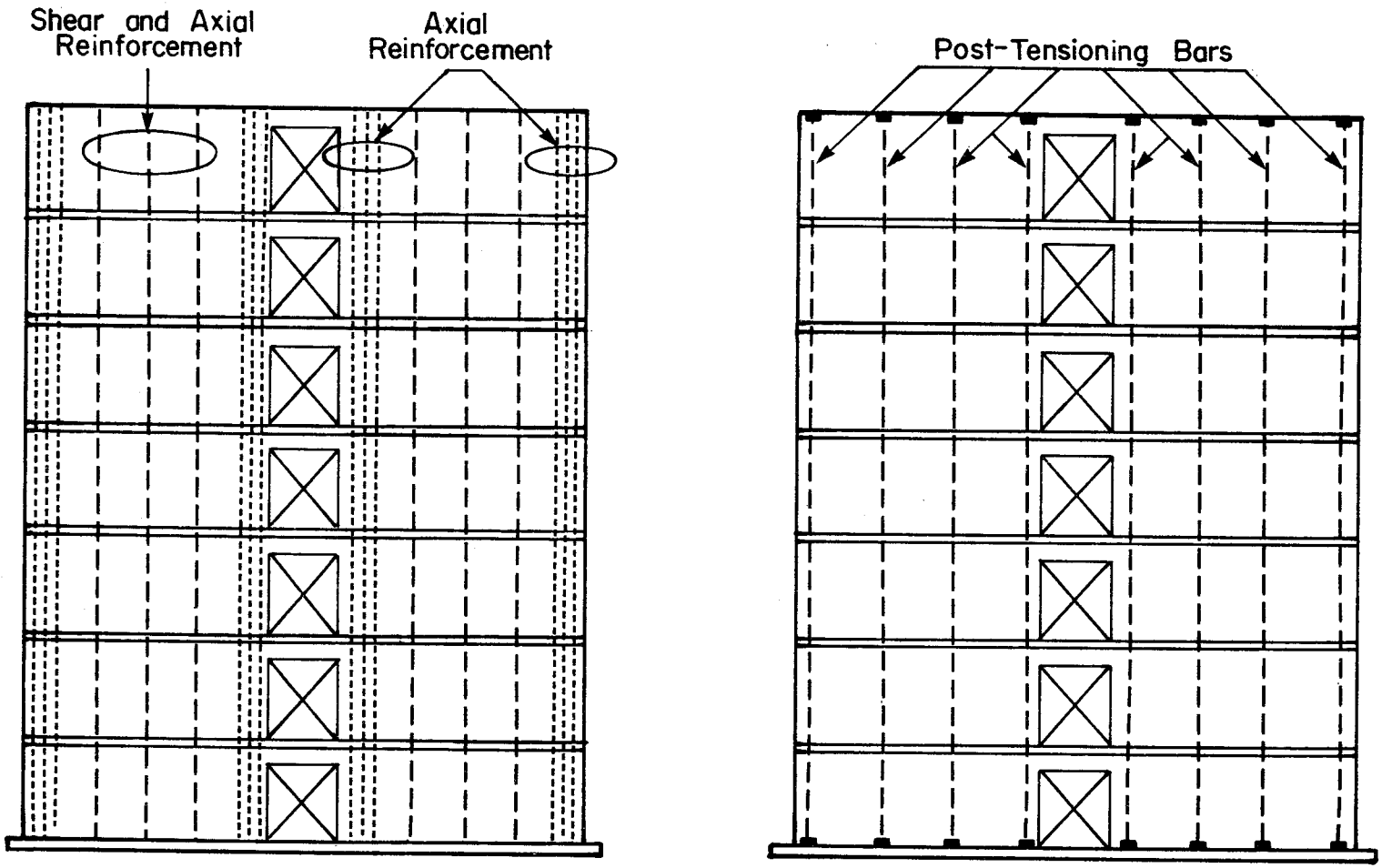

Figure 2-11 Vertical Continuity in Coupled Wall Systems

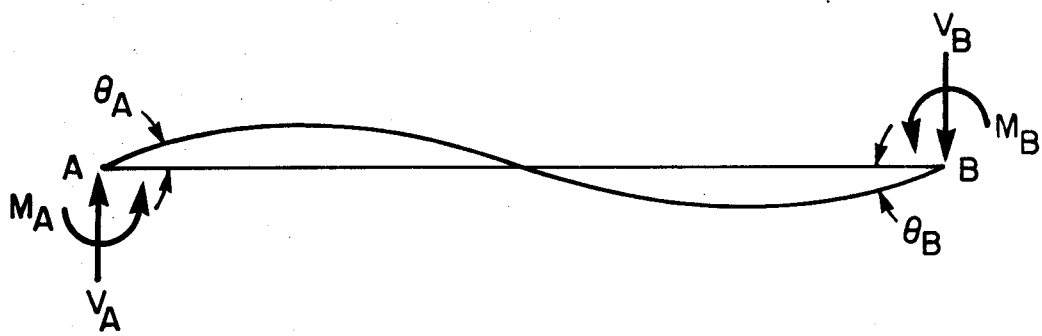

(a) Displaced Configuration of Coupling Beams

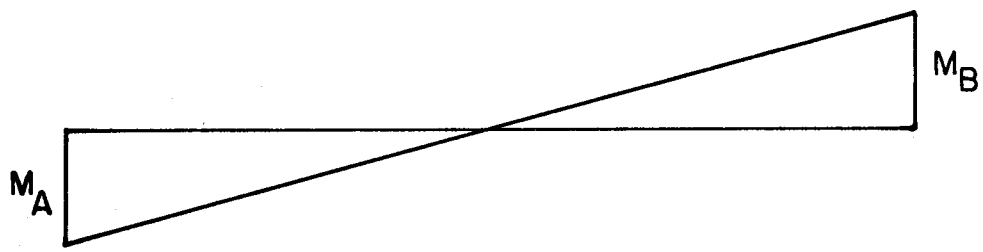

(b) Moment Diagram

Figure 2-12 Behaviour of Coupling Beams

ratios behave quite differently if conventional reinforcement consisting of a group of horizontal bars at the top and at the bottom of the beams is used. Because of their behaviour, coupling beams are classified into two categories, namely slender beams and deep beams. Beams with small depth/length ratios are called slender beams and those with large depth/length ratios are called deep beams.

Eight 1/3-scale specimens were tested by Barney et al. (1978). The models were subjected to in-plane reversing loads simulating those in beams of coupled structural walls. Controlled variables were the type and arrangement of primary reinforcement, span to depth ratio and size of concrete core. Details of the specimens are listed in Table 2-1.

Beams with different span to depth ratios and different arrangements of reinforcing were tested by Paulay (1971a-b) and Paulay and Binney (1974). These beams were cast with heavily reinforced end blocks and were subjected to alternate cyclic loading as shown in Figure 2-13. Two one-quarter full size seven story reinforced concrete coupled shear wall models with differently reinforced coupling beams were also tested by Paulay (1977) and Paulay and Santhakumar (1976). These specimens were subjected to high intensity alternating cyclic loading simulating seismic effects.

A study of the test results mentioned above shows that the behaviour of slender beams and deep beams with different reinforcement arrangements are different. For this reason,

Table 2-1 Test Program Variables for Coupling Beams

Specimen	Core Width a (in.)	Span Length b (in.)	Primary Reinforcement
C1	2.63	16.67	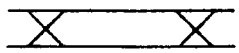
C2	2.63	16.67	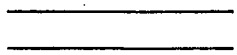
C3	2.63	16.67	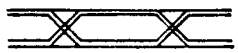
C4	3.50	16.67	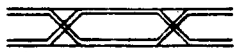
C5	3.50	16.67	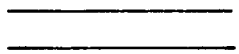
C6	3.50	16.67	
C7	3.50	33.33	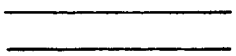
C8	3.50	33.33	

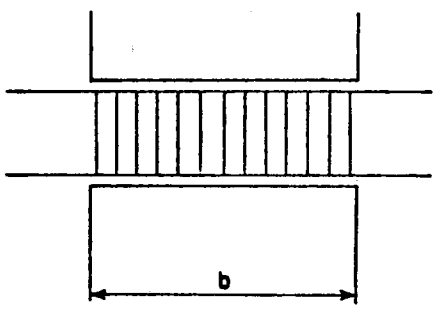

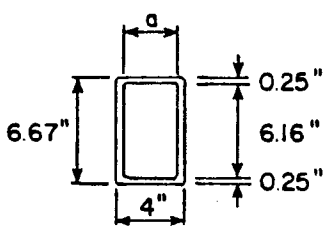

1 in. = 25.4mm

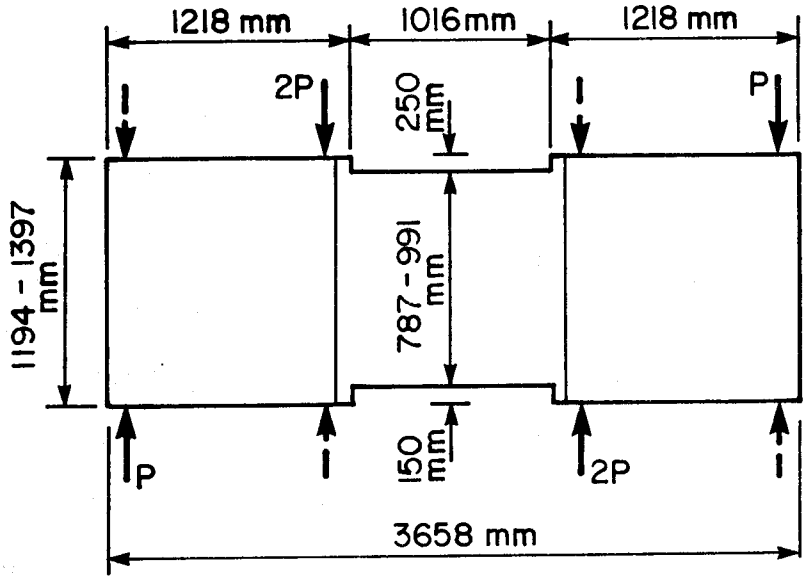

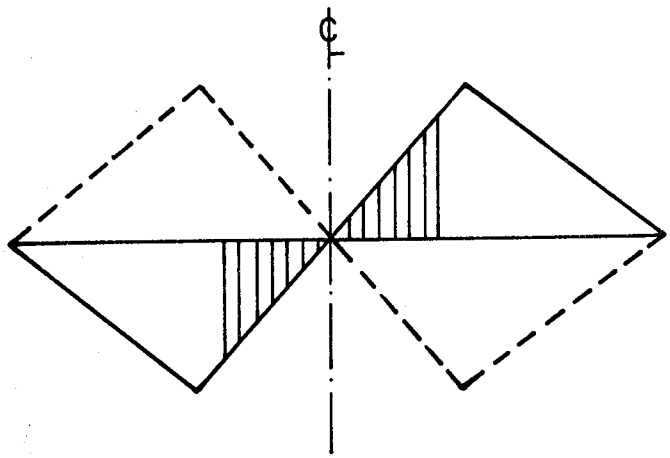

Bending Moment Diagram

Figure 2-13 Test Program Carried Out by Paulay

the behaviour of slender coupling beams and deep coupling beams are discussed separately.

2.4.3.1 Behaviour of Slender Coupling Beams

Experimental studies carried out on the inelastic behaviour of slender coupling beams has shown that the conventional reinforcement consisting of horizontal flexural bars at the top and the bottom of the beams and surrounded by closely spaced vertical stirrups as shown in Figure 2-14(a) is suitable. Test results have also indicated that the mode of failure is of flexural type and adequate ductility of such beams can lead to the formation of plastic hinges at the beam ends. A typical load versus deflection relationship for specimen C7 tested by Barney et al. (1978) at Portland Cement Association (PCA) is shown in Figure 2-14(b). Deflections are the relative displacements between the ends of the beams.

2.4.3.2 Ductility of Slender Coupling Beams

Ductility of a structure is commonly used as a measure of its inelastic performance. A ductile structure must be capable of large inelastic deformation at near maximum load carrying capacity without brittle failure. The available ductility in a structure is dependent on the amounts of longitudinal tension and compression steel, the amounts of transverse steel for concrete confinement and restraint against buckling of bars, the concrete and steel strengths

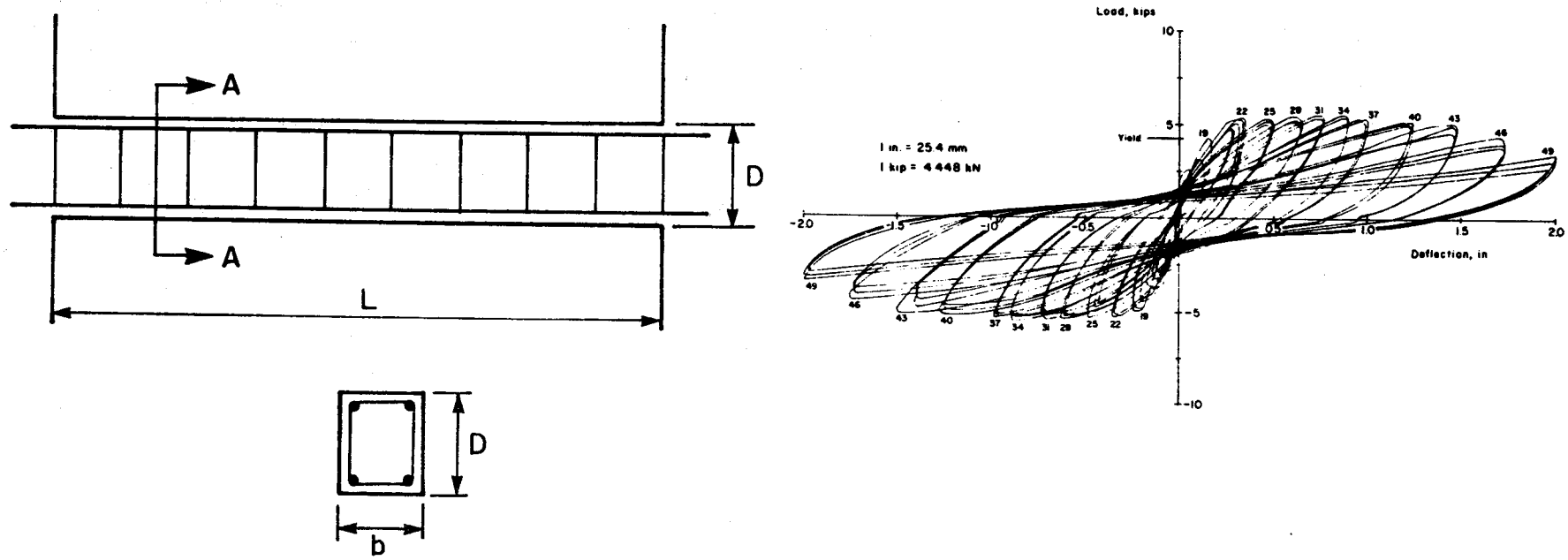

Section A-A

(a) Reinforcement Detailing for Slender Coupling Beam (b) Load versus Deflection Relationship for Specimen C7

Figure 2-14 Slender Coupling Beams

and the level of axial load. A ductile structure should avoid the possibility of shear and bond failure.

The rotation ductility factor or ratio is used here to define the measure of inelastic action in slender coupling beams.

$$u_\theta = \frac{\theta_{max}}{\theta_y} \qquad (2.1)$$

where

u_θ = rotation ductility ratio

θ_{max} = maximum rotation

θ_y = yield rotation

The ductility ratio in coupling beams can also be defined in terms of curvature given by

$$u_\phi = \frac{\phi_{max}}{\phi_y} \qquad (2.2)$$

The definitions for the above equation are synonymous to Equation 2.1.

2.4.3.3 Behaviour of Deep Coupling Beams

Experimental studies mentioned earlier have indicated that conventional longitudinal reinforcement is not suitable when the coupling beams which are relatively deep are subjected to alternate cyclic loading. Deep coupling beams may be subjected to high shearing stress when the ultimate

flexural strength is to be developed. The shear forces not only inhibit the full development of flexural capacity, they also restrict the ductility obtainable. It is therefore important to assess the ductility demand on the coupling system when the overall ultimate strength of the coupled shear wall structure is considered.

Experimental studies carried out on deep coupling beams with conventional reinforcement have indicated that the shear strength allocated to the concrete in accordance with ACI (1977) design practice diminishes with reverse loading and gradually the stirrups become overloaded and yield excessively; these beams fail in diagonal tension when stirrup reinforcement is provided for the whole or in excess of the maximum shear force that may be developed. When the flexural reinforcement enters the strain hardening range, it is possible to supress a diagonal tension failure. However the coupling beams fail by sliding shear. A sliding shear failure cannot be considered as being ductile enough for the purpose of seismic resistance. Moreover, a sliding shear failure means a near total loss of beam strength and stiffness.

It has been revealed that the ductility and strength of coupling beams can be considerably improved if instead of conventional steel arrangement, the principal reinforcement is placed diagonally in the beam as shown in Figure 2-15(a). The load versus deflection plot for specimen C6 tested at PCA is shown in Figure 2-15(b). Tests carried out by Paulay

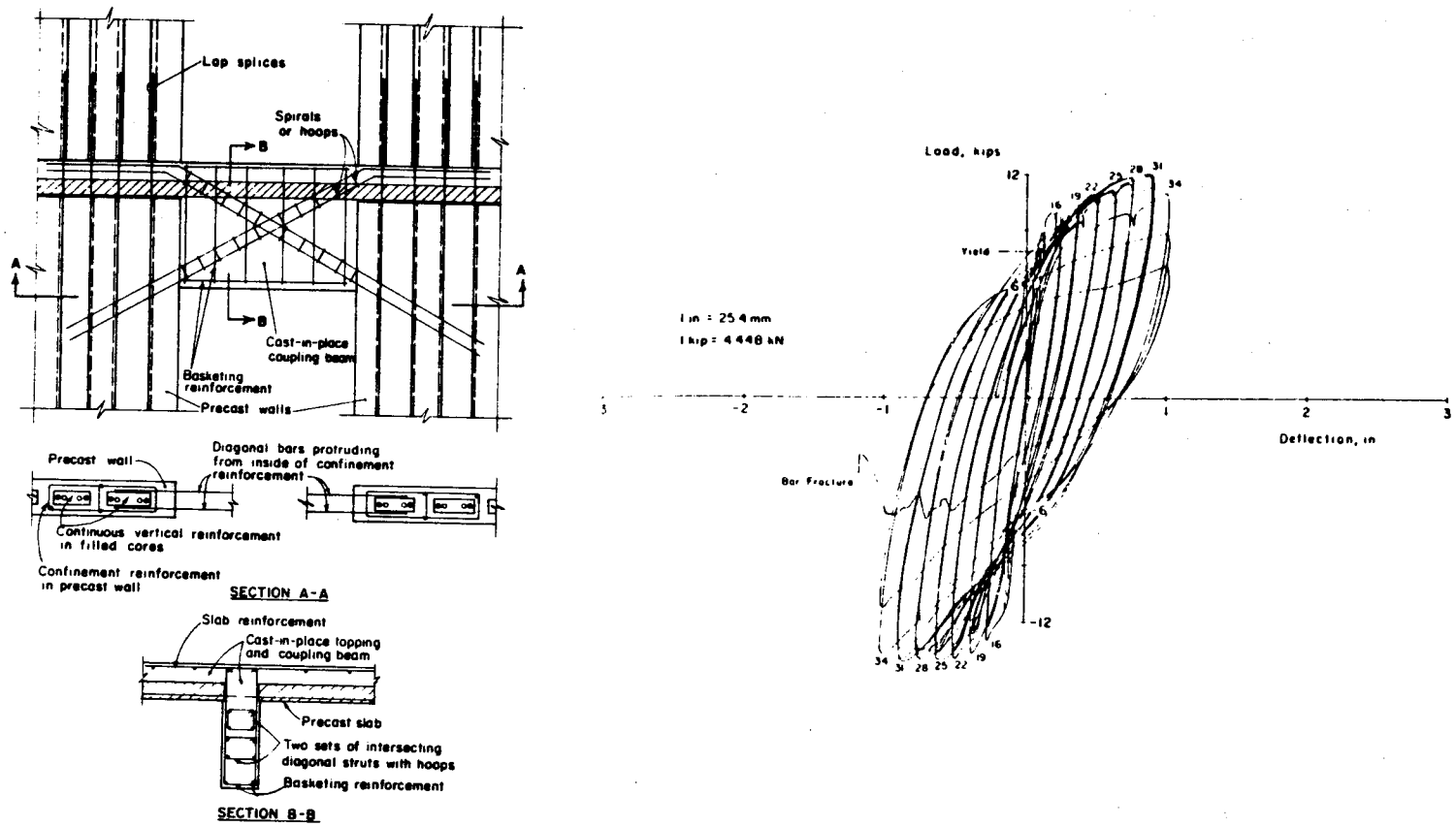

(a) Reinforcement detailing of deep coupling beams

(b) Load versus deflection for Specimen C6

Figure 2-15 Deep Coupling Beams

show similar behaviour. These results indicate that the behaviour of such beams is elasto-plastic and adequate ductility can be achieved. Test results also show that the cause of failure in such beams is the buckling of compression bars after the surrounding concrete has broken away. However if these bars are closely tied together or spiral winding is provided, particularly at the four corners of the beam which are likely to contain the heavily cracked concrete during cyclic loading, the lateral stability of these bars can be assured. Additional light secondary or basketing reinforcement consisting of a mesh in both faces of a coupling beam will also be required to hold the broken concrete particles in place when large plastic displacements occur during a catastrophic earthquake.

2.4.3.4 Energy Dissipation Capacity of Deep Coupling Beams

To illustrate the better performance of deep coupling beams containing full diagonal reinforcing bars rather than other reinforcing arrangements as shown in Table 2-1, the energy dissipation capacities of deep coupling beams with different reinforcing details are compared. This is the result of a series of experimental studies carried out at PCA described earlier.

A measure of energy dissipation is given by the area within the load versus deflection loop. For equivalent loads and deflections, specimens dissipating the most energy are considered to have the best performance. Figure 2-16

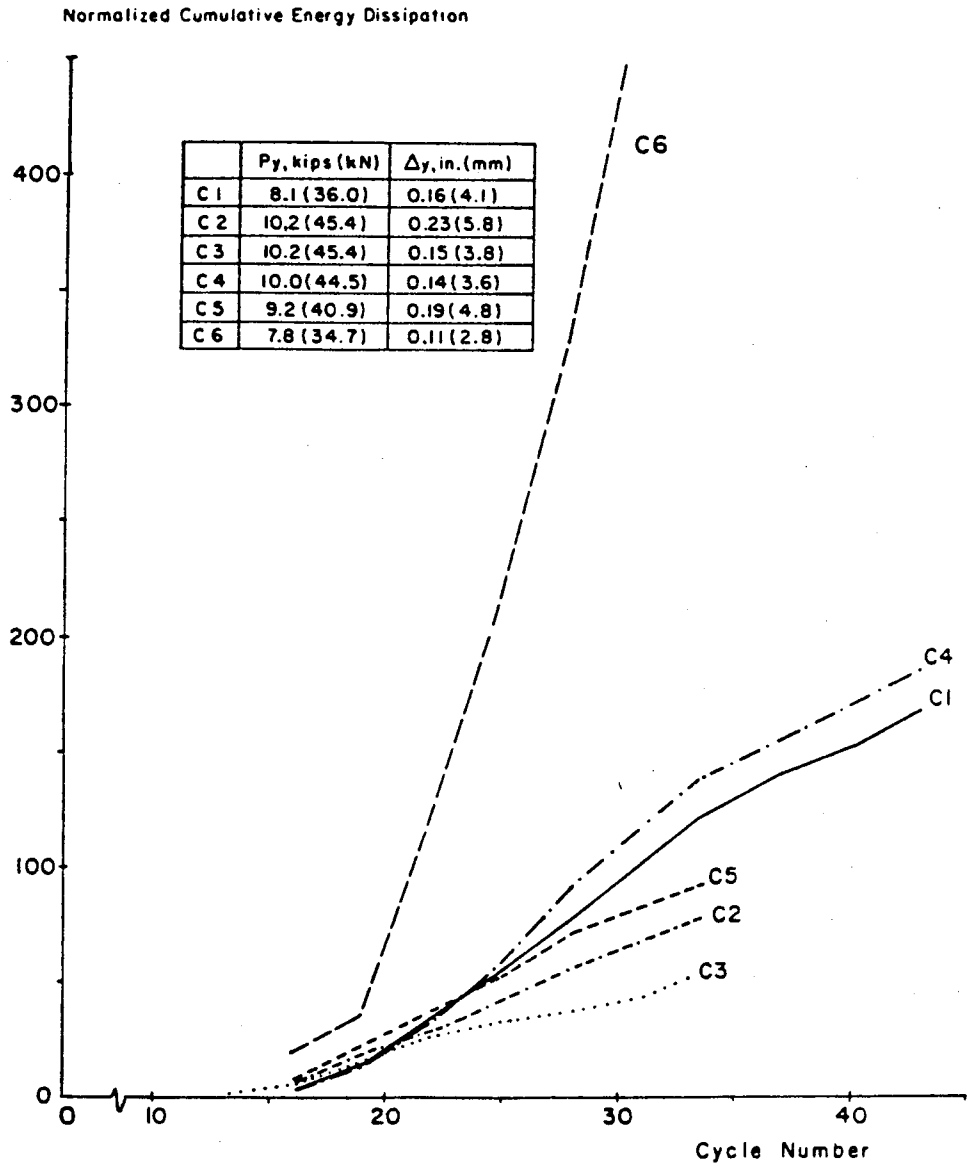

Figure 2-16 Normalized Cumulative Energy Dissipation Versus Cycle (Barney et al., 1978)

shows the normalized cumulative energy dissipated versus number of cycles for different beams. The normalized cumulative energy dissipated E_{ij}, is defined as the cumulative energy dissipated divided by the yield load and yield deflection as follows.

$$E_{ij} = \frac{1}{P_y \Delta_y} \sum_{k=1}^{n} e_k \qquad (2.3)$$

where

E_{ij} = normalized cumulative energy dissipated

P_y = yield load

Δ_y = yield deflection

e_k = energy dissipated in the kth load cycle

k = load cycle.

These curves confirm the better performance of the specimen C6 with full length diagonals compared to other specimens with different reinforcing arrangements.

2.4.4 Experimental Test Results of Precast Concrete Structures

There have been some experimental tests of precast panel wall systems in the past few years. The tests have been carried out on small scale models under quasi-static conditions or on shaking tables to simulate earthquake motions. There are only limited results of the experiments available at present.

Oliva and Shahrooz (1984) carried out tests using a

shaking table on one-third size scale models of three stories high structures of plain solid wall, wall panels with door openings and wall panels with adjoining end flange walls. Shear-slip motion was constrained by shear keys. Test results showed dominant rocking behaviour with limited shear slip. Rocking motion induced stress concentration at wall ends which led to concrete crushing.

Velkov et al. (1984) tested specimens similar to those described above under quasi-static conditions. Their results showed that coupled walls have sufficient ductility behaviour with displacement ductility greater than 5. They concluded that large panel systems with carefully designed details of connections allow their applications in seismic conditions.

Harris and Caccese (1984) tested simple walls of 1/32 scale models of five stories high structures using a small shaking table. The model was chosen to study the behaviour of the simple walls studied analytically by Becker and Llorente (1979). The dynamic response of the model showed the failure mechanism of the system to be the slip and the crushing of the panel corners caused by rocking. The behaviour of the model was close to the behaviour predicted by an MIT analysis.

Chu et al. (1984) tested a 1/5 scale mode of an eight story coupled wall building constructed in Beijing, China. Static and dynamic loading was applied to the structure. Dynamic loading was applied with an exciter placed at roof

level. The static and dynamic tests were interchanged in the whole test program. Results of the test showed that large panel structures possess adequate ability of energy dissipation to resist earthquakes and that even if the walls are damaged the structural stability/integrity is maintained.

2.5 Material Behaviour of the Connections

2.5.1 Material Behaviour of Concrete

In considering the failure mechanism of reinforced concrete or prestressed concrete, it has often been stated that reinforcement or prestress alters the nature of the material and therefore changes the criteria of failure. In the development of failure mechanism, the bond between concrete and reinforcement and deformation in the reinforcement are important. However, as Bresler and Pister (1964) suggest, a reasonable assumption can be made in which the conditions producing local failure in concrete are essentially the same for both plain and reinforced concrete. Therefore, knowledge of the conditions producing local failure in plain concrete should lead to a better understanding of the failure mechanism in reinforced or prestressed concrete.

The behaviour of concrete under a biaxial state of stress is quite different than that under a uniaxial state of stress. Figure 2-17 shows typical experimental stress-strian curves for concrete under biaxial compression.

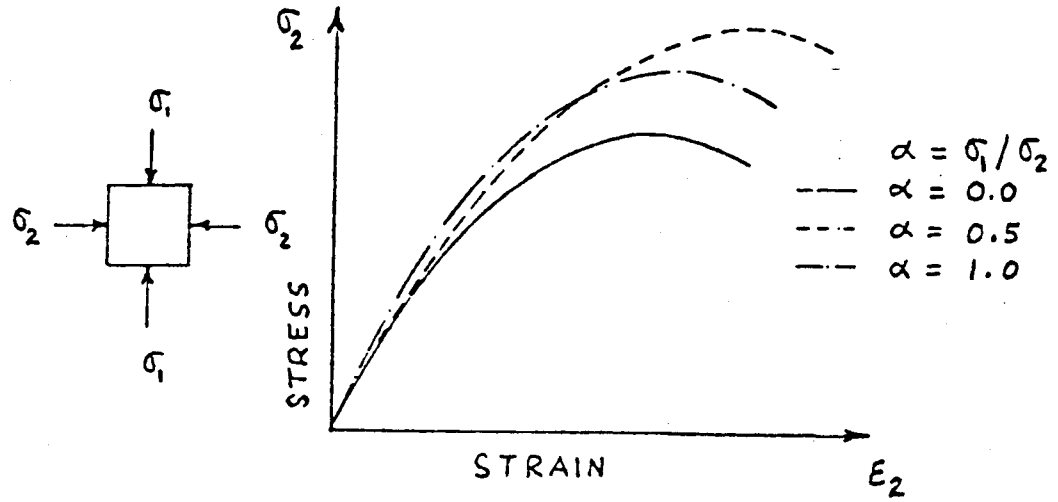

Figure 2-17 Behaviour of Concrete under Biaxial Compression (Kuper et al., 1969)

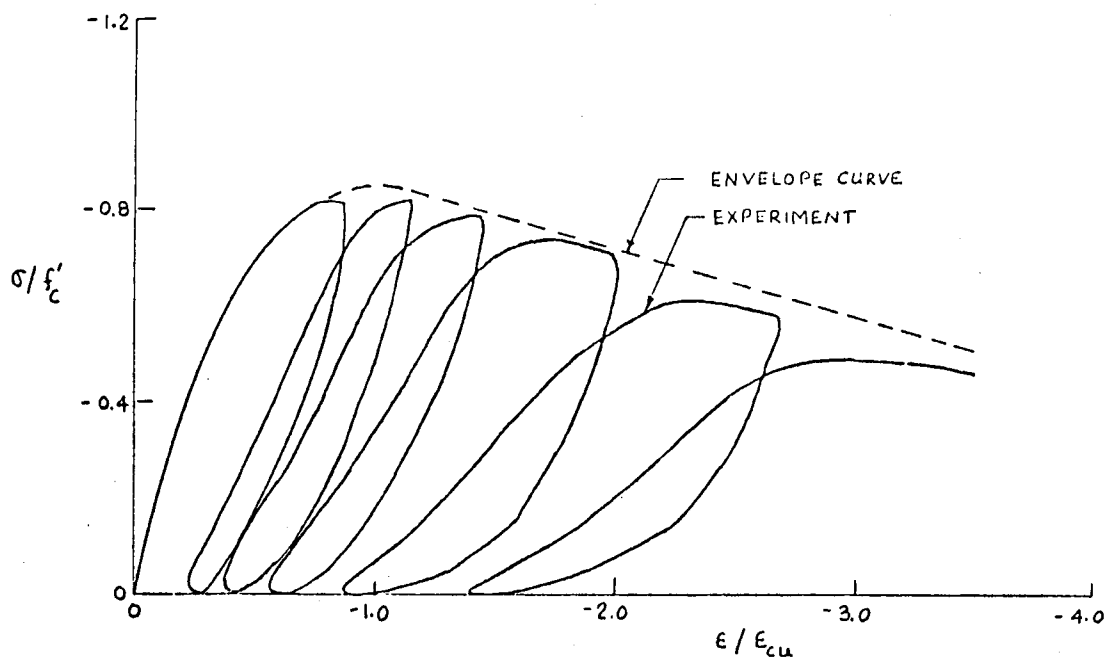

Figure 2-18 Behaviour of Concrete under Uniaxial Cyclic Load

Recognizing the fact that the constitutive relationship in the biaxial state of stress will be different from that in the uniaxial case, several investigators presented experimental data on specimens under biaxial states of stress.

Liu et al. (1972) modeled concrete as an orthotropic material under biaxial loading. For biaxial compression, they proposed a constitutive relationship of the form:

$$\sigma_i = \frac{\varepsilon_i E_o}{(1 - \nu\alpha)\left[1 + \left(\frac{1}{1 - \nu\alpha}\frac{E_o}{E_s} - 2\right)\left(\frac{\varepsilon_i}{\varepsilon_p}\right) + \left(\frac{\varepsilon_i}{\varepsilon_p}\right)^2\right]} \qquad (2.4)$$

where

σ_i, ε_i = stress and strain in the principal stress direction

σ_p, ε_p = maximum biaxial compressive stress and corresponding strain

ν = Poisson's ratio

E_o = initial tangent modulus

E_s = secant modulus at maximum stress σ_p/ε_p

α = stress ratio σ_1/σ_2, $\sigma_1 > \sigma_2$

The above equation is valid for biaxial compression only and does not take into account load reversals.

It should be noted that the material behaviour of the connection is under a uniaxial state of stress only and the

transverse stresses are assumed to be zero which is also the case in simple beam theory.

Setting α equal to zero in Equation 2.4 will reduce the stress-strain relationship to an equivalent uniaxial stress state.

Karsan and Jirsa (1969) have carried out experiments under cyclic loads on concrete under uniaxial conditions; the results are shown in Figure 2-18. Based on the envelope curves, Darwin and Pecknold (1974) have extended Liu's model to incorporate cyclic loading and strain softening in compression; this model is shown in Figure 2-19. The constitutive relationship is of the form:

$$\sigma_i = \frac{E_o \, \varepsilon_i}{1 + \left(\frac{E_o}{E_s} - 2\right)\left(\frac{\varepsilon_i}{\varepsilon_c}\right) + \left(\frac{\varepsilon_i}{\varepsilon_c}\right)^2} \qquad (2.5)$$

where

ε_i = uniaxial strain in the principal stress direction

σ_c, ε_c = maximum compressive stress and corresponding strain in the principal direction

E_o = initial tangent modulus

E_s = secant modulus σ_c/ε_c

The concete material model adopted for the present study is similar to the model suggested by Darwin and Pecknold (1974) with some modifications. This will be discussed in the next chapter.

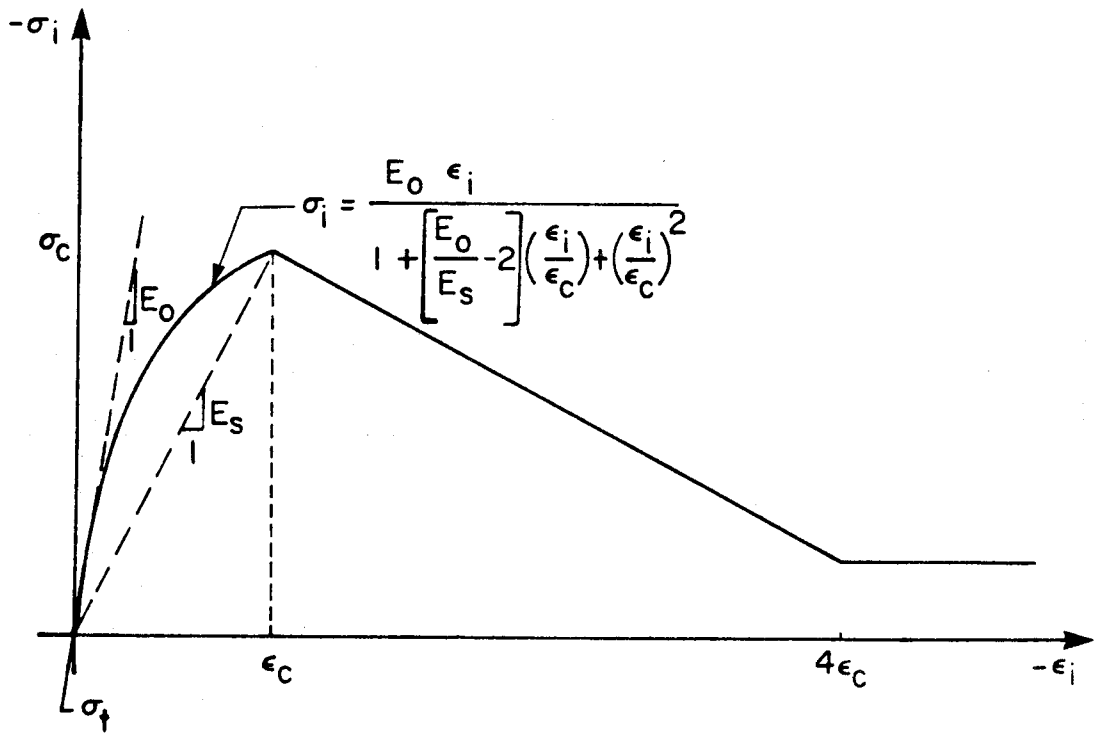

Figure 2-19 Equivalent Uniaxial Stress-Strain Model for Concrete

2.5.2 Shear Behaviour of the Connections

The transfer of shear forces across the horizontal connections is made either by Coulomb friction in the presence of gravity load and/or post-tensioning and, by shear friction in the presence of mild reinforcing bars. The transfer of shear by Coulomb friction is provided essentially by a friction force between the panel and the connections which is given by the coefficient of friction multiplied by the compressive force on the connection. If the induced shear force increases by this value, slip will occur. A typical test result carried out by Hanson at PCA (1979) is shown in Figure 2-20(a). The connection is of platform type and the transfer of shear is by Coulomb friction. The figure shows an abrupt initial loss of strength probably due to loss of bond. For subsequent loading, the connection exhibits elastic-plastic strain-hardening behaviour. The elastic part is associated with the deformation of the material and the plastic part is associated with the slippage along the connection panel interface.

The inelastic behaviour of the connections have also been investigated by Verbic (1977) for the type used in the Yugoslavian "Vranica" building system. The shear behaviour of the unreinforced connection when the panel self weight is producing vertical load is shown in Figure 2-20(b). The figure shows a strain hardening degradation under repeated cyclic loading. The loss of stiffness can be attributed to

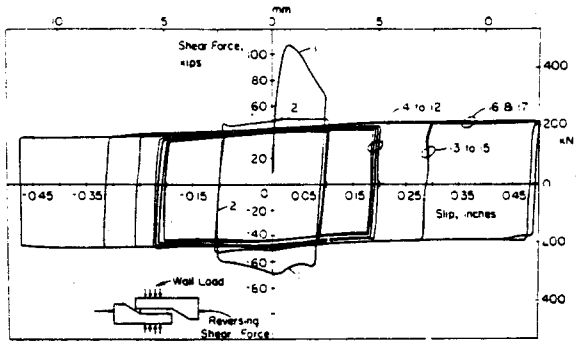

(a) Test results by Hanson (1979)

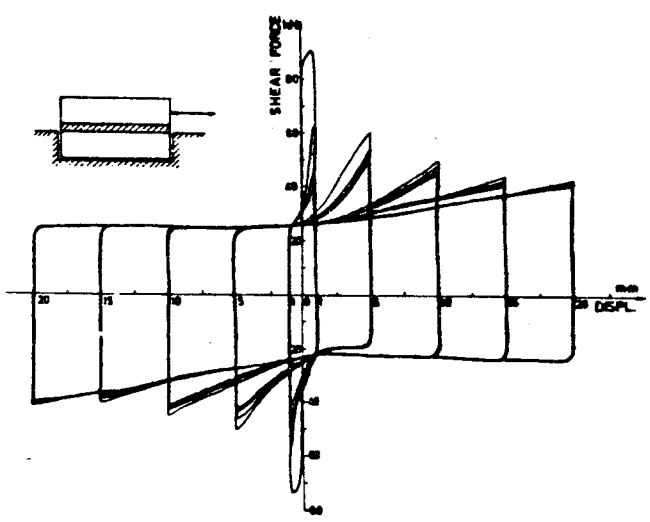

(b) Test results by Verbic (1977)
(No applied vertical load)

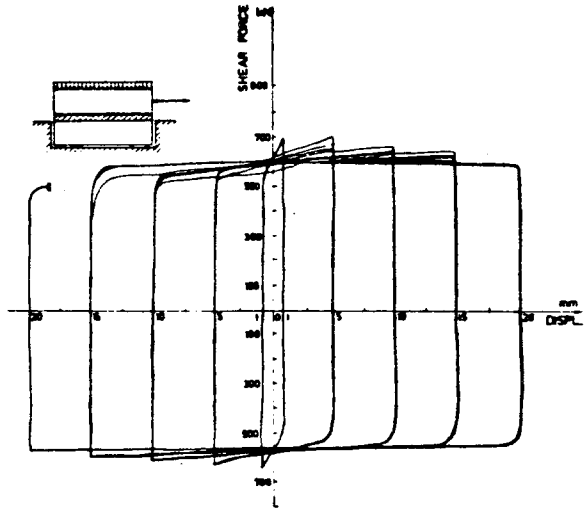

(c) Test results by Verbic (1977)
(Applied vertical load)

Figure 2-20 Shear Force Versus Shear Displacement Relationships for Connections Without Vertical Reinforcement

polishing of the connection surfaces and to accumulation of loose sand particles which facilitate sliding. Under applied vertical load, the connection shows a similar behaviour except the initial strength loss is smaller and the degradation of the strain hardening stiffness is less noticeable as shown in Figure 2-20(c). These results show similar behaviour to those tested at PCA shown in Figure 2-20(a).

When mild reinforcing bars are provided cross the connections, shear forces are carried mainly by aggregate interlock, interface shear transfer and dowel action of the reinforcement. When the connections are subjected to shear, slip will occur along the shear plane if the shearing stresses are greater than $\mu\sigma$, where μ is the coefficient of friction and σ is the normal stress. Since the faces of the crack are rough and irregular, the crack faces are forced to separate. As a result, tension is developed in the reinforcement which produces equal amount of normal compression or clamping force on the connection surface as shown in Figure 2-21, and hence it increases the friction. This mechanism is termed interface shear friction. Researchers have called this mechanism surface roughness shear transfer, shear friction or tangential shear transfer (MacGregor, 1973). The transfer of shear forces across the connections is also produced by the dowelling action in the reinforcing bars. However, test results by Paulay et al. (1974) on shear transfer across the construction joints and

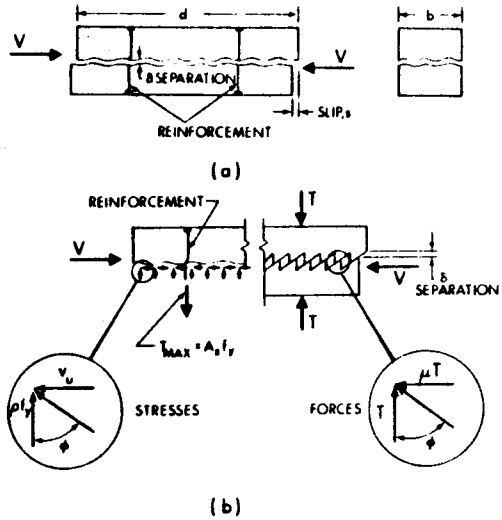

Figure 2-21 Interface Shear Transfer (MacGregor, 1973)

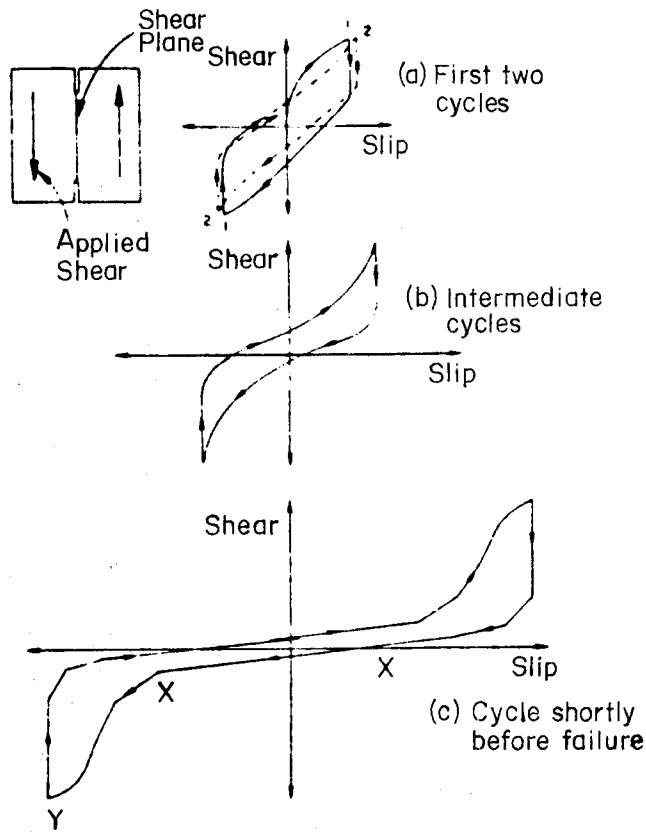

Figure 2-22 Shear Versus Slip for Precracked Reinforced Specimens (Mattock, 1974)

also tests by Mattock (1977) have indicated that the contribution of dowel forces is relatively minor and most of the shear across the connections is carried by interface shear transfer and the aggregate interlock mechanism. It should be noted that a small proportion of the shear resistance across the connections is also provided by shearing of small asperities projecting from the faces of the crack.

There are few experimental test results available on the shear strength of connection with longitudinal reinforcement perpendicular to the plane of the connections. Such results indicate that the presence of reinforcement significantly affects the shear strength of the connections. Mattock (1974, 1976) carried out a series of tests on the shear behaviour of precracked specimens. The tests were load controlled. Results of the test show elasto-plastic behaviour during the first few cycles as illustrated in Figure 2-22. As the number of cycles increase, the hysteresis loops show pinching behaviour which is not a desirable mechanism for energy dissipation. At cycles before failure, large inelastic deformations are developed which do not show elasto-plastic ductile behaviour. In the region X-X, the specimen has very little shear stiffness and therefore very little shear resistance is developed. This is due to the fact that the crack is open and the reinforcement provides no clamping action in this region. Since the concrete surrounding the reinforcing

bars becomes damaged, the resistance from aggregate interlock is lost. In the region X-Y, reinforcement develops tension force and provides clamping action which increases both friction and aggregate interlock effects.

A complete hysteretic response on specimen similar to those described above and tested by Mattock (1976) is shown in Figure 2-23. These results also show pinched hystertic behaviour.

Verbic (1977) carried out tests on specimens containing reinforcing bars. The results are shown in Figures 2-24(a) and (b) for cases containing no vertical loading and with vertical loading, respectively. The results of these tests are similar to those with no reinforcing bars shown in Figures 2-20(b) and (c). However, in this case, the deterioration of strain-hardening stiffness is less severe as the number of cycles are increased and also larger amount of shear forces are carried by the specimen.

Harris and Abboud (1981) tested 16 3/32 scale models of the interior American type horizontal connections under both monotonic and cyclically reversing load. Vertical continuity was provided with threaded steel rods. Uniform load distribution as well as triangular load distribution increasing from the center of the connection to the edge of the connection was applied across the shear plane. This produces a moment in the center in addition to the slight moment introduced by the applied horizontal shear load. A typical test result is shown in Figure 2-25. These results

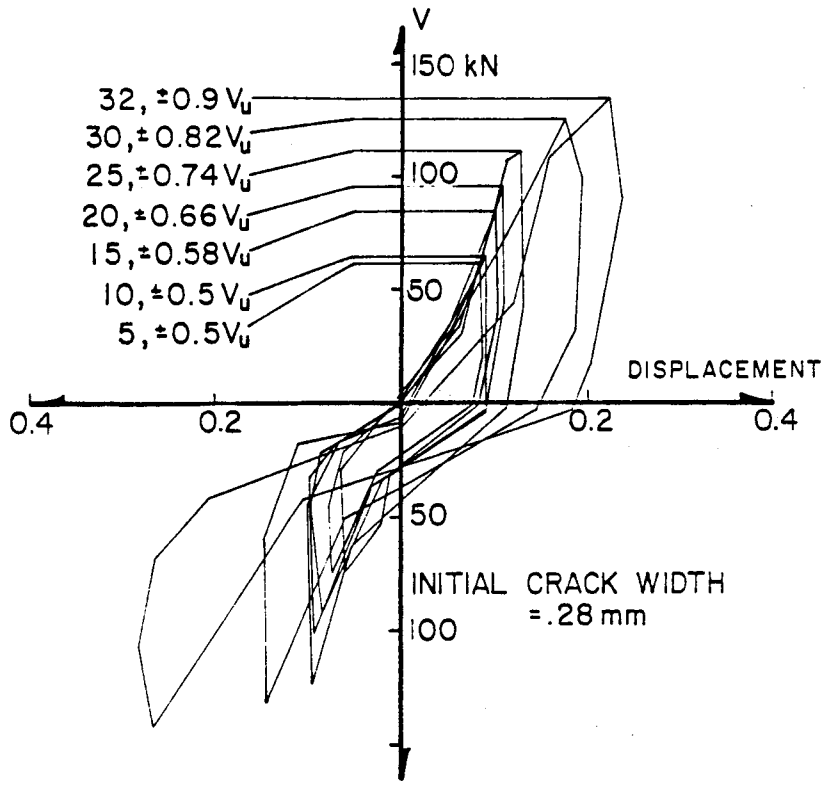

Figure 2-23 Shear Transfer by Shear-Friction (Mattock, 1976)

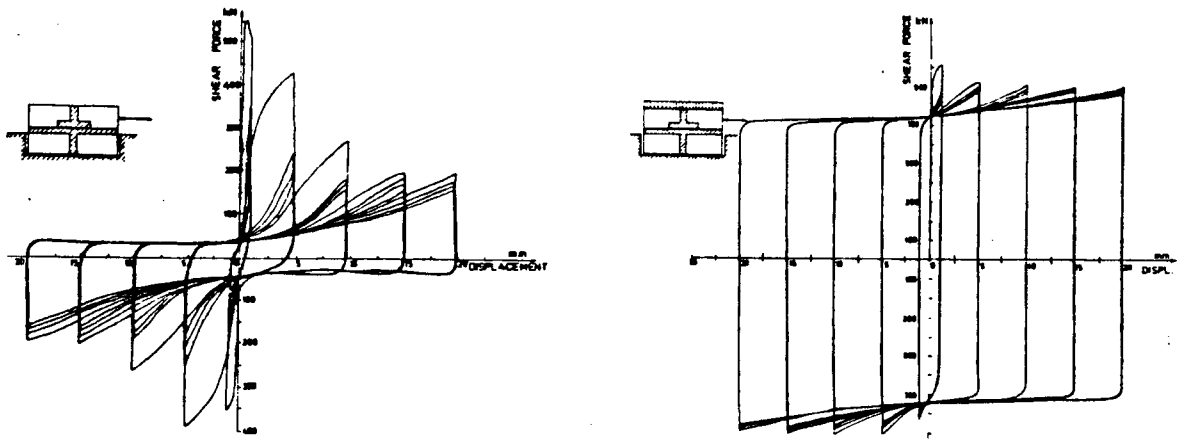

Figure 2-24 Shear Force Versus Shear Displacement Relationships for Connections with Vertical Reinforcement (Verbic, 1977)

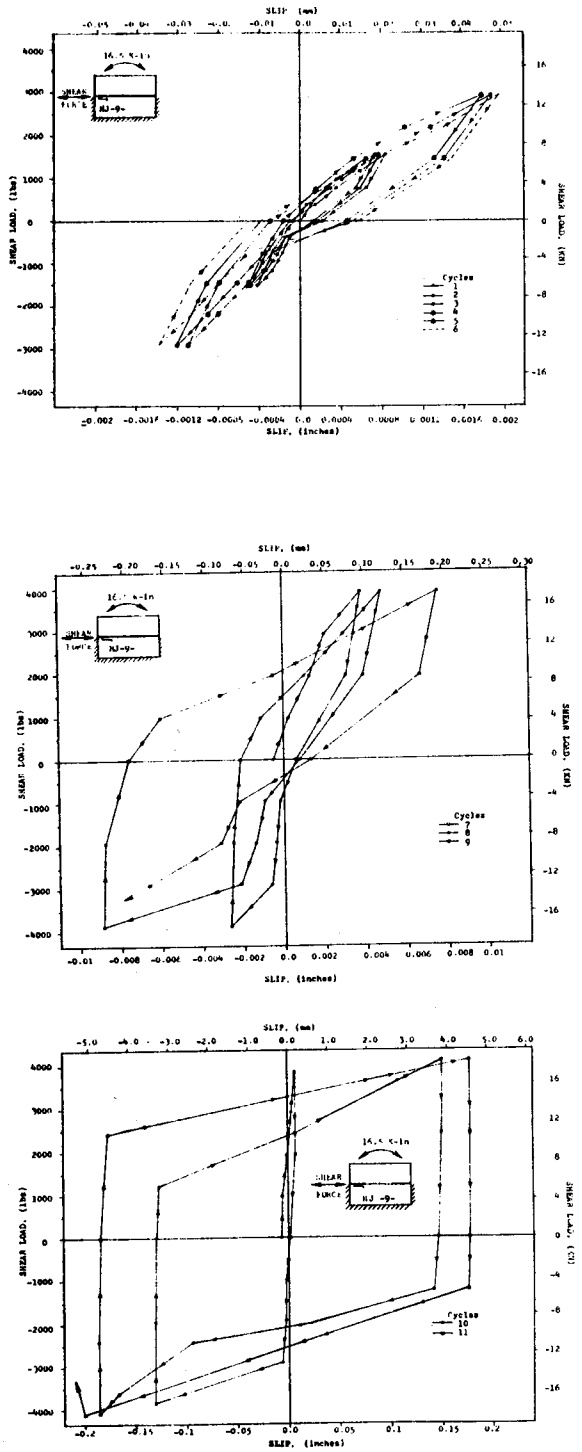

Figure 2-25 Shear Versus Slip Relationship (Harris and Abboud, 1981)

show an irregular pinching appearance at lower shear cycles. The shape of shear slip curves prior to failure changes to rectangular or elasto-plastic type. In these specimens, failure occurred suddenly due to rupture of vertical ties. The sudden failure was followed by local failure of the edges of the wall at the point of the shear load application. Their test results also showed that the ultimate shear capacity of the specimens tested under cyclic loading was between 5 to 33 percent less than under monotonic loading.

2.5.3 Coefficient of Friction (μ)

The coefficient of friction across the connections can have a significant effect on the response of precast wall panels. There have been experimental tests carried out on full and small scale models to estimate a value for the coefficient of friction. These results show a wide range between 0.2 and 1.81 as shown in Figure 2-26.

Gaston and Kriz (1964) investigated the shear strength of the connections between precast pieces. Bonding between the blocks was provided with a 1/2 inch layer of mortar and rods for applying normal stress to the specimen were passed through oversized holes. For these specimen, the minimum and maximum values of coefficient of friction were 0.79 and 1.81 respectively.

Jones (1959) tested the shear strength of units which were mortared together and post-tensioned. The maximum and

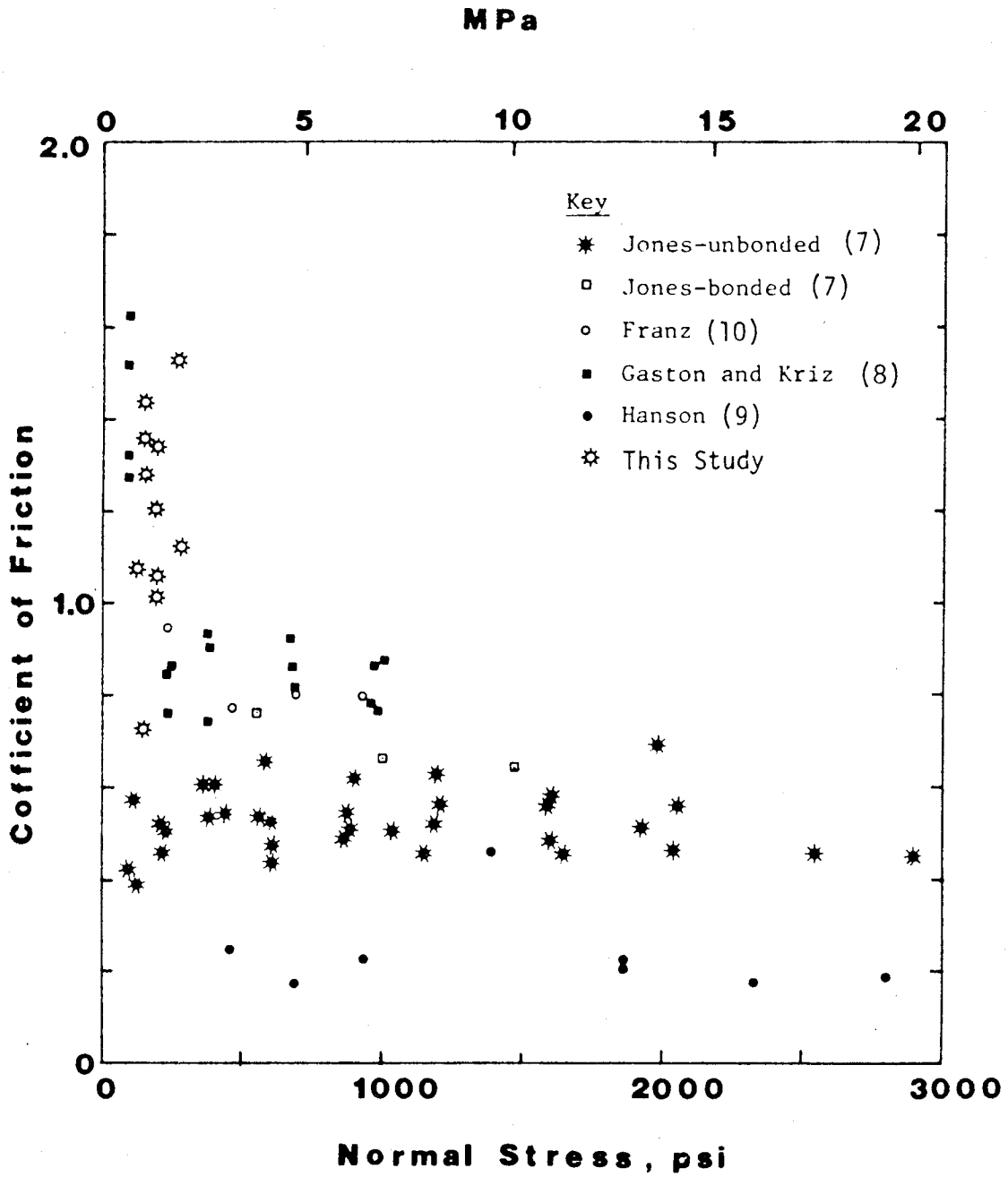

Figure 2-26 Coefficient of Friction (Harris and Abboud, 1981)

minimum values of the coefficient of friction reported were 0.765 and 0.645 respectively.

Harris and Abboud (1981) carried out a series of 16 tests to study the cyclic shear behaviour of the connections. Normal load was applied to specimens in such a manner to produce a compression and an overturning moment about the mid length of the connections. The values of the coefficient of friction were in the range of 0.72 to 1.52.

Hanson (1979) investigated the force-deformation characteristics of the interior horizontal wall-to-floor joint subjected to repeated reversals of shear forces applied along the joint, simulating seismic loading. Five full scale joints of 1.22 meter and 0.609 meter sections were tested. In each case, the formed surfaces of the end of the wall at the joint were cast against plastic-coated plywood to produce an extremely smooth surface for sliding of the joint. The values of coefficient of friction measured were between 0.2 and 0.4.

2.6 Summary

In this chapter, the results of experimental tests and analyses carried out by other researchers on the parameters affecting the response of precast wall panels and the coupling beams were described. It was shown that the type of reinforcing detail can have a significant effect on the behaviour of coupling beams. Conventional longitudinal reinforcement is most suitable for slender beams while full

diagonal reinforcing bars are most effective for deep beams. It was also shown that the presence of reinforcing bars significantly affects the shear behaviour of the connections. The range of the value of the coefficient of friction reported from different test results varied significantly.

3. ANALYSIS AND MODELING OF WALLS

3.1 General

In this chapter, the finite element modeling techniques used for analysis of coupled wall structures are discussed. Wall panels are modeled assuming linear-elastic behaviour. Inelastic action is assumed to take place in the horizontal connections and the coupling beams. Based on experimental results discussed in the previous chapter, several models are described which are incorporated into the computer program DRAIN-2D. The modeling of coupling beams is described and the procedure used for the compatibility of beam elements with plane-stress panel elements is discussed. The behaviour of deep coupling beams is reviewed and a truss model for modeling of deep beams is described.

3.2 Previous Analyses

The behaviour of cast-in-place walls has been studied extensively by several researchers. There are some well known techniques in which the elastic and/or inelastic behaviour of monolithic walls can be modeled and analysed. Simple cast-in-place walls can be modeled as simple vertical cantilevers using simple bending theory for elastic analysis with masses uniformly distributed or lumped at floor levels.

A large number of walls have at least one vertical row of openings and the analyses of such structures is less straightforward. The shear-connection method or the wide

column frame analysis are used for walls with a single row or several rows of openings. In the shear connection method, the row of openings can be effectively treated as a continuous medium in pure shear as shown in Figure 3-1(b). A second order differential equation is formed and solved to give deflections, moments and shears. To use this method, Coull and Choudhury (1967) have provided charts. This method is simple to use for walls with a single row of openings and constant properties with height. However, the arithmetic becomes cumbersome with several rows of openings and other variations.

In the wide-column frame analysis, the structure can be idealized as shown in Figure 3-1(c). This requires a frame program in which the finite width of the column should be considered. Spring supports can be used to model the foundation effects and rotational springs can be used between the rigid and the flexible parts of the frame to model the action of connecting beams which may not be fully fixed at their ends.

Saatcioglu (1981) studied the inelastic behaviour of earthquake resistant cast-in-place coupled walls. In his study, he idealized the walls as line elements with inelastic action allowed by the formation of plastic hinges at the ends of line elements. The element idealization consists of an inelastic beam with point hinges at each end as shown in Figure 3-2. For the earthquake analysis of coupled wall specimens, Takayanagi et al. (1981) used a

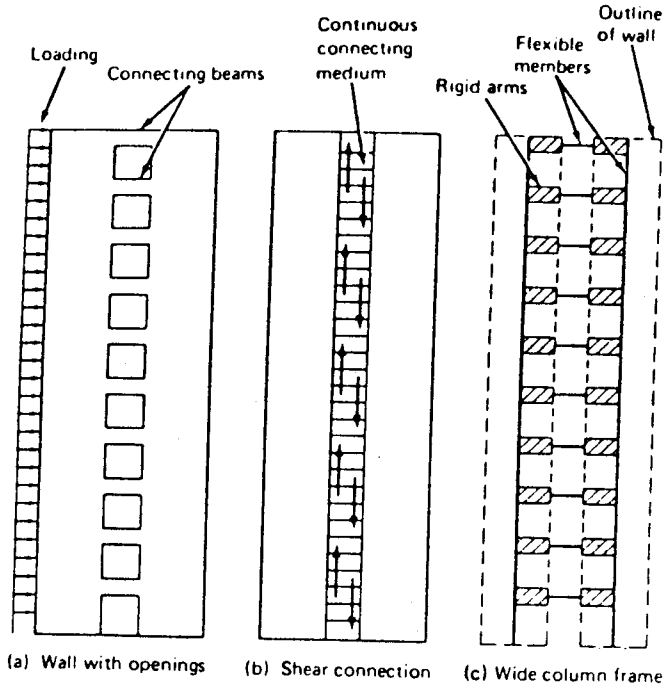

Figure 3-1 Analysis Techniques for Monolithic Shear Walls with Openings

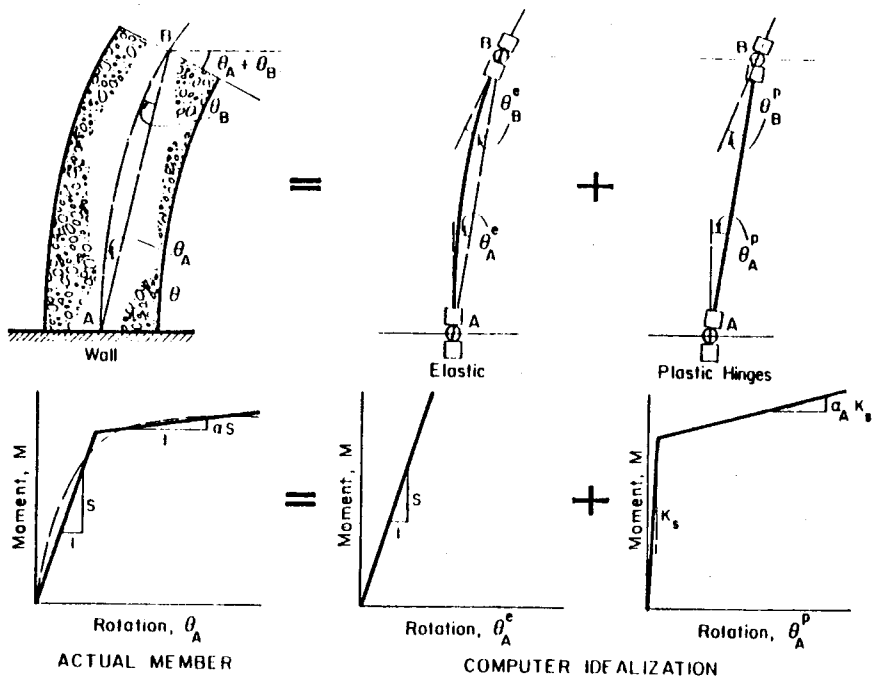

Figure 3-2 Modeling Technique for Wall Elements (Saatcioglu, 1981)

structural model which is shown in Figure 3-3. They divided the wall members into subelements in order to consider the inelastic action over the length of the wall. Finer arrangement of subdivision was allowed in the lower part of the structure since the major inelastic action is expected to occur at the base of the wall.

The modeling techniques described so far applies to monolithic structures such as cast-in-situ structural walls. As mentioned in the previous chapter, the behaviour of precast walls is different from cast-in-place walls and therefore different modeling techniques are required. However, if the connections are strong enough to resist the forces associated with the formation of a plastic hinge at the wall base, i.e. seismic behaviour similar to cast-in-place walls, then it can be assumed that the structure behaves monolithically and the modeling procedure similar to those described above could be adopted.

Muller and Becker (1979) have used an extended version of the shear connection method to obtain an explicit expression for the fundamental period of precast simple and composite shear walls. However, their analysis is based on a strong horizontal connection and a weak vertical connection. The frame model has been used by Pall and Marsh (1979) for the nonlinear analysis of precast composite walls containing vertical connections only.

In the previous studies carried out by Pall and Marsh (1979), Llorente and Becker (1981), Schricker and Powell

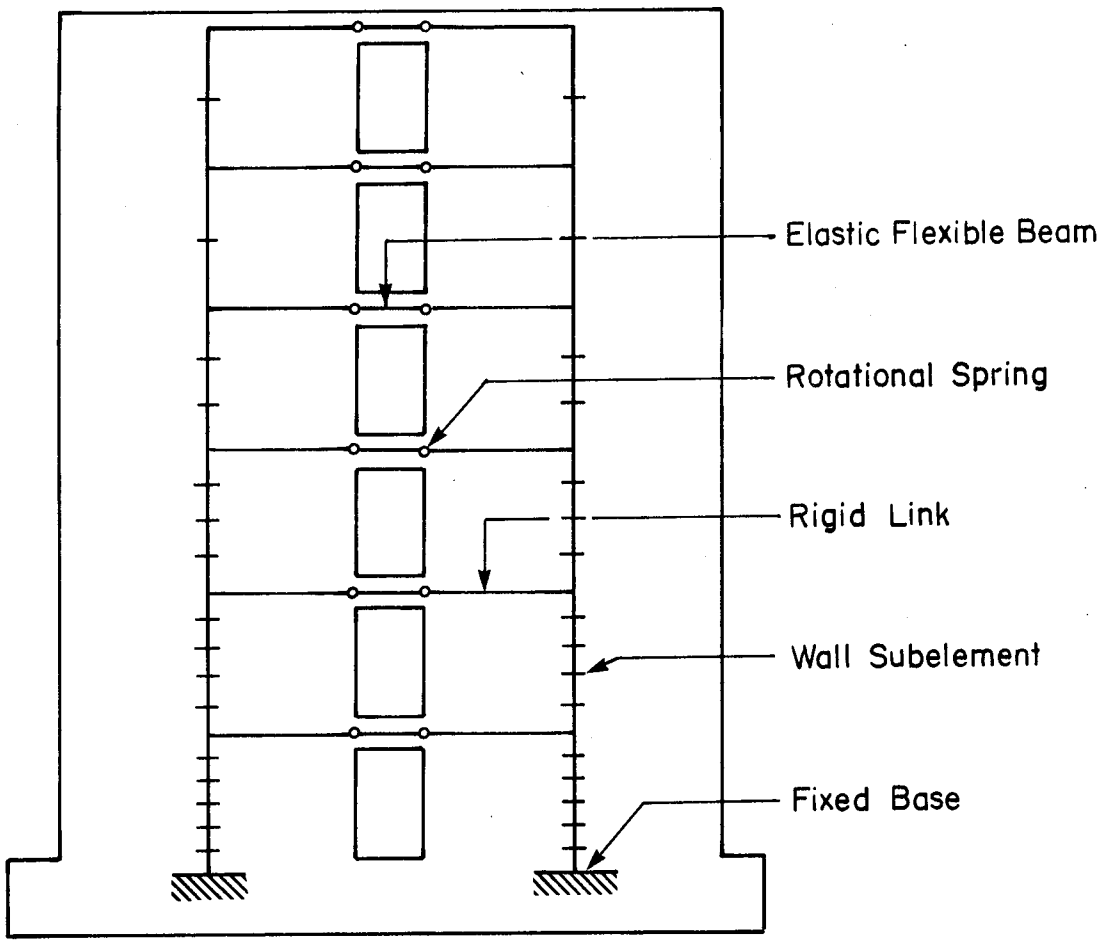

Figure 3-3 Structural Modeling of Monolithic Coupled Wall Systems

(1980), Brankov and Sachanski (1977), Velkov et al. (1978), and Velkov (1977) on static and dynamic analysis of precast walls, it was assumed that wall panels remain linear-elastic throughout the analysis. Simple walls in panelized structures can be modeled as simple vertical cantilevers described earlier. Connection regions can be modeled as short flexible beams having axial, shear and rotational stiffnesses. However the assumption of plane section after joint opening is unrealistic and therefore such modeling technique cannot be very accurate. The technique also becomes more complicated when material inelasticities are included in the analysis.

On the inelastic seismic analysis of large panel buildings, Shricker and Powell (1980) have used a modified beam element to model wall panels; this is shown in Figure 3-4(a). For the connections, they used axial and shear springs which is shown in Figure 3-4(b). The modified beam element assumes that the horizontal joint planes remain flat. For cases in which joint opening occurs, gap opening is progressive and the rigid plane assumption is no longer valid. For this reason, they have also used a four node rectangular plane stress finite element to model the wall panels with several spring elements placed across the connection.

The inelastic behaviour of precast concrete shear walls has also been analytically studied by Llorente and Becker (1981). They used finite elements to model the wall panels

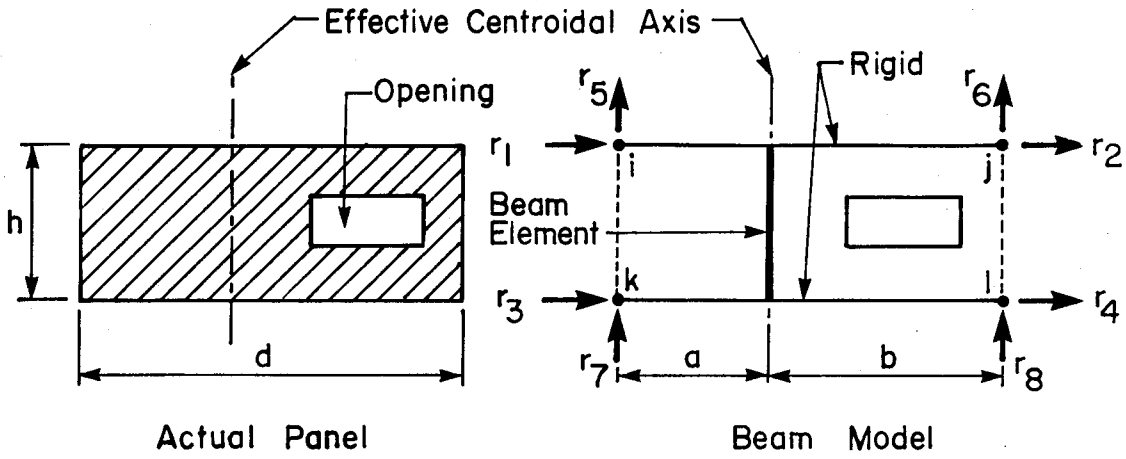

(a) Panel Element : Modified Beam Model

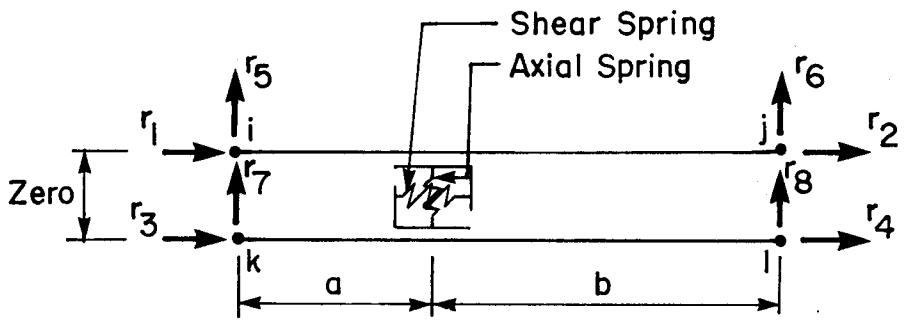

(b) Horizontal Connection

Figure 3-4 Modeling Technique for Precast Wall Systems (Schricker and Powell, 1980)

as well as the connections. For cases in which gap opening occurs, their model takes into consideration the distributed nature of the force transfer and allows for the gradual opening and closing of the connections. This modeling procedure has been used in the present study to model the connections and will be further discussed in this chapter.

3.3 The Computer Program DRAIN-2D

DRAIN-2D is a general purpose computer program for dynamic analysis of inelastic plane structures. The program was developed by Kanaan and Powell (1975) at the University of Berkeley, California. Modifications to the program were carried out for the present study for inelastic seismic analysis of precast shear walls. The program consists of a number of "base" subroutines which read and print the structure and loading data, carry out a variety of bookkeeping operations, assemble the structure stiffness and loading, and determine the displacement response of the structure. The structure stiffness matrix is assembled from the individual element stiffness matrices by direct stiffness method. The program makes provisions for static loads to be applied prior to dynamic loads, but no yielding is allowed to take place under such conditions. Viscous damping effects may be included, if desired. Damping coefficients proportional to mass, initial elastic stiffness and/or tangent stiffnesses can be specified. The damping matrix is of the form

$$[C] = \alpha\ [M] + \beta\ [K_T] \tag{3-1}$$

where

[C] = damping matrix

[M] = diagonal mass matrix

$[K_T]$ = tangent stiffness matrix

α and β = constants to be specified by the program.

The values α and β can be obtained from the following equations when the first two modes of vibration are considered.

$$\alpha = \frac{4\pi(T_j\lambda_j - T_i\lambda_i)}{T_j^2 - T_i^2} \tag{3-2}$$

$$\beta = \frac{T_iT_j\ (T_j\lambda_i - T_i\lambda_j)}{T_j^2 - T_i^2} \tag{3-3}$$

where

λ_n = proportion of critical damping in the nth mode

T_n = period of vibration in the nth mode.

Because of change in the yield status of the structural elements, the tangent stiffness matrix may change from one step to the next. Hence, if stiffness dependent damping is assumed, the damping matrix may also change suddenly between time steps. This introduces an equilibrium unbalance at the beginning of the new time step which may lead to the accumulation of significant errors if not corrected. The

computer program has the capability to minimize this problem by applying a correction load during the next integration time step.

The program uses the step by step technique with constant average acceleration method (Newmark, $\beta = 1/4$) during each time step for the dynamic analysis. This method has the advantage of being stable for all periods and time steps, and of not introducing damping into the system. Appendix A shows the procedure for the solution of the equations of dynamic equilibrium using this technique. Greater accuracy can be obtained using small integration time steps; however, for vibration modes with periods which are short relative to the time step, the response will be inaccurate with respect to time, but the amplitudes will be of the correct order of magnitude. Selecting the optimum time step for analysis in terms of accuracy and computational efforts requires both experience and experiment.

Several models which are described in this chapter have been incorporated into the program. In the seismic analysis and the seismic design of structural systems, time history plots of response provide a better understanding of the structural behaviour. A graphical option has been developed which is a post processor that operates on analysis data saved upon request. The program, originally developed by Casey (1979), is capable of plotting the time history response of nodal displacements as well as the element

internal forces.

3.4 Finite Element Modeling Adopted for the Present Study

3.4.1 Basic Assumptions

The basic assumptions made in modeling of precast wall systems are as follows:

1. Wall panels are assumed to remain linear-elastic throughout the analysis. Inelastic action is assumed to be concentrated in the horizontal connections and the coupling beams.
2. Soil-structure interaction is not considered. Fully fixed conditions are assumed at structural base.
3. The floor slabs are infinitely rigid in their own planes and distribute the lateral forces on the structure between different walls in proportion to their stiffness. A study by Unemori (1978) on dynamic behaviour of crosswall building systems has shown that the rigid floor assumption is valid for buildings having more than 10 stories. For shorter buildings, the lateral distribution of wall forces is noticably different from that predicted under the rigid floor assumption.
4. The degradation in the coefficient of friction is ignored.
5. Shear-compression interaction across the horizontal connections is ignored.

3.4.2 Modeling of Wall Panels

In modeling of wall panels, it is assumed that the panels remain linear elastic during a major earthquake. The wall panels are idealized as four node rectangular plane stress elements having eight degrees of freedom (d.o.f.). The finite element matrices can be obtained in an explicit form, given by Gallager (1975). However, to make it more general, the well known formulation of isoparametric elements as discussed by Bathe and Wilson (1976), and Cook (1974) are used. Isoparametric elements are formulated using an intrinsic coordinate system ξ η which is defined by element geometry as shown in Figure 3-5 and not by element orientation in the global coordinate system. Having obtained the shape function and strain displacement matrices, the element stiffness can be obtained from the expression

$$[K] = \int_{vol} \int \int [B]^T [C] [B] \, dvol \qquad (3\text{-}4)$$

or

$$[K] = t \int_{-1}^{+1} \int_{-1}^{+1} [B]^T [C] [B] \det [J] \, d\xi \, d\eta \qquad (3\text{-}5)$$

where

$[B], [B]^T$ = strain displacement matrix and its transpose

$[C]$ = constitutive matrix

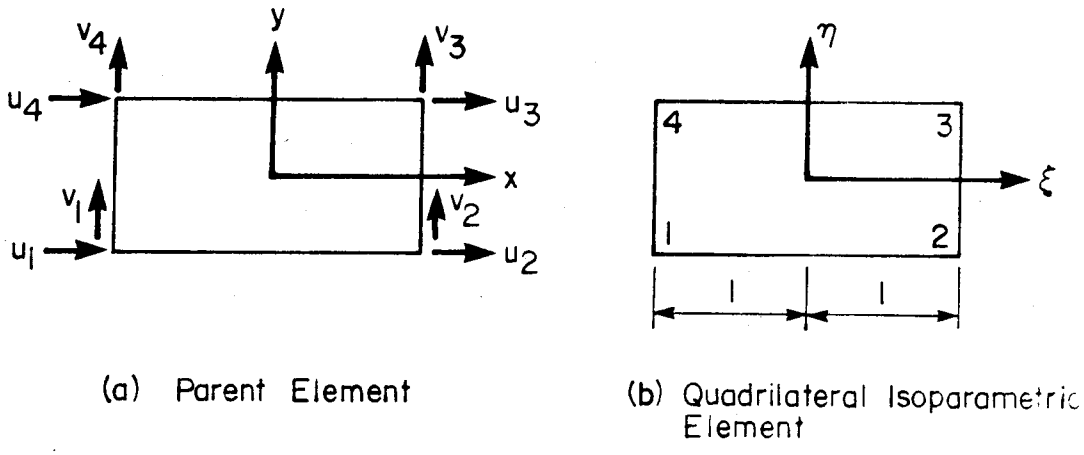

Figure 3-5 Four-Node Rectangular Plane Stress Element

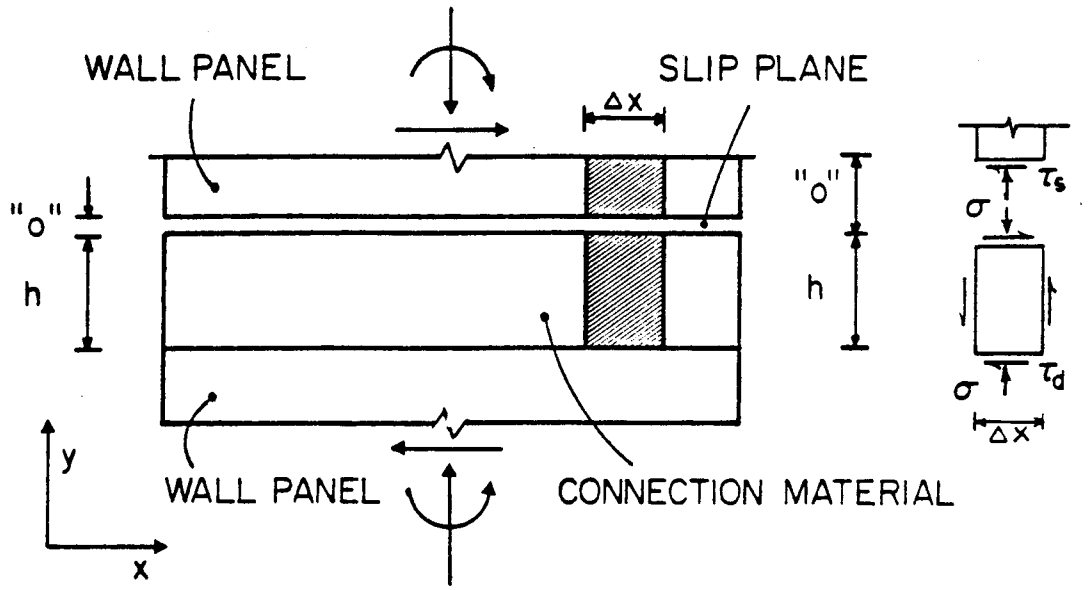

Figure 3-6 State of Stress Within the Connection Region (Llorente and Becker, 1981)

t = panel thickness

[J] = Jacobian matrix

The integration of the above expression was obtained approximately and numerically by Gauss Quadrature Procedure using two Gauss integration points for each element.

The constitutive matrices for plain concrete and reinforcing bars are as follow:

$$[C_c] = \frac{E_c}{1 - \nu^2} \begin{bmatrix} 1 & \nu & 0 \\ \nu & 1 & 0 \\ 0 & 0 & \frac{1-\nu}{2} \end{bmatrix} \tag{3-6}$$

$$[C_r] = E_s \begin{bmatrix} \rho_x & 0 & 0 \\ 0 & \rho_y & 0 \\ 0 & 0 & 0 \end{bmatrix} = nE_c \begin{bmatrix} \rho_x & 0 & 0 \\ 0 & \rho_y & 0 \\ 0 & 0 & 0 \end{bmatrix} \tag{3-7}$$

and the total constitutive relation for both concrete and steel are:

$$[C] = [C_c] + [C_r] = \frac{E_c}{1-\nu^2} \begin{bmatrix} 1+(1-\nu^2)n\rho_x & \nu & 0 \\ \nu & 1+(1-\nu^2)n\rho_y & 0 \\ 0 & & (\frac{1-\nu}{2}) \end{bmatrix} \tag{3-8}$$

where

E_c = elastic modulus of concrete

E_s = elastic modulus of steel

n = Poisson's ratio

ρ_x, ρ_y = reinforcement ratios in x and y directions, respectively

n = modular ratio, E_s/E_c

To obtain accurate results, it is necessary to divide each panel into several finite rectangular elements. This will increase the computational effort to solve a problem if the mesh size is small and/or if the structure is very tall or very wide. The computational effort can be decreased using static condensation or substructuring techniques. However, the program DRAIN-2D at the present time does not have this capability.

3.4.3 Modeling of Connections

The modeling procedure used for the present study for the connection regions is similar to the model used by Llorente and Becker (1981) for the inelastic analysis of precast concrete simple walls. In this approach, interface elements are used to model the horizontal connections which allows for gradual opening and closing of the connections. The shear behaviour of the connections is modeled using two shear elements; one element is used to model the deformation of the connection and a contact element is used to model the shear slip behaviour along the connection panel interface as shown in Figure 3-6. The deformed configuration of the connection region under shear deformation and shear slip are

shown in Figures 3-7(a) and (b) respectively.

3.4.3.1 Formulation of Element Matrices

A tyical connection element with eight degrees of freedom is shown in Figure 3-8. The displacement field is defined by interpolation function:

$$u = \sum_{i=1}^{n} \phi_i \, u_i \tag{3-9}$$

$$v = \sum_{i=1}^{n} \phi_i \, v_i \tag{3-10}$$

where

$$\phi_1 = \frac{1}{4} (1 - \xi) (1 - \eta) \tag{3-11}$$

$$\phi_2 = \frac{1}{4} (1 + \xi) (1 - \eta) \tag{3-12}$$

$$\phi_3 = \frac{1}{4} (1 + \xi)(1 + \eta) \tag{3-13}$$

$$\phi_4 = \frac{1}{4} (1 - \xi) (1 + \eta) \tag{3-14}$$

The axial strain is given by

$$\varepsilon = \frac{\partial v}{\partial y} \tag{3-15}$$

The shear strain consists of shear deformation and shear slip. The shear strain corresponding to shear deformation

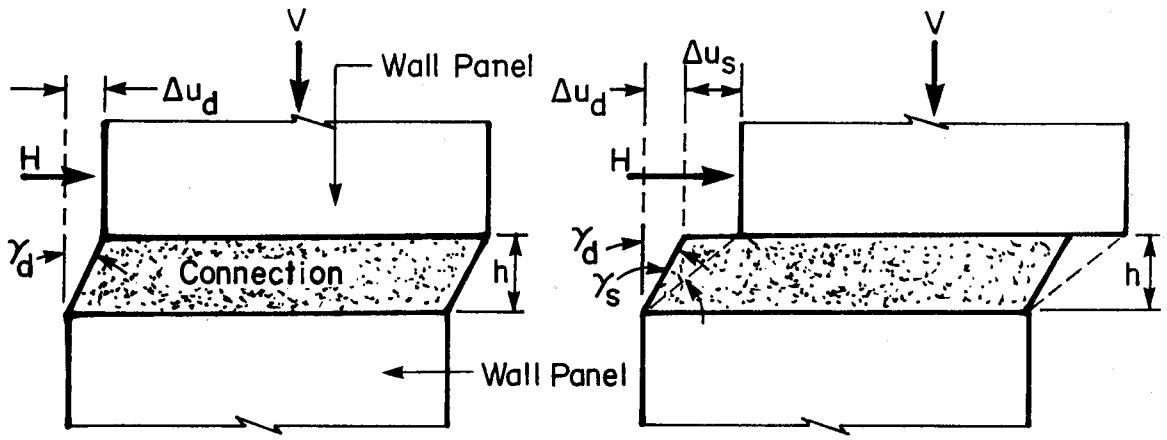

(a) Deformation (b) Deformation and Slip

Figure 3-7 Deformed Configuration of the Connection

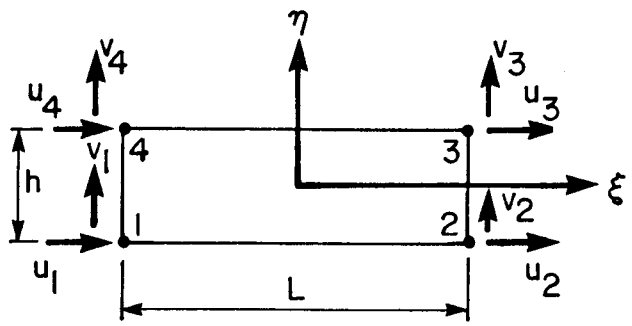

Figure 3-8 Typical Connection Element

is given by:

$$\gamma_d = \frac{\partial u_d}{\partial y} + \frac{\partial v}{\partial x} \tag{3-16}$$

Shear strain corresponding to shear slip is given by

$$\gamma_s = \frac{\Delta u_s}{h} \tag{3-17}$$

where

- u = increment in horizontal displacement field of the entire connection region
- v = increment in vertical displacement field of the entire connection region
- u_d = increment in horizontal displacement field within the finite region of the connection
- u_s = increment in horizontal displacement field along the slip plane
- h = connection height.

Therefore, the total shear strain is given by:

$$\gamma = \gamma_d + \gamma_s = \frac{\partial u_d}{\partial y} + \frac{\partial v}{\partial x} + \frac{\Delta u_s}{h} \tag{3-18}$$

or

$$\gamma = \frac{\tau_d}{G_d} + \frac{\tau_s}{G_s} = \tau \left(\frac{1}{G_d} + \frac{1}{G_s}\right) \tag{3-19}$$

$$\gamma = \tau / G_{eff}$$

$$G_{eff} = \frac{1}{(\frac{1}{G_d} + \frac{1}{G_s})} = \frac{G_s}{1 + \frac{G_s}{G_d}} = \frac{G_d}{1 + \frac{G_d}{G_s}} \qquad (3\text{-}20)$$

where

G_d = tangent shear modulus of the connection material

G_s = tangent shear modulus of the slip surface

It should be mentioned that shear stress is assumed to remain constant over the height of the connection, i.e. $\tau_s = \tau_d = \tau$.

The strain increment is given by

$$\{\varepsilon\} = \begin{Bmatrix} \varepsilon_y \\ \gamma_{xy} \end{Bmatrix} = [B]\{u\} \qquad (3\text{-}21)$$

where $$\{u\}^T = \{u_1 \; v_1 \; u_2 \; v_2 \; u_3 \; v_3 \; u_4 \; u_4\} \qquad (3\text{-}22)$$

and

$$[B] = \frac{1}{2h} \begin{bmatrix} 0 & -(1-\xi) & 0 & -(1+\xi) & 0 & (1+\xi) & 0 & (1-\xi) \\ -(1-\xi) & -\frac{h}{L} & -(1+\xi) & \frac{h}{L} & (1+\xi) & \frac{h}{L} & (1-\xi) & -\frac{h}{L} \end{bmatrix}$$

(3-22)

The element stiffness matrix can be obtained from the expression:

$$[K]_{8x8} = t \int_A [B]^T [C] [B] \, dA \qquad (3\text{-}24)$$

and the restoring nodal forces are given by:

$$\{R\} = t \int_A [B]^T \{S\} \, dA \qquad (3\text{-}25)$$

where

$[C] = \begin{bmatrix} E & 0 \\ 0 & G \end{bmatrix}$

E = axial tangent modulus per unit thickness of the connection

G = shear tangent modulus per unit thickness of the connection

$[B], [B]^T$ = matrix relating assumed displacement field parameters to nodal displacement and its transpose

t = connection thickness

L = connection length

$\{S\} = \begin{Bmatrix} \sigma_y \\ \tau_{xy} \end{Bmatrix}$

$\{R\}$ = vector of unbalanced forces

The element stiffness matrix can be obtained in an explicit form using Equation 3-24.

$$[K] = t\begin{bmatrix} 2\alpha_1 & \alpha_2 & \alpha_1 & -\alpha_2 & -\alpha_1 & -\alpha_2 & -2\alpha_1 & \alpha_2 \\ & 2\beta+\alpha_3 & \alpha_2 & \beta-\alpha_3 & -\alpha_2 & -\beta-\alpha_3 & -\alpha_2 & -2\beta+\alpha_3 \\ & & 2\alpha_1 & -\alpha_2 & -2\alpha_1 & -\alpha_2 & -\alpha_1 & \alpha_2 \\ & & & 2\beta+\alpha_3 & \alpha_2 & -2\beta+\alpha_3 & \alpha_2 & -\beta-\alpha_3 \\ & & & & 2\alpha_1 & \alpha_2 & \alpha_1 & -\alpha_2 \\ & & & & & 2\beta+\alpha_3 & \alpha_2 & \beta-\alpha_3 \\ & \text{symmetric} & & & & & 2\alpha_1 & -\alpha_2 \\ & & & & & & & 2\beta+\alpha_3 \end{bmatrix}$$

(3-26)

where

$$\alpha_1 = \frac{1}{6} G \frac{L}{h}$$

$$\alpha_2 = \frac{1}{4} G$$

$$\alpha_3 = \frac{1}{4} G \frac{h}{L}$$

$$\beta = \frac{1}{6} E \frac{L}{h}$$

The unbalanced forces can be obtained using equation 3-25 as follows.

$$\{R\}^T = \frac{1}{2} Lt \left\{-\tau \quad \left(-\sigma - \tau \frac{h}{L}\right) \quad -\tau \quad \left(-\sigma + \tau \frac{h}{L}\right) \right.$$
$$\left. \tau \quad \left(\sigma + \tau \frac{h}{L}\right) \quad \tau \quad \left(\sigma - \tau \frac{h}{L}\right)\right\} \qquad (3\text{-}27)$$

It was mentioned earlier that the computer program DRAIN-2D has the capability to eliminate the equilibrium unbalance and this is done using the above relationship.

3.4.3.2 Connection Models Incorporated into the Computer Program DRAIN-2D

3.4.3.2.1 Linear Elastic Model

In the linear elastic model, it is assumed that the material under both compressive and tensile normal stresses remain linear elastic throughout the analysis; shear stresses are also assumed to remain linear elastic as shown in Figure 3-9. The assumption of linear elastic behaviour in the design and modeling of the connections is of little significance. However, such assumptions can be reasonable for structures which have short periods in which inelastic energy dissipation is of little benefit. The linear elastic assumption is also valid for regions of low to moderate earthquakes where seismic forces are low compared with the forces the structure has been designed for considering other effects. To investigate the distribution of forces and the reduced force levels in the structure due to ductility and energy dissipation by the inelastic action of the connections, the linear elastic model can be useful as a comparison with inelastic models.

3.4.3.2.2 Zero-Tension Model

It was mentioned in the previous chapter that due to the effects of creep and shrinkage, horizontal connections are considered as precracked planes. For this reason, the material model under consideration is asumed to have specified strength and stiffness under compression and zero

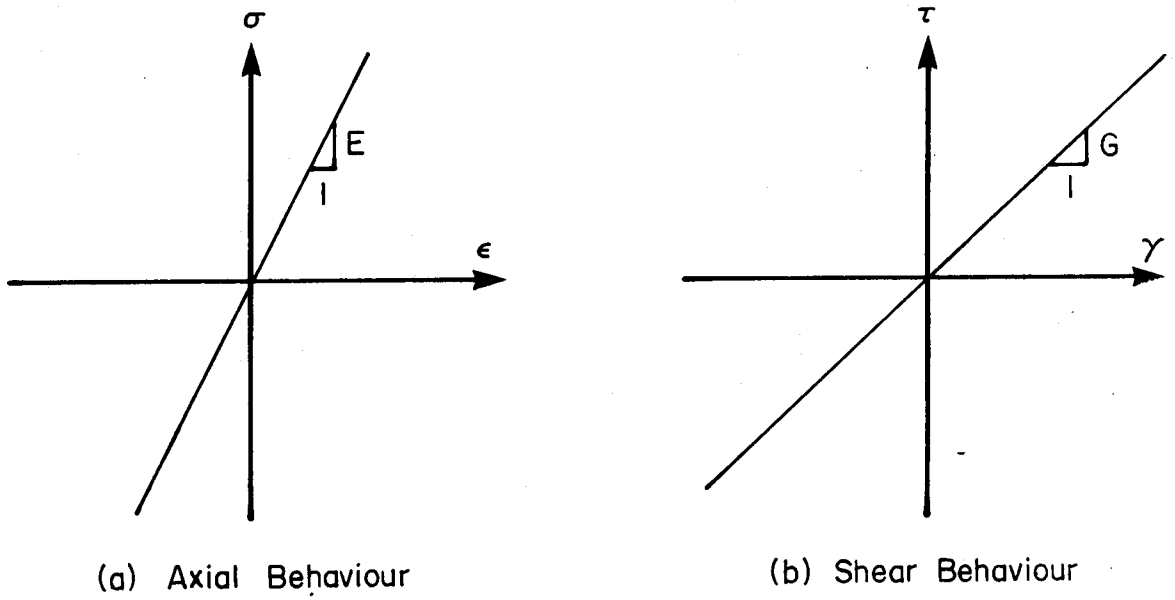

(a) Axial Behaviour (b) Shear Behaviour

Figure 3-9 Linear-Elastic Model

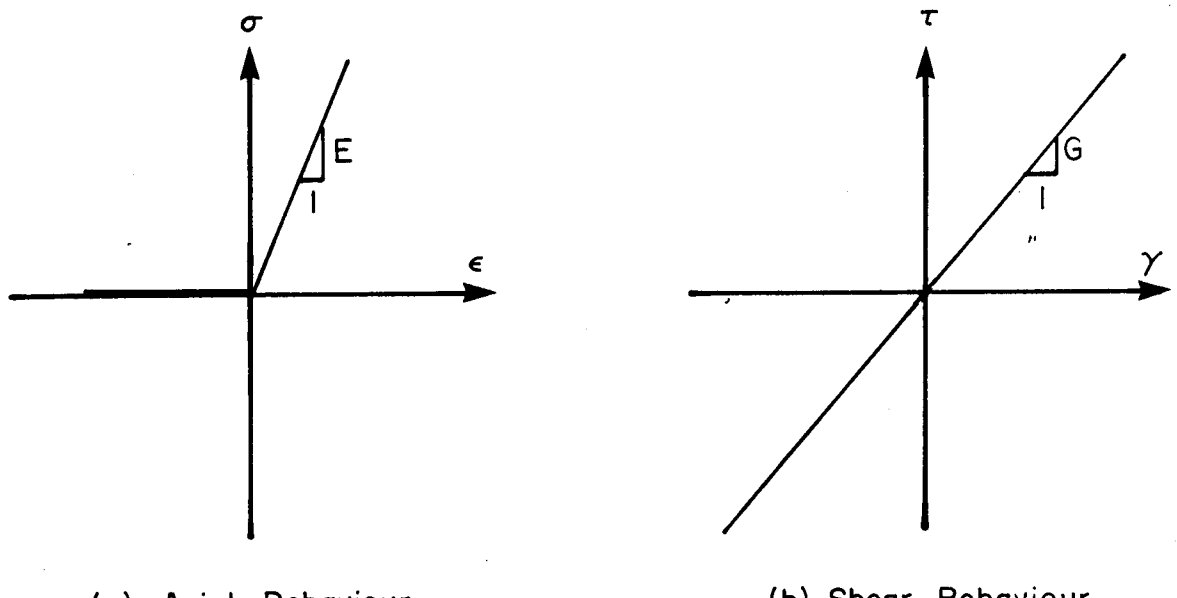

(a) Axial Behaviour (b) Shear Behaviour

Figure 3-10 Zero-Tension Model

strength and stiffness under tension as shown in Figure 3-10. The shear behaviour is assumed linear-elastic throughout the analysis. However, when the connection material is under tension, the shear strength and stiffness is assumed to be zero.

3.4.3.2.3 Concrete Stress-Strain Model

The concrete stress-strain model described in the previous chapter and developed by Darwin and Pecknold (1974) is adopted here with some modifications. The concrete model selected is shown in Figure 3-11. Modifications which are made to the model include the initial compression loading part which is divided into two linear segments with slopes of E_1 and E_2. This is done mainly to reduce the amount of computation effort and reduce the cost of analysis. Figure 3-11(a) shows the parameters involved in obtaining the initial bilinear part of the diagram. The tangent modulus and the compressive stress at any given time t is as follows:

For $0 < {}^{t}\varepsilon \leq 0.425\ \varepsilon_c$

$$ {}^{t}\sigma = E_o\ {}^{t}\varepsilon \left(\frac{1}{\frac{1}{2} + \frac{E_o}{E_s}} + \frac{1}{2}\right) \qquad (3\text{-}28) $$

$$ E_1 = E_o \left(\frac{1}{\frac{1}{2} + \frac{E_o}{E_s}} + \frac{1}{2}\right) \qquad (3\text{-}29) $$

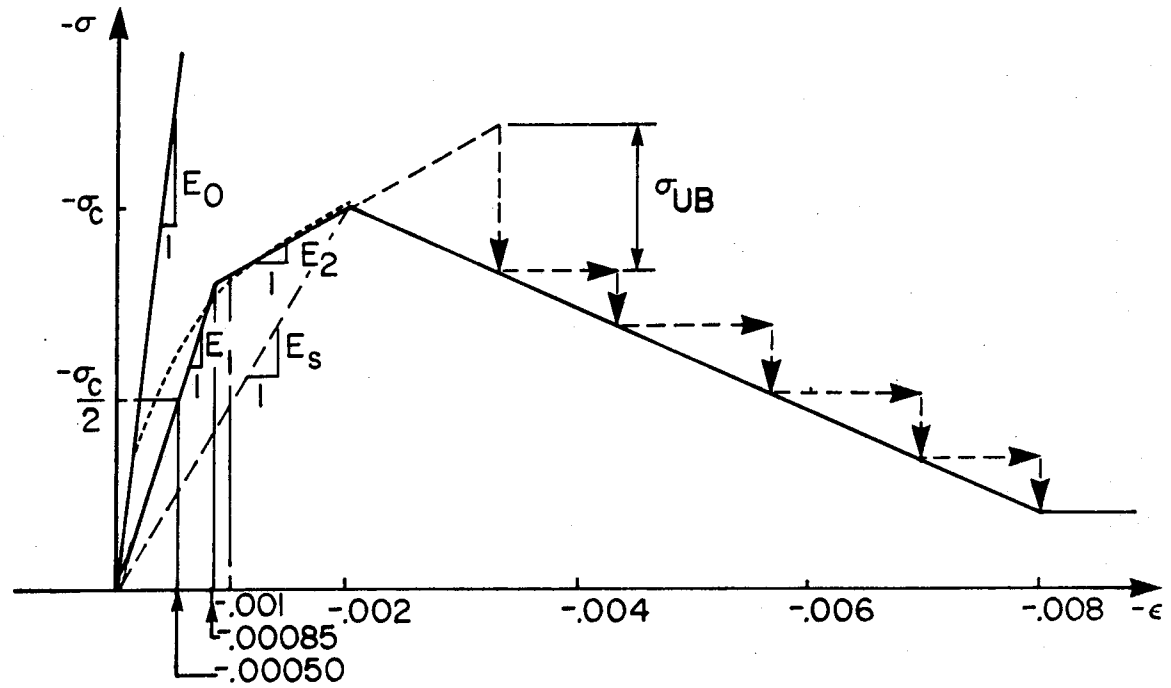

(a) Zero Stiffness on Descending Branch

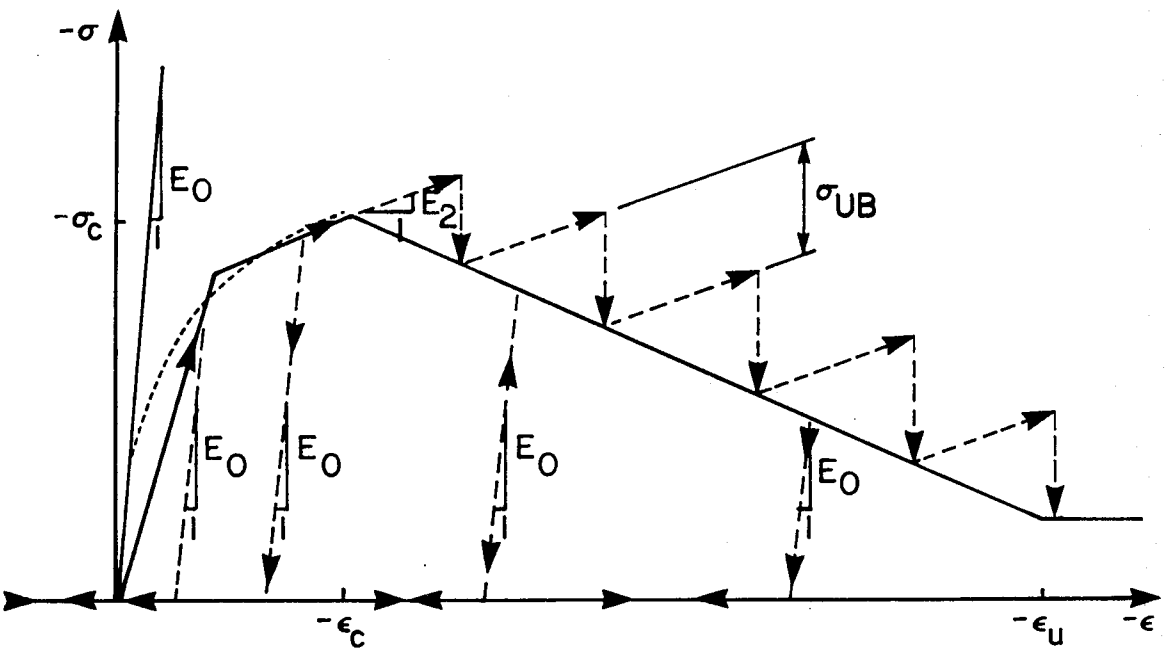

(b) Finite Stiffness on Descending Branch

Figure 3-11 Concrete Stress-Strain Model

For $0.425\varepsilon_c < {}^t\varepsilon \leq \varepsilon_c$

$$t_\sigma = \sigma_c - \frac{\sigma_c - 0.425\varepsilon_c E_1}{0.575}\left(1 - \frac{t_\varepsilon}{\varepsilon_c}\right) \qquad (3\text{-}30)$$

$$E_2 = \frac{\sigma_c - 0.425\varepsilon_c E_1}{0.575\varepsilon_c} \qquad (3\text{-}31)$$

where

t_σ = stress at time t

t_ε = compressive strain at time t

ε_c = compressive strain at maximum stress level

E_o = initial tangent modulus

E_s = secant modulus, σ_c/ε_c

The unloading and reloading model chosen for this study is shown in Figure 3-11(b). Unloading is assumed to take place with a slope equal to initial slope E_o until the material undergoes tension in which the concrete stiffness is lost completely. Reloading is assumed to take place on the same path as the unloading. This is a simple approximation which avoids additional computational effort.

The tangent modulus of the descending part of the stress-strain diagram is negative and this may cause numerical problems. To avoid this, the following technique is used. When the compressive strain exceed the maximum compressive strain, ε_c, at a particular time step, yielding is assumed to have occurred. The tangent modulus is assumed to be zero for the next time step. In this case, an

unloading of σ_{UB} occurs which is the unbalanced stress as shown in Figure 3-11(a). The unbalanced stress is redistributed in the next time step. The above procedure is repeated until concrete reaches its ultimate strain ε_u and then crushing of concrete occurs. An alternative option is also available to avoid numerical problems as shown in Figure 3-11(b). In this case, when the concrete compressive strain exceeds ε_c, the tangent stiffness modulus is assumed to follow the slope E_2, and the unbalanced stresses are calculated at every time step.

3.4.3.2.4 Steel Stress-Strain Model

A simple bilinear model is used for steel reinforcement in this study. The model is elasto-perfectly plastic and does not consider strain hardening as shown in Figure 3-12. In this model, the amount of steel is spread over the element area. The initial slope is equal to ρE_s where ρ is area of steel bars divided by the gross area of concrete and E_s is the elastic modulus of steel. When the maximum strain in steel bars exceed the yield strain, the slope is zero and the maximum stress in steel is equivalant to ρf_y where f_y is the yield stress in steel.

It should be noted that the existing truss model in the computer program DRAIN-2D can also be used to represent the reinforcing bars. However, the above model is much simpler to use since three variables of ρ, E_s and f_y represent the input parameters.

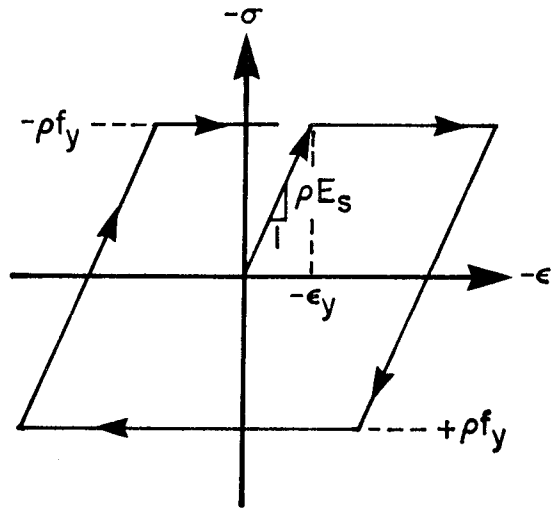

Figure 3-12 Steel Stress-Strain Model

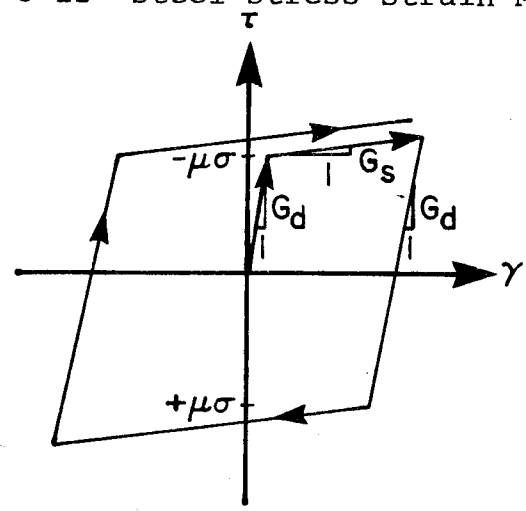

(a) Constant Normal Stresses

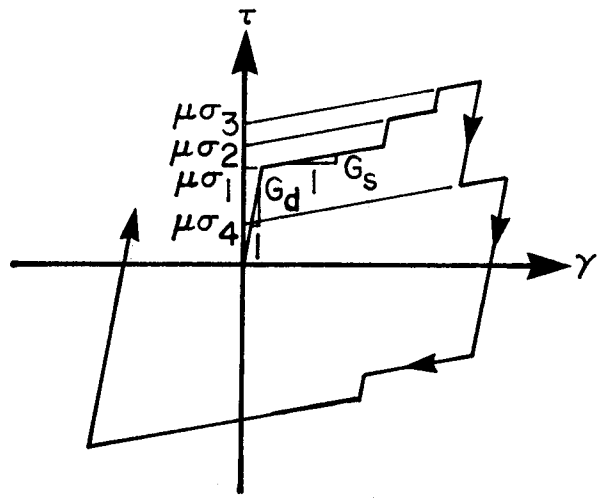

(b) Vary Normal Stresses

Figure 3-13 Shear-Slip Model

3.4.3.2.5 Post-tensioning Steel Model

The existing truss model in the computer program DRAIN-2D is used to model the post-tensioning bars. The post-tensioning bars are assumed to be ungrouted and extend their full length from the foundation up to the roof level with no intermediate connection to the wall. It is also assumed that these bars do not reach the yield level, therefore post-tensioning bars are modeled with linear elastic properties.

3.4.3.2.6 Shear-Slip Model

The results of the experimental studies described in the previous chapter show that if a horizontal connection has no reinforcing or it has very little reinforcing, the shear transfer is by Coulomb friction. These tests show that for constant normal compressive stresses, the hysteresis loops for shear-slip relationship is of elasto-plastic type.

Figure 3-13 shows the shear slip model selected for the present study. Figure 3-13(a) shows the behaviour for the case when normal stresses remain constant throughout the analysis. The model is essentially composed of two components, elastic component and plastic component. The elastic part is associated with shear deformation of the connection with a slope of G_d. The plastic part is associated with slip along the connection panel interface.

It is assumed that when shear stresses reach $\mu\sigma$, where μ is the coefficient of friction and σ is the normal compressive stress, slip will occur. It is assumed that the value of coefficient of friction remains constant throughout the analysis. The degradation of the coefficient of friction is not considered here. Unloading is assumed to take place parallel to the initial slope until shear stresses reach $\mu\sigma$ in the reverse direction in which slip will begin.

For any step in the step by step analysis, the amount of shear deformation or shear slip and the accumulated slip, if any is calculated.

Up to now, there are no test results available on the shear behaviour of the connections with varying normal stresses. However, due to the effects of overturning and the vertical component of acceleration, normal stresses do not remain constant during an earthquake. Also for situations when gap opening occurs, normal stresses drop to zero at the gap since concrete has zero strength under tension and shear resistance is lost. When normal stresses vary throughout the analysis, the shear slip behavour is assumed to be similar to Figure 3-13(b). The amount of slip and deformations are also calculated at every time step in the analysis. When normal stresses vary from one step in the analysis ($\mu\sigma_1$ at time t) to the next step ($\mu\sigma_2$ at time t + Δt) and shear stresses are greater than both $\mu\sigma_1$ and $\mu\sigma_2$, it is assumed that the shear stiffness is unchanged. However, there is an equilibrium unbalance equal to ($\mu\sigma_1$ -

$\mu\sigma_2$) at the end of the time step. The unbalanced force is calculated and applied in the following step to restore equilibrium.

3.4.3.2.7 Shear-Friction Model

The behaviour of horizontal connections containing mild reinforcing bars was discussed in the previous chapter. Test results show that these connections exhibit shear-friction type behaviour with pinched hysteresis loops for each cycle. Different test results show different types of behaviour in terms of the shape of the hysteresis loops. After each cycle of loading, the shape of the hysteresis loops also changes. For this reason, it is very difficult to select a model which represents the actual behaviour of the connections.

The shear-friction model selected for the present study under constant normal stresses is shown in Figure 3-14(a). It is assumed that the contribution of reinforcing bars is minor until the level of shear stresses reach $\mu\sigma$. Up to the level of $\mu\sigma$, the deformation of the connections is governed by shear modulus of concrete. When shear stresses exceed the value $\mu\sigma$, reinforcing bars provide some resistance against slip and the shear stiffness is governed by G_s. The value of G_s obtained from the test results and discussed in the previous chapter is about 10% of G_d.

Unloading is assumed to take place parallel to the initial slope until shear stresses reach $\mu\sigma$ in the reverse

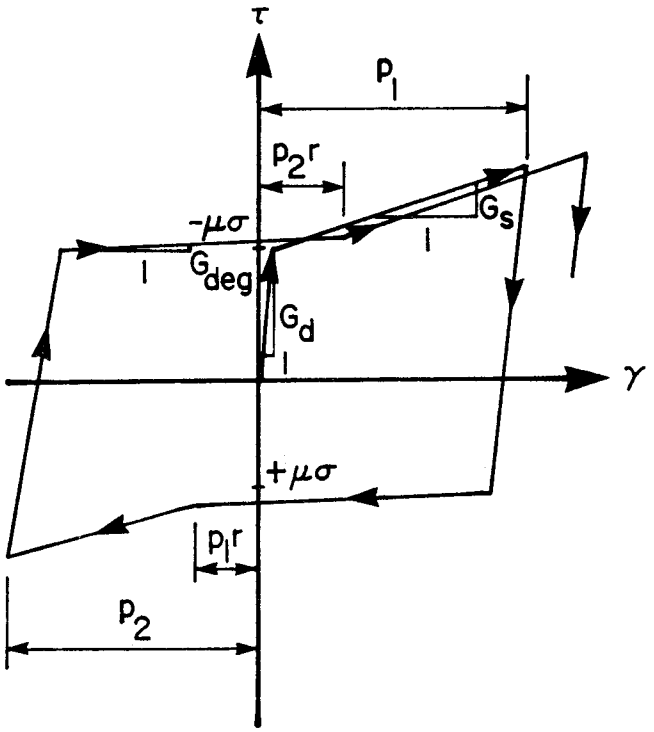

(a) Constant Normal Stresses

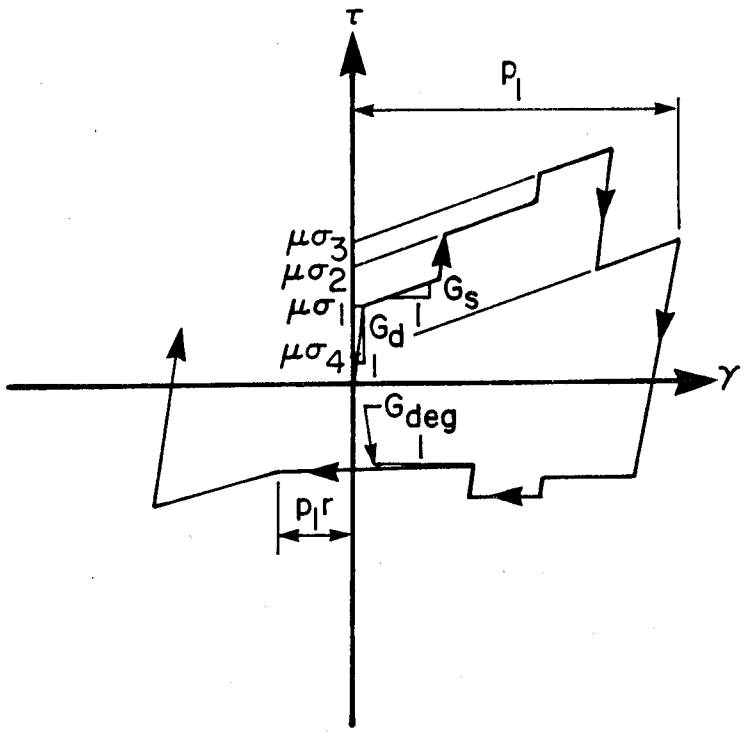

(b) Varying Normal Stresses

Figure 3-14 Shear-Friction Model

direction. In this situation, reinforcement provides no clamping action and the shear resistance of the connection is reduced considerably. At some point along the hysteresis loop, the reinforcement develops tension force and provides clamping action. The point at which tension develops in the reinforcement is controlled by a parameter r. The value for this parameter obtained from test results is about 0.15. The rest of the hysteresis loops are modeled in the same fashion as described above. The effect of the amount of reinforcement is not considered in the selected model. Test results by Harris and Abboud (1981) have shown that the amount of reinforcement across the shear plane of the connections does not have a significant effect on the response.

The behaviour of the connections under varying normal stresses is assumed to be similar to Figure 3-14(b). When gap opening occurs, normal stresses drop to zero and shear resistance is mainly controlled by reinforcing bars.

3.4.4 Coupling Beam Models

It was mentioned in the previous chapter that the behaviour of coupling beams is dependent on the depth/span ratio. For this reason, different modeling techniques have been used for slender coupling beams and deep coupling beams. Beams with small depth/span ratio are classified as slender beams and those with large depth/span ratio are classified as deep beams. The modeling techniques for the

two cases are discussed separately.

3.4.4.1 Slender Coupling Beams

The slender coupling beams have been idealized as beam elements. The existing reinforced concrete beam element in the computer program DRAIN-2D is used to model the slender coupling beams. The model exhibits degrading flexural stiffness properties when beams are subjected to cyclic loads. It is assumed that yielding takes place only in concentrated plastic hinges at element ends. Strain hardening and degrading flexural stiffness are approximated assuming that the element consists of a linear elastic beam element with nonlinear rotational springs at each end as shown in Figure 3-15(a). The element deformations are considered as the sum of the elastic component and the plastic component as shown in Figure 3-15(b) and (c) respectively. The moment rotation relationship for each hinge is the extended version of Takeda's model (1970) which has the behaviour as shown in Figure 3-16. The extension to the Takeda model includes a reduction in unloading stiffness and a variable reloading stiffness.

In the inelastic range, chord rotations are calculated as the sum of the elastic beam rotation and plastic hinge rotations as follows:

$$\Delta\theta_A = \Delta\theta_A^e + \Delta\theta_A^P \qquad (3\text{-}32)$$

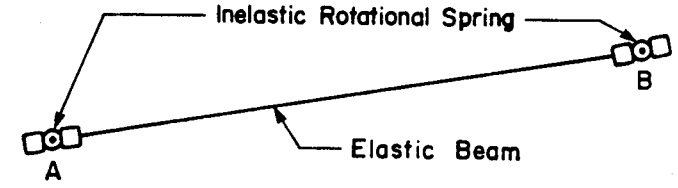

(a) Element Idealization

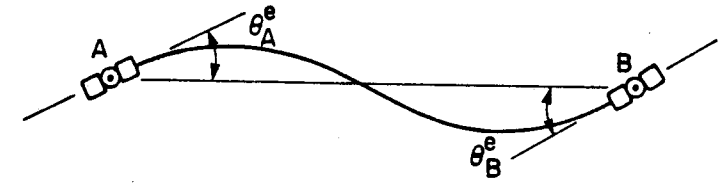

(b) Elastic

(c) Plastic

Figure 3-15 Beam Element Idealization and Deformation

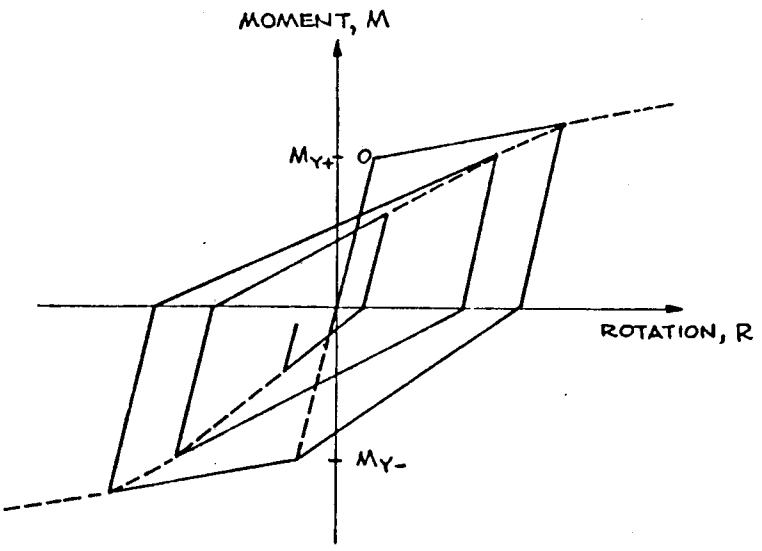

Figure 3-16 Hinge Moment-Rotation Relationship for Takeda Model

$$\Delta\theta_B = \Delta\theta_B^e + \Delta\theta_B^P \qquad (3\text{-}33)$$

where

$\Delta\theta_A^e, \Delta\theta_B^e$ = increments of chord rotations due to bending of elastic beam at ends A and B respectively

$\Delta\theta_A^P, \Delta\theta_B^P$ = increments of hinge rotations at ends A and B respectively.

In order to prevent rotation of hinges in the elastic range, the spring stiffness should be assigned a very large initial value so that each hinge is essentially rigid up to yield. The computer program DRAIN-2D is also capable of providing automatic generation of the spring properties. The incremental moment-rotation relationship for elastic and plastic components are given by:

$$\begin{Bmatrix} \Delta\theta_A^e \\ \Delta\theta_B^e \end{Bmatrix} = \begin{bmatrix} \frac{L}{3EI} & -\frac{L}{6EI} \\ -\frac{L}{6EI} & \frac{L}{3EI} \end{bmatrix} \begin{Bmatrix} \Delta M_A \\ \Delta M_B \end{Bmatrix} \qquad (3\text{-}34)$$

$$\begin{Bmatrix} \Delta\theta_A^P \\ \Delta\theta_B^P \end{Bmatrix} = \begin{bmatrix} \frac{1}{\alpha_A K_s} & 0 \\ 0 & \frac{1}{\alpha_B K_s} \end{bmatrix} \begin{Bmatrix} \Delta M_A \\ \Delta M_B \end{Bmatrix} \qquad (3\text{-}35)$$

where

L = length of beam

EI = flexural stiffness of beam

α_A, α_B = ratios of the slope of the post-yield branch to the slope of the bilinear moment-rotation curves at member ends A and B respectively

K_s = spring stiffness

It should be mentioned that the ratio of the second slope to the first slope of the moment-chord rotation relationship of a member in the computer program DRAIN-2D is computed on the basis of linearly varying moment distribution with zero magnitude at one end. However the coupling beams have a linear moment distribution with double curvature and for this reason the value of α should be modified and the corrected value of α must be specified as an input into the program. The procedure to calculate the correct value of α has been described in detail by Saatcioglu (1981).

3.4.4.2 Plane-Stress to Line Element Compatibility

The reinforced concrete beam element in the computer program DRAIN-2D has been used for the analysis of slender coupling beams in the coupled wall structures. Incompatibility arises due to the existance of the rotational d.o.f. of beam elements when they are connected to the corresponding rectangular plane-stress wall panel elements as shown in Figure 3-17.

There are several ways in which this problem can be solved. Some of these are explained by Cook (1974), Macleod

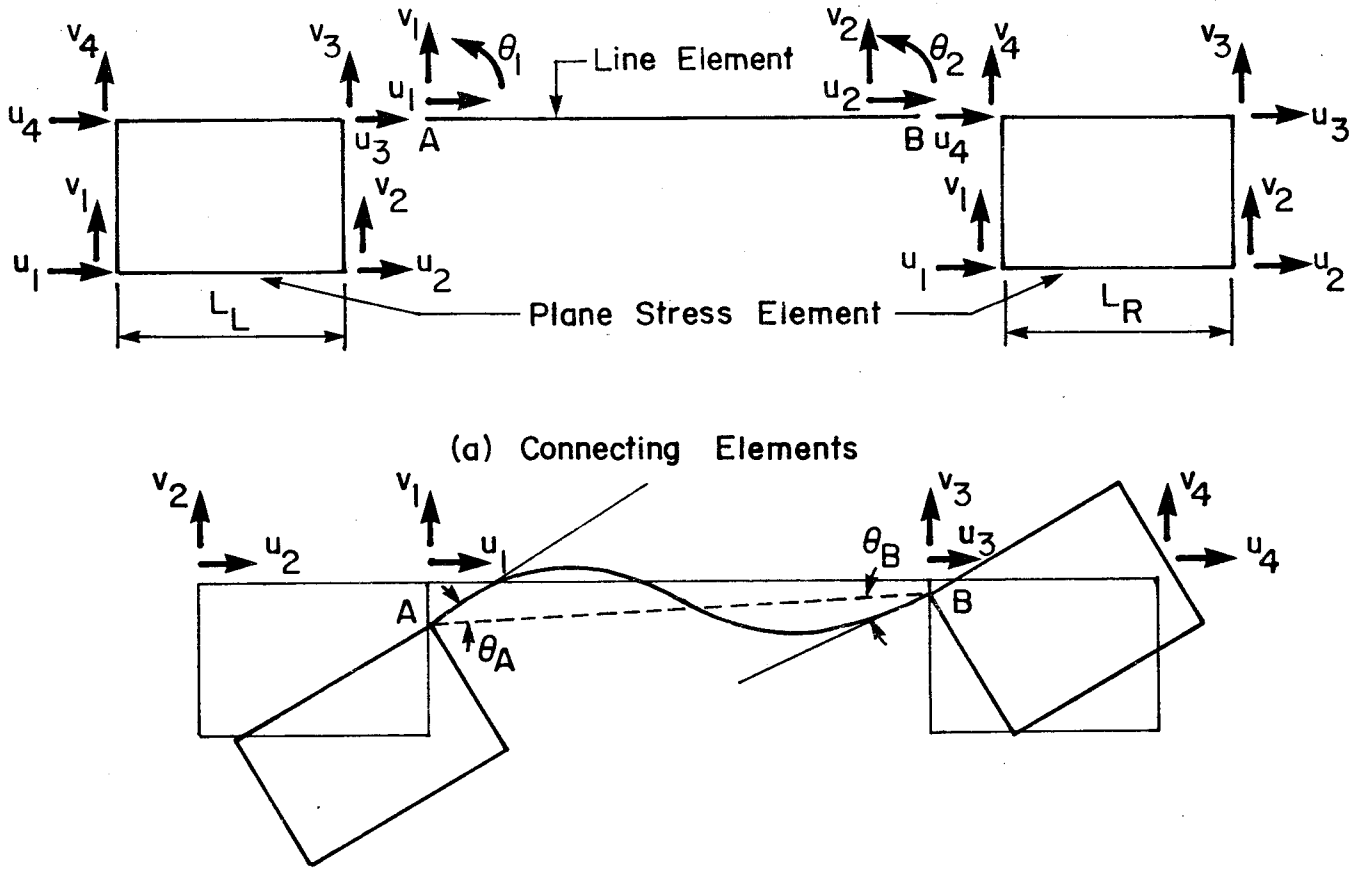

Figure 3-17 Compatibility of Plane-Stress Element with Line Element

(1969), and Spira and Sokal (1970). For the present study, the connecting beam elements are idealized as line elements. The rotational d.o.f. of coupling beams are replaced by the translational d.o.f. of the corresponding plane-stress elements as shown in Figure 3-17(b) using the following relationships:

$$\theta_A = \frac{v_1 - v_2}{L_L} \tag{3-36}$$

$$\theta_B = \frac{v_4 - v_3}{L_R} \tag{3-37}$$

where

θ_A, θ_B = rotations at ends A and B respectively

$v_1, \ldots v_4$ = translational d.o.f.

L_L, L_R = length of plane-stress elements for left panels and right panels respectively

From the above relationships, the following transformation matrix can be constructed

$$[T] = \begin{array}{c} \begin{matrix} u_1 & v_1 & v_2 & u_3 & v_3 & v_4 \end{matrix} \\ \begin{bmatrix} 1.0 & 0 & 0 & 0 & 0 & 0 \\ 0 & 1.0 & 0 & 0 & 0 & 0 \\ 0 & \frac{1}{L_L} & \frac{-1}{L_L} & 0 & 0 & 0 \\ 0 & 0 & 0 & 1 & 0 & 0 \\ 0 & 0 & 0 & 0 & 1 & 0 \\ 0 & 0 & 0 & 0 & \frac{-1}{L_R} & \frac{1}{L_R} \end{bmatrix} \end{array} \tag{3-28}$$

The element stiffness matrix for the compatible line element can be obtained from the expression:

$$[K]_T = \underset{(6x6)}{[T]^T} \quad \underset{(6x6)}{[K]} \quad \underset{(6x6)}{[T]} \tag{3-29}$$

where

$[T]^T$ = transpose of [T]

[K] = element stiffness matrix corresponding to translational and rotational d.o.f.

$[K]_T$ = element stiffness matrix corresponding to translational d.o.f.

To obtain the element deformation and forces, the translational d.o.f. are transformed into rotational d.o.f. at the element level.

When yielding begins in the coupling beams and hinges start to rotate, the above formulations are still applicable. However, the stiffness matrix $[K]_T$ is different. Figure 3-18 shows the way in which the compatibility of plane-stress element and line element is maintained after the formation of plastic hinges at beam ends.

If there is a change in stiffness at any time step, equilibrium unbalance arises and the unbalanced nodal forces must be calculated and applied in the next time step. To maintain full compatibility between the line-elements and

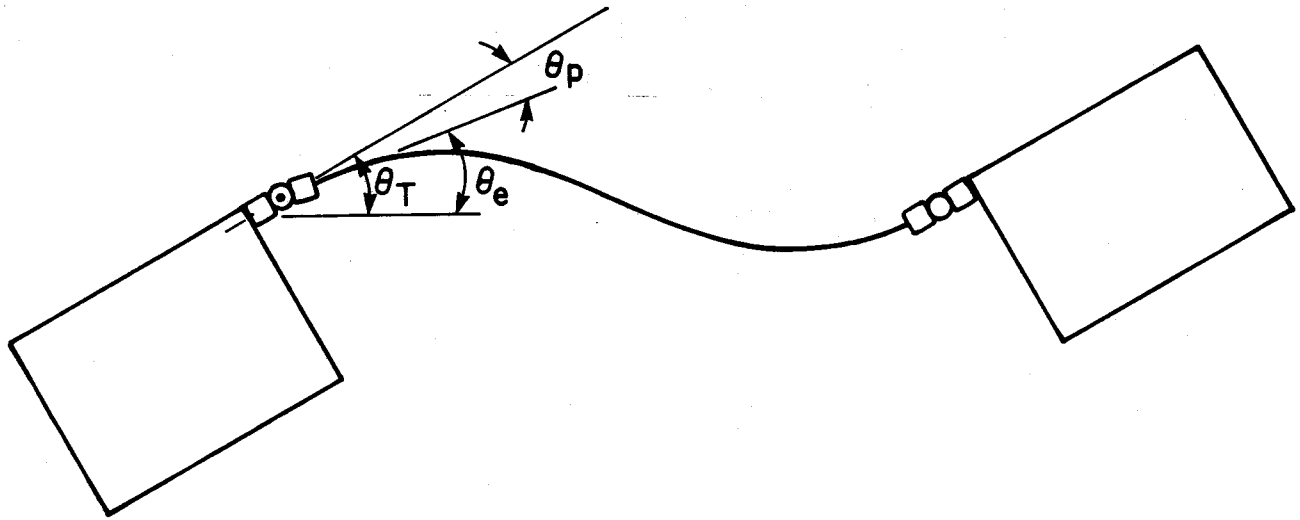

Figure 3-18 Compatibility of Plane-Stress Element with Line Element After the Formation of Plastic Hinges

plane-stress elements, the unbalanced moments in the coupling beams must be expressed in terms of the translational forces. The unbalanced forces at ends of the coupling beams are calculated as follows.

$$F_{uB}(v_1) = \frac{(M_{uB})_A}{L_L} \tag{3-30}$$

$$F_{uB}(v_2) = \frac{(M_{uB})_A}{L_L} \tag{3-31}$$

$$F_{uB}(v_3) = -\frac{(M_{uB})_B}{L_R} \tag{3-32}$$

$$F_{uB}(v_4) = -\frac{(M_{uB})_B}{L_R} \tag{3-33}$$

where

$F_{uB}(v_1)$ ..., $F_{uB}(v_4)$ = unbalanced forces corresponding to translational d.o.f. v_1 ... v_4

$(M_{uB})_A$, $(M_{uB})_B$ = unbalanced moments at ends A and B respectively

3.4.4.3 Deep Coupling Beams

It was shown in the previous chapter that deep coupling beams with diagonal reinforcing bars improve the strength and the ductility of coupling beams considerably. Experimental results have shown that when these beams are subjected to cyclic loading, the steel bars make an insignificant contribution initially and the diagonal

compression is mainly carried by concrete. When the diagonal reinforcing bars enter the yield range, large cracks form and remain open until the load is reversed. As the load is reversed, the bars are subjected to large compressive stresses and perhaps yield before the previously formed cracks close. As suggested by Paulay (1977), it is reasonable to assume that at the development of yield strength, the cracked concrete along the diagonal bars do not make a significant contribution to resist the shear. The behaviour of the beams is then governed by the diagonal bars which are expected to be equally effective in both tension and compression. The load versus deflection relationship shown in Figure 2-15(b) in the previous chapter indicates that the behaviour of such beams is of elasto-plastic type and is similar to the behaviour of steel members.

The design of diagonally reinforced coupling beams can be based on the statically determinate model shown in Figure 3-19. At the development of yield strength,

$$T_u = C_u = A_s f_y \tag{3-34}$$

$$V_u = 2\ T_u \sin \alpha \tag{3-35}$$

$$A_s = \frac{V_u}{2\ f_y \sin \alpha} \tag{3-36}$$

The resisting moment at the supports of the beam:

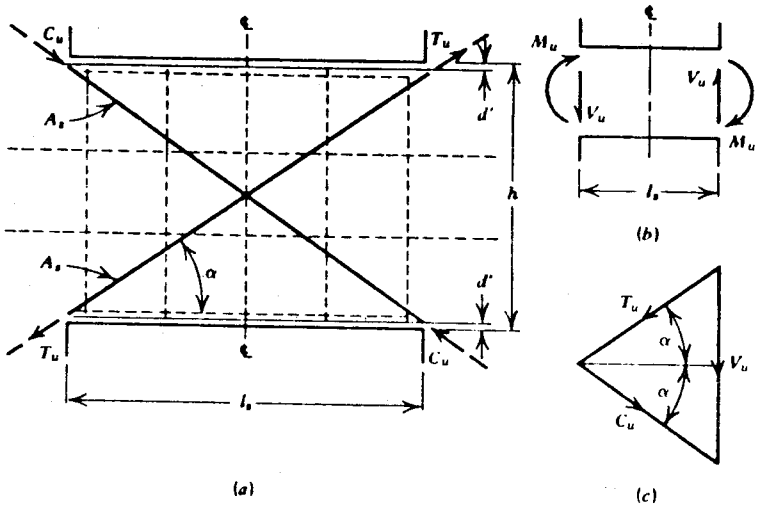

Figure 3-19 Behaviour of Deep Coupling Beams (Paulay, 1977)

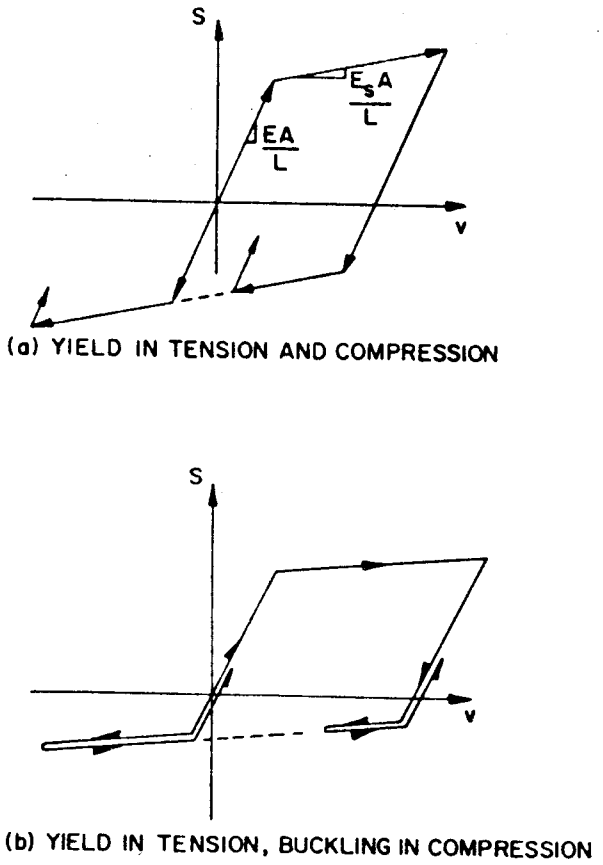

Figure 3-20 Truss Model Used for Deep Beams

$$M_u = V_u \frac{\ell}{2} = T_u \ell \sin \alpha \qquad (3\text{-}37)$$

or

$$M_u = (h - 2d') T_u \cos \alpha \qquad (3\text{-}38)$$

where

T_u, C_u = maximum tensile and compressive forces respectively

A_s = cross sectional area of diagonal reinforcement

f_y = yield stress of diagonal reinforcement

V_u = maximum shear force

α = angle between diagonal bar and horizontal

ℓ = total length of the coupling beam

d' = distance from extreme concrete fibre to centroid of reinforcement at beam ends.

3.4.4.4 Truss Model

The hysteresis loops described earlier show that deep coupling beams have the characteristics of a steel member. The inelastic truss element in the computer program DRAIN-2D is used to model deep coupling beams. The truss element considers two alternative modes of inelastic behaviour either by yielding in both tension and compression as shown in Figure 3-20(a) or by yielding in tension and elastic buckling in compression as shown in Figure 3-20(b).

In this study, it is assumed that the inelastic behavior of coupling beams is governed by yielding of

reinforcing bars in tension or compression. More details on the characteristics of elements are explained in the program manual of DRAIN-2D.

3.5 Summary

The finite element technique used for modeling precast wall systems was discussed in this chapter. Several hysteretic models which are incorporated into the computer program DRAIN-2D were discussed. The models considered include wall panels, the material behaviour of the connections, vertical continuity across the connections, and coupling beams. The effect of these models on the response of precast walls will be examined in the following chapter.

4. EFFECT OF MODELING FEATURES ON STATIC AND DYNAMIC RESPONSE

4.1 General

The purpose of this chapter is to investigate the effect of individual models on the response of precast wall systems. The accuracy of modeling techniques and their computer implementation are verified. The effects of some of the parameters that may affect the response of precast walls are also studied. Some of the analytical results described in this chapter are compared with reported analytical or experimental test results.

4.2 Static and Dynamic Response of Wall Panels

As discussed in Chapter 3, wall panels are modeled using linear elastic plane stress elements. Static analyis was carried out on structures consisting of plane stress elements. Several structural models with a minimum of four nodes, up to a maximum of 66 nodes with varying mesh sizes were analysed and compared with results obtained using SAPIV, a general purpose computer program for linear elastic static and dynamic analysis developed by Bathe et al. (1973). The results showed good agreement. The response of two of the selected models with their properties are shown in Figure 4-1.

Dynamic analyses were carried out on structural models similar to those described above. Figure 4-2 shows a

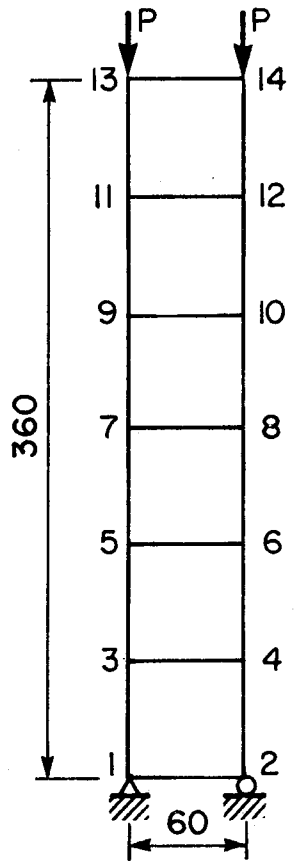

Properties:

P = 60
E = 30,000
ν = 0.3
thickness = 1.0

Vertical Displacement at Node 14

DRAIN-2D	SAPIV
-0.012	-0.012

(a) 14 Nodes

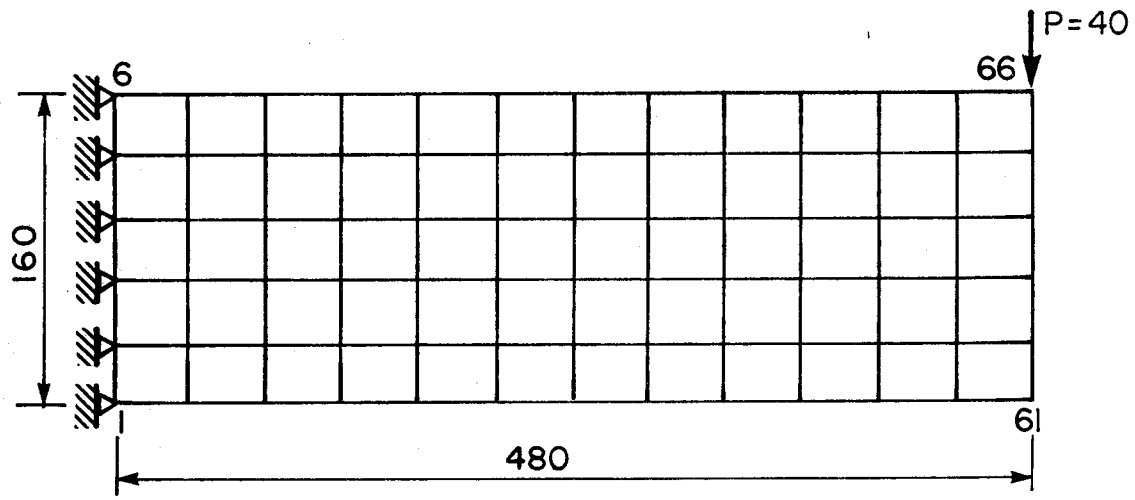

Vertical Displacement at Node 66

DRAIN-2D	SAPIV
-0.153	-0.158

(b) 66 Nodes

Figure 4-1 Description of Structural Model Selected for Static Analysis

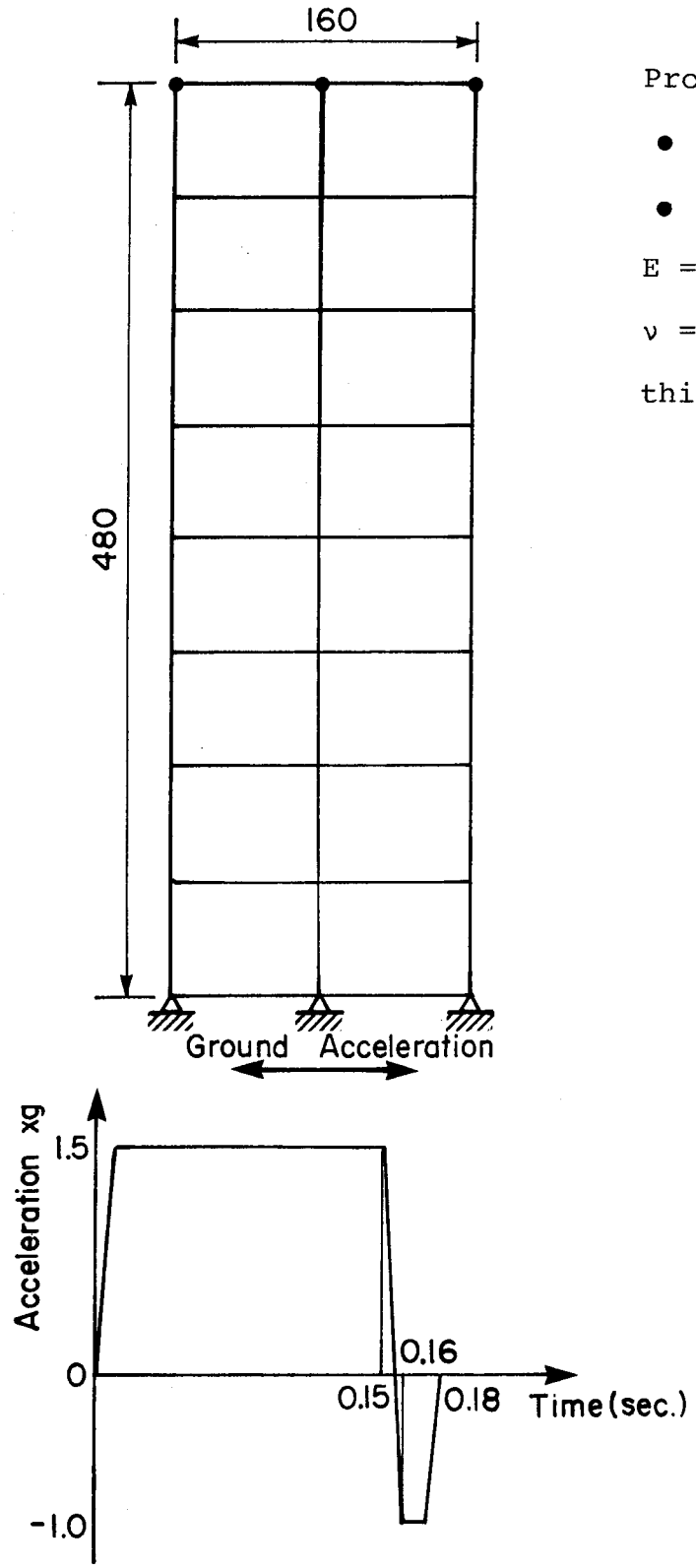

Figure 4-2 Description of Structural Model Selected for Linear-Elastic Dynamic Analysis

selected model and its properties used for linear elastic dynamic analysis. A trapezoidal acceleration pulse was applied at the base of the structure. Loads and masses were applied at roof level as shown in the same figure. Similar analysis was also carried out using the computer program SAPIV. The displacement time history response at roof level is plotted and shown in Figure 4-3. The results show good agreement in terms of peak displacements. However, the period of vibrations are slightly out of phase which can be attributed to the different step-by-step integration procedure used by the two programs.

4.3 Linear Elastic Response of Horizontal Connections

A 15-story building model was chosen to study the response of walls with horizontal connections in the linear elastic range. The structure which has a horizontal connection at its base only was analysed by Llorente and Becker (1981) in their study of the response of simple walls. Details and the properties of the wall panels and the connection are shown in Figure 4-4. The entire mass of the wall as well as dead loads are concentrated at roof level. A triangular pulse of 0.2 seconds duration with a peak acceleration of 23% of gravity was applied at the base of the wall. The structure was analysed using the computer programs SAPIV and DRAIN-2D. The time history response at roof level is plotted and shown in Figure 4-5(a). The results show good agreement.

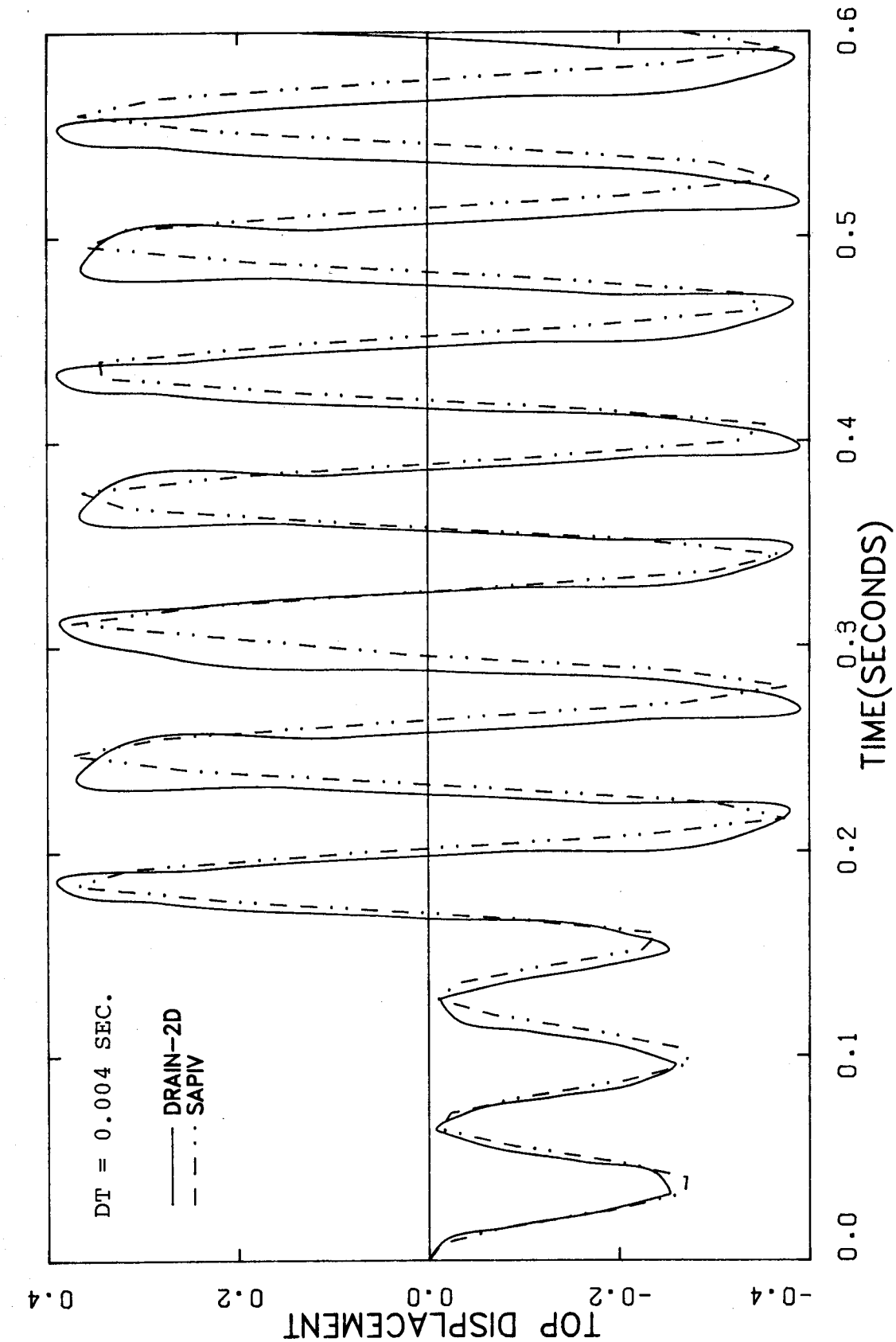

Figure 4-3 Linear-Elastic Time History Response

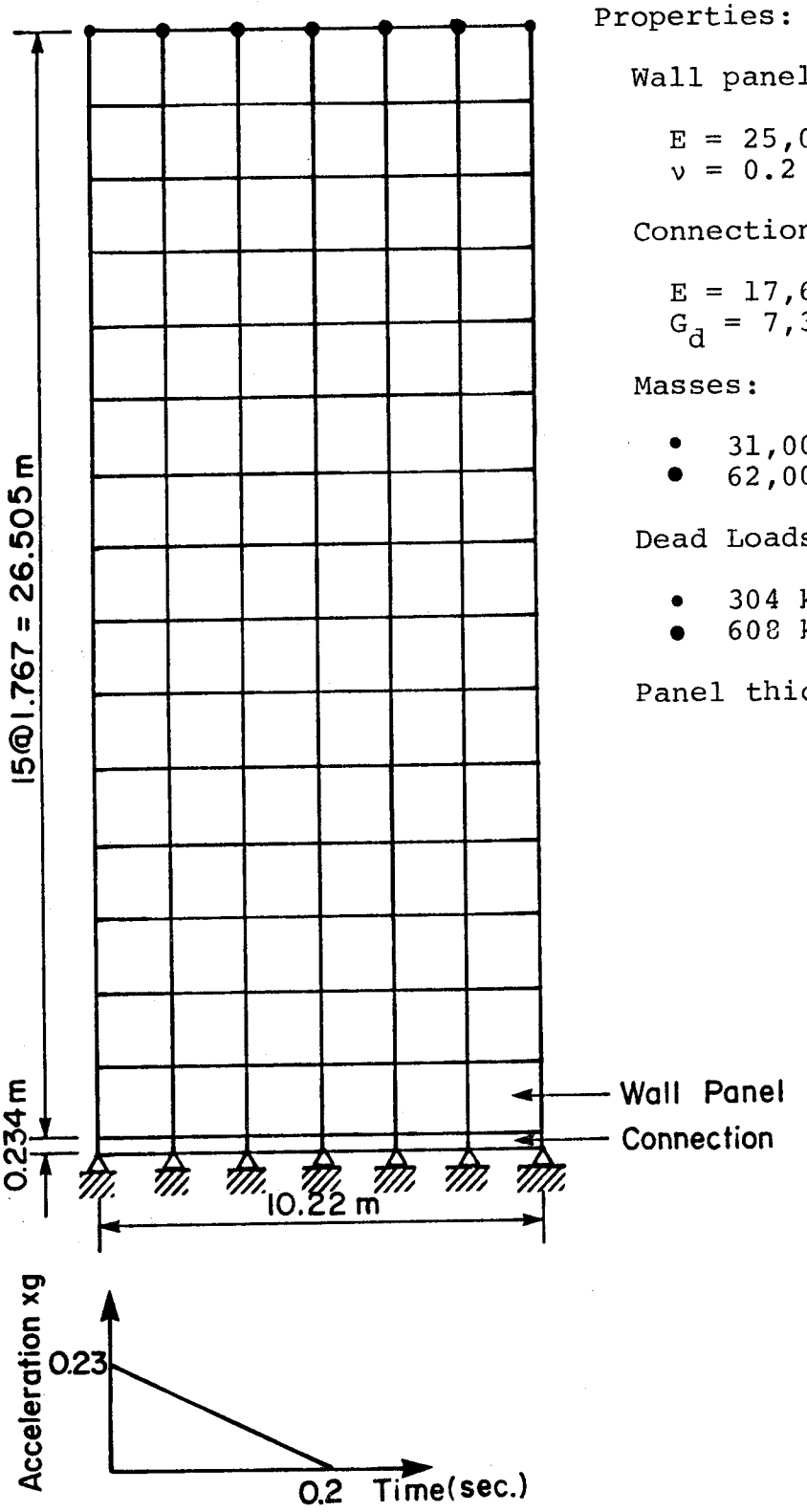

Properties:

Wall panel:

E = 25,000 MPa
ν = 0.2

Connection:

E = 17,600 MPa
G_d = 7,330 MPa

Masses:

- 31,000 kg
- 62,000 kg

Dead Loads:

- 304 kN
- 608 kN

Panel thickness = 200 mm

Figure 4-4 Description of 15-Story Building Model Used for Dynamic Analysis

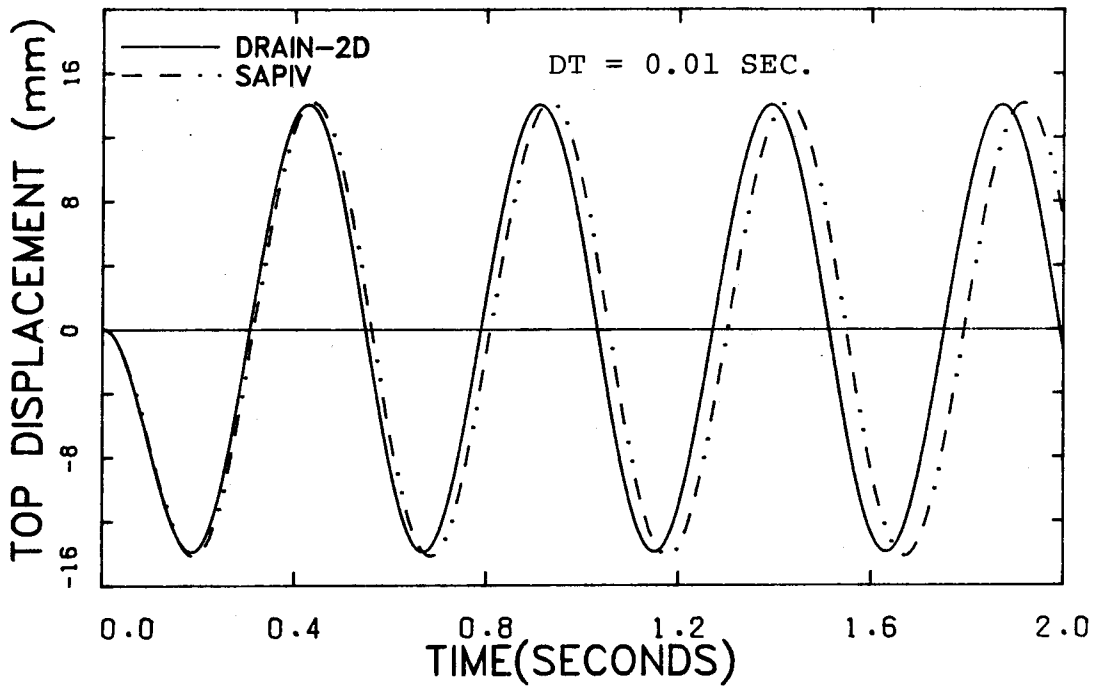

(a)

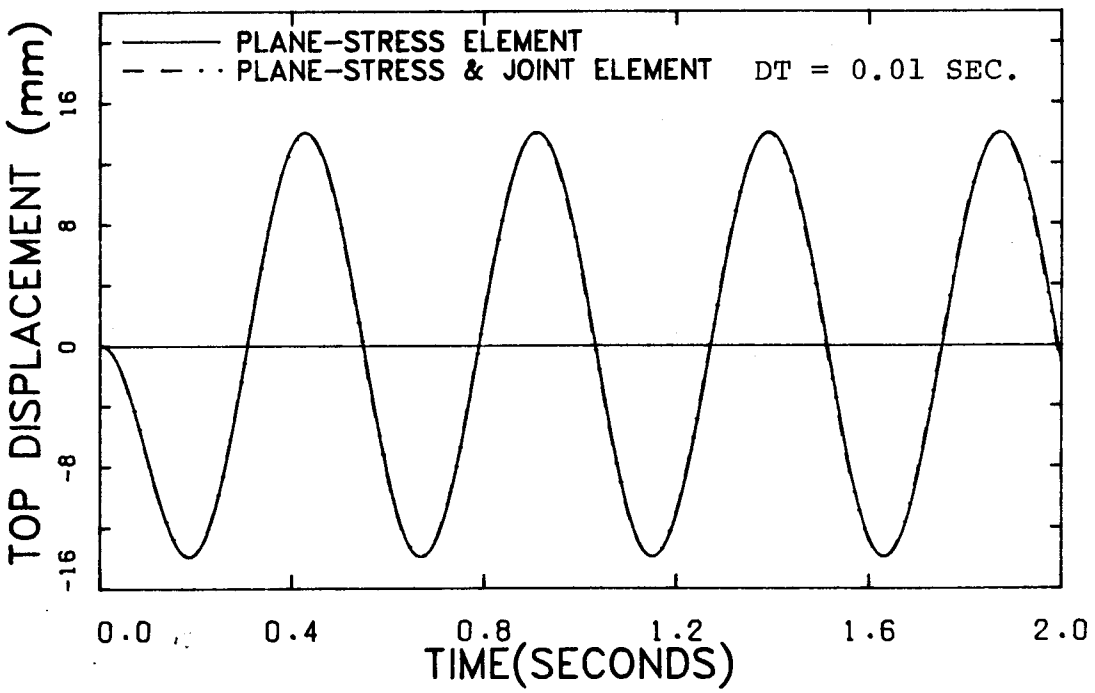

(b)

Figure 4-5 Linear-Elastic Time History Response of 15-Story Building Model

The structure was reanalysed with the connection elements chosen to be of the same type as wall panel elements. The displacement time history response shown in Figure 4-5(b) shows excellent agreement.

4.4 Inelastic Response of Horizontal Connections

4.4.1 Static Response Due to Overturning

It was mentioned in the previous chapter that due to the effects of creep and shrinkage, horizontal connections are recognized as precracked planes. For this reason, the connection material under compression is assumed to have finite strength and stiffness, while under tension the connection is assumed to have zero strength and stiffness.

Overturning response is associated with continuing opening and closing of horizontal connections in which plane sections after opening no longer remain plane. The 15 story building model described in the previous section was used to investigate the overturning response of the horizontal connection. It was assumed that opening occurs only at the ground floor connection. This assumption was made to isolate gap opening to one level and thus simplify the interpretation of results.

The computer program DRAIN-2D does not allow yielding in the structure under static conditions. For this reason, the static response due to overturning was carried out by step-by-step load increment as follows. The wall was subjected to a point load at the top which was increased by

a small amount during each increment until tensile stresses developed in the first element in the horizontal connection. Zero stiffness was assigned to the first element and the load was increased until tension developed in the second element. Zero stiffness was assigned to the second element and similar procedure to those described above was repeated. The point load at roof level was increased up to a maximum of 580 kN. Using the above procedure, the load versus deflection curve was constructed. These results are compared with those obtained by Llorente and Becker (1981) as shown in Figure 4-6. The results show good agreement.

Previous analyses carried out by Schricker and Powell (1980) and Llorente and Becker (1981) on the response of simple walls have shown that overturning response reduces the force levels in the structure compared to the corresponding elastic response. However, the lateral deflection of the wall associated with overturning may be lower or higher than its elastic response. This will depend on the rigid body displacement caused by overturning and the relative contribution between wall panel deformation associated with lower moments.

4.4.2 Dynamic Response Due to Overturning

4.4.2.1 Effect of Zero-Tension Model and Reinforcing on Overturning Response

The 15 story building model described in Section 4.3

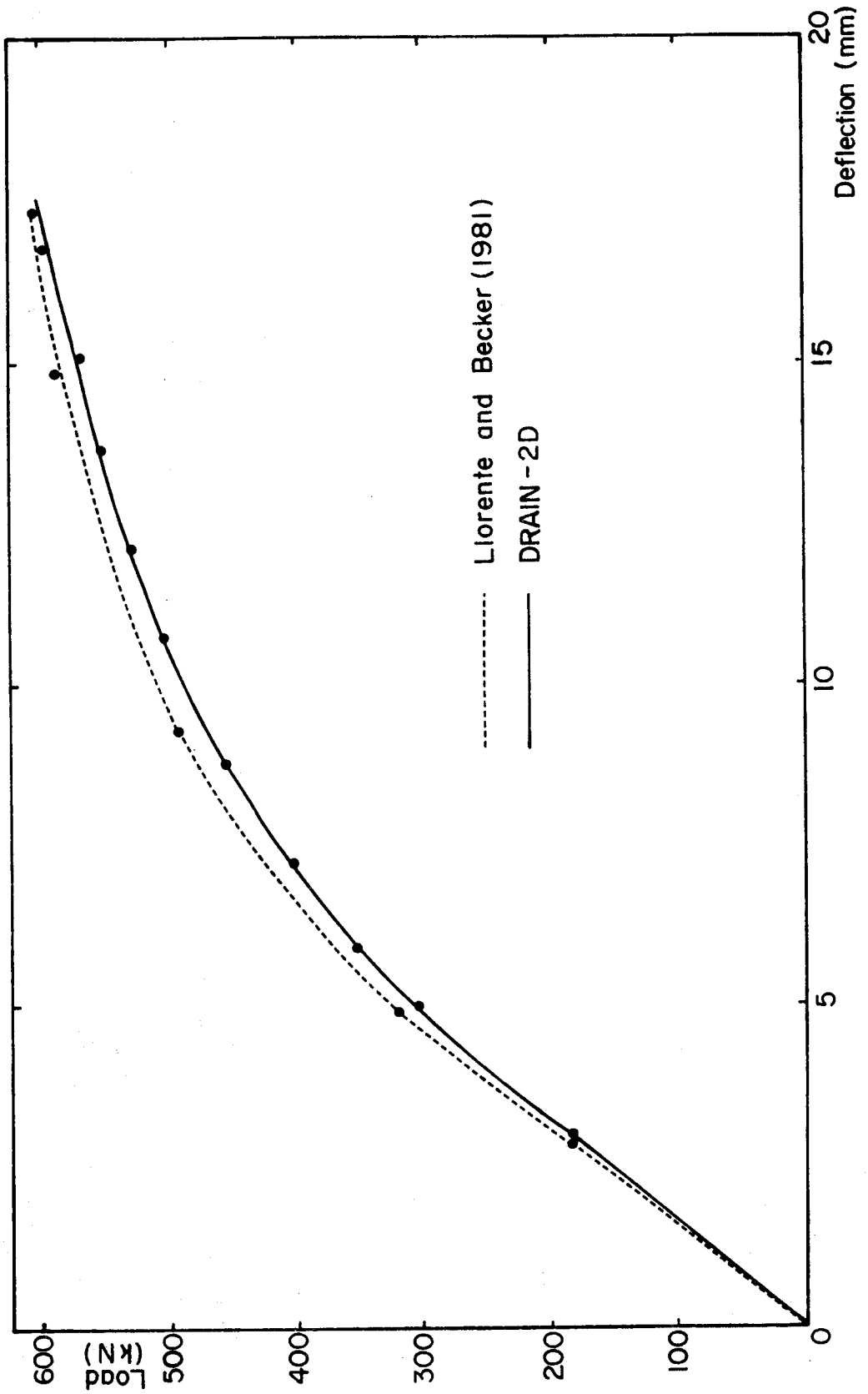

Figure 4-6 Static Response of 15-Story Building Model

was used to study the dynamic response due to overturning. The wall was subjected to a triangular pulse of two seconds duration and a peak ground acceleration of 23% of gravity. Three different types of material models were considered for the connections; linear elastic model, zero-tension material model and zero-tension material model with mild-reinforcing bars for vertical continuity. The reinforcing bars were assumed to have elasto-plastic stress-strain curve as discussed in the previous chapter. The properties of the reinforcing bars are as follows.

E_s = 204000 MPa

F_y = 297 MPa

ρ = 0.15%

The displacement time history response at roof level for the three cases mentioned above are plotted and shown in Figure 4.7(a). These results show an elongation in periods in the inelastic cases compared to the elastic case. The elongation in period which is associated with softening in the connections is higher for the case with no reinforcing bar for vertical continuity than the other cases.

The displacement-time history response discussed above was compared with those obtained by Llorente and Becker (1981) as shown in Figure 4-7(b). These results indicate similar trend in their behaviour, however, there are small differences in peak displacements and the periods of vibration. The differences are attributed mainly to the different step-by-step integration schemes. The computer

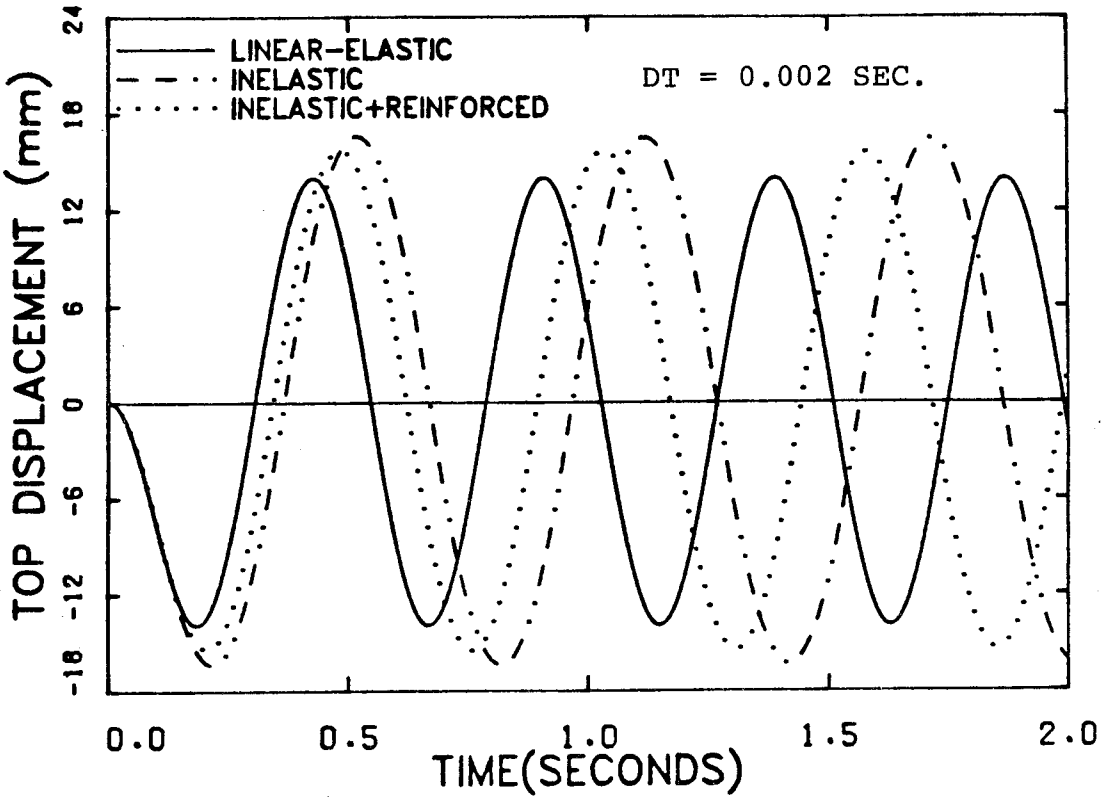

(a)

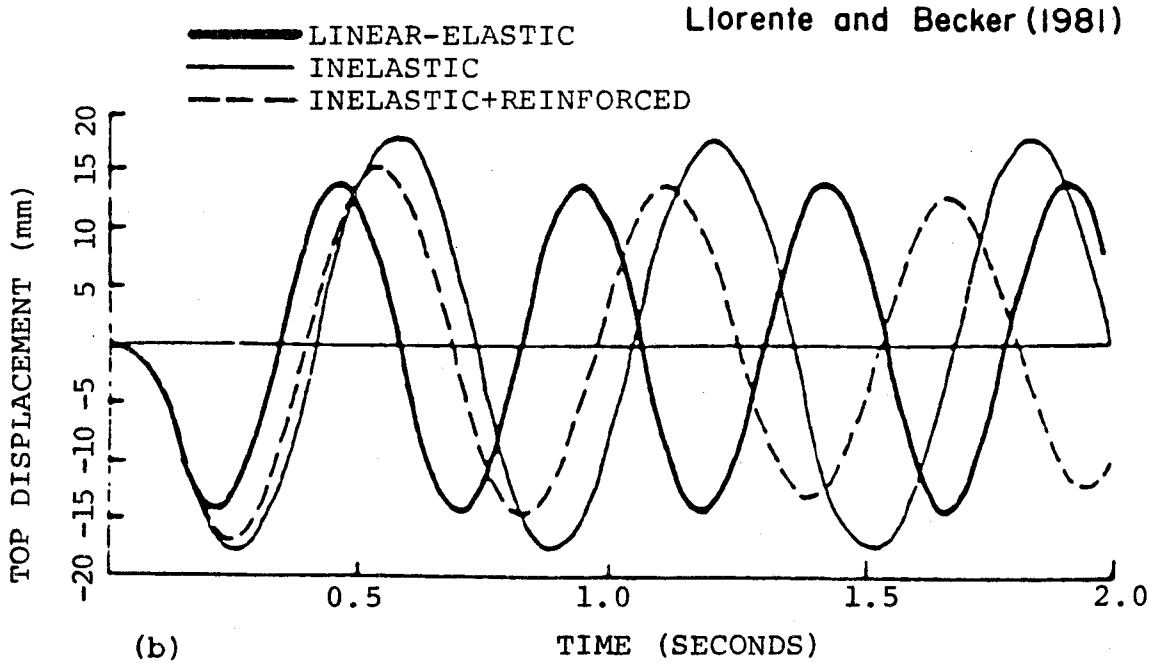

(b)

Figure 4-7 Time History of 15-Story Building Model due to Overturning

program DRAIN-2D uses the constant average acceleration method while Llorente and Becker use the central difference method for step-by-step integration.

The overturning response of the walls was further investigated using a 5 story building model shown in Figure 4-8. The properties and dimensions of wall panels and the connection are shown in the same figure. A triangular pulse with peak acceleration of 3.5 times gravity was applied at the base of the structure. Two cases were considered for the connections: a zero-tension material model with no vertical continuity and a zero-tension material model with mild reinforcing bars for vertical continuity. The displacement-time history responses are plotted and shown in Figure 4-9(a). These results indicate that the addition of a small amount of reinforcement equal to 0.25% of the gross cross-sectional area of the wall can significantly affect the response.

4.4.2.2 Effect of Multi-linear Concrete Model on Response

The 5 story building model described in the previous section and shown in Figure 4-8 was used to study the effect of the multi-linear concrete model on response of the structure. As mentioned in the previous section, a high level of acceleration was applied at the base of the structure; this was done mainly to increase the maximum strain in the connection beyond the concrete capacity and examine the response of the structure when the concrete is

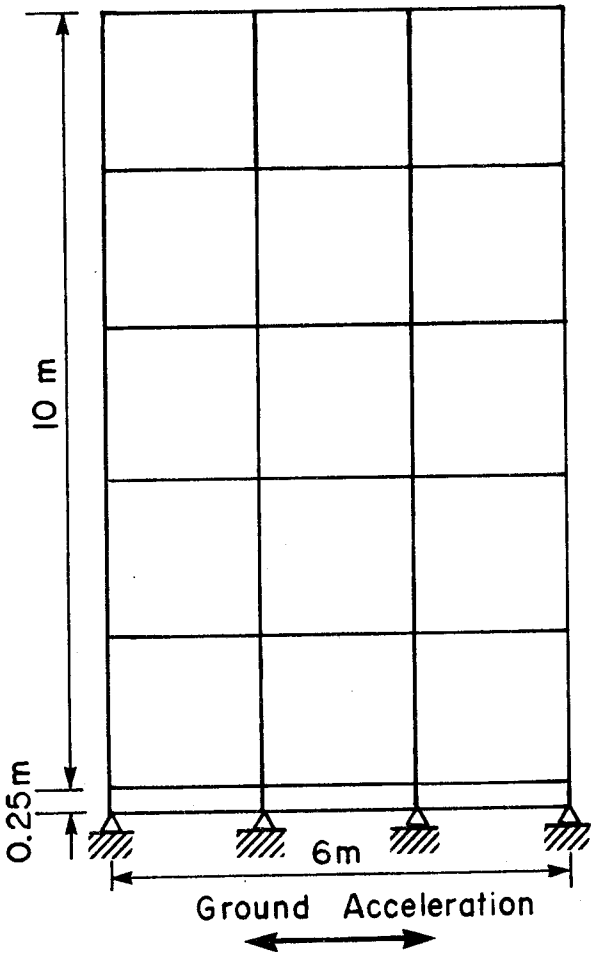

Properties:

Wall panel:

$E = 25{,}000$ MPa
$\nu = 0.2$

Connection:

$E = 13{,}000$ MPa
$G = 7000$ MPa
$f'_c = 15$ MPa
$\nu = 0.0$

Steel bars:

$E_s = 200{,}000$ MPa
$f_y = 300$ MPa
$\rho = 0.25\%$

Loads:

Roof = 480 kN
Floor = 720 kN

Masses:

Roof = 48930 kg
Floor = 73394 kg

Panel thickness = 200 mm

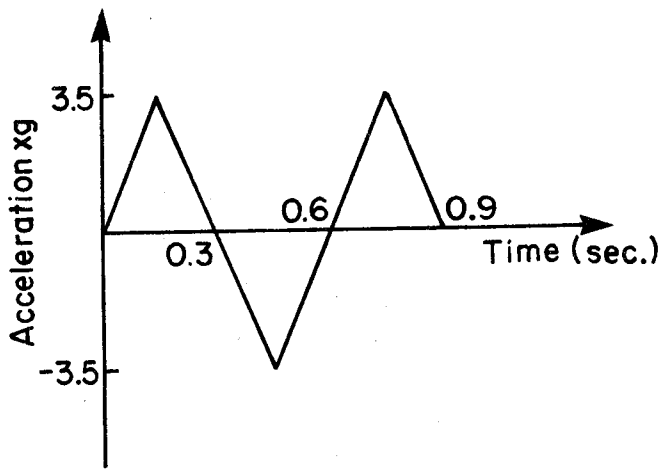

Figure 4-8 Description of 5-Story Building Model Studied for Overturning

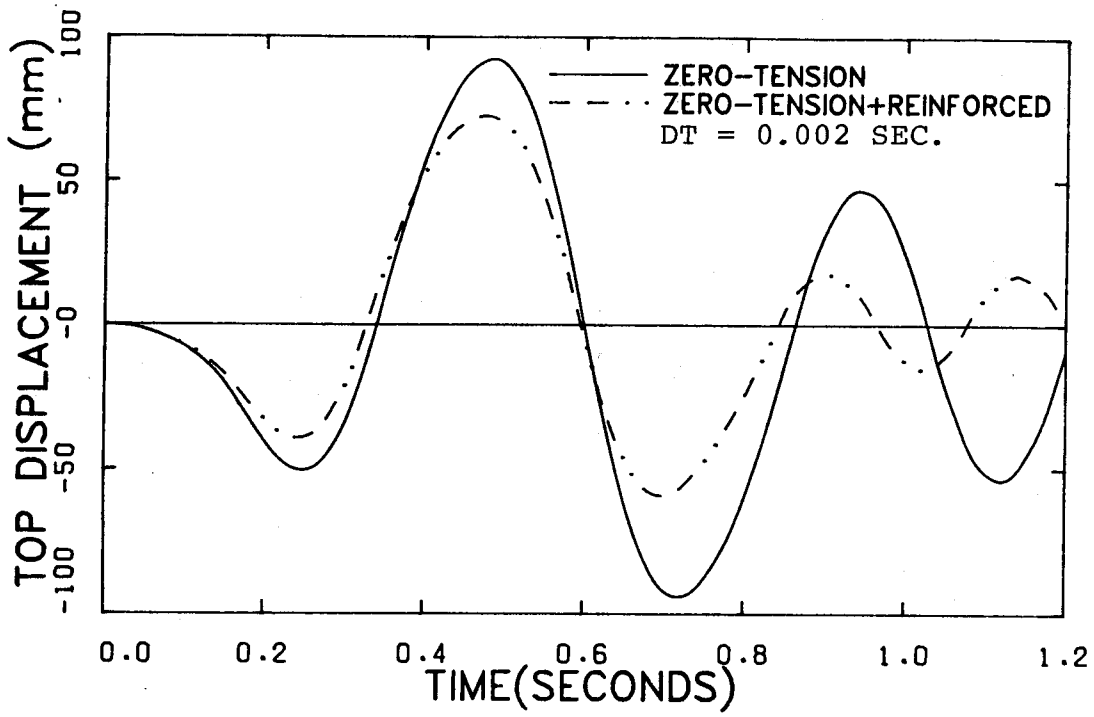

(a)

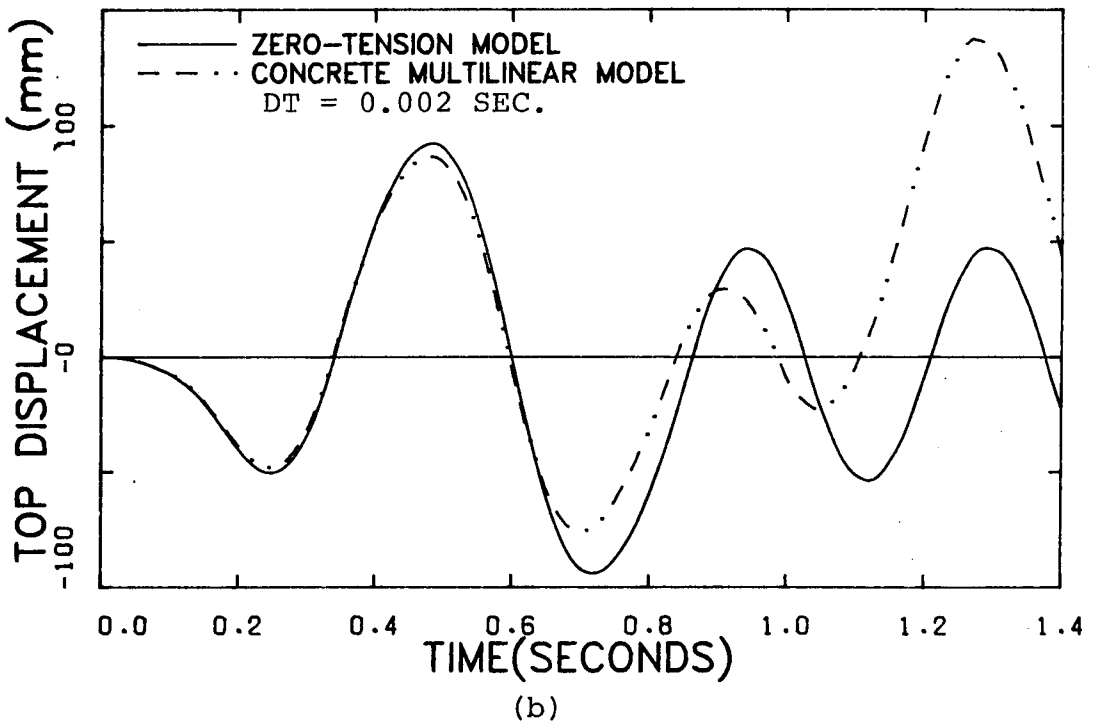

(b)

Figure 4-9 Time History Response of 5-Story Building Model due to Overturning

on the descending branch on the stress-strain diagram.

The displacement-time history response at roof level is plotted and compared with the response of the structure with the zero-tension material model for the connections as shown in Figure 4-9(b). Results show that the displacements are initially lower for the structure when multi-linear stress-strain models are used. This is mainly due to the different unloading stiffnesses assigned to the two different models. In the zero tension model, unloading is assumed to take place on a slope E_1 as shown in Figure 4-10(a). In the multi-linear concrete model, the unloading stiffnesss is E_o which is effectively higher than the slope E_1 as shown in Figure 4-10(b).

When the strain in concrete exceeds its capacity at maximim stress level, the stiffness is lost in the connection, and hence large displacements occur as shown in Figure 4-9(b). The stress-strain response of concrete in the connection region was followed throughout the analysis as illustrated in Figure 4-10(b).

4.4.3 Dynamic Response Due to Shear

4.4.3.1 Response Due to Shear-Slip

The transfer of shear forces across the horizontal connection due to the presence of gravity loads and post-tensioning (if any) is by Coulomb friction. The resultant of these loads and the magnitude of the coefficient of friction determine if slip has occurred.

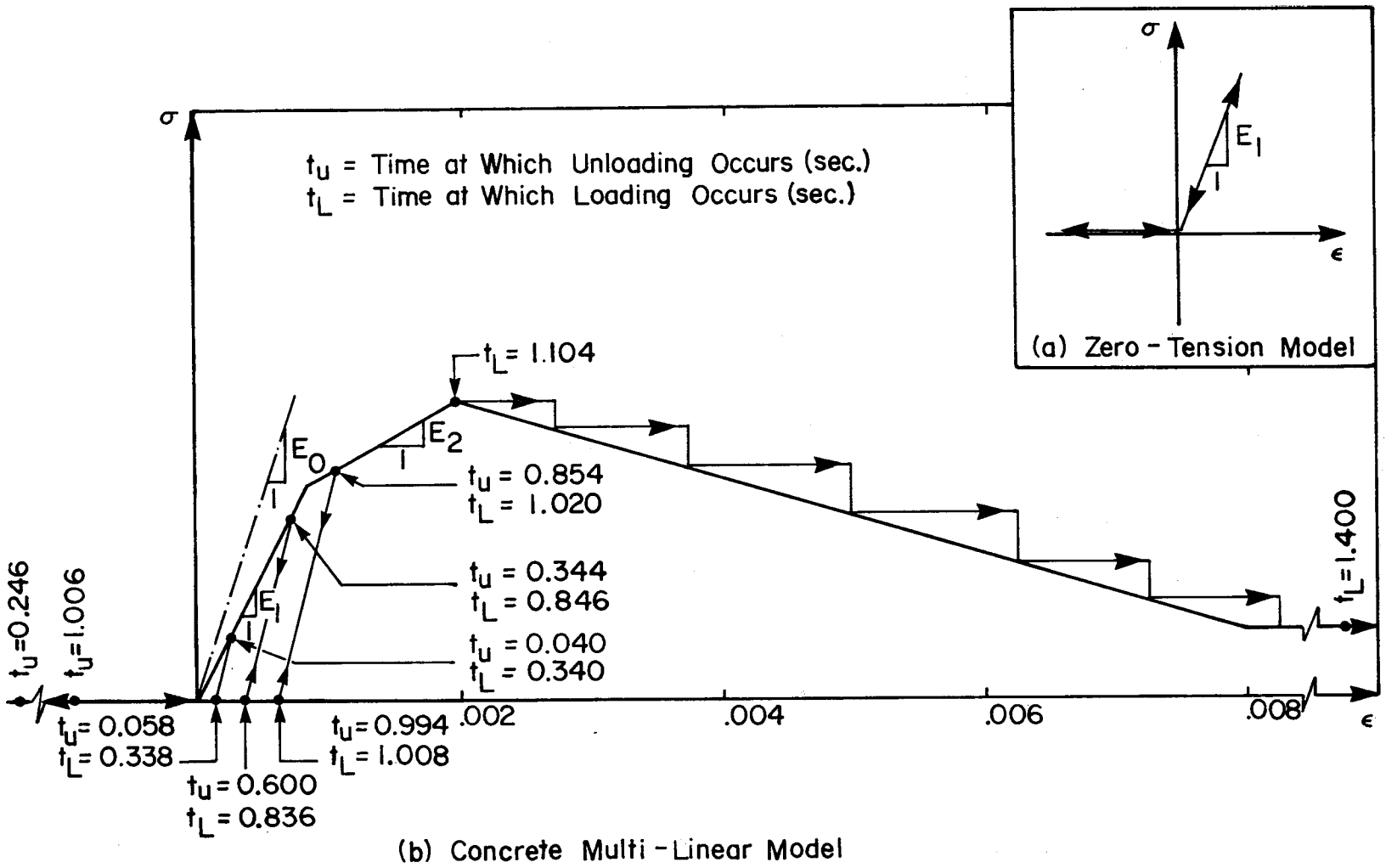

Figure 4-10 Concrete Behaviour in the Connection Region in the 5-Story Building Model

To study the shear slip behaviour across the connections and verify the shear slip model, the six-story building model analysed by Llorente and Becker (1981) was selected. The structural dimensions and its properties are shown in Figure 4-11. The structure was subjected to a rectangular pulse at its base and was allowed to slip at the connection level at the base of the wall. The displacement-time history response at roof level is plotted and shown in Figure 4-12. These results are compared with those obtained by Llorente and Becker. The two cases show close agreement up to 0.2 seconds. Disagreement in response is evident beyond 0.2 seconds. The discrepancies may be due to causes such as the sensitivity of the shear slip model, the integration time step, step-by-step integration techniques or other effects. The value of the integration time step used by Llorente and Becker is not known. The effect of integration-time step on the response is investigated in this study and is described later in this chapter.

The sensitivity of the shear slip model to different values of strain hardening slope is investigated in this study. The selected values of the strain-hardening slope are 0.2% and 3.0% of its elastic slope. The displacement-time history response of the six-story building model corresponding to different ratios of strain hardening are plotted and compared with the case with zero strain hardening as shown in Figure 4-13. These results show that a small amount of strain hardening can significantly reduce

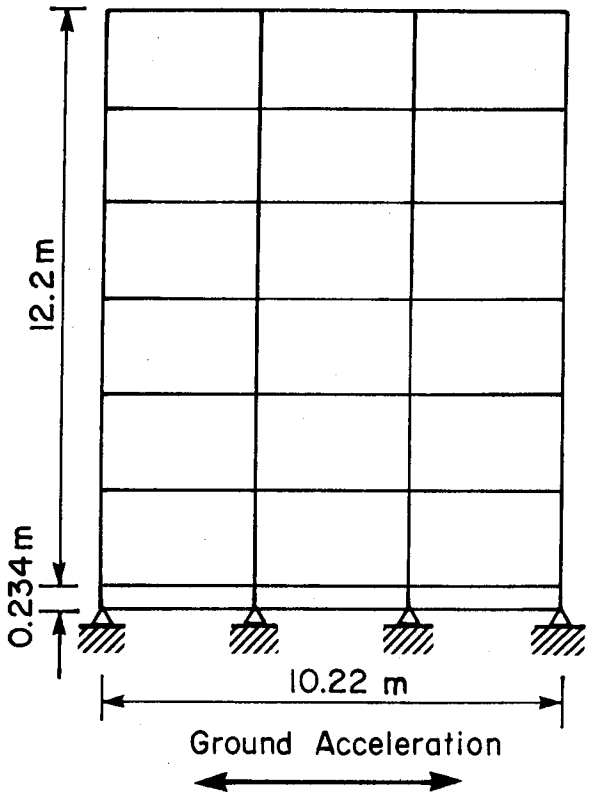

Properties:

Wall panels:

E = 25,000 MPa
ν = 0.2

Connections:

E = 19,600 MPa
G_d = 7330 MPa
μ = 0.1

Loads = 3647 kN

Masses = 371760 kg

Panel thickness = 200 mm

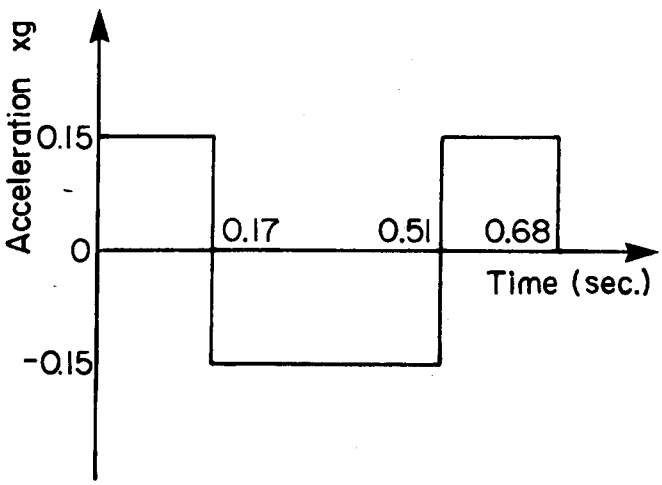

Figure 4-11 Description of the 6-Story Building Model Studied for Shear Transfer

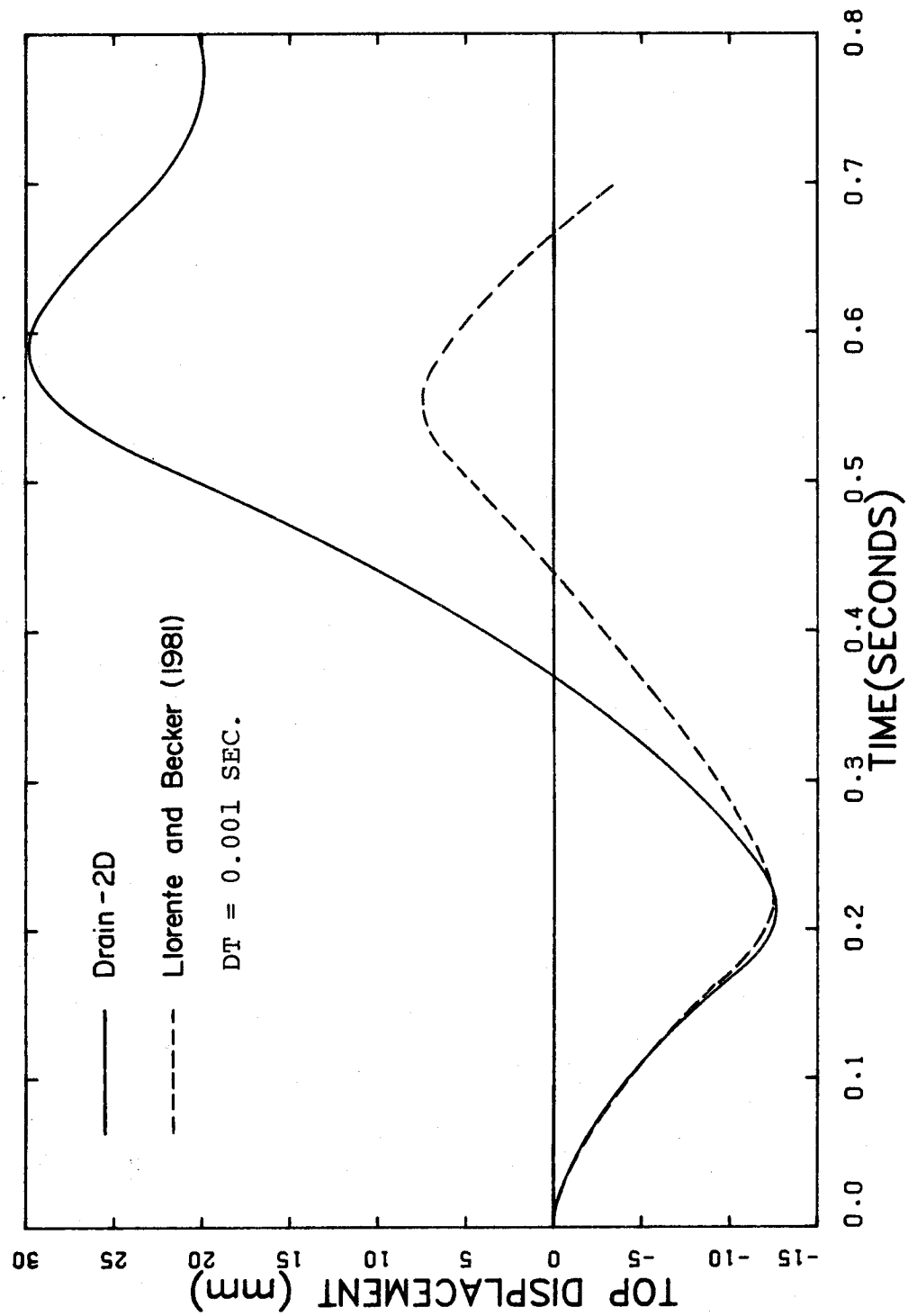

Figure 4-12 Comparison of Time History Response of 6-Story Building Model due to Shear-Slip with Previous Analysis

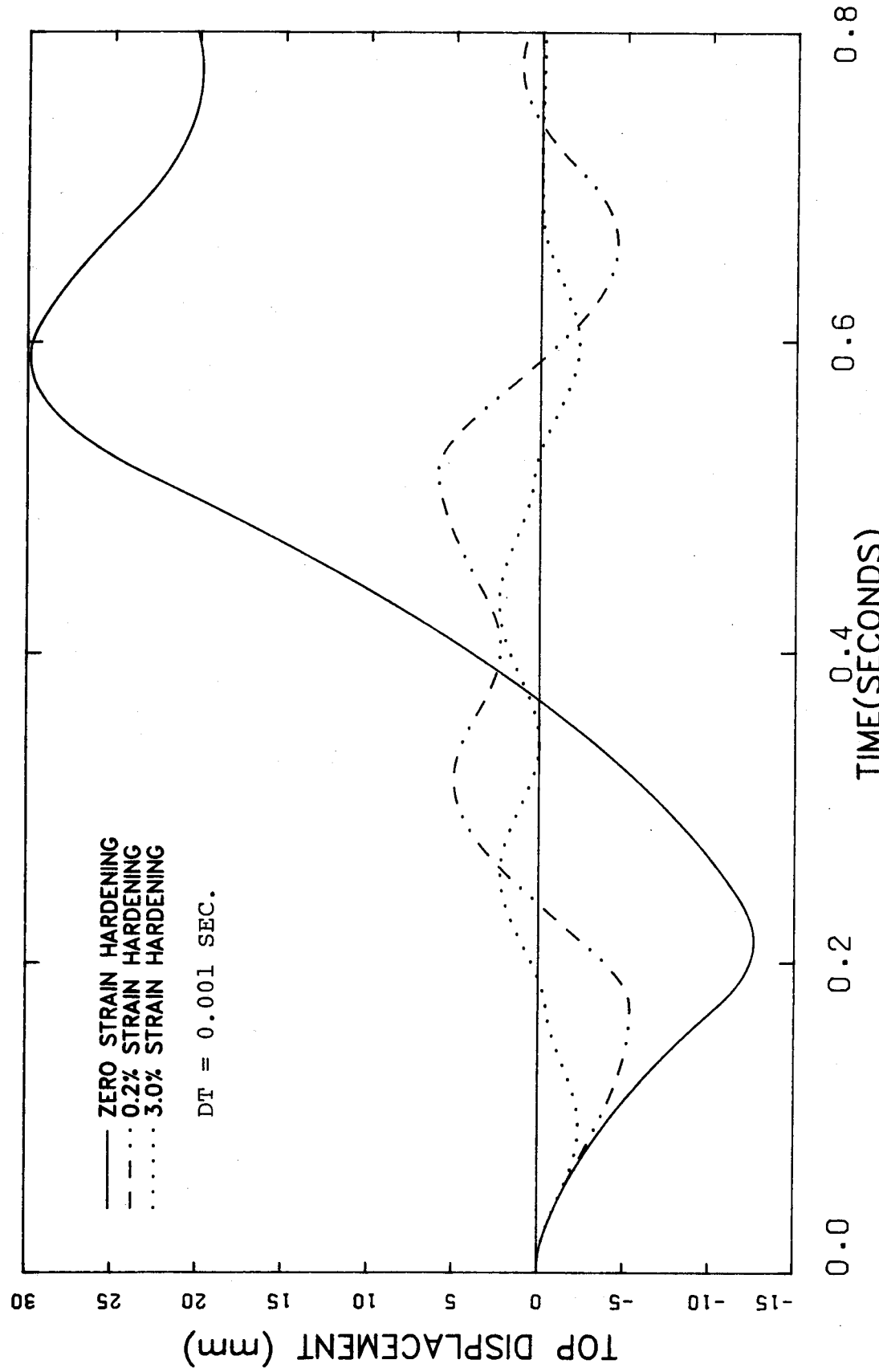

Figure 4-13 6-Story Building Model - Effect of Strain Hardening on Response

the maximum displacement. It is very difficult to select the exact value of strain hardening from the reported test results. It is believed that the strain hardening varies with the number of slip cycles and any degradation that may occur across the connections.

To investigate the energy disipation capacity of horizontal connections due to the variation in strain hardening in the shear slip model, the hysteresis loops were examined. Figures 4-14(a) and (b) show the hysteretic response corresponding to zero strain hardening and strain hardening of 1% strain hardening of elastic slope respectively. The shape of the hysteresis loops clearly demonstrates the reasons for variation in the structural response due to variation in strain hardening.

To study the effect of the magnitude of the strain hardening on the response, the same structure described above was analysed with strain hardening ratios of 0.2%, 1.0% and 3.0% of the elastic slope. The displacement time history response is shown in Figure 4-15. Analytical results indicate that for the type of structure considered, the values of strain hardening below 1% of the elastic slope do not have a significant effect on maximum response. However, for zero strain hardening, large displacements occur. For strain hardening higher than 0.2% of the elastic slope, the maximum displacements are reduced significantly.

The above analyses were carried out on the assumption that normal stresses remain constant throughout the

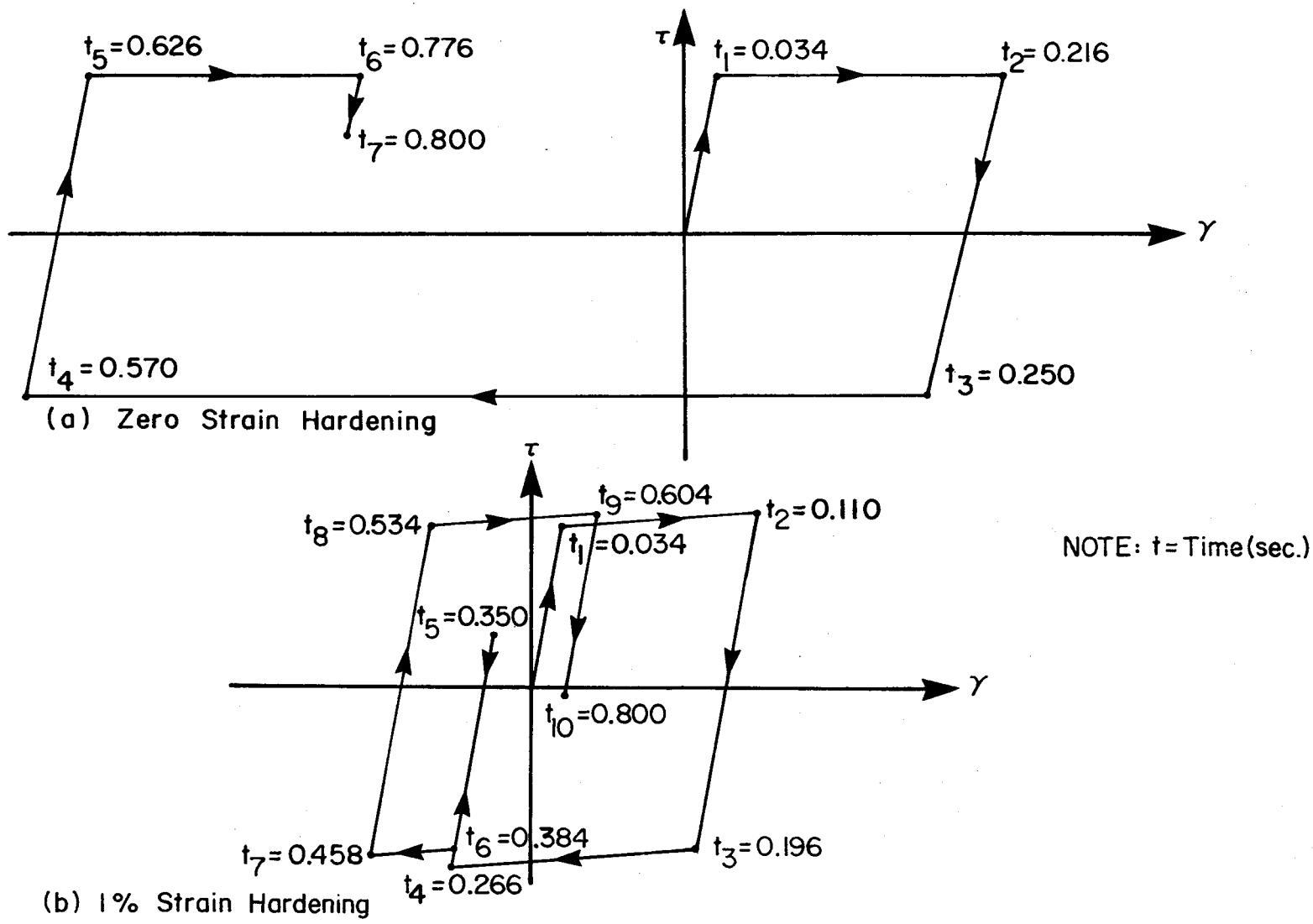

Figure 4-14 6-Story Building Model - Effect of Variation in Strain Hardening on Hysteretic Response

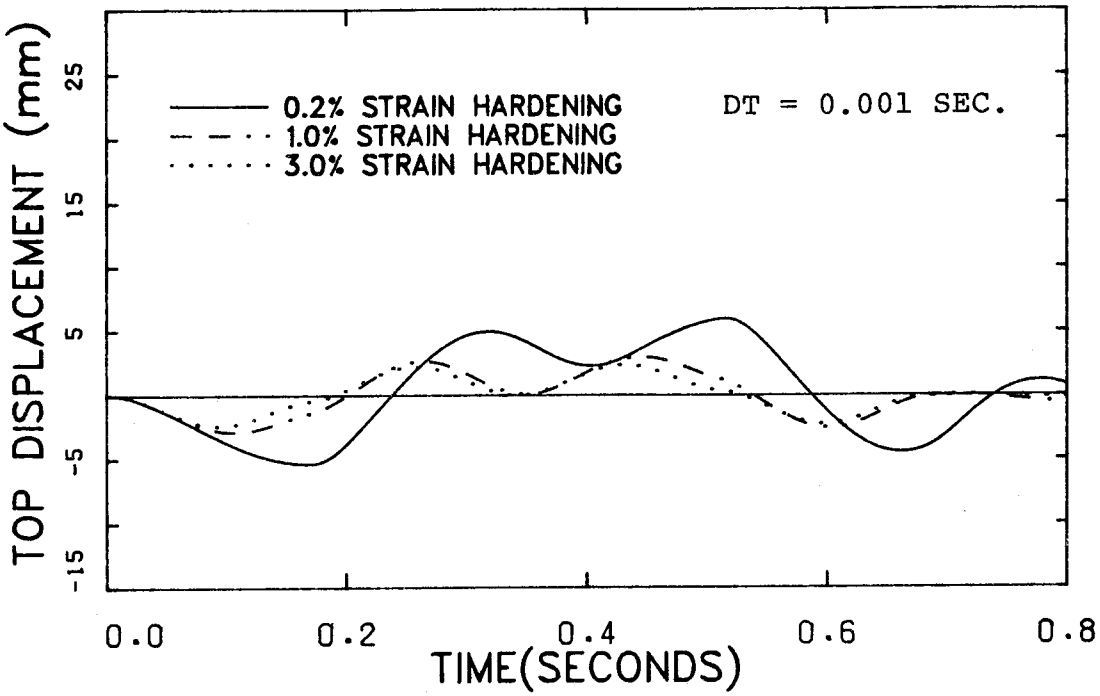

Figure 4-15 6-Story Building Model - Effect of Strain Hardening on Response

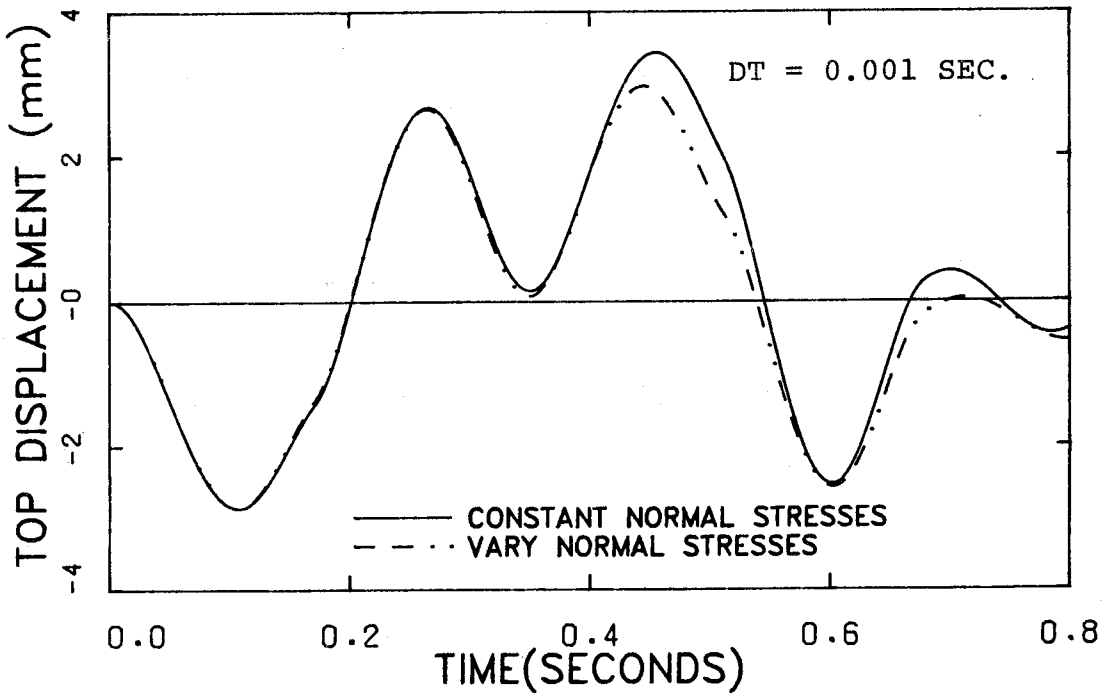

Figure 4-16 6-Story Building Model - Effect of Varying Normal Stresses on Response

analyses. The normal stress across the connection was selected to be the stress corresponding to static loads prior to dynamic loads. However, due to the effects of overturning and vertical component of acceleration, normal stresses do not remain constant throughout the analysis. For this reason, further analysis was carried out on the six story building model to study the effect of variation of normal stresses across the connection. The strain hardening was assumed to be 1% of the elastic slope. Figure 4-16 compares the displacement time history response at roof level for constant normal stresses and variable normal stresses across the connection. Results show small variation in response due to variation in normal stresses.

4.4.3.2 Response Due to Shear-Friction

It was discussed in Chapter 2 that the behaviour of horizontal connections is controlled by shear friction mechanism when mild reinforcing bars are placed perpendicular to the plane of the connections.

The six story building model described in the previous section was selected to study the response of the wall due to shear friction mechanism. The properties of reinforcing bars and the parameters corresponding to the shear friction model selected for this purpose are shown in Figure 4-17. Results of dynamic analysis indicate that the response of the wall is considerably improved when mild reinforcing bars are provided across the horizontal connections. Figure 4-18

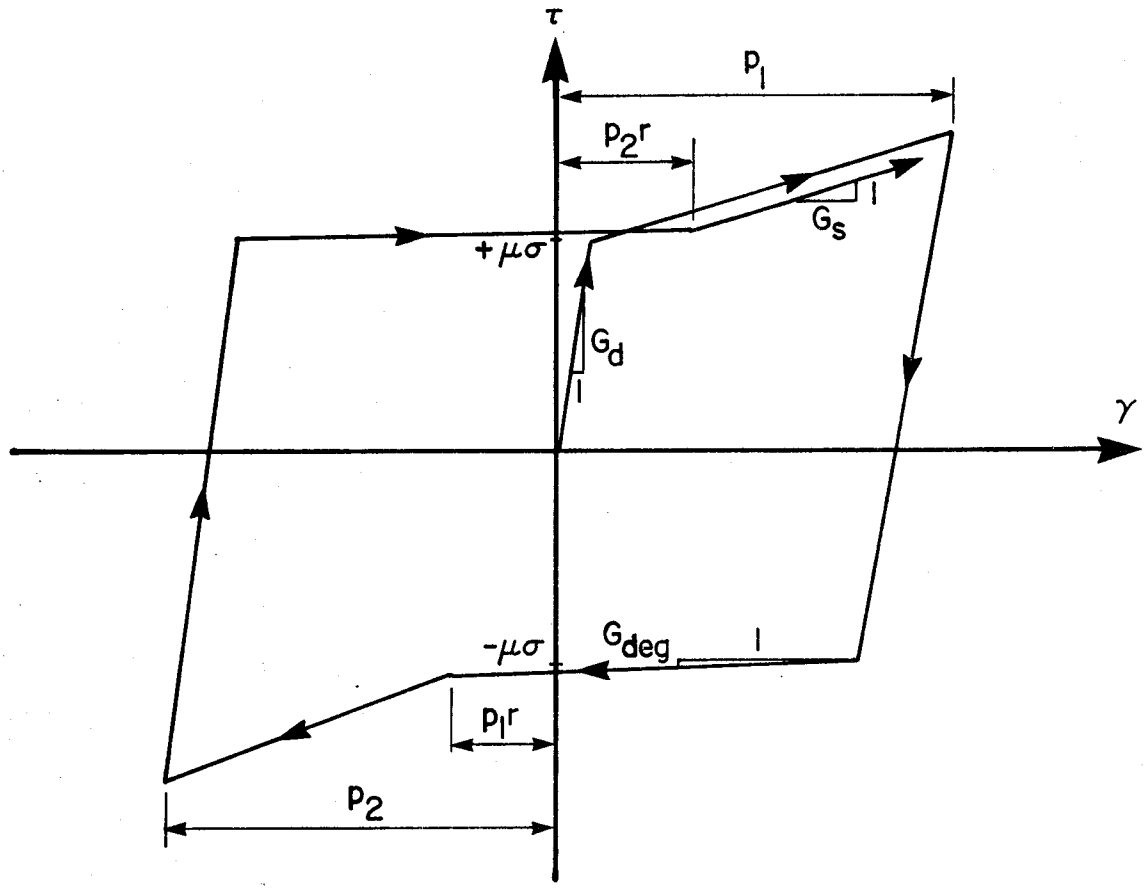

Properties:

E_s = 200,000 MPa
f_y = 300 MPa
G_s/G_d = 0.1
G_{deg}/G_d = 0.002
ρ = 0.25%
r = 0.15

Figure 4-17 Shear Friction Parameters

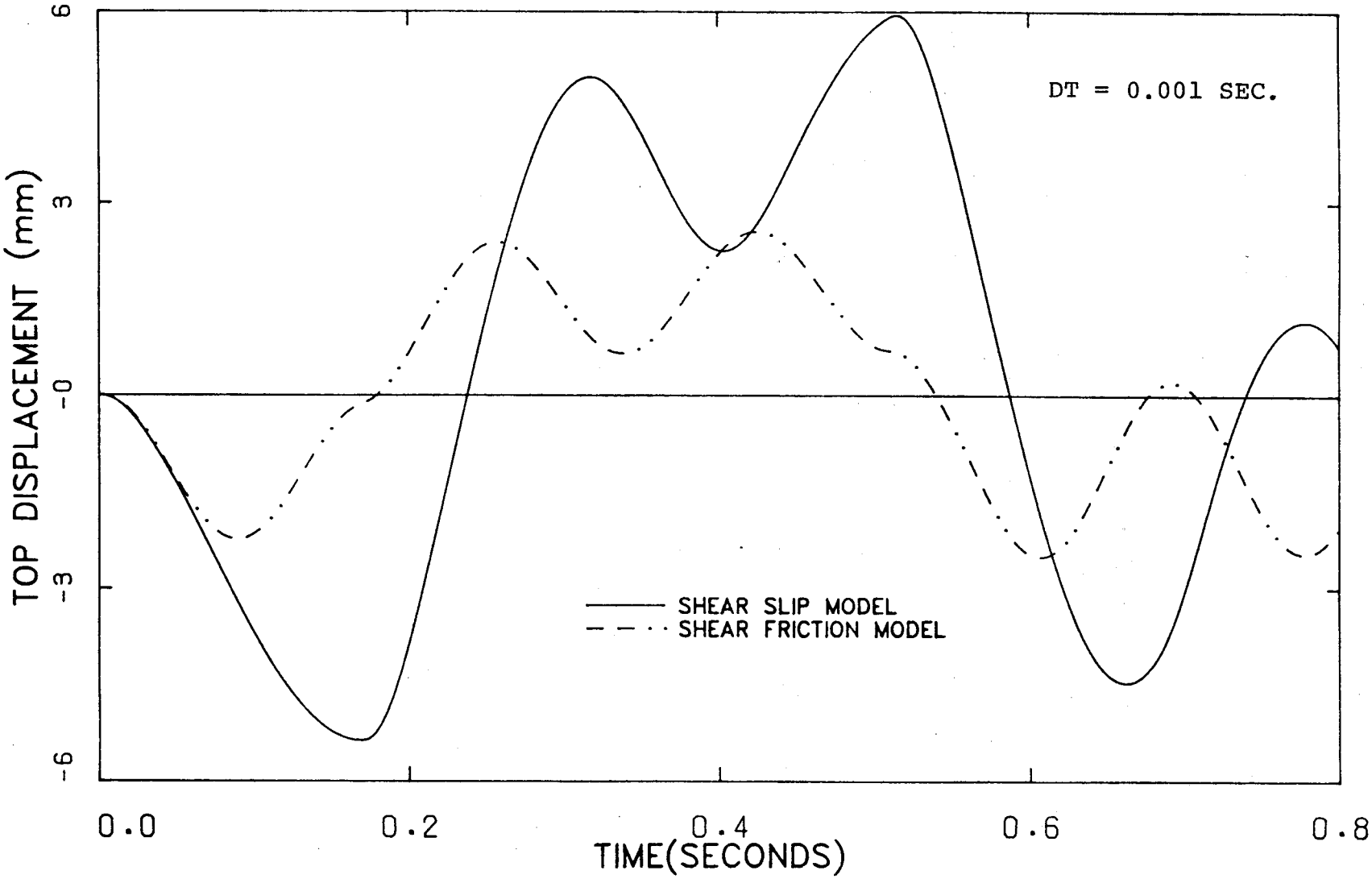

Figure 4-18 6-Story Building Model - Response due to Shear-Slip Versus Response due to Shear-Friction

compares the displacement time history response at roof level for both the reinforced and unreinforced connection. The amount of strain hardening for the shear slip model was assumed to be 0.2% of the elastic slope. These results show that due to the presence of reinforcement across the connection, the maximum displacements are reduced by at least 50% of those obtained from the unreinforced connection.

The above analysis was carried out assuming constant normal stresses across the connection. Results of dynamic analysis showed that the effect of variation in normal stress across the connection was not significant as was also the case with the shear slip model.

4.5 Effect of Integration Time Step

Selection of integration time step is of primary concern in dynamic analysis. The integration time step should be as small as possible to ensure accurate results, but at the same time the computational cost should also be considered. Inaccuracies usually result if the integration time steps are large compared to the periods of the vibrational modes of the structure. In order to verify the accuracy of the results described so far with respect to integration time step, some of the structural models described earlier were reanalyzed with varying integration time steps.

To investigate the effect of integration time step in

the linear elastic range, the structural model described in Figure 4-2 was selected. The displacement time history at roof level for three different time steps are plotted and shown in Figure 4-19. These results show variation in peak displacement and period of vibration due to the variation in integration time steps.

The 15-story building model described in Figure 4-4 was selected to study the effect of integration time step on gap opening. The range of integration time steps considered were between 0.002 seconds to 0.01 seconds. The displacement time history response shown in Figure 4-20 indicate that the integration time step do not have a significant effect on the response for the range of values considered. It should be noted that the above analyses were carried out based on the amount of axial reinforcement equal to 0.25% of the gross concrete area provided for vertical continuity across the connection.

The sensitivity of the shear slip model due to the variation in the integration time step was studied using the six-story building model described in Figure 4-11. The range of values considered for the integration time step were between 0.0001 seconds to 0.02 seconds. Results of dynamic analysis shown in Figures 4-21(a) and (b) indicate that the response is not significantly affected for the integration time steps below 0.01 seconds and excellent agreement can be observed for time steps below 0.005 seconds. For values higher than 0.01 seconds, the response

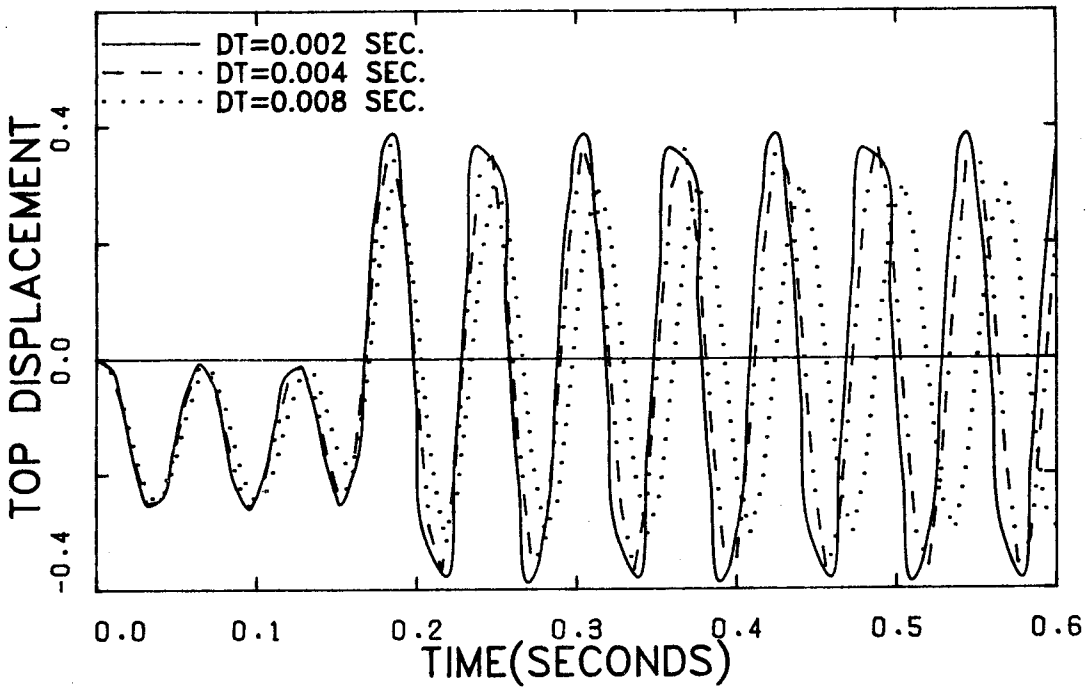

Figure 4-19 Effect of Integration Time Step on Linear-Elastic Response

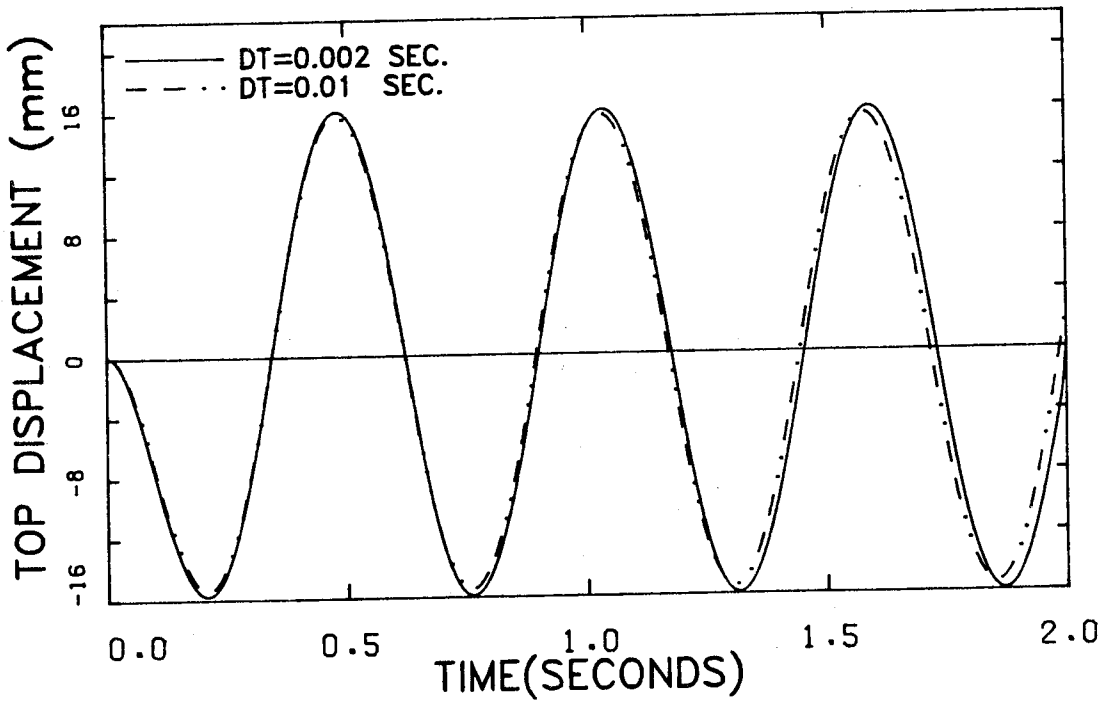

Figure 4-20 Effect of Integration Time Step on Gap Opening

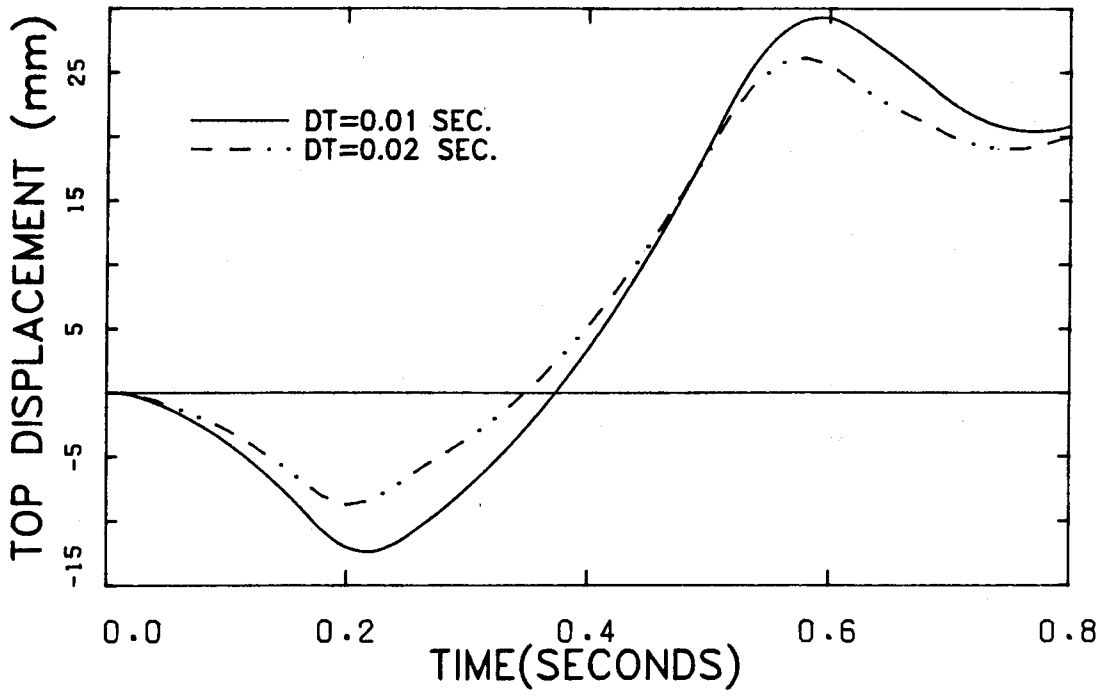

(a)

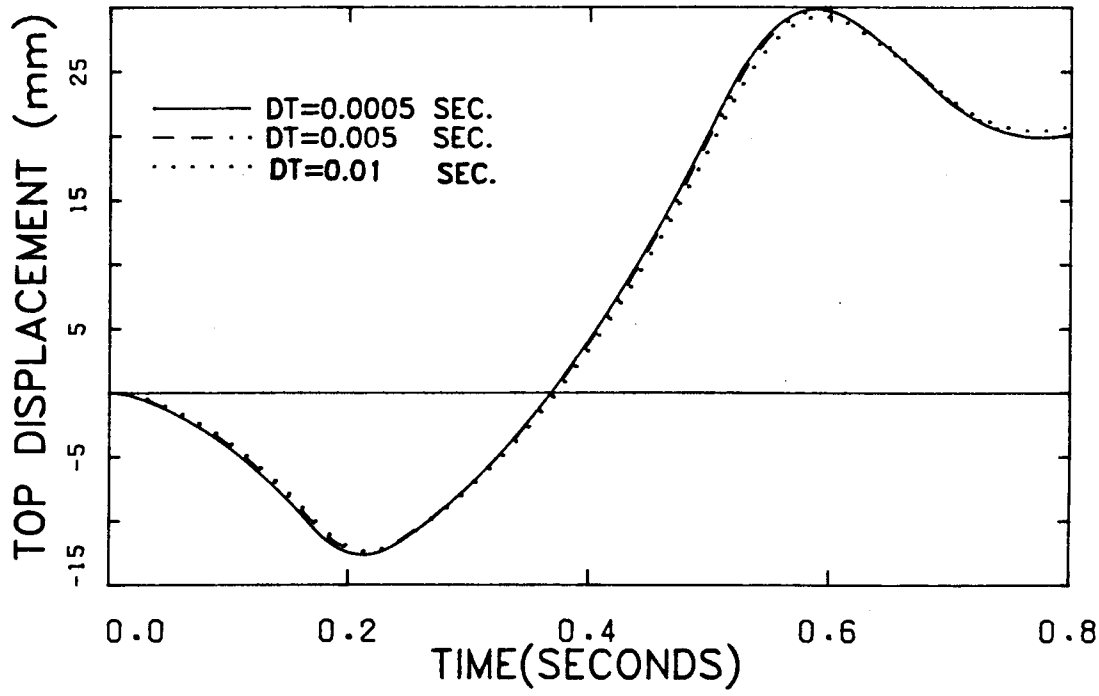

(b)

Figure 4-21 Effect of Integration Time Step on Shear Slip

is very sensitive to the selected time step. The above analyses were made assuming zero strain hardening for the shear slip model.

It should be noted that the discussion made regarding the integration time step is valid for the type of model and the type of structure considered for the analysis and cannot be generalized to other models or other structural types. The integration time step is greatly dependent on the numerical integration procedure and the vibrational period of the structure. Selection of a proper value for the integration time step requires both experience and experiment to ensure accurate results and reduce the computational cost as much as possible.

4.6 Compatibility of Plane Stress Element with Beam Element

To verify the compatibility of wall panel element with coupling beam element, a comparison was made between the results of a dynamic test on a building model and an analysis of the same structure. A 10 story small scale coupled wall structure of monolithic construction was tested by Aristizabal-Ochoa (1977) at the University of Illinois on an earthquake simulator. The properties of the test specimen and the experimental data are described by Saatcioglu (1981). Structural properties used in the analysis are listed in Table 4-1. The overall dimensions of the test specimen are illustrated in Figure 4-22(a). Cross sectional dimensions of walls and beams were 1.0 x 7.0 inch

Table 4-1 Properties of Test Specimen Used in the Analysis

Fundamental Period	0.2 sec
Number of Stories	10
Wall Stiffness Parameter (EI)	5.77×10^4 k-in.^{2} (165.6 kNm^2)
Stiffness Taper	1.00 EI at base 0.67 EI at 4th floor
Beam Stiffness Parameter (EI)	1.0×10^2 k-in.^{2} (0.287 kNm^2)
Wall Yield Moment, M_y	39.0 k-in. (4.4 kNm)
Strength Taper	1.00 M_y at base 0.51 M_y at 4th floor
Beam Yield Moment, M_y	1.56 k-in. (0.176 kNm)
Damping	2.0% of critical
Post-Yield Stiffness on Primary Curve	2.0% of elastic
Weight	2.5 K/wall (11.22 kN/wall)
Base Fixity Condition	Fully fixed
Base Motion	El Centro 1940 N-S

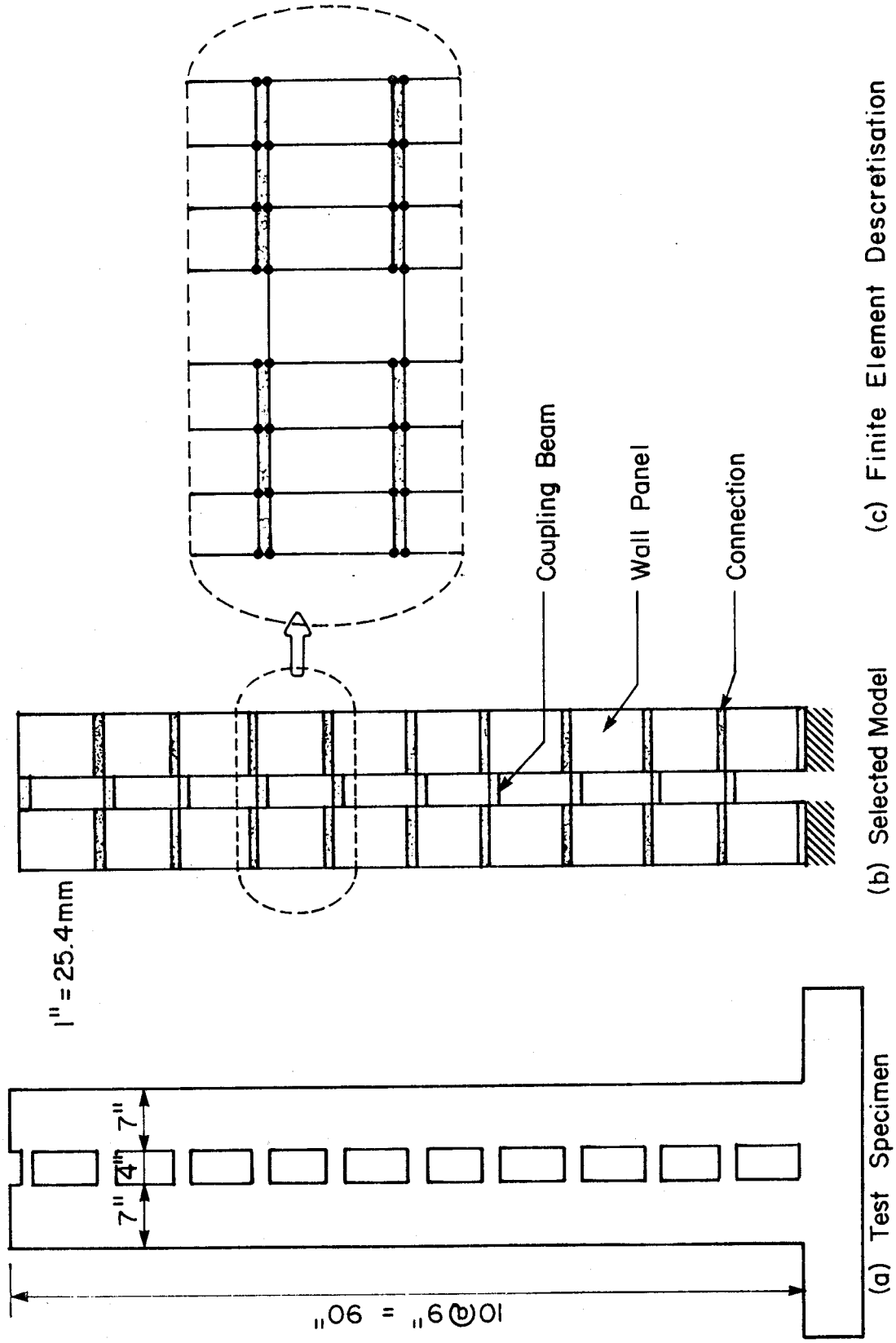

Figure 4-22 Descretization of 10-Story Test Specimen for Analytical Study

(15.4 x 177.88 mm) and 1.0 x 1.5 inch (25.4 x 38.1 mm), respectively. Structure weight was simulated by placing a 0.5 kip (2.22 kN) weight at each floor.

The input motion used was the N-S component of the 1940 El Centro record with a peak acceleration of 0.33 g. The original time axis was compressed by a factor of 2.5, which implies that 3.0 seconds of analysis corresponds to 7.5 seconds of actual ground motion.

Figure 4-22(b) shows the 10 story building model and Figure 4-22(c) shows the finite element descretisation of the structure selectd for the analysis. The available test results do not indicate whether yielding has occurred in the walls or in the coupling beams. However, to account for yielding in the walls, gap opening was assumed to take place across the connections. The zero-tension material model described in the previous chapter was assumed for the connections. Results of dynamic analysis showed large gap opening across the connections which led to the eventual failure of the structure. Further analysis was carried out assuming linear elastic behaviour for the connection material. Results of dynamic analysis showed yielding in most of the coupling beams. Figure 4-23 compares the roof displacement time history response of the analytical results with simulator test results. These results indicate that the maximum displacements are considerably higher for experimental results than the analytical values. After 1.0 seconds of the applied acceleration, the experimental

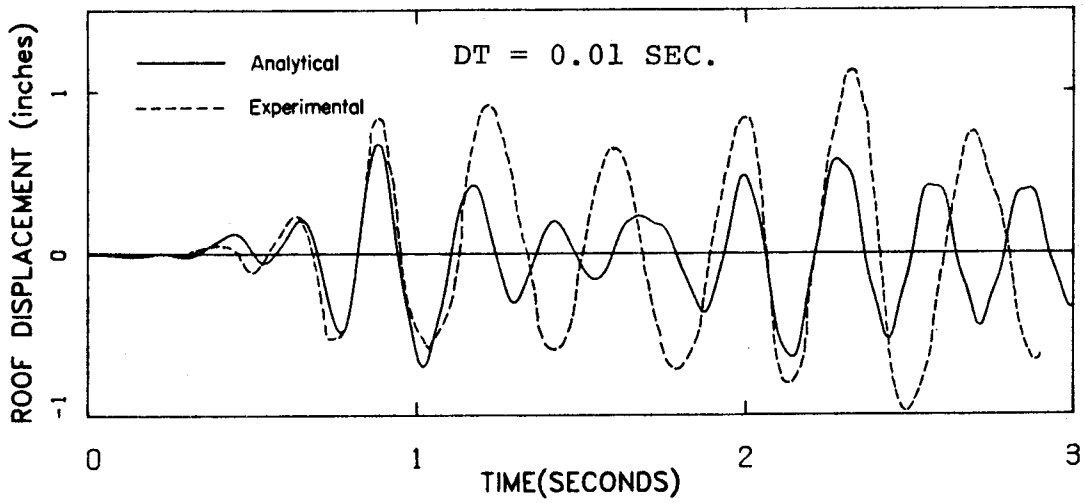

Figure 4-23 Comparison of Top Displacement Time History of Analytical and Simulator Test Results

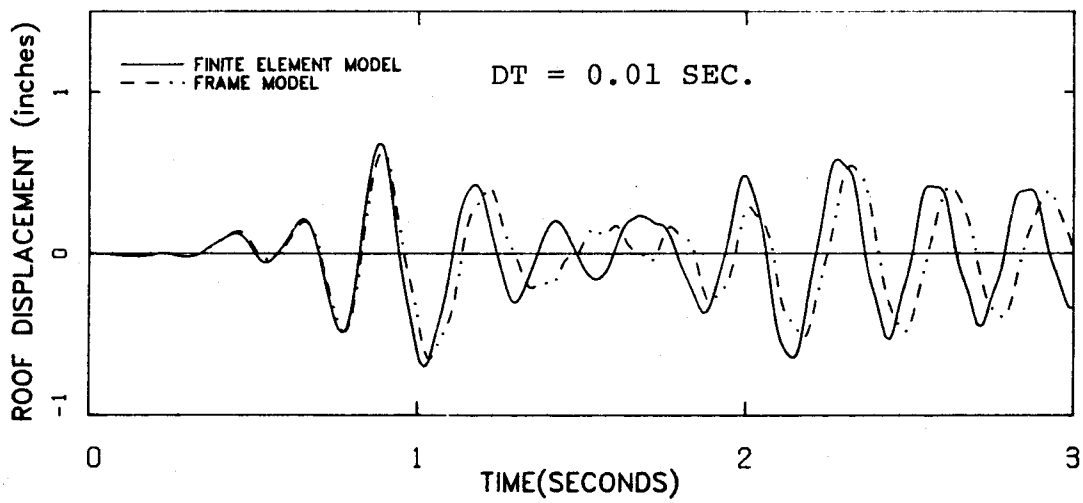

Figure 4-24 Comparison of Top Displacement Time History of Frame Model and Finite Element Model

results show higher periods of vibration than the analytical results. The increase in the period of vibration can be attributed to softening in the cast-in-place wall due to inelastic action that was not modeled in the analytical results.

The compatibility of plane stress element with coupling beam element was further investigated using a standard frame analysis and the concrete beam element in the computer program DRAIN-2D. Frame analysis showed linear elastic behaviour in wall elements. Yielding occurred in the coupling beams with similar magnitudes to those obtained from the finite element model described above. The displacement time history response of the finite element model and the frame model shown in Figure 4-24 are in good agreement.

4.7 Summary

In this chapter, the effect of the individual models on the response of precast wall panels was studied. The validity of the analytical models incorporated into the computer program DRAIN-2D was also investigated. Results of linear elastic static and dynamic analyses showed good agreement with those obtained using the computer program SAPIV. The overturning response of the structure showed good agreement with reported analytical results. It was shown that the shear behaviour of the connections was significantly affected by the variation of some of the

structural parameters and the integration time step. The strain hardening stiffness in the shear slip model had a significant effect on the response of simple walls. Results of dynamic analyses showed that the response is affected considerably when mild reinforcing bars are provided for vertical continuity or for shear transfer across the horizontal connections. The inelastic dynamic response of the walls was also affected by the variation of the integration time step. However, the response was not affected for integration time steps as low as 0.005 seconds.

The compatibility of plane stress element with coupling beam element showed close agreement with available experimental test results. The finite element results showed very good agreement with the analytical frame results.

5. SELECTION OF VARIABLES FOR PARAMETRIC STUDY

5.1 General

In this chapter, the selected variables for parametric study are described. A 10-story, large panel coupled wall system with horizontal connections at each floor level was used as the basis for the study. The selected properties and dimensions of the structure are described in Section 5-2. It is assumed that the structure rests on a rigid base, and the effect of soil-structure interaction is not considered in the analysis.

Dynamic analyses were carried out using three different earthquake records. An input motion that is potentially critical and likely to cause the most damage to the structure is used for the parametric study.

5.2 Preliminary Design of Structure

5.2.1 Structure Dimensions

Details and dimensions of the structure are shown in Figure 5-1. This type of large panel system is commonly used in residential buildings in North America. Figure 5-1(a) shows the elevation of the building. The panels are 7200 mm wide, 200 mm thick and 3000 mm high; the total height of the building is 32500 mm. Figure 5-1(b) shows a plan of the building. Precast columns are provided which are shown in the same figure. Figure 5-1(c) shows the platform type connection detail commonly used in North

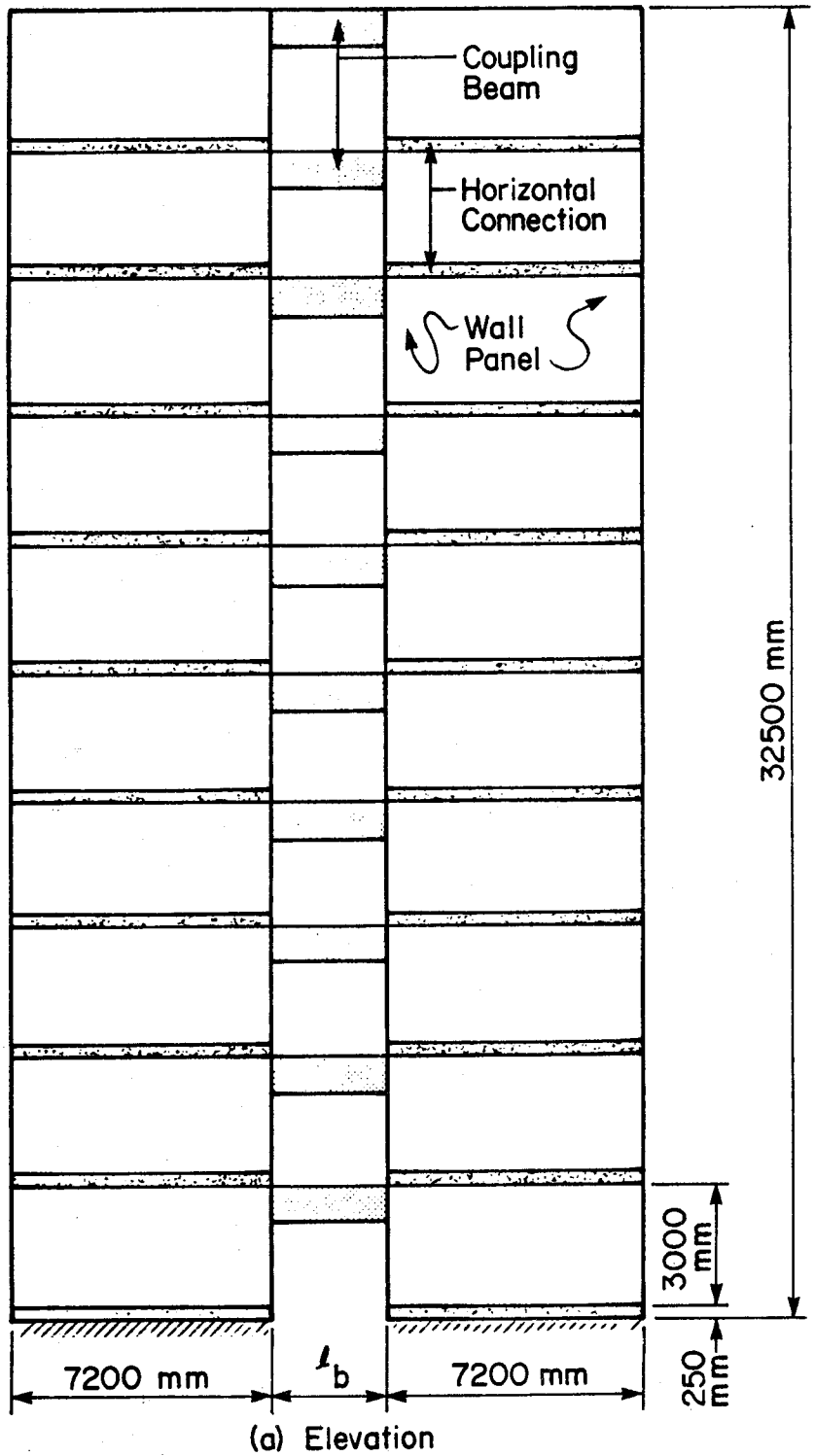
Coupling Beam
Horizontal Connection
Wall Panel
32500 mm
3000 mm
250 mm
7200 mm
l_b
7200 mm

(a) Elevation

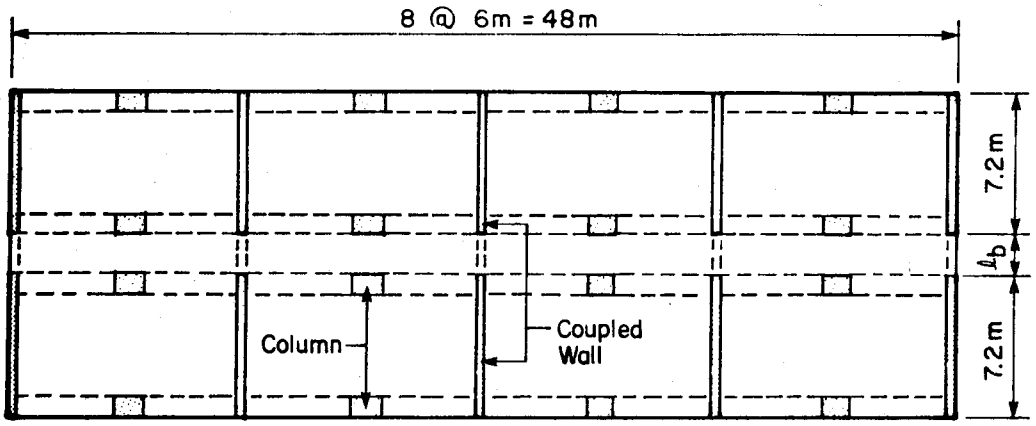

(b) Plan

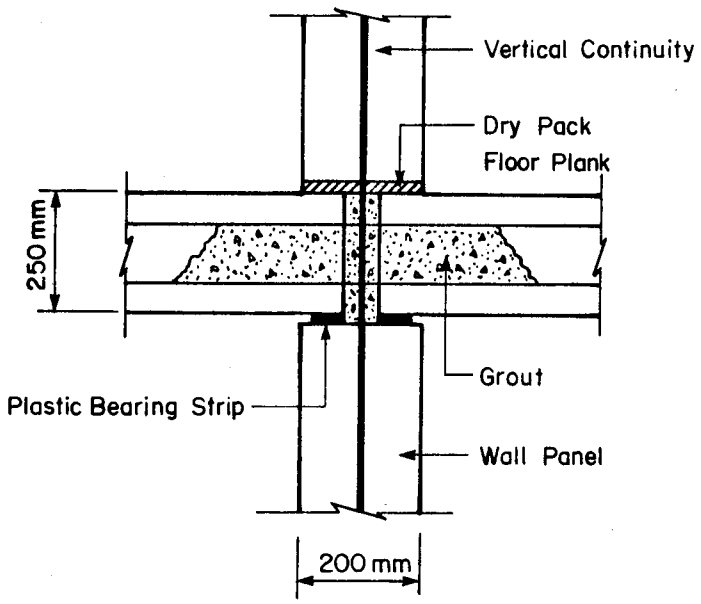

(c) Connection Detail

Figure 5-1 Details of the Coupled Wall System Selected for Parametric Study

America. Such connection detail is described in Section 2.3. The total height of the connection is assumed to be 250 mm. Two types of coupling beams are used for the analysis; slender coupling beams and deep coupling beams. The slender coupling beams are 1800 mm long and the length of deep coupling beams varies from 1000 mm to 1800 mm. Figures 5-2(a) and 5-2(b) show the reinforcement details used for slender coupling beams and deep coupling beams respectively. It is assumed that coupling beams are precast with wall panels and that they are detailed adequately to prevent premature failure.

5.2.2 Loads

The specified loads for the structure were selected using the National Building Code of Canada (NBCC, 1985) and a report on the design and construction of large panel structures by Kripanarayanan and Fintel (1976). The specified loads include partition load, mechanical load, slab dead load, live load, snow load and the panel self weight as follows:

Floor:

Partition load	0.5 kPa
Mechanical load	0.25 kPa
Slab dead load	4.1 kPa
Live load	1.9 kPa

Roof:

Built up roof	0.3 kPa

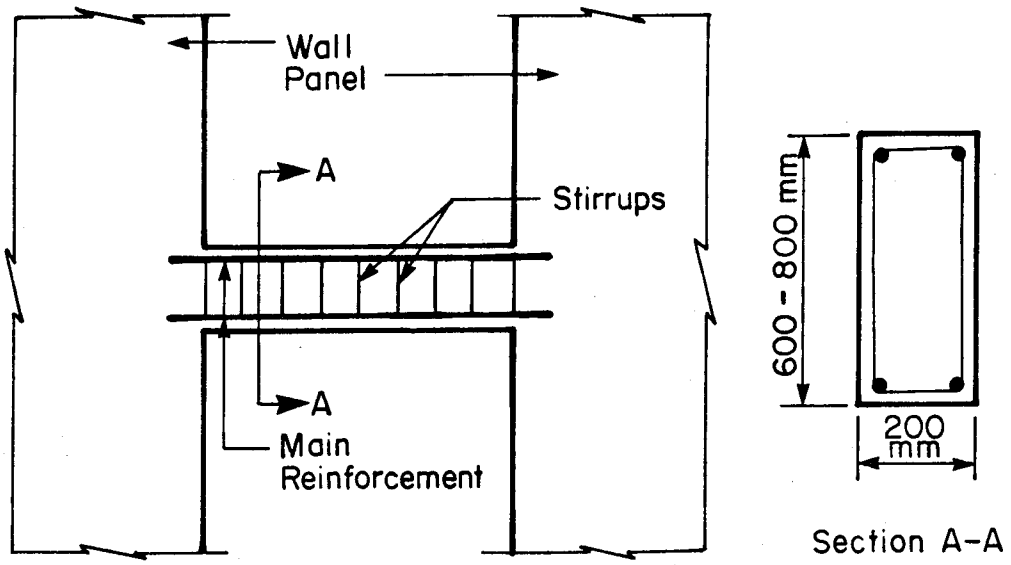

(a) Slender Beam

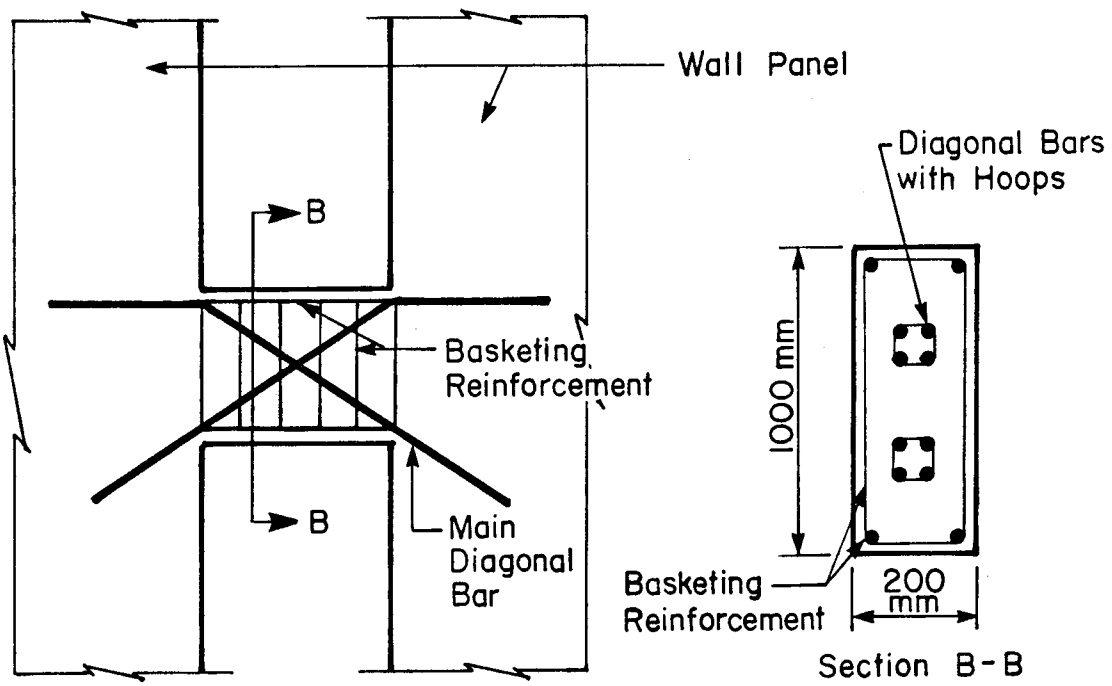

(b) Deep Beam

Figure 5-2 Reinforcing Details for Coupling Beams

Slab dead load	4.1 kPa
Live load	1.9 kPa
Snow load	1.0 kPa
Panel self weight:	34.0 kN/m height of wall

The specified loads used in the analysis for parametric study include partition load, mechanical load, built up roof and slab dead load. The effects of live load and snow load were not included in the dynamic analyses. The slab dead load is based on a 250 mm thick slab. The specified loads were used to calculate the gravity loads and the masses applied at each floor level and at the roof level; these are listed in Table 5-1. The earthquake loads were obtained using the lateral seismic force, V, given in Section Four of the NBCC (1985) as follows:

$$V = v\ S\ K\ I\ F\ W \qquad (5\text{-}1)$$

where

v = zonal velocity ratio

S = seismic response factor

K = ductility factor

I = importance factor

F = foundation factor

W = dead load + 25 percent of snow load

The values selected for the relationship (5-1) are as follows:

v = 0.5

Table 5.1 Loads and Masses Selected for Parametric Study

Loads:

Roof = 469 kN

Floor = 726 kN

Masses:

Roof = 57400 kg

Floor = 74000 kg

S = 0.25

K = 1.3

I = 1.0

F = 1.0

W = 7000 kN

i.e. V = 1138 kN

The selected value of v was based on the assumption that the building is located in zone six which is the highest velocity zone specified by the NBCC (1985). The upper limit for the value of v for zone six is not specified in the code. A value of v = 0.5 was selected as suggested by MacGregor (1985). The suggested magnitude of v corresponds directly to the maximum peak acceleration used for the parametric study.

Using the lateral seismic force, V, given above, the lateral forces at each story level were evaluated using the NBCC (1985) method. The specified dead loads and earthquake forces were multiplied by appropriate load factors as given in CAN3-A23.3-M77 (1977) to obtain loads for use in an analysis of the structure to determine internal forces.

5.2.3 Analysis

The 10-story building model discussed in Section 5.2.1 was analysed based on the "equivalent static load" method of the NBCC (1985). The analysis was carried out to provide a basis for selecting an appropriate range of structural parameters for the parametric study. The 10-story building

model was idealized as a frame and the computer program DRAIN-2D was used for linear-elastic static analysis. The selected properties of the coupled wall for frame analysis are listed in Table 5.2.

In the frame analysis, deep coupling beams were idealized as truss elements while slender coupling beams were idealized as beam elements. It is known that concrete beams crack during the application of cyclic loading. To account for this cracking, the frame analysis with slender coupling beams was repeated using the effective moment of inertia calculated using the procedure outlined in Section 9.5 of ACI-318 (1983). Figure 5-3 shows the maximum beam moment at each story level using the gross and effective moment of inertia. The results of the frame analysis are listed in Table 5-3.

5.2.4 Vertical Continuity

Amounts of mild reinforcement and post-tensioning steel required to provide vertical continuity were selected based on requirements for seismic design of special shear walls outlined in Section A of the ACI Code (1977).

5.2.4.1 Mild Reinforcing Bars

To estimate the amount of reinforcement required for the 10-story coupled wall system, results of the equivalent static analysis described earlier in this chapter were used. The total amount of reinforcement required was

Table 5.2 Properties of the Selected Structure for Frame Analysis

Wall Stiffness Parameters

$E = 27400$ MPa

$I = 6.22\ m^4$

$A = 1.44\ m^2$

Beam Properties

Slender Beams

$E = 27400$ MPa

$I_{gross} = 85 \times 10^8\ mm^4$

$I_{effective} = 68 \times 10^8\ mm^4$

$A = 160{,}000\ mm^2$

Deep Beams

$E = 200{,}000$ MPa

$A_s = 1200\ mm^2$

$F_y = 300$ MPa

Table 5.3 Maximum Internal Forces Obtained from Frame Analysis

	Max. Base Moment (kNm)	Max. Base Shear (kN)	Max. Base Axial (kN)	Max. Beam Moment (force)
Slender Beams	10006	1051	10546	413 (kNm)
Deep Beams	13460	1016	9691	278 (kN)

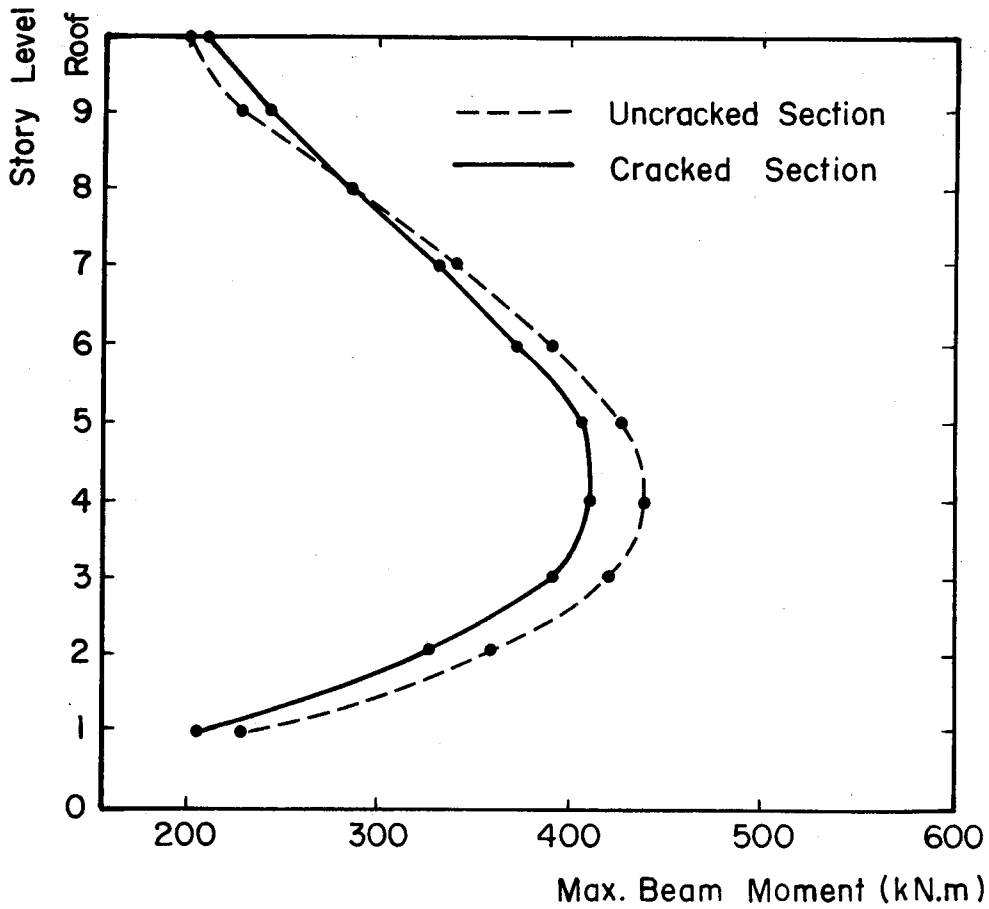

Figure 5-3 Maximum Beam Moments from the Equivalent Static Frame Analysis

calculated based on maximum shear, maximum moment and maximum axial force at the base of the walls. Minimum reinforcement requirements outlined in the Code were also determined. In all cases, the minimum amount of reinforcement required by the ACI Code (1977) governed. Connection reinforcement used in the parametric study consisted of an area of 0.25% of the gross concrete area spread uniformly along the length of the horizontal connection in addition to 0.5% of the gross concrete area concentrated at the two ends of the connection as shown in Figure 5-4(a).

5.2.4.2 Post-tensioning bars

An alternative method of providing vertical continuity in precast wall construction is by vertical post-tensioning. It is assumed that the post-tensioning bars are ungrouted and that they extend from roof level to the foundation. In the absence of vertical mild reinforcement, the shear and bending resistance in the walls is provided by post-tensioning bars. As such, the vertical load is the sum of the gravity and post-tensioning and the transfer of shear forces across the connections is by Coulomb friction.

The type of post-tensioning bars selected for this study are alloy steel bars. The properties of steel bars are as follows.

D = 25.4 mm

A = 503 mm^2

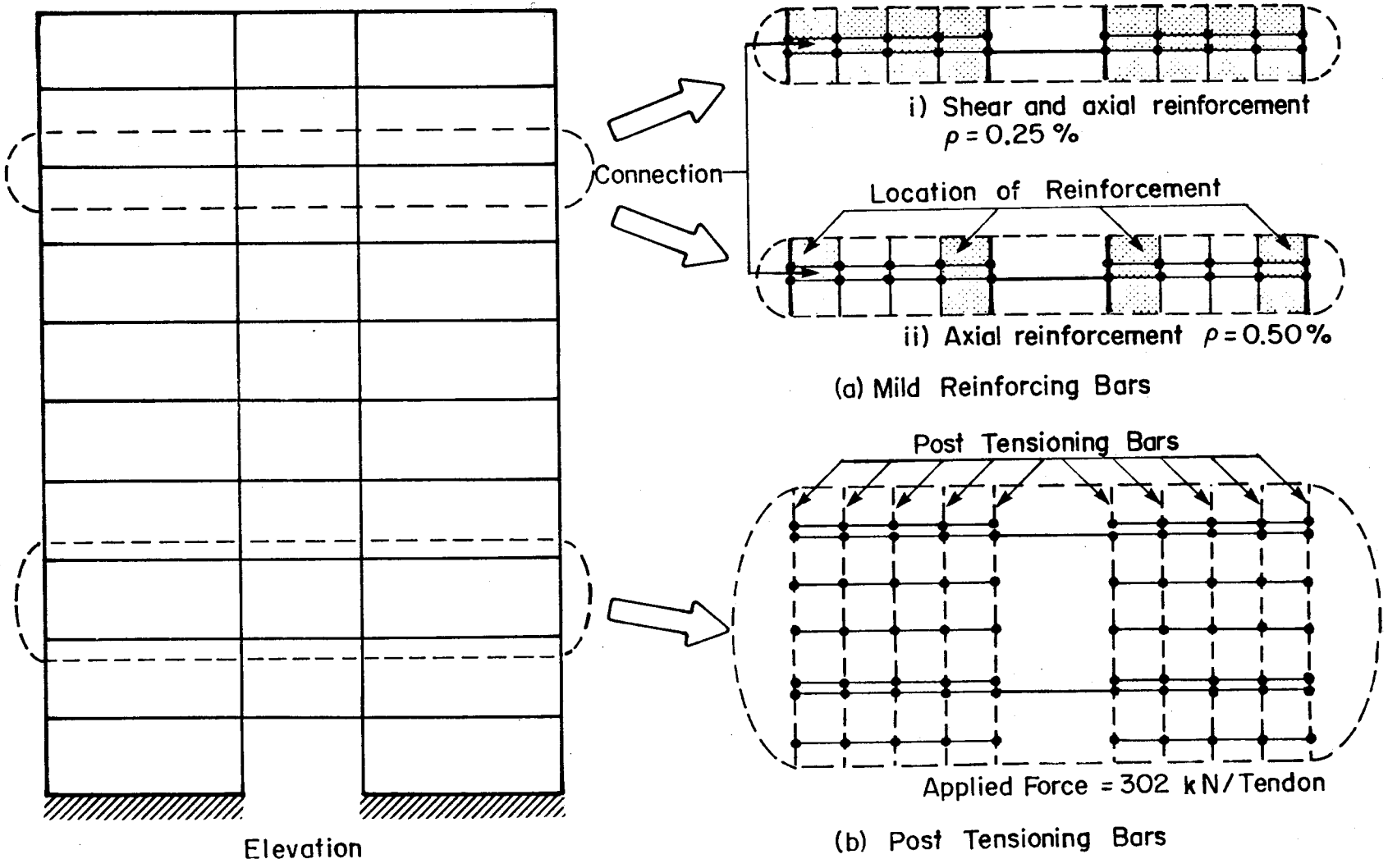

Figure 5-4 Details of Vertical Continuity on the 10-Story Coupled Wall System

f_u = 1000 MPa

where

D, A = diameter and cross-sectional area of bar

f_u = minimum ultimate strength of bars

The amount of post-tensioning was provided on the basis of developing tensile force equal to the yield force developed by mild reinforcing bars of 0.25% of the gross concrete area distributed over the entire wall section. It is normal practice to stress bars up to 70% of their ultimate stress. However as recommended by Mujumdar (1977), the bars are stressed up to 60% of their ultimate strength. This reduces the risk of high stress concentrations across the connections. The total force carried by each tendon is 302 kN. Figure 5-4(b) shows the locations of post-tensioning bars in coupled walls selected for parametric study. Post-tensioning bars are connected from roof level to the base of the walls with no intermediate connections. Five tendons are provided for each of the walls which are equally stressed.

5.3 Range of Structural Parameters Considered in Parametric Study

Table 5-4 summarizes the range of variables selected for parametric study. Tables 5-5 through 5-9 summarize the properties of wall panels, the horizontal connections and the coupling beams selected. The beam properties selected for parametric study are based on the preliminary design of

Table 5.4 Selected Variables Considered for Parametric Study

(a) Coupling Beam Strength

Parameter Study		Variables			Constants
		M_y (kNm)	F_y (kN)	Vertical Continuity	
Coupling Beam Strength	Slender Beams	0	-	R.C.	EI = 122060 kNm^2
		90	-	R.C.	
		180	-	R.C.	
		Elastic	-	R.C.	
		0	-	P.T.	
		90	-	P.T.	
		180	-	P.T.	
		270	-	P.T.	
		180	-	R.C.+P.T.	
	Deep Beams	-	0	R.C.	$\frac{L}{D}$ = 1.0
		-	180	R.C.	

(b) Coupling Beam Stiffness

Parameter Study		Variables			Constants
		EI (kNm^2)	L/D	Vertical Continuity	
Coupling Beam Stiffness	Slender Beams	0	-	P.T.	M_y = 180 kNm
		61030	-	P.T.	
		122060	-	P.T.	
		183090	-	P.T.	
	Deep Beams	-	0	P.T.	F_y = 180 kN
		-	1.0	P.T.	
		-	1.4	P.T.	
		-	1.8	P.T.	

Note: P.T. = Post-tensioned
R.C. = Reinforced concrete

Table 5.5 Properties of Wall Panels for Parametric Study

Wall Properties

$E = 27400$ MPa

$\nu = 0.15$

$f'_c = 30$ MPa

$\rho_x = 0.25\%$

$\rho_y = 0.25\%$ and 0.75%

panel thickness = 200 mm

Table 5.6 Properties of Connections for Strength Analysis (Reinforcing Bars Across the Connections)

$E_s = 200{,}000$ MPa

$F_y = 300$ MPa

$G_d = 6850$ MPa

$G_s/G_d = 0.1$

$G_{deg}/G_d = 0.002$

$\mu = 0.2$

$\nu = 0$

Table 5.7 Properties of Slender Coupling Beams for Strength Analysis

Flexural Stiffness, EI = 122 060 kNm^2

Axial Stiffness, EA = 4.03×10^6 kN

Shear Stiffness, GA = 4.03×10^5 kN

Yield Moments, M_y (kN.m)

Beam No. 1 90

Beam No. 2 180

Beam No. 3 ∞ (Elastic Beams)

Beam No. 4 0 (Simple Wall)

Strain Hardening Stiffness = 5% of elastic

Table 5.8 Properties of Deep Coupling Beams for Strength and Stiffness Analysis

E = 200,000 MPa

A = 600 mm^2

(= area of reinforcement in diagonal elements)

σ_y = 300 MPa

Strain hardening stiffness = 8% of elastic

Table 5.9 Properties of Connections and Slender Coupling Beams for Stiffness Analysis

(a) Properties of the Connections (Post-tensioning bars across the connections)

$E = 13700$ MPa

$G_d = 6850$ Mpa

$\nu = 0$

$\mu = 0.2$

$f'_c = 15$ MPa

$G_s/G_d = 0.001$

(b) Properties of the Slender Coupling Beams

Beam No. 1

Flexural Stiffness EI = 61 030 kNm^2

Axial Stiffness EA = 3.30×10^6 kN

Shear Stiffness GA = 3.30×10^5 kN

Beam No. 2

Flexural Stiffness EI = 122 060 kNm^2

Axial Stiffness EA = 4.03×10^6 kN

Shear Stiffness GA = 4.03×10^5 kN

Beam No. 3

Flexural Stiffness EI = 183 090 kNm^2

Axial Stiffness EA = 4.55×10^6 kN

Shear Stiffness GA = 4.55×10^5 kN

Strain Hardening Stiffness = 5% of elastic

Yield Moment = 180 kNm

the 10-story coupled wall discussed in Section 5.2.3. The ratio of inelastic stiffness to the elastic stiffness for slender coupling beams is assumed to be 5%. This value was selected by examining moment-rotation curves obtained from test results carried out by Barney et al. (1978). For deep coupling beams, the ratio was assumed to be 8%. This value was selected by examining a large number of moment-rotation curves or load-deformation curves obtained from test results carried out by Barney et al. (1978), Paulay (1971(a), 1977), Paulay and Binney (1974), and Paulay and Santhakumar (1976).

5.4 Dynamic Analysis

5.4.1 Finite Element Mesh Layout

The finite element modeling of wall panels and connections, and the modeling of coupling beams were discussed in Chapter 3. Figure 5-5 shows the finite element descretization of the wall panels and connections of the structure. The panels are made up of four-node rectangular plane-stress elements which are assumed to behave linear-elastically throughout the analysis. The rectangular elements of the connections as well as the coupling beams are the locations of inelastic action in the coupled wall structure. Figure 5-5(b) shows the coupling of the two walls through slender beams idealized as line elements and Figure 5-5(c) shows the coupling of deep beams idealized as diagonal truss elements. The 10-story building model selected for parametric study consists of 410 nodes, 240

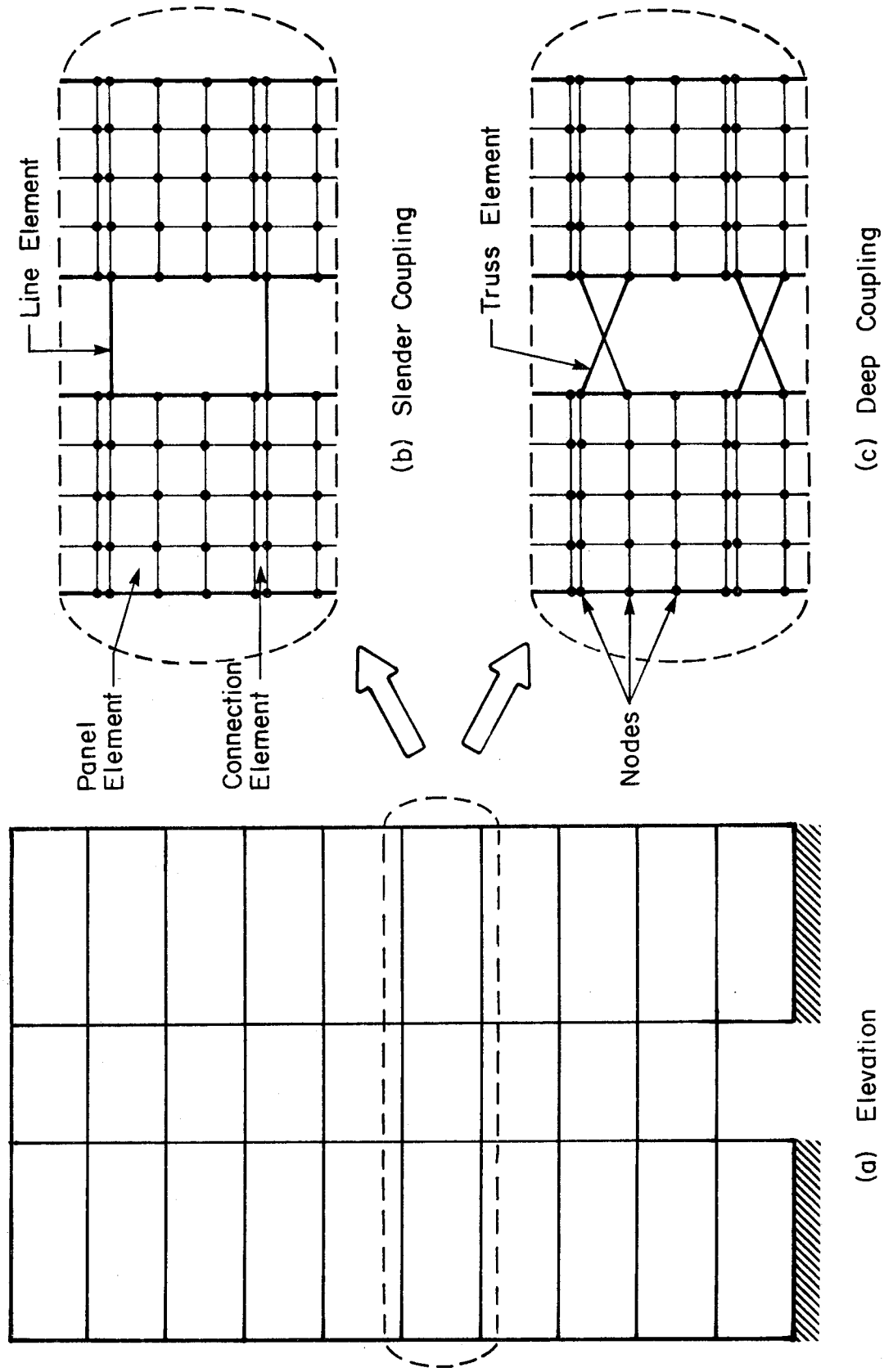

Figure 5-5 Descretization of the 10-Story Coupled Wall System

panel elements and 80 horizontal connection elements. Figure 5-6 shows the way in which masses and loads have been lumped and distributed at the connection nodes. Masses have been distributed at the upper and lower nodes of the connections. The masses assigned to the interior nodes are assumed to be twice those at exterior nodes. The dead loads have been distributed at the upper nodes of the connections. It is assumed that the load at each level is the weight of the floor slab and the panels above it as well as partition loads and mechanical loads.

5.4.2 Selection of Earthquake Record

For the dynamic analyses, three different acceleration records were considered as input ground motions. The three accelerograms selected for the analysis are: (1) El Centro, California, 1940, N-S component; (2) Taft, California, July 1952, S69E component, and (3) Pacoima Dam S16E component, 1971. These accelerograms were selected as examples of strong ground motions which have been recorded to date. The acceleration records were obtained from the Earthquake Engineering Research Institute (1976).

A ground accelerogram has three important characteristics: a) frequency, b) intensity, and c) duration. The frequency characteristic of an earthquake, as reflected in its velocity response spectrum is an important factor in selecting a suitable earthquake record. In the inelastic seismic analysis of structures, the stiffness and

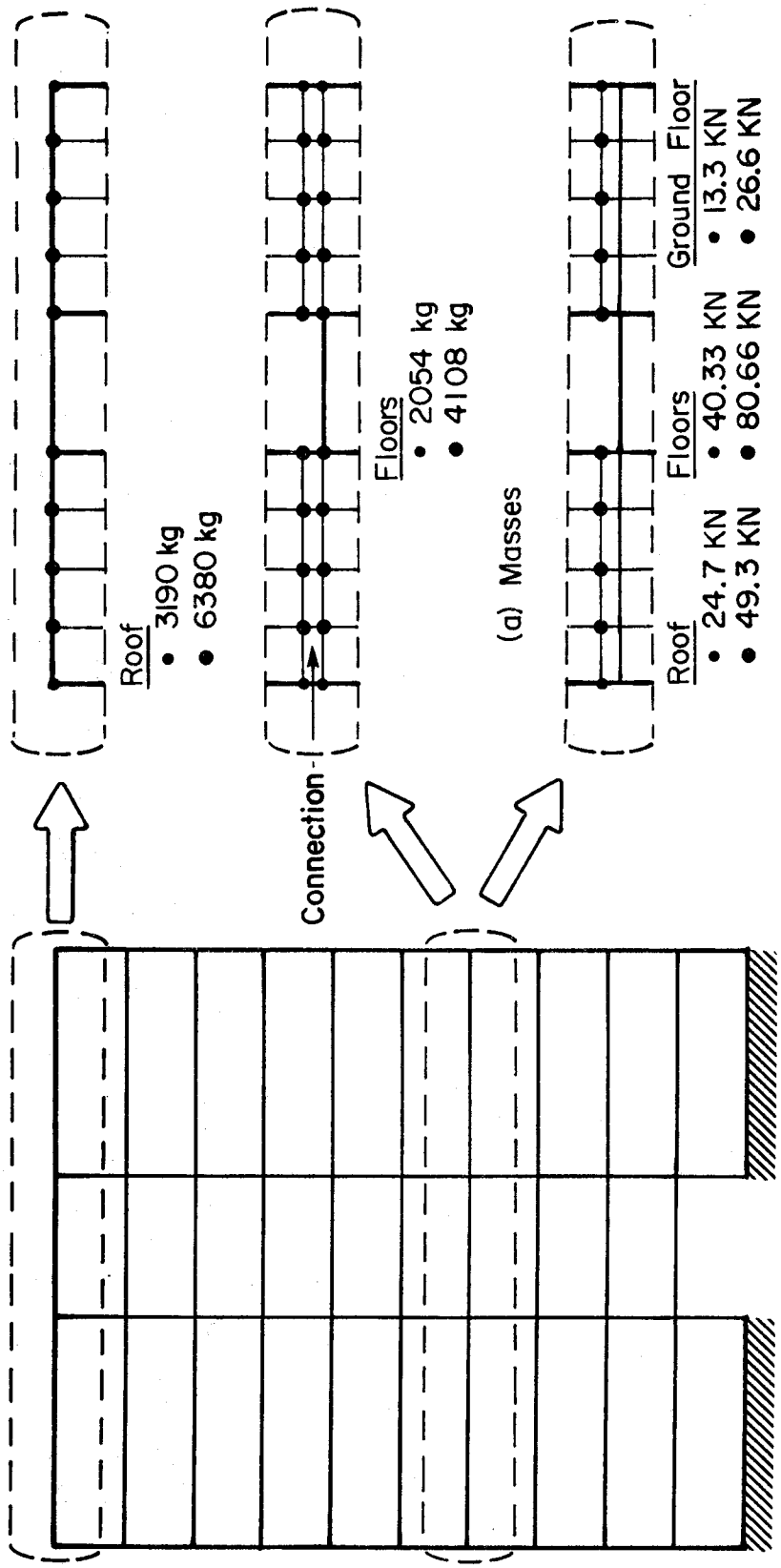

Figure 5-6 Distribution of Masses and Loads on the 10-Story Coupled Wall System

periods of vibration change throughout the analysis. As inelasticity develops in some part of the structure, softening occurs and this leads to reduced stiffness and period elongation. The elastic period of vibration for the 10-story building model under consideration is about 0.4 seconds and it is expected that the structure will undergo period elongation as yielding develops. The N-S component of El Centro was chosen as one of the accelerograms because it has almost uniform velocity spectrum peaks over the range of the fundamental periods of the structure under consideration.

Intensity of earthquake is associated with damage or potential destructiveness. Saatcioglu (1981), and Goel and Berg (1968) have used peak acceleration as a measure of intensity. In order to use a stronger earthquake (in magnitude) than the ones recorded to date, they multiplied the ordinates of the El Centro record, by a factor of 1.5. This has also been adopted for the present study. Spectrum intensity was used in this investigation as a measure of earthquake intensity. The spectrum intensity here is defined as the area under the 5%-damped relative velocity response spectrum between periods of 0.1 and 3.0 seconds. The intensities of the Taft and Pacoima Dam have been adjusted to yield a spectrum intensity equal to 1.5 times the spectrum intensity of the N-S component of the 1940 El Centro record. The response spectra for the three cases are shown in Figure 5-7 and the 10 seconds normalized

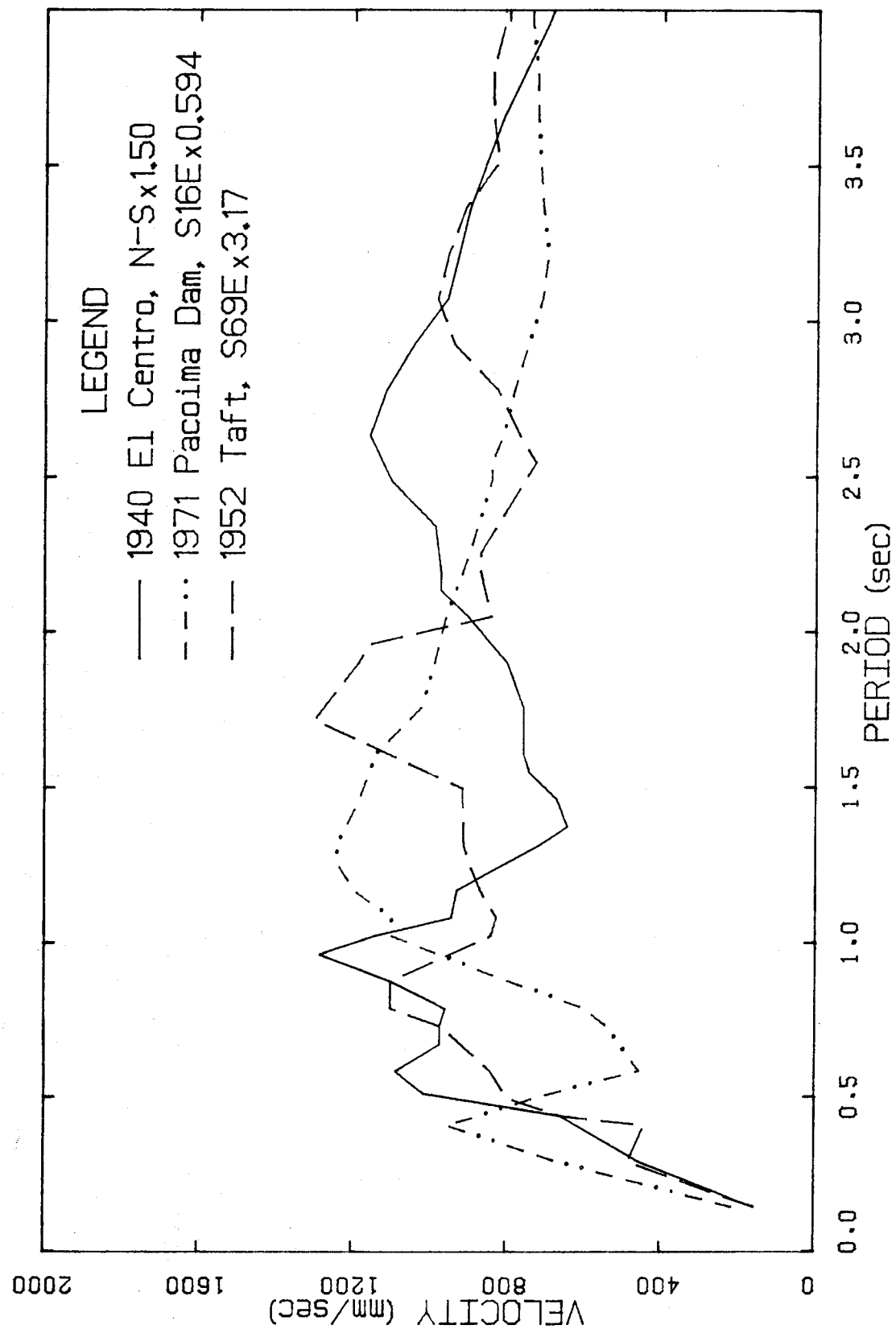

Figure 5-7 Relative Velocity Response Spectra for First 10 Seconds of Normalized Input Motions

accelerograms considered are shown in Figure 5-8.

All of the structures analysed for the parametric study were subjected to 10 seconds of ground motion. Drenink (1972) and Clough and Benuska (1964) have shown that damage to a structure is most likely to occur during the first 5 to 10 seconds of strong ground motion. The effect of duration of earthquake on the inelastic seismic response of cast-in-place coupled walls has been studied analytically by Saatcioglu (1981). He analysed the response of a 10-story cast-in-place concrete building model using the 20-second duration by repeating a 10-second accelerogram. The primary effect of earthquake duration on structural response was to increase cumulative plastic deformations. To limit the computer time required for analysis, a duration of 10 seconds of ground motion was used in the present study.

The 10 story building model described earlier was subjected to the three earthquake records mentioned above. The response of the structure was compared both in the elastic and in the inelastic range. The following computer models were selected to study the response in the inelastic range.

1. Wall panels - Linear-elastic plane stress elements
2. Connections - Zero-tension axial model
   - Shear slip model
3. Post-tensioning bars - Linear elastic truss element
4. Slender beams - Linear elastic coupling beams.

The properties of wall panels and post-tensioning were

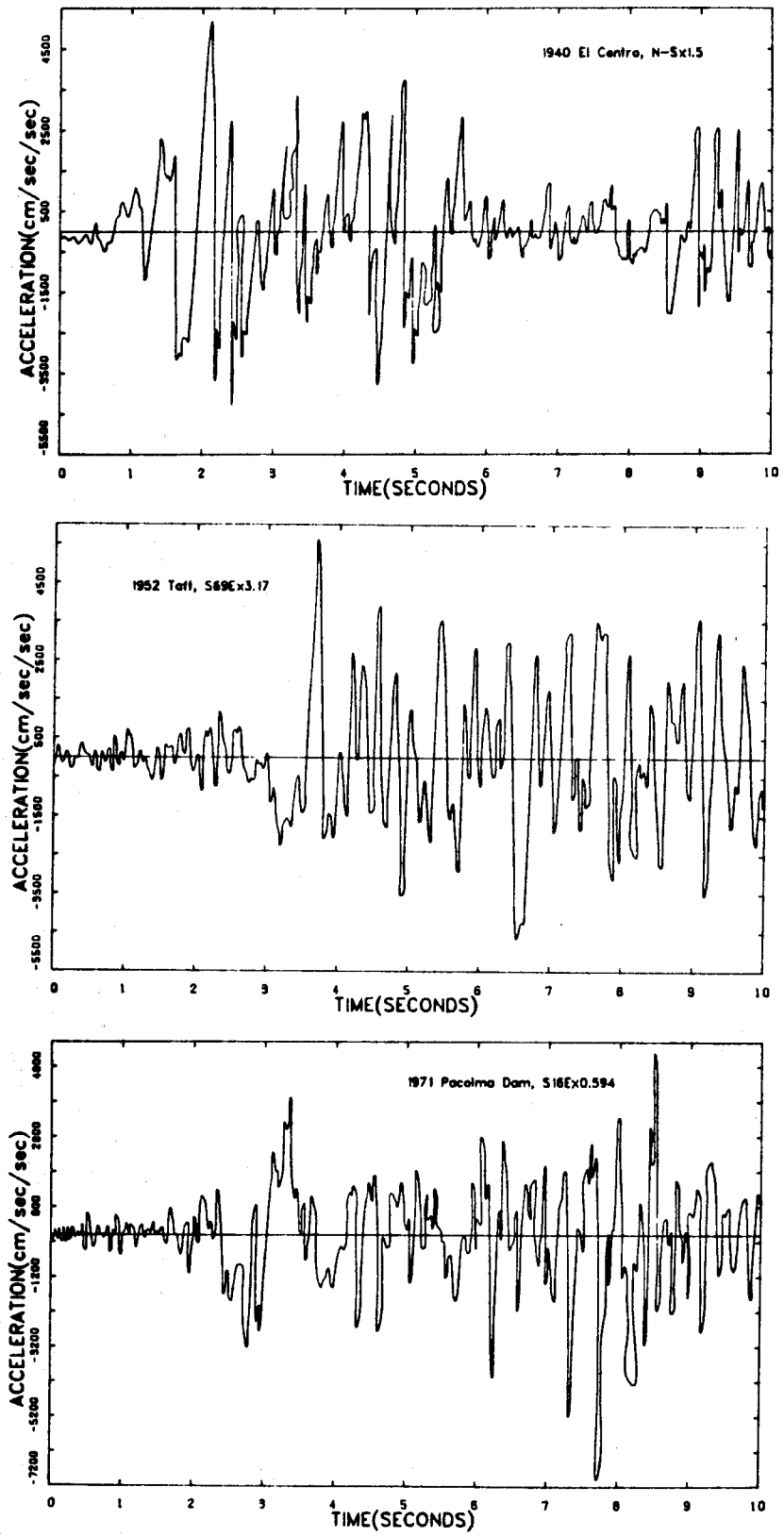

Figure 5-8 10-Second Duration Normalized Accelerograms Used for Parametric Study

described in Sections 5.2 and 5.3. The properties of the connections and coupling beams are listed in Table 5-10. Slender coupling beams were used in the analysis and vertical masses were not considered. Based on linear-elastic analysis, Figure 5-9(a) shows the maximum horizontal displacement at each story level and Table 5-11 shows the maximum forces at the base of the walls for the three different earthquakes considered. Results show that the response of Pacoima Dam is the largest followed by El Centro and Taft. A similar trend can also be seen on the velocity response spectra shown in Figure 5-7 using elastic period of vibration corresponding to the first mode.

In the inelastic range, the maximum horizontal displacements at each story level are shown in Figure 5-9(b). Due to change in the period of vibration, the trend of maximum response is different in the inelastic range compared to the elastic range. In this case, the maximum displacements for Pacoima Dam are largest followed by Taft and El-Centro. However the trend of maximum forces at the base of the walls is different than for maximum displacements as shown in Table 5-12. The main reason for this is the effect of the combination of slip and gap opening that occurs in the structure. The effect of gap opening and slip on maximum displacements and maximum forces in the walls are discussed in detail in the next chapter. The response of Taft earthquake is largest in terms of maximum forces at the base of the walls followed by El

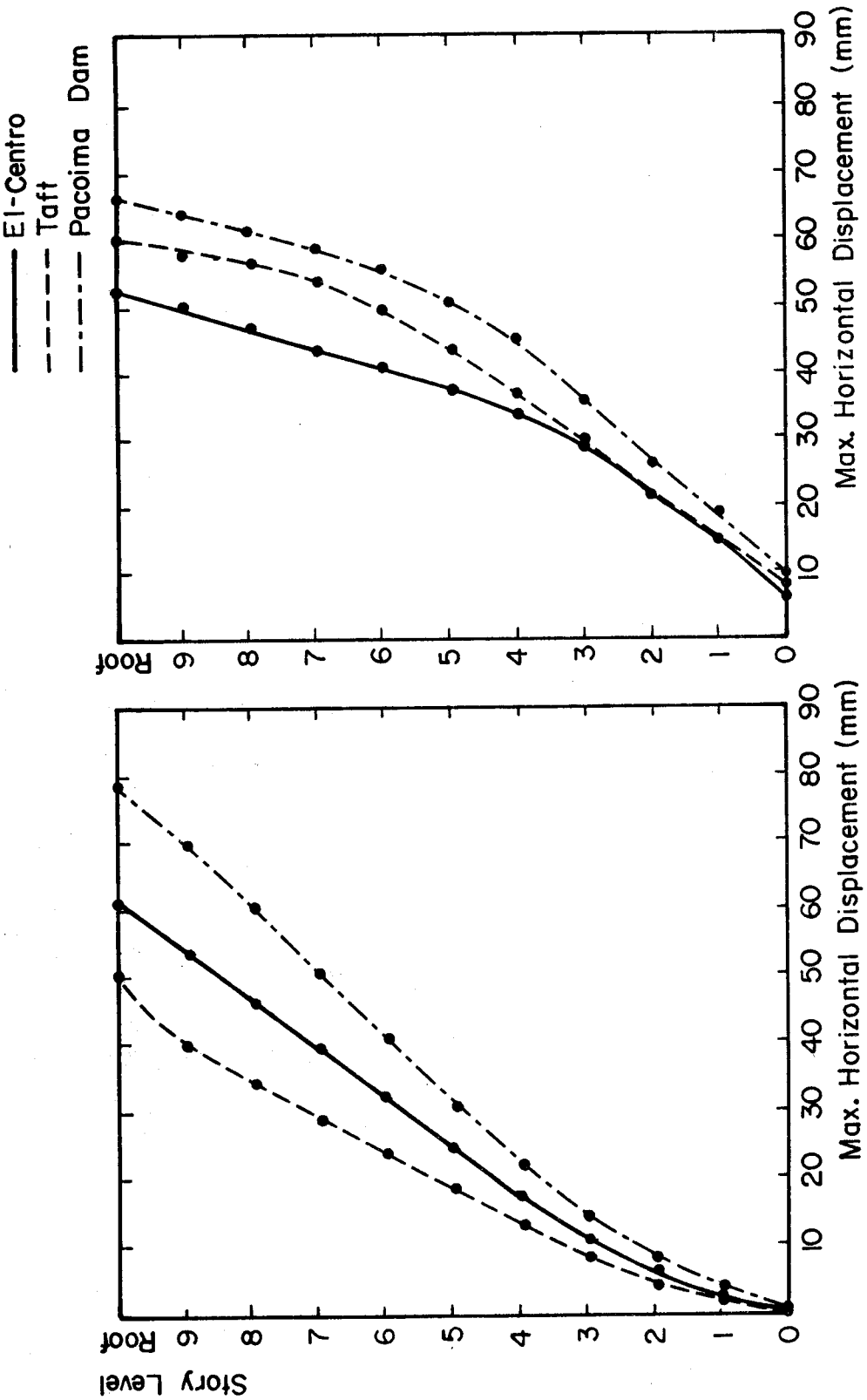

a) Linear-elastic Response

b) Inelastic Response

Figure 5-9 Effect of Different Ground Accelerograms on Maximum Displacements

Table 5.10 Properties of Connections and Coupling Beams for Selecting an Earthquake Record

Connections:

$E = 15000$ MPa

$G = 7500$ MPa

$\nu = 0$

$\mu = 0.2$

$f'_c = 15$ MPa

$G_s/G_d = 0.001$

Coupling Beams:

Flexural stiffness: $EI = 61030$ kNm^2

Axial stiffness: $EA = 3.3 \times 10^6$ kN

Shear stiffness: $GA = 3.3 \times 10^5$ kN

Strain hardening stiffness: 5%

Yield moment = 340 kNm

Table 5.11 Linear Elastic Response of 10-Story Walls Due to Different Ground Motions

Case	Roof Displ. (mm)	Base Axial Force (kN)	Base Shear Force (kN)	Base Bending Moment (kNm)
El-Centro	61.7	13 312	3295	26 974
Taft	45.1	10 364	2252	20 067
Pacoima Dam	78.9	15 922	3681	32 577

Table 5.12 Inelastic Response of 10-Story Walls due to Different Ground Motions

Case	Roof Displ. (mm)	Axial Force (kN)	Shear Force (kN)	Bending Moment (kNm)	Max Gap (mm)	Max Slip (mm)	Max % of Crack Length
El-Centro	52.14	5655	1394	13845	2.05	6.12	80
Taft	58.86	5280	1582	14885	3.37	8.15	85
Pacoima Dam	65.17	5169	1189	11772	0.77	9.75	50

Centro and Pacoima Dam. A similar trend can also be seen for gap opening as shown in Figure 5-10(a). As expected, the maximum crack lengths across the horizontal connections are in the same order as the gap opening. In terms of slip, Pacoima Dam shows the largest amount followed by Taft and El-Centro.

It was assumed that the coupling beams remain linear-elastic throughout the analysis. Figure 5-10(b) shows the maximum beam moments at each story level. The response of Taft earthquake shows the highest values followed by El-Centro and Pacoima Dam.

From the above discussion, it can be concluded that in the linear-elastic range, the response to the Pacoima Dam record is the most severe among the three selected earthquakes. However, in the inelastic range, the maximum response of the structure varies and it is more difficult to conclude which ground motion is most severe. The Taft earthquake was considered to be the most severe because the maximum forces at the base of the walls were the largest and the rocking was the most intense. For this reason, the Taft earthquake was selected as the base accelerogram for the parametric study.

5.4.3 Damping

Rayleigh damping ($C = \alpha M + \beta k$) corresponding to approximately 5% of critical damping in the first and second mode was assumed. The first two periods of vibration of the

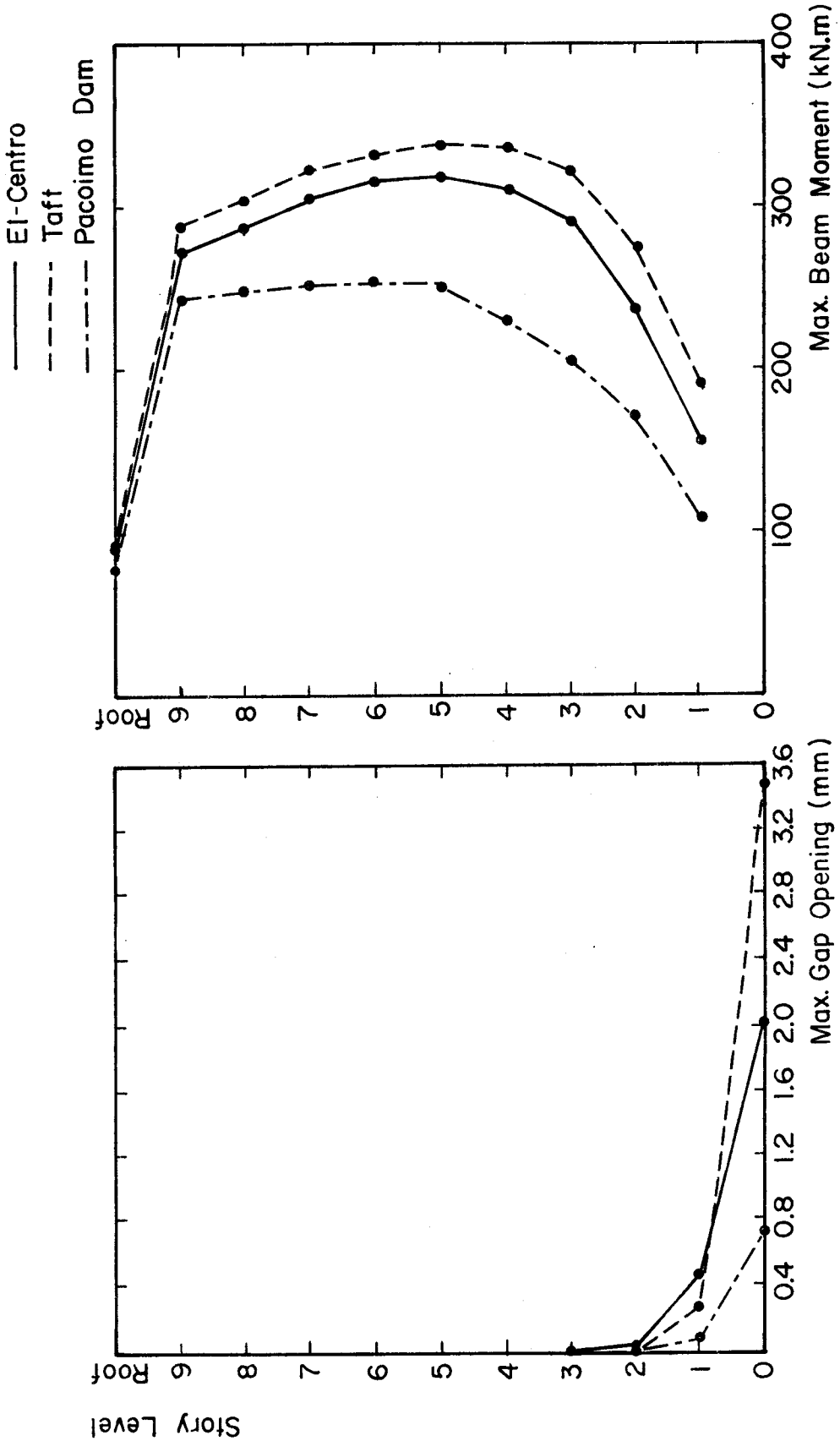

Figure 5-10 Effect of Different Ground Accelerograms on Maximum Gap Opening and Maximum Beam Moments

wall were estimated using the computer program SAPIV (Bathe et al., 1973). The periods of vibration were found to be 0.38 seconds and 0.09 seconds corresponding to the first and second mode respectively. The values of α and β were found to be 1.34 and 0.0037 respectively, using the relationships (3-1) and (3-2) described in Chapter 3. These values were used as input parameters in the computer program DRAIN-2D.

5.4.4. Integration time step

For all the analysis carried out herein, integration time steps of 0.01 seconds and 0.001 seconds were used for elastic analysis and inelastic analysis respectively. Selection of the integration time step was based on the limited studies carried out on precast coupled wall systems. Results of inelastic dynamic analysis showed that the effect of integration time step was not significant for time steps as low as 0.002 seconds. Schricker and Powell (1980) used the computer program DRAIN-2D to study the inelastic seismic response of simple wall panels. In their study they compared results with different time steps. Their results showed only small changes in computed response for time steps as large as 0.005 seconds. A similar conclusion was made regarding a study on the integration time step carried out on the structures described in Chapter 4. However, to ensure accurate results, 0.001 seconds was used as the integration time step.

5.4.5 Coefficient of friction (μ)

In all the analyses carried out in this chapter, the value of the coefficient of friction for the connection model was assumed to be 0.2. As mentioned in Chapter 2, the reported values from test results fall in the range of 0.2 to 1.81. A conservative value of the coefficient of friction was used in the analysis because of the large variation in reported test results. A low value of the coefficient of friction can also approximately account for degradation that may occur across the horizontal connections during cyclic loading.

5.5 Summary

In this chapter, the selected variables for a 10-story coupled wall structure used for parametric study were described. The range of structural parameters was selected on the basis of a simplified frame analysis using the "equivalent static load" method. An earthquake record that is critical in terms of its frequency characteristics and likely to cause most damage to the structure was selected based on the response of a structure subjected to three different earthquakes. It was shown that the S-E component of the 1952 Taft record caused the most damage to the structure and for this reason was selected as the base accelerogram for the parametric study which is described in the following chapter.

6. RESULTS OF DYNAMIC ANALYSES

6.1 General

In this chapter, the effects of structural parameters on the inelastic dynamic response of large panel coupled walls are studied. The selected properties of the structure and the variables for parametric study were described in the previous chapter.

The effect of coupling beam parameters on the response of the coupled walls is the major part of the parametric study. A series of dynamic analyses was carried out to investigate the effect of coupling beam strength and stiffness on the structural response of coupled walls. Since dynamic response is also significantly affected by behaviour of horizontal connections, analyses were made for several arrangements of reinforcement across the connections using both mild reinforcement and post-tensioning steel.

Beam strength plays a major role in the behaviour of coupled walls. Coupling beams with various yield strengths were selected to investigate the effect of beam strength on the behaviour of coupled walls. Beams of various depth/length ratios were also selected to study the effect of beam stiffness on response. The effect of the strength of the coupling beams on the response of coupled walls was studied with mild reinforcing bars and/or post-tensioning bars as vertical continuity reinforcement. The effect of the beam stiffness on response was studied assuming that

vertical continuity is provided by post-tensioning bars.

6.2 Variation in Strength of Coupling Beam

6.2.1 Response of Walls with Slender Coupling Beams

6.2.1.1 Horizontal Connections with Mild Reinforcement for Vertical Continuity

To investigate the effect of the strength of coupling beams on the response of coupled walls, identical structures except for varying degrees of coupling beam strength were analysed. In this part of the investigation, vertical continuity was assumed to be provided by reinforcing bars. The transfer of shear forces in this case is by shear friction mechanism. The following computer models were used to study the effect of beam-strength on the dynamic response of coupled walls.

1. Wall panels - Linear elastic plane stress element
2. Connections - Concrete multilinear stress-strain model
   - Elasto-plastic steel model
   - Shear-friction model
3. Slender coupling beams - Inelastic concrete beam model

Tables 5-6 and 5-7 list the properties of the connections and the coupling beams selected for this purpose. Yielding was allowed in Beam no. 1 and Beam no. 2 while Beam no. 3 remained elastic throughout the analysis. The fourth structure analysed had no coupling beams to provide results

for a simple wall.

Results of dynamic analyses showed material failure of both concrete and steel in the connection regions prior to completing the full 10 seconds of motion. The connection was considered to have failed when the mild reinforcement yielded and the concrete compressive strain exceeded the strain at maximum stress, simultaneously. Results of dynamic analyses presented here correspond to the case prior to material failure. Since structures with elastic coupling beams showed failure at an early stage, their results are not presented.

Figure 6-1(a) shows the maximum horizontal displacement at each story level. These results show that the maximum displacements for coupled walls are less than those for a simple wall. For coupled walls, variations in beam strength have only a minor effect on maximum displacements. Figure 6-1(b) shows maximum slip at each story level. In this case, the amount of slip for simple walls is generally higher than for coupled walls. Figure 6-2 shows the plots of maximum gap opening at each story level and maximum strain distribution at the base of the walls. These results show that an increase in beam yield moment results in a slight increase in gap opening at the base of the structure.

Figure 6-3 shows the effect of beam strength on maximum beam moment and maximum beam ductility factor at each story level. The ductility factor is defined here as the maximum

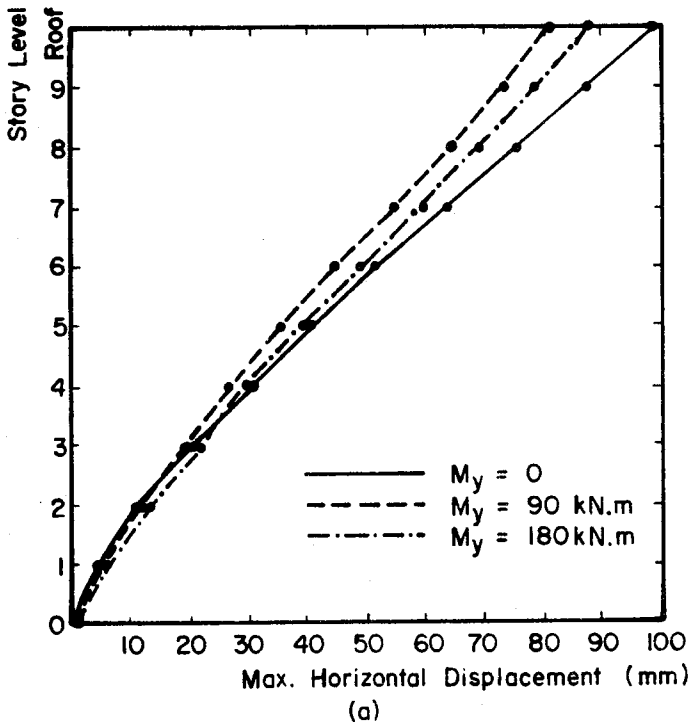

(a)

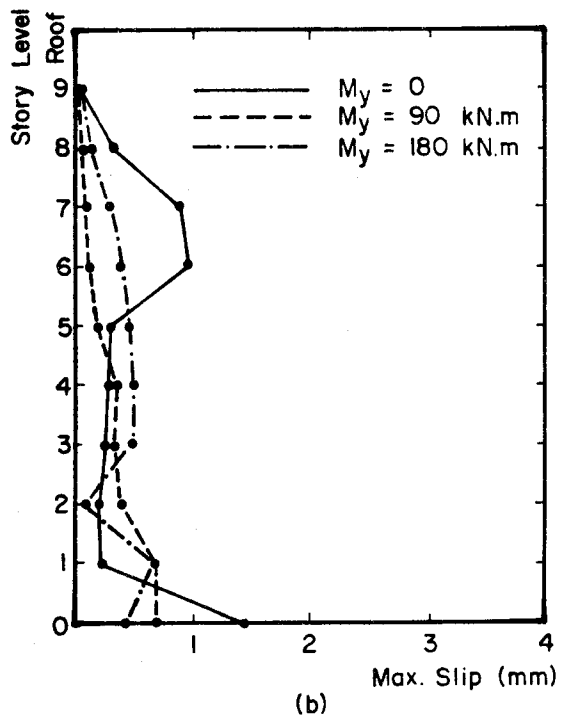

(b)

Figure 6-1 Displacement and Shear Slip Envelopes Showing the Effect of Beam Strength (Slender Beams, R.C.)

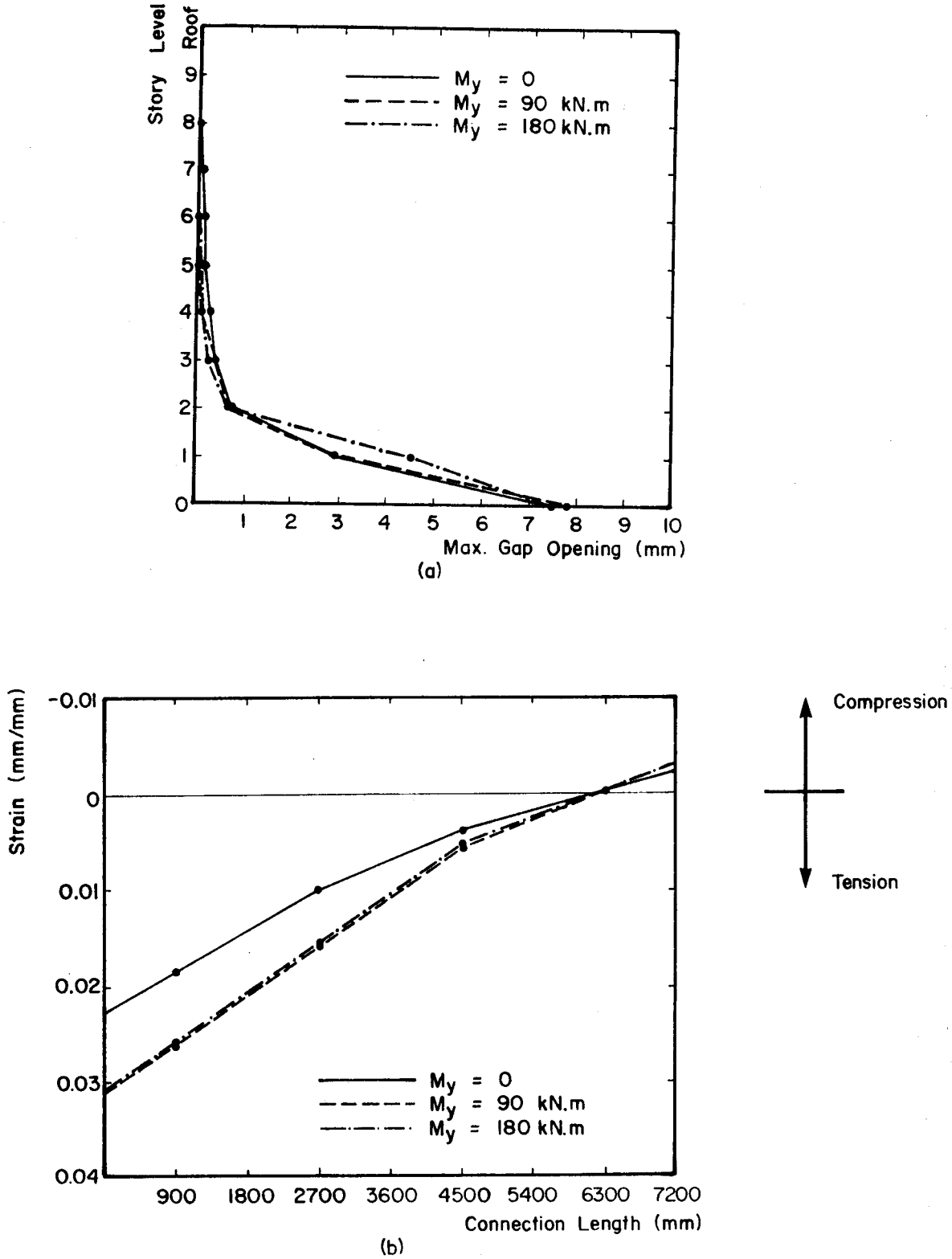

Figure 6-2 Gap Opening and Strain Distribution Showing the Effect of Beam Strength (Slender Beams, R.C.)

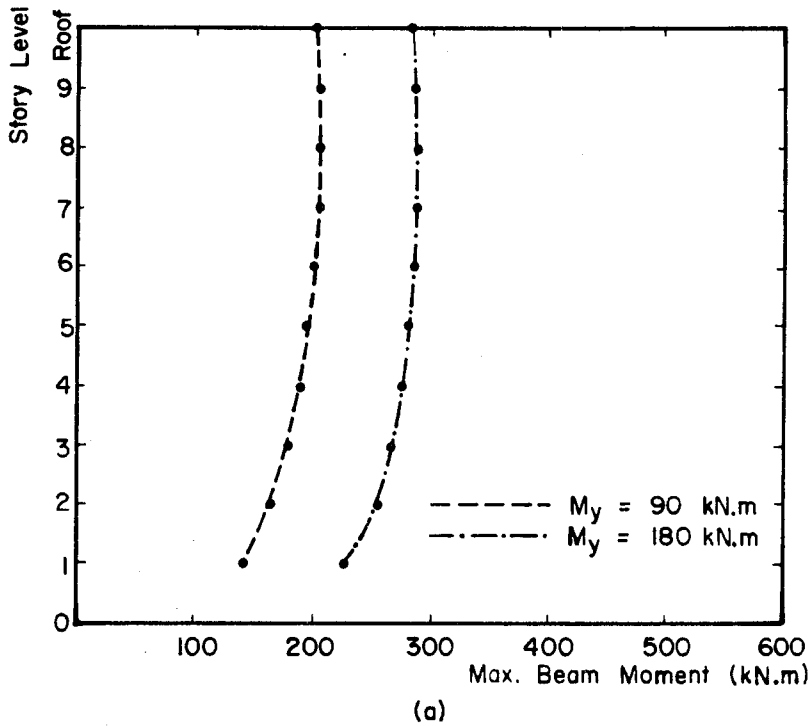

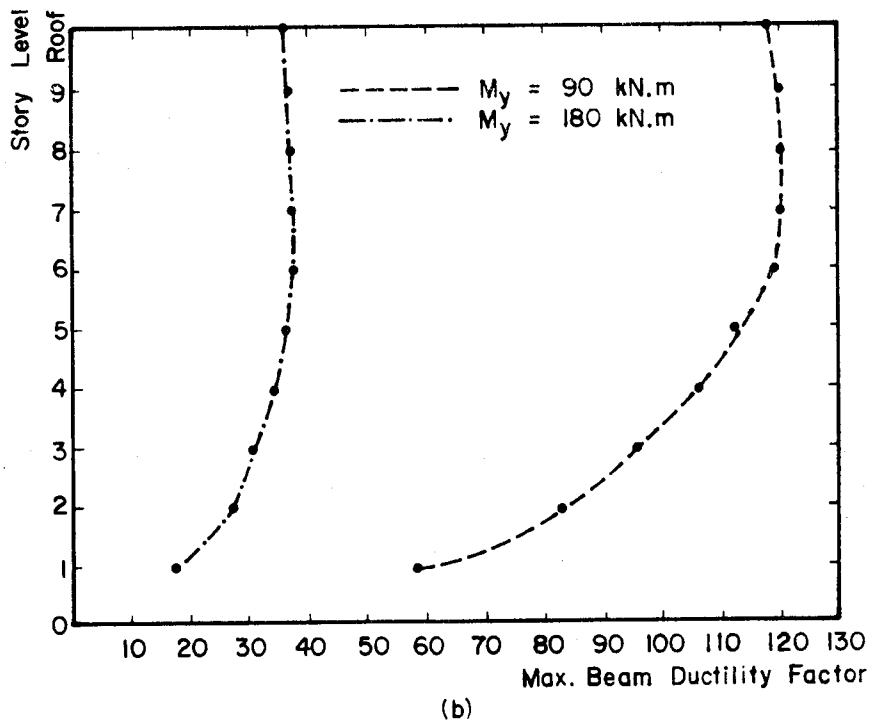

Figure 6-3 Maximum Beam Moments and Maximum Beam Ductility Factor Showing the Effect of Beam Strength (Slender Beams, R.C.)

rotation divided by the rotation at yield level. These results show that all the coupling beams yield and that maximum moments are very high compared to the yield moments. Consequently, the beam ductility demands are very large. Coupling beams with lower yield moments show higher ductility demands.

The effect of coupling beam strength on maximum axial force, shear force and bending moment at the base of the structure is shown in Table 6-1. Simple walls show lower forces than the coupled walls. Figure 6-4 shows the slip-time history response at the base of the structure and Figure 6-5 shows the displacement-time history response at roof level for the 10 seconds duration of the base acceleration. Slip at the base of the structure moves in one direction. In this case, once slip occurs, movement takes place in the same direction and the wall has a tendency to shift away from the original neutral position.

Figure 6-6 shows the time history response of base axial force, base shear force and base bending moment for a coupled wall with beam yield moment of 90 kNm. Since the two walls of the coupled wall structure are identical, their behaviour is also very similar. For this reason, the time history response shown corresponds to only one of the two walls of the coupled wall structure. The response of walls with other values of beam yield strength is illustrated in Appendix C.

Table 6-1 Maximum Base Forces for Different Values of Beam Yield Strength (Slender Beams, R.C.)

M_y	Axial Force (kN)	Shear Force (kN)	Bending Moment (kNm)
0	4984	1370	15 101
90	5187	1794	18 452
180	5767	2089	19 737

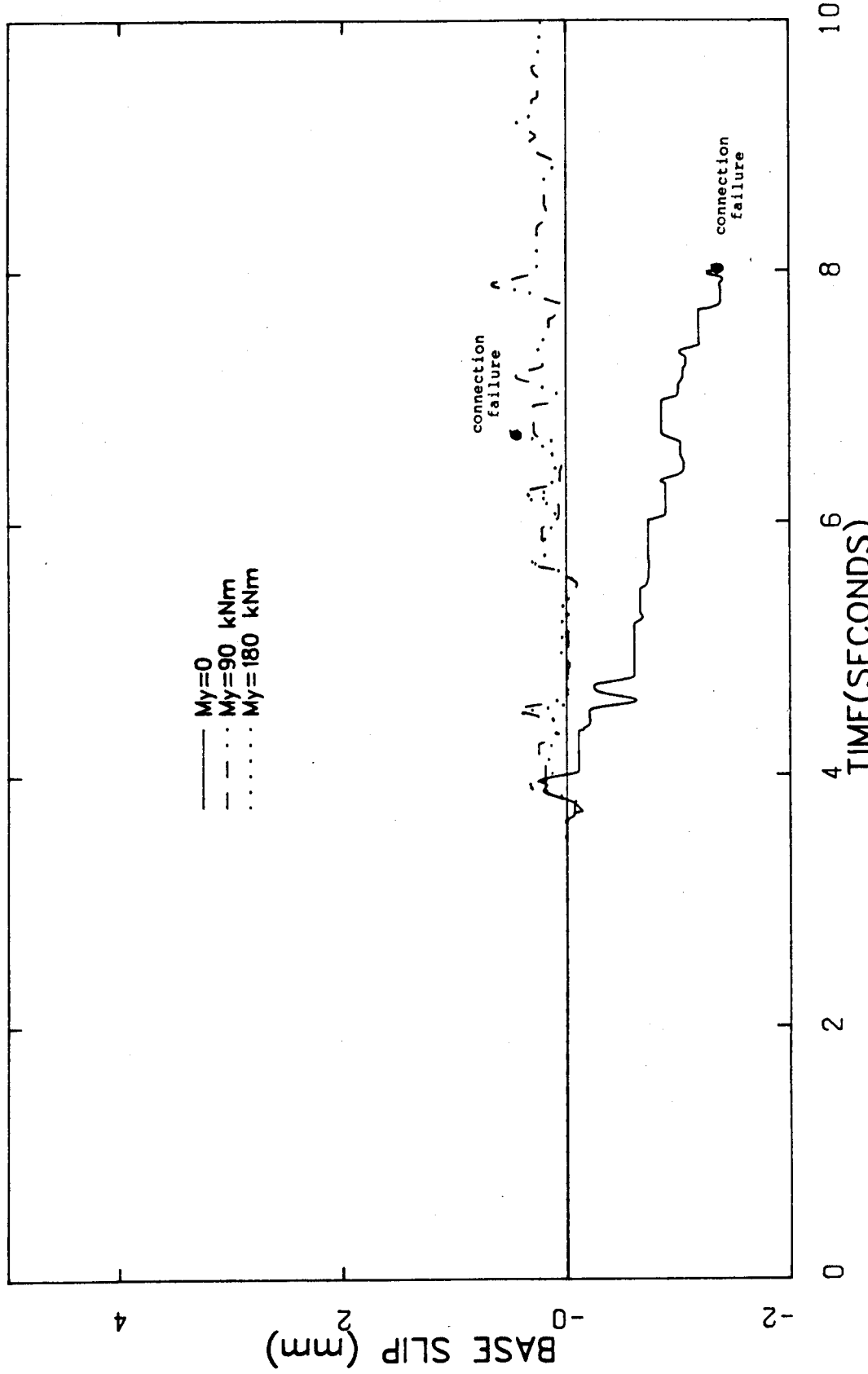

Figure 6-4 Slip-Time History Response Showing the Effect of Beam Strength (Slender Beams, R.C.)

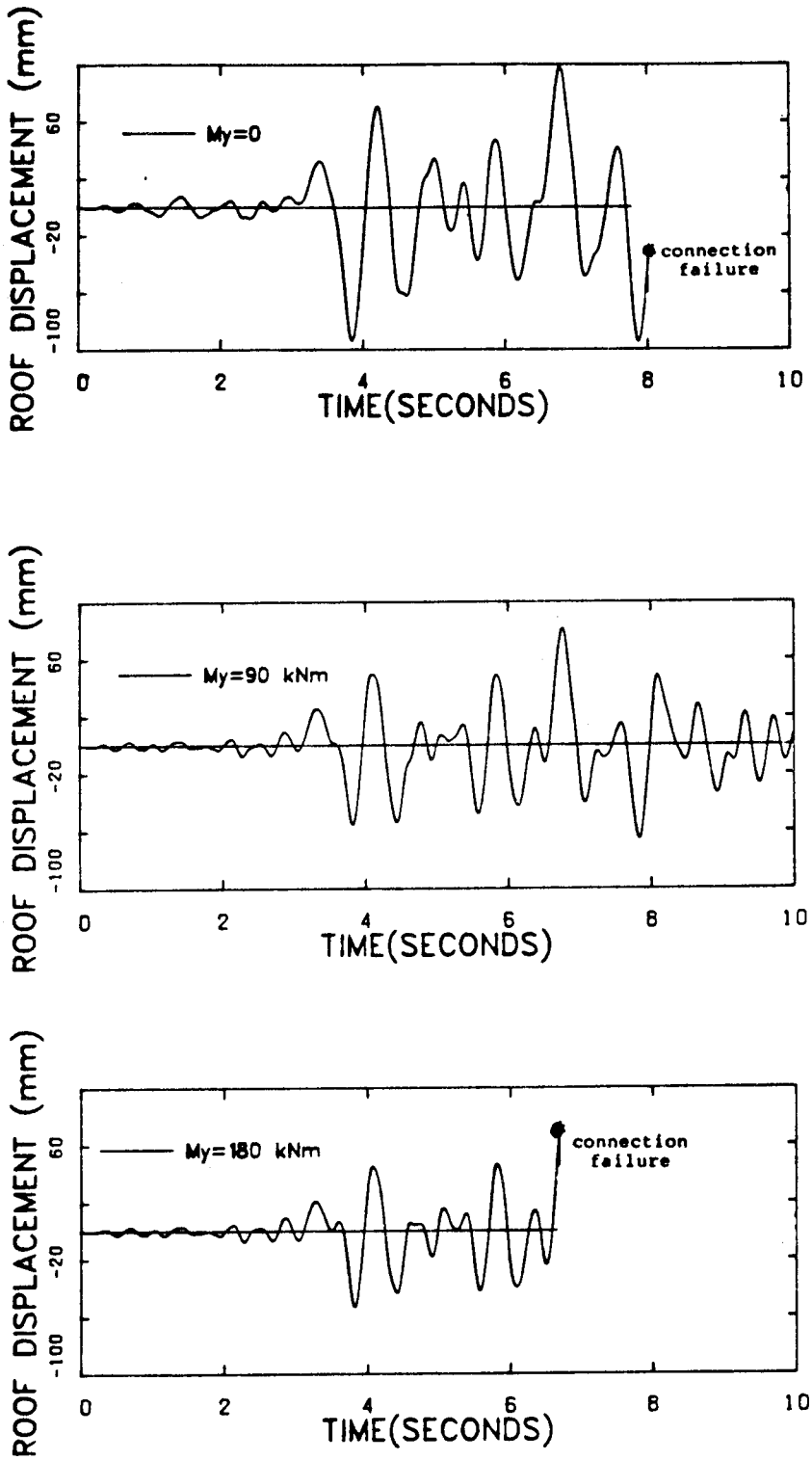

Figure 6-5 Displacement Time History Response Showing the Effect of Beam Strength (Slender Beams, R.C.)

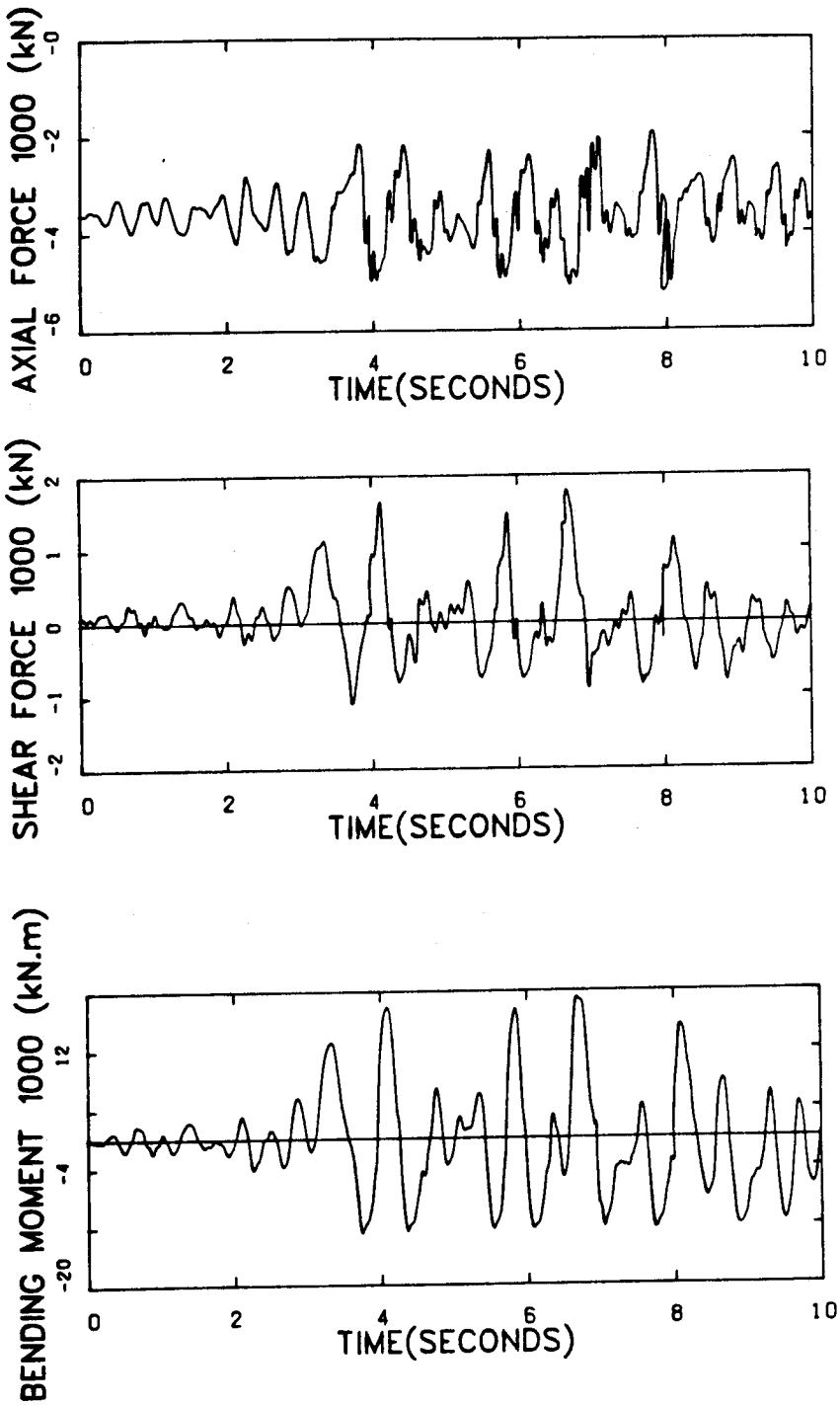

Figure 6-6 Time History Response of Base Forces (Slender Beams, M_y = 90 kNm, R.C.)

6.2.1.2 Horizontal Connections with Mild Reinforcement and Post-Tensioning for Vertical Continuity

In an attempt to reduce the amount of gap opening at the base of the walls, post-tensioning bars were combined with the mild reinforcement considered in the previous section. The amount and properties of post-tensioning are described in section 5.2.4.2. The effect of post-tensioning on maximum gap opening is shown in Figure 6-7. The results show that the maximum gap opening at the base of the structure due to the addition of post-tensioning is unchanged. However, the amount of gap opening at other story levels is reduced slightly. The response of other parameters were found to be similar to the response of those with mild reinforcing bars only.

6.2.1.3 Horizontal Connections with Post-Tensioning for Vertical Continuity

The results outlined in the section 6.2.1.1 showed that the effect of shear friction mechanism associated with mild reinforcement across horizontal joints was to increase the gap openings at the base of the structure. In some cases, a large gap opening resulted in lifting one of the walls of the coupled wall. Large gap opening developed large moments in the coupling beams. This increased the ductility demands of the coupling beams beyond practical limits. To minimize the size of gap opening, a series of analyses was made using post-tensioning as vertical continuity. The properties of

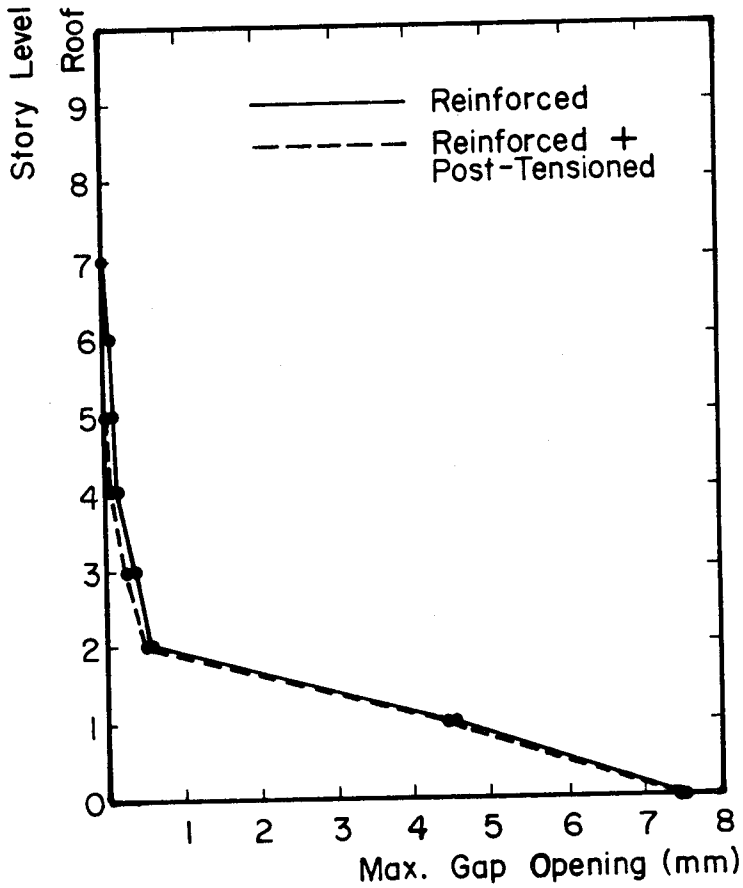

Figure 6-7 Effect of Method of Vertical Continuity on Gap Opening

beams are the same as in the previous series, as listed in Table 5-7, except that the elastic beam was replaced with a beam with a yield strength of 270 kNm. Figure 6-8 shows the maximum horizontal displacement and the maximum slip at each story level. Maximum displacement occurs in the structure with coupling beam strength of 90 kNm. The maximum slip for all structures occurs at the base or at the first story level. The values of maximum slip for all cases are very similar. Walls coupled with beams of strength of 90 kNm show lower slip at lower levels and higher slip at upper story levels.

The maximum gap opening at each story level and maximum strain distribution at the base of the walls are shown in Figure 6-9. These results show a significant drop in maximum gap opening and maximum strain distribution as the yield strength of coupling beams is increased.

The effect of beam strength on maximum beam moments and maximum beam ductility factor are shown in Figure 6-10. The increase in beam yield moments resulted in an increase in maximum moments and a decrease in beam ductility factors. Coupling beams with yield strength of 90 kNm show large ductility demands.

Table 6-2 shows the maximum forces at the base of the walls for different values of beam yield strength. Figures 6-11 and 6-12 shows a series of plots of maximum response versus the coupling beam strength. The effect of coupling beam strength on maximum slip and maximum gap opening are

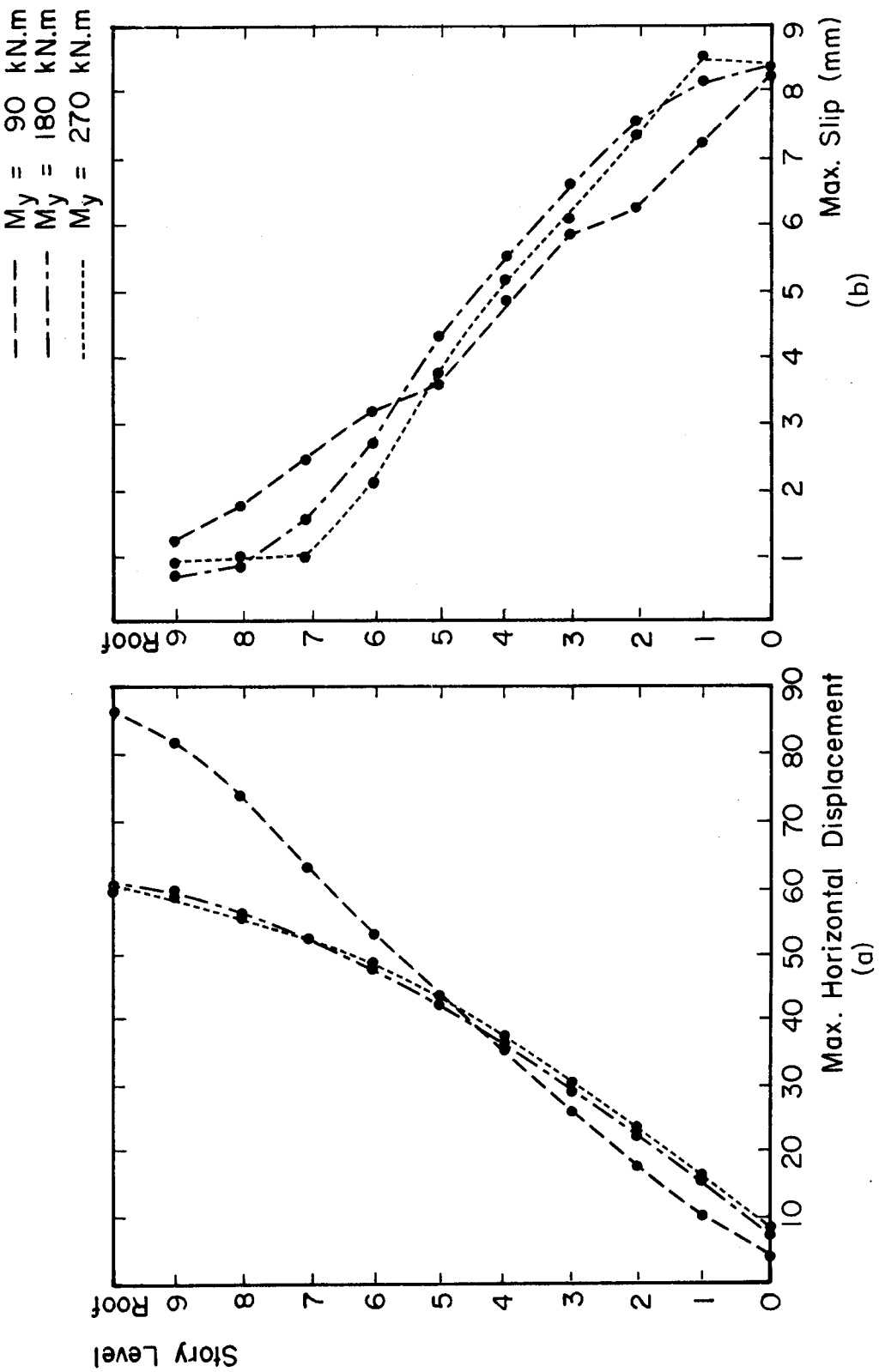

Figure 6-8 Displacement and Shear Slip Envelopes Showing the Effect of Beam Strength (Slender Beams, P.T.)

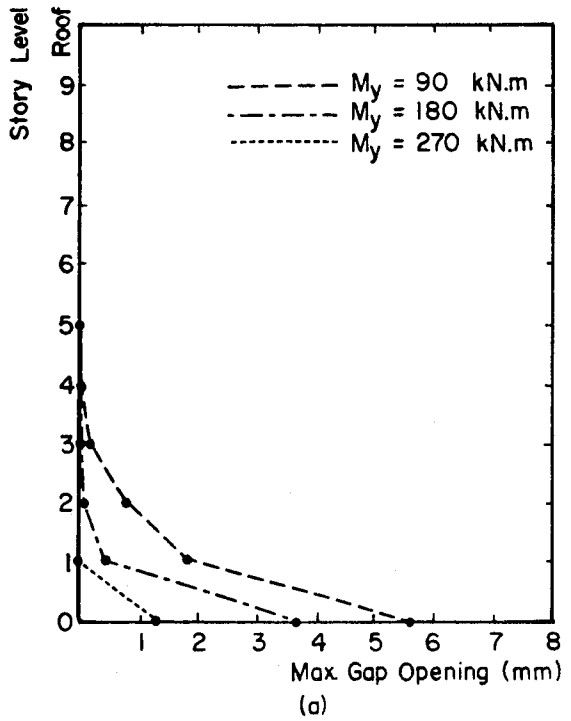

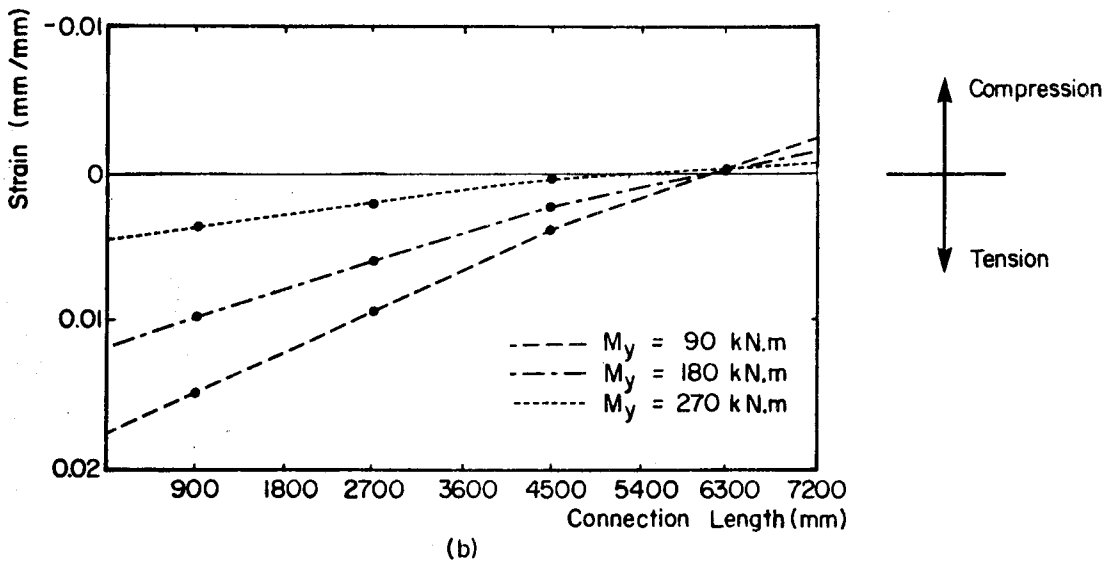

Figure 6-9 Gap Opening and Strain Distribution Showing the Effect of Beam Strength (Slender Beams, P.T.)

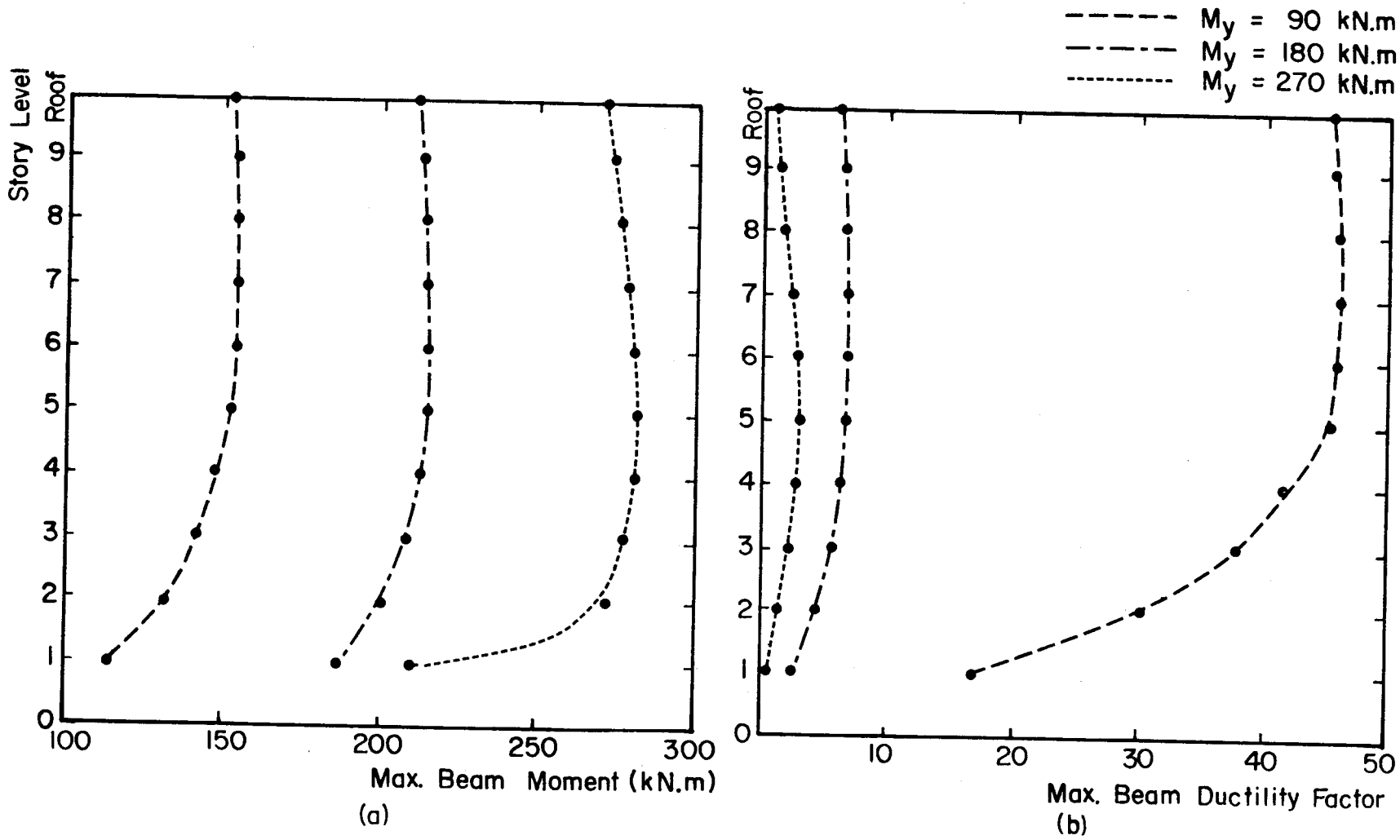

Figure 6-10 Maximum Beam Moments and Maximum Beam Ductility Factor Showing the Effect of Beam Strength (Slender Beams, P.T.)

Table 6-2 Maximum Base Forces for Different Values of Beam Yield Strength (Slender Beams, P.T.)

M_y (kNm)	Axial Force (kN)	Shear Force (kN)	Bending Moment (kNm)
0	4252	839	9967
90	4949	1271	13273
180	5422	1422	14007
270	5728	1524	14056

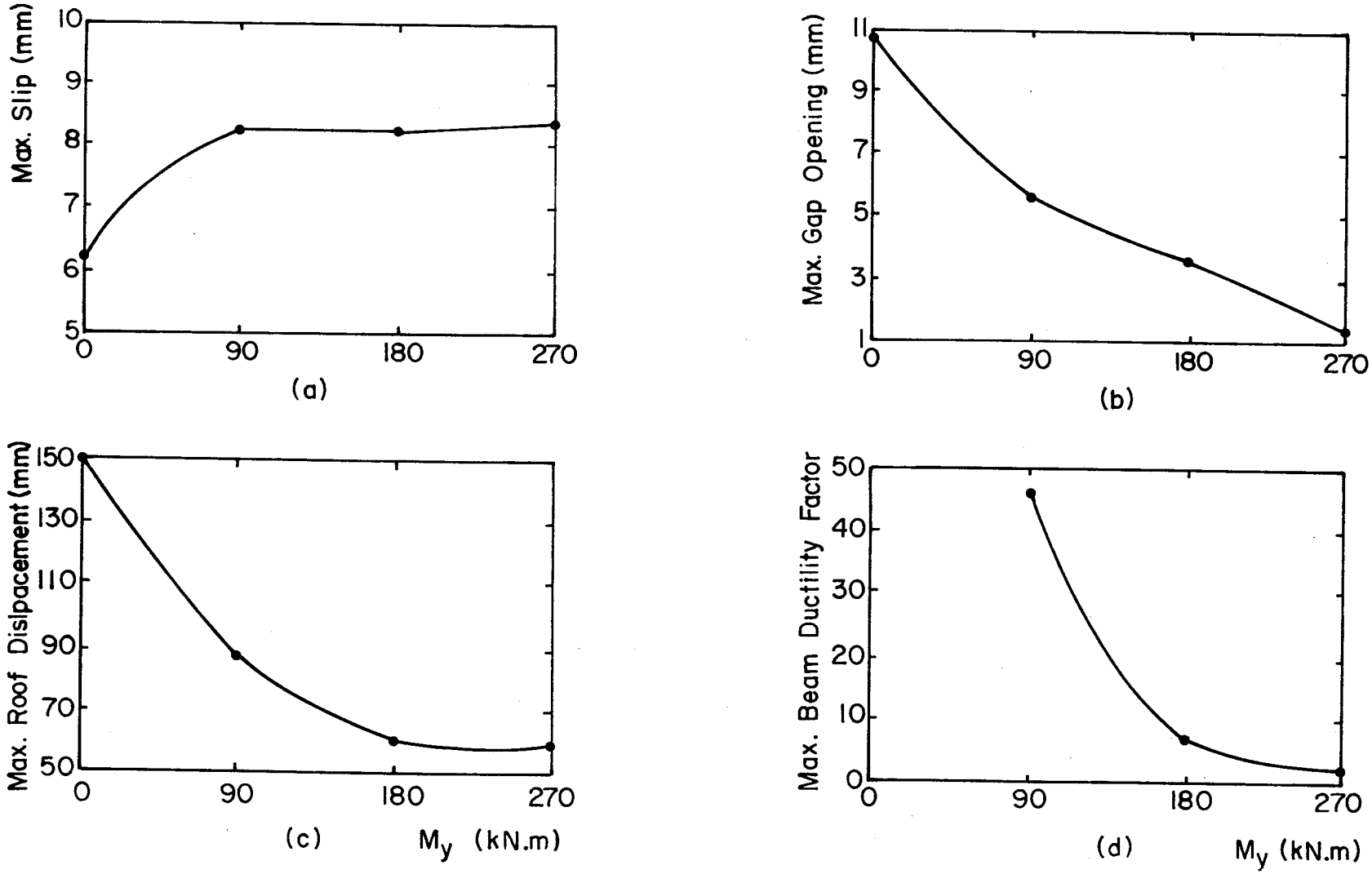

Figure 6-11 Effect of Beam Strength on Maximum Response (Slender Beams, P.T.)

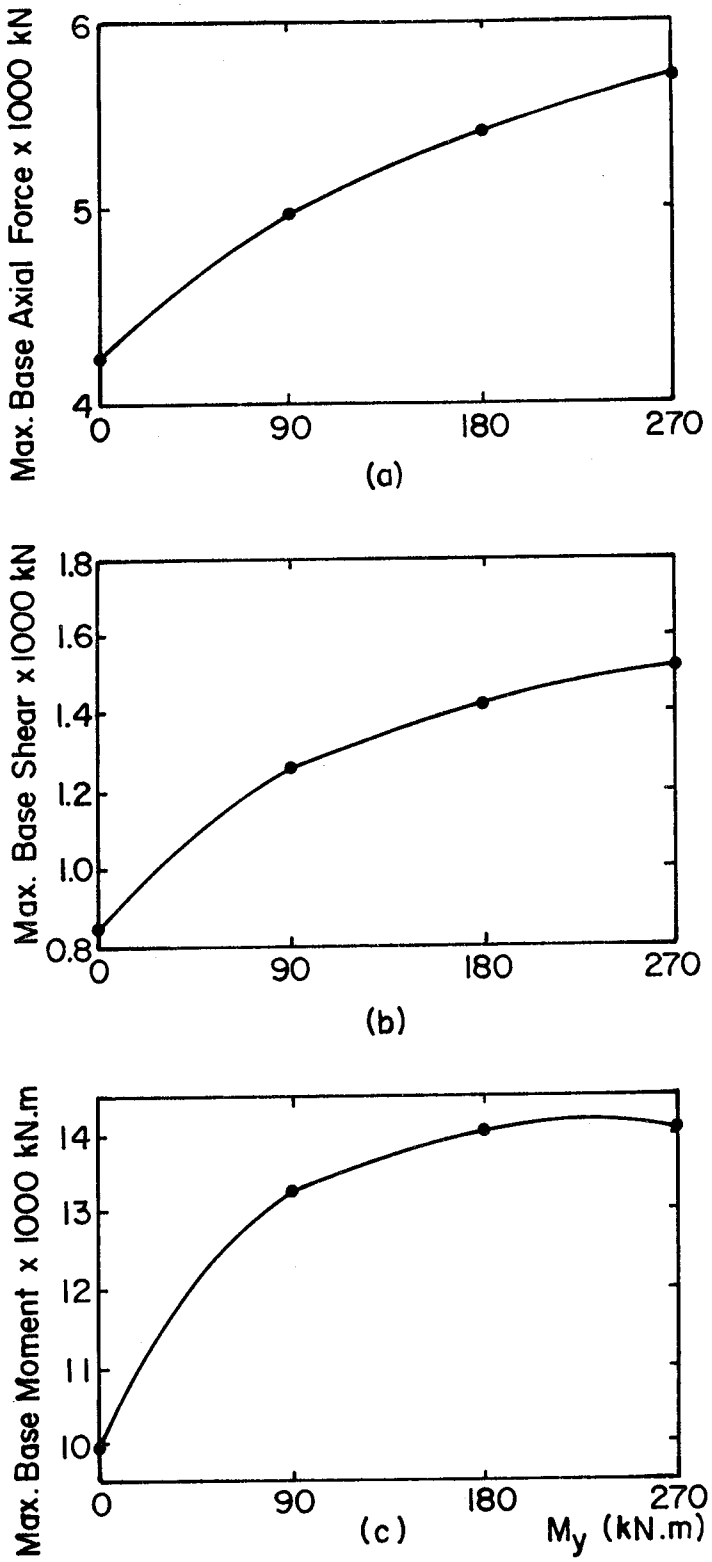

Figure 6-12 Effect of Beam Strength on Maximum Base Forces (Slender Beams, P.T.)

shown in Figures 6-11(a) and (b) respectively. The maximum roof displacements and maximum beam ductility factors decrease as the coupling beam strengths increase as shown in Figures 6-11(c) and (d), respectively. The increase in beam moments increases the maximum axial force, shear force and bending moment at the base of the walls; these are shown in Figures 6-12(a), (b) and (c), respectively.

The time history response of forces at the base of the walls are shown in Appendix C.

The effect of the strength of slender coupling beams on the behaviour of coupled walls with post-tensioning for vertical continuity are summarised as follows.

1. The increase in coupling beam strength reduced the maximum horizontal displacements. However, the maximum displacements for beams with yield strengths of 180 kNm and 270 kNm were similar. The maximum amounts of slip for all cases were similar.
2. Increase in beam strength produced a reduction in maximum gap opening.
3. As the coupling beam strength was increased, the maximum beam moments increased but the maximum beam ductility factor decreased.
4. The maximum base axial force, base shear force and base bending moments increased as the coupling beam strength was increased.

6.2.2 Response of Walls with Deep Coupling Beams

To study the effect of the strength of deep coupling beams on the response of coupled walls, a structure with beams having a length/depth ratio of 1.0 was analysed. The strength of deep coupling beams is dependent on the yield strength and area of reinforcement. Reinforcement yield strength was taken as 300 MPa and reinforcement area as 600 mm^2. In this series, only connections with mild reinforcement were considered.

The analysis of walls coupled with deep beams showed more severe response than walls with slender beams. Large gap openings as high as 12.8 mm occurred at the base of one wall leading to complete lifting of the wall at its base.

6.3 Variation in Stiffness of Coupling Beams

6.3.1 Response of Slender Coupling Beams

The effect of the initial elastic stiffness of the coupling beams on the behaviour of coupled wall structures was studied using different cross-sectional areas of coupling beams. Beams with depths varying from 600 mm up to 800 mm were selected for this purpose. The length/depth ratios of the coupling beams ranged between 3 and 4. Post-tensioning bars were assumed to provide vertical continuity across the connections. The following computer models were used in the analysis.

1. Wall Panels - Linear-elastic plane stress element
2. Connections - Concrete multi-linear stress strain

model

- Shear slip model

3. Vertical Post-Tensioning - Linear-elastic truss model

4. Beam Element - Inelastic concrete beam model.

To study the effect of the stiffness of the coupling beams, three different values of EI were selected. The properties of the connections and the coupling beams are listed in Table 5-9.

Four separate cases were considered. In the first three cases, the coupling beams were considered to have finite strength and stiffness while in the last case, the structure was idealized as a simple wall (no coupling between the walls) having the same properties and dimensions as one of the walls of the coupled wall system. The yield strength of coupling beams were 180 kNm.

Figures 6-13 shows the envelopes of maximum displacement and maximum slip at each story level. Figure 6-13(a) shows that the effect of increase in beam stiffness is to reduce the maximum horizontal displacements. In this case the maximum roof displacement is reduced by at least 56% due to the effect of coupling. Figure 6-13(b) shows the maximum shear slip at each story level. These results indicate that the amount of slip in the structures with coupling beams is larger than for the structure with no coupling beams (i.e. simple wall). These results also show that in most cases, the maximum slip occurs at the base of

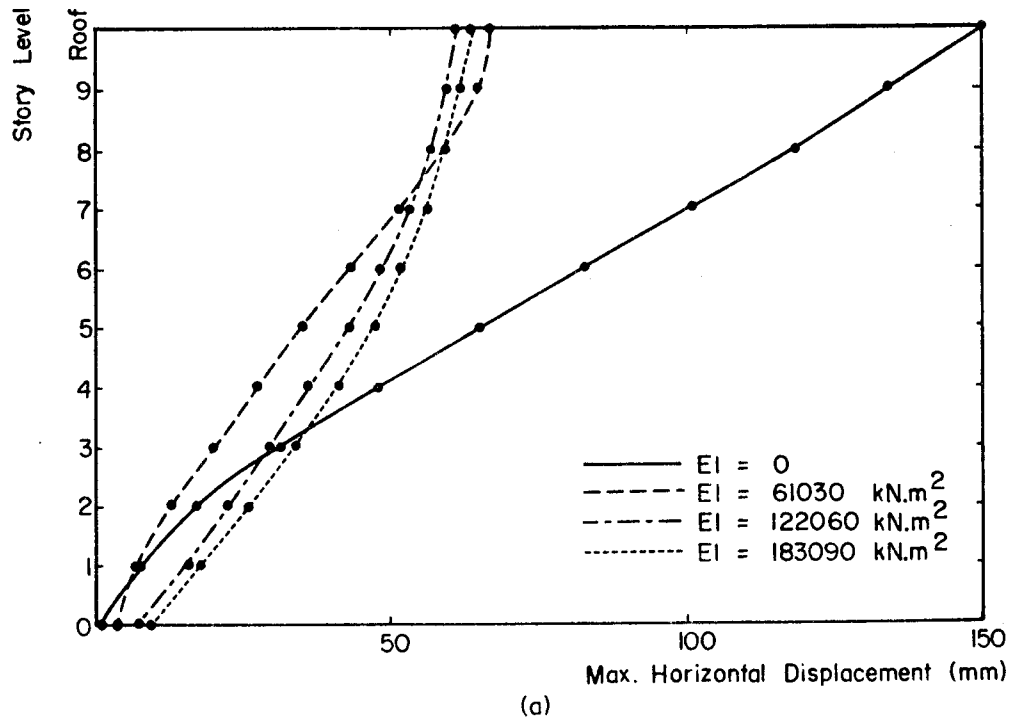

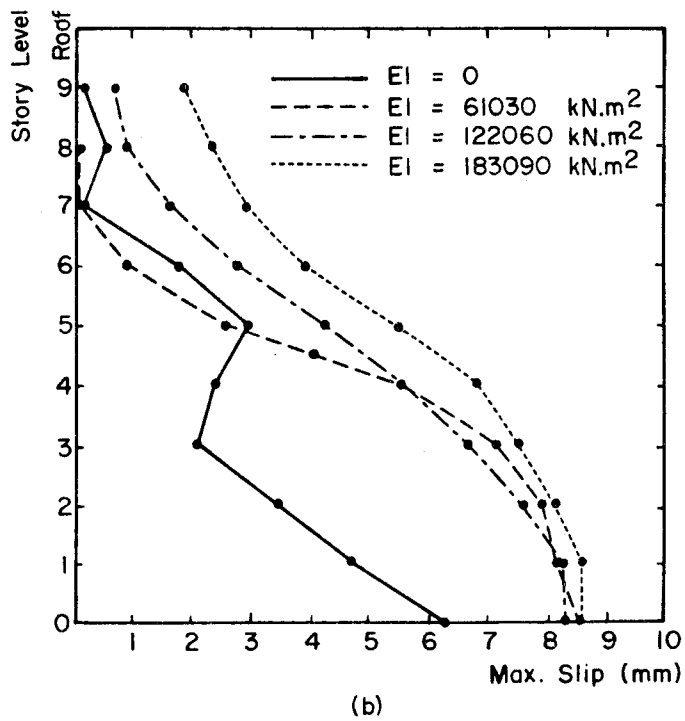

Figure 6-13 Displacement and Shear Slip Envelopes Showing the Effect of Beam Stiffness (Slender Beams, P.T.)

the structure and that slip decreases with increasing story level.

Figure 6-14 illustrates the maximum gap opening at each story level and the maximum strain distribution at the base of the structure. Maximum gap openings occur at the base of the structure as shown in Figure 6-14(a). These results also show that the amount of gap opening for coupled wall structures is considerably lower than for the structure with no coupling beams. In this case, the amount of gap opening has been reduced by at least 66% due to the effect of coupling. However, variation of the beam stiffness within the range considered does not yield a significant effect on the gap opening. Figure 6-14(b) shows the maximum strain distribution at the base of a wall for a coupled wall structure. In this case, the maximum compressive strain at the corner of the wall was calculated assuming linear strain distribution. Using this assumption, the maximum compressive strain at the corner of the simple wall was 0.007 which is very close to the assumed ultimate concrete strain capacity of 0.008. For coupled wall structures, the maximum compressive concrete strain was found to be 0.0018. This value is less than the maximum concrete compressive strain of 0.002 at maximum stress. The maximum crack length along the connections were found to be approximately 85% of the total connection length at the base of the structure for the simple wall and the coupled walls.

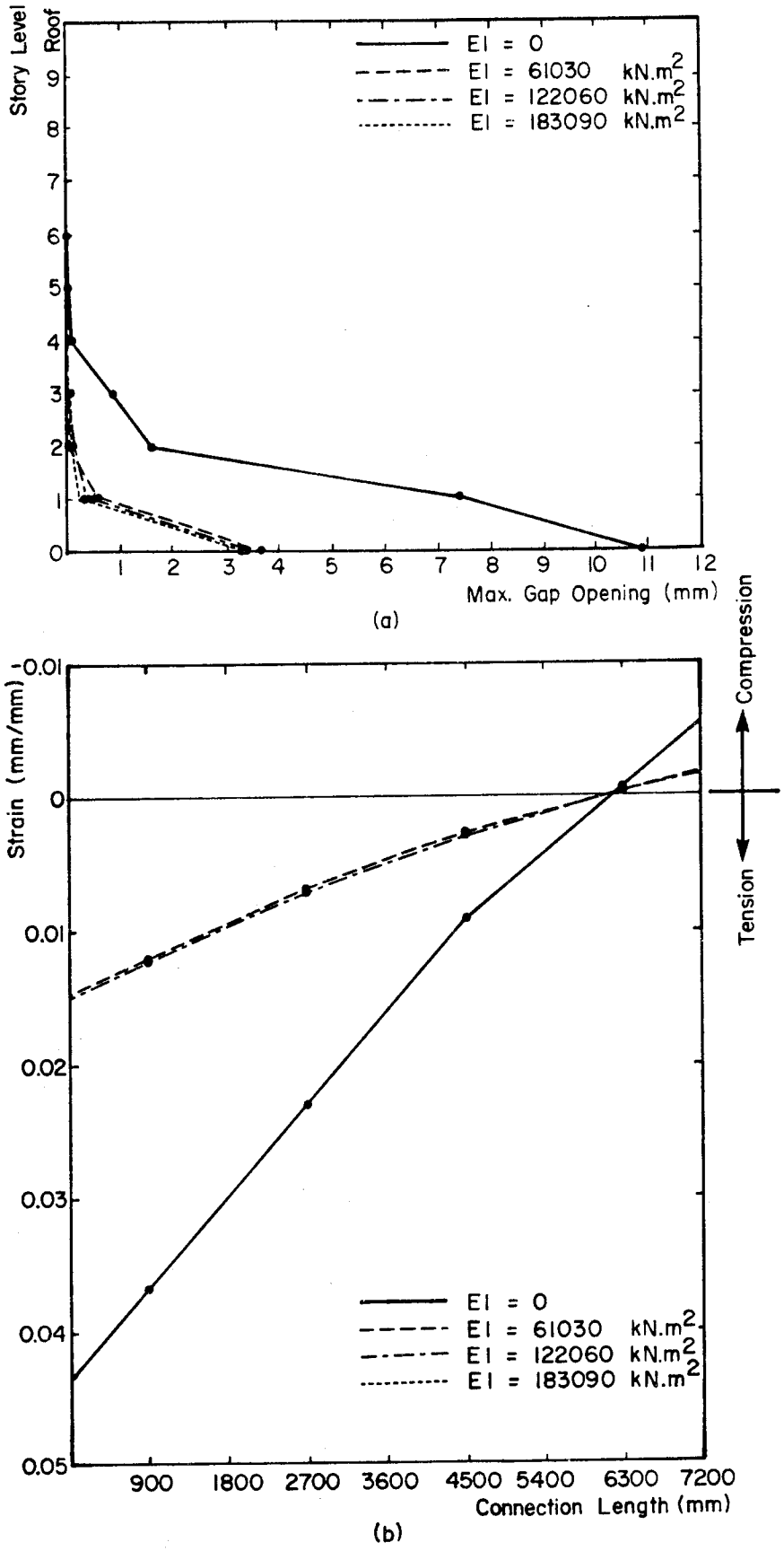

Figure 6-14 Gap Opening and Strain Distribution Showing the Effect of Beam Stiffness (Slender Beams, P.T.)

Figures 6-15(a) and (b) show the maximum beam moment and the maximum beam ductility factor respectively at each story level. The increase in beam stiffness results in an increase in beam moments and beam ductility factor. In this investigation, the rotational ductility factor is used as a measure of inelastic action and is defined as the maximum rotation divided by the rotation at yield level.

Table 6-3 shows the maximum forces at the base of the walls for different coupling beam stiffness values. Figure 6-16 shows a series of plots that indicate the effect of beam stiffness on the structural response. Figure 6-16(a) shows the response corresponding to maximum base slip. These results show that the effect of variations in initial beam stiffness on the amount of slip is insignificant for the range considered. However when there is no coupling between the walls, the amount of slip is considerably less compared to coupled wall systems. A plot of maximum horizontal displacement versus beam stiffness is shown in Figure 6-16(c). The maximum displacements are considerably lower for coupled walls than for simple walls. However, the effect of variation in beam stiffness on maximum displacement is not very significant. The effect of beam stiffness on the maximum values of the base axial force, base shear force and base bending moment are shown in Figures 6-17(a), (b) and (c), respectively. The increase in beam stiffness shows an increase in forces at the base of the structure. The simple wall shows lower forces than the

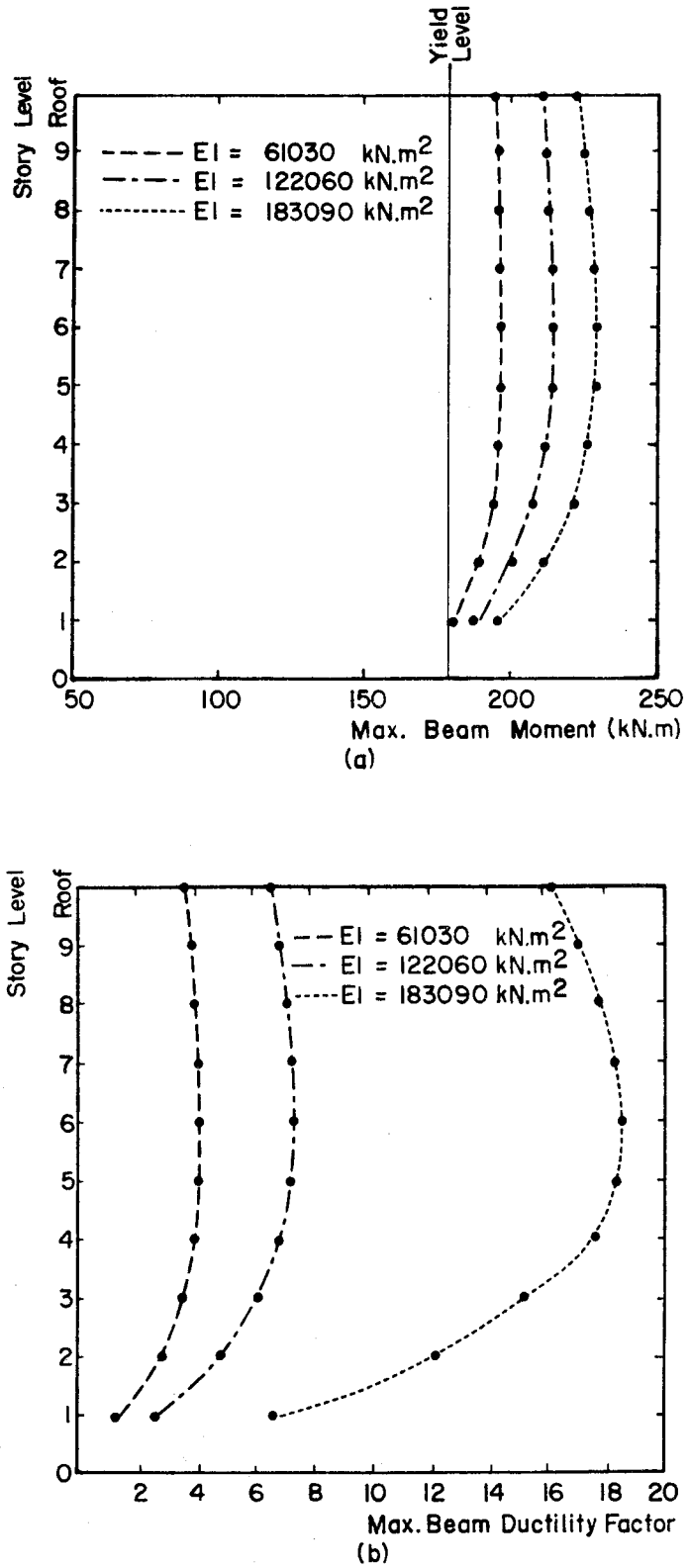

Figure 6-15 Maximum Beam Moments and Maximum Beam Ductility Factor Showing the Effect of Beam Stiffness (Slender Beams, P.T.)

Table 6-3 Maximum Base Forces for Different Values of Beam Initial Stiffness (Slender Beams, P.T.)

EI (kNm^2)	Axial Force (kN)	Shear Force (kN)	Bending Moment (kNm)
0	4252	839	9967
61030	5370	1382	13687
122060	5422	1422	14007
183090	5465	1444	14115

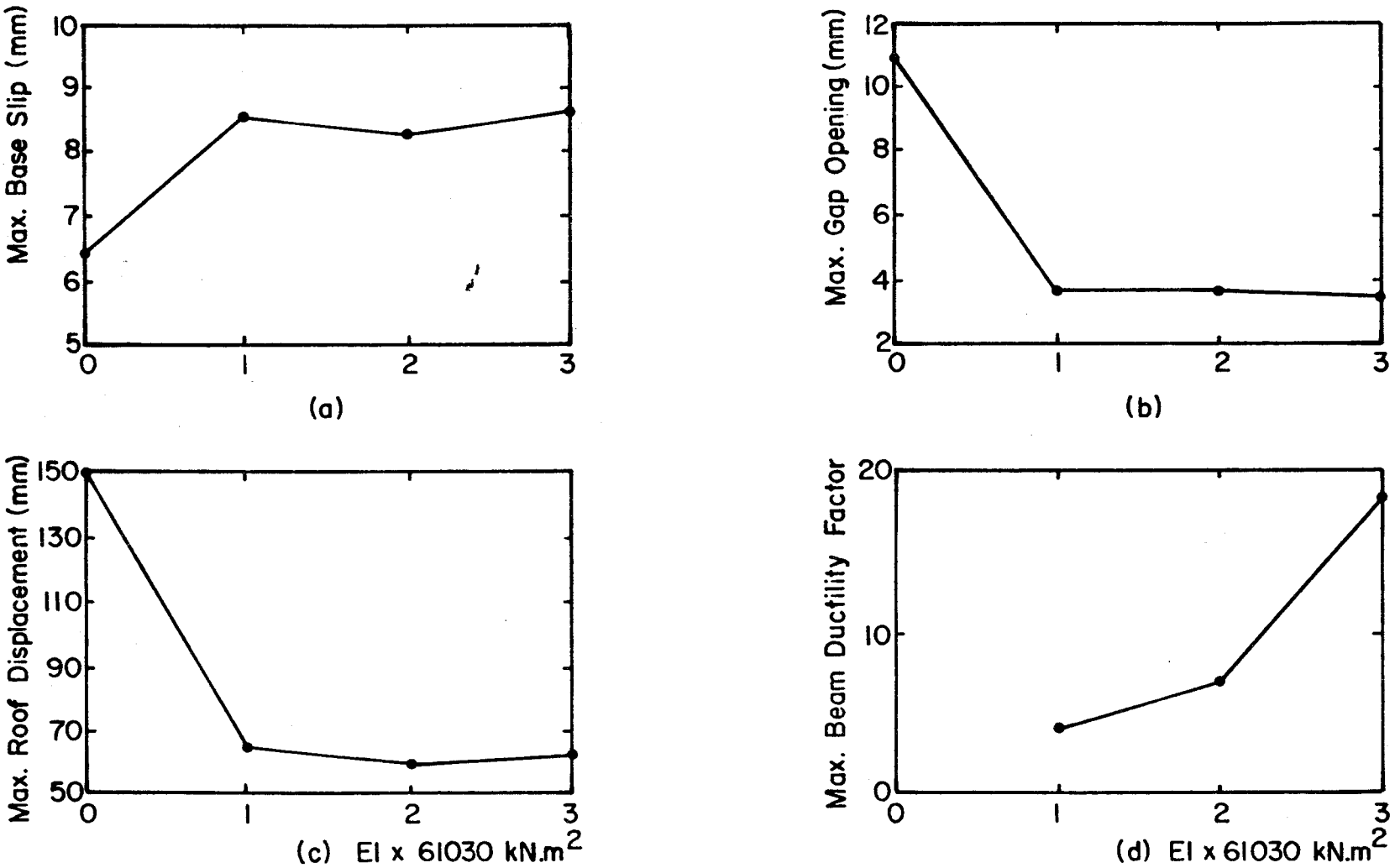

Figure 6-16 Effect of Beam Stiffness on Maximum Response (Slender Beams, P.T.)

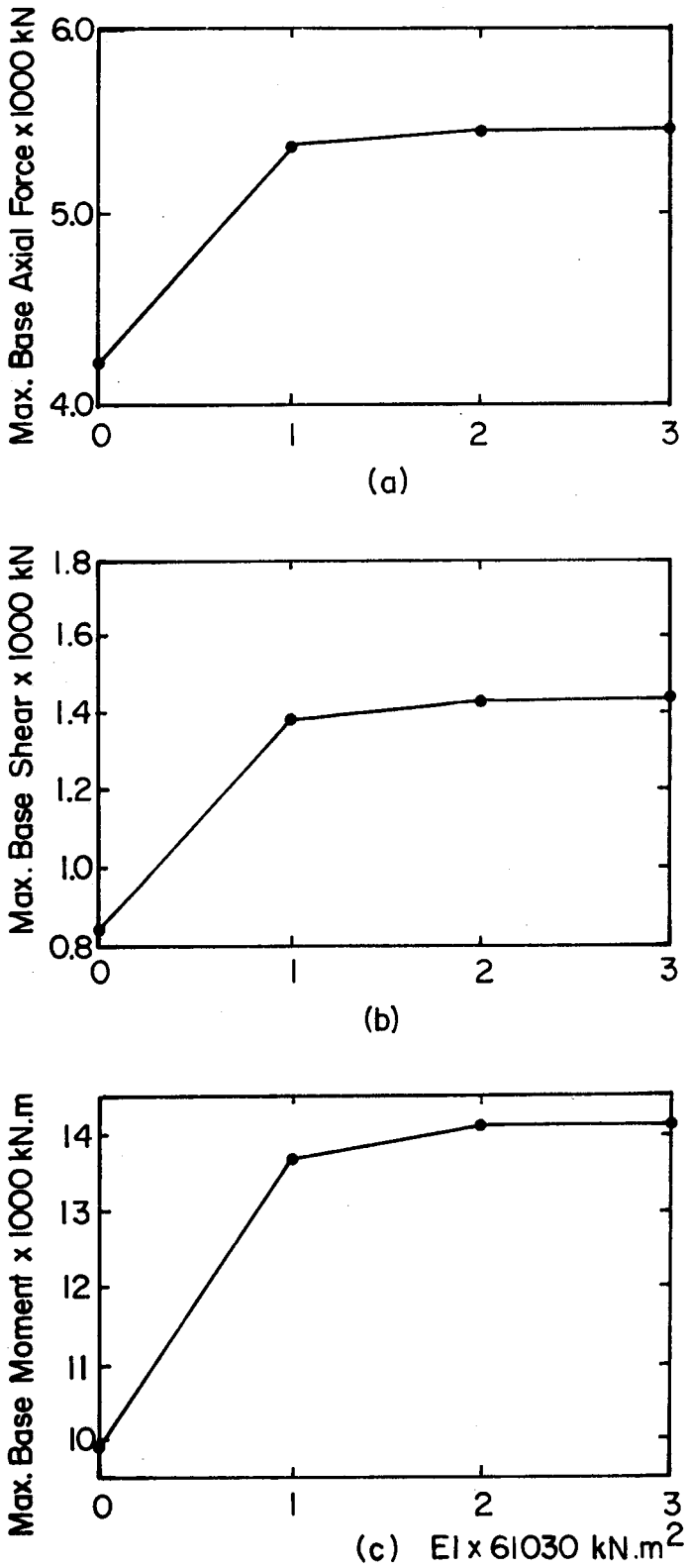

Figure 6-17 Effect of Beam Stiffness on Maximum Base Forces (Slender Beams, P.T.)

coupled walls.

The effect of beam stiffness on the time history response of the structures is illustrated in Figures 6-18 and 6-19. Figure 6-18(a) compares the time history response of roof displacement of a simple wall and a coupled wall of finite beam stiffness. These results show a dramatic reduction in peak displacements due to the effect of coupling. There is also a slight change in the period of vibration. Figure 6-18(b) shows the displacement time history response corresponding to three different values of beam stiffness. These results indicate that the effect of variation in beam stiffness on peak displacements is minor. Figure 6-19(a) compares the time history response of slip at the base of a simple wall and of a coupled wall structure. These results show that the amount of slip for the coupled wall is higher than for the simple wall. However, towards the end of the analysis, the amount of slip in the coupled wall structure drops significantly. These results also show that the slip has a tendancy to accumulate in one direction. Figure 6-19(b) shows that the effect of variation of initial beam stiffness on shear slip is not significant for the range considered.

Figure 6-20 and 6-21 show a series of plots showing the time history response of axial force, shear force and bending moment at the base of the structure. These results represent the response of a simple wall and a coupled wall with beam flexural stiffness, EI = 61030 kNm^2. The time

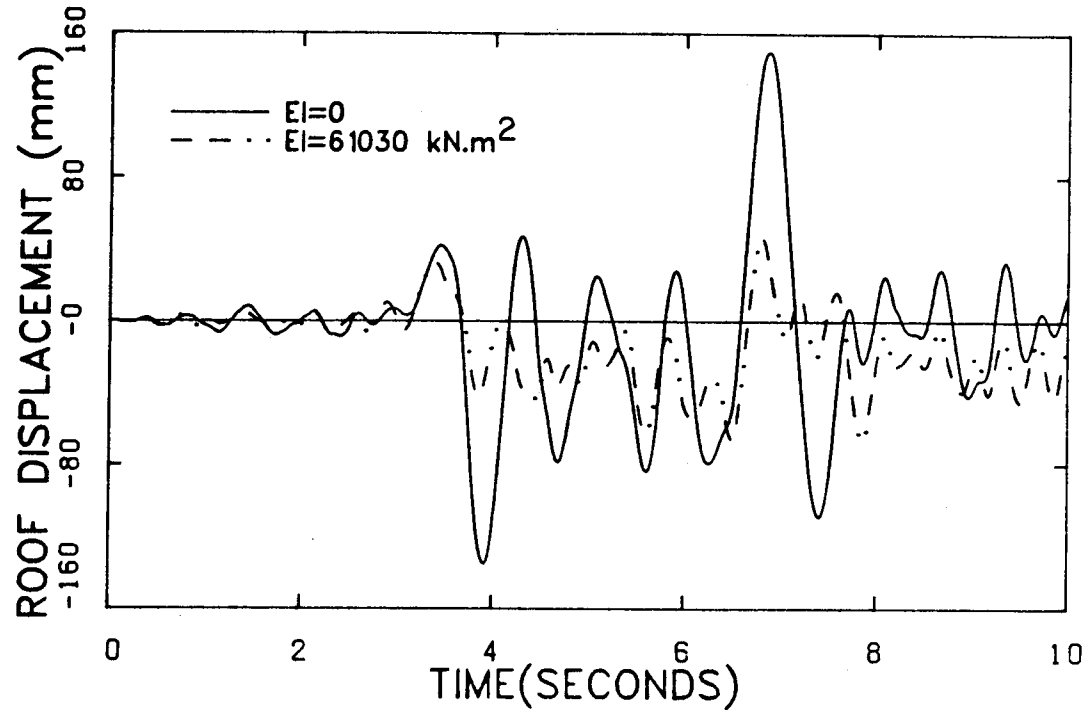

(a)

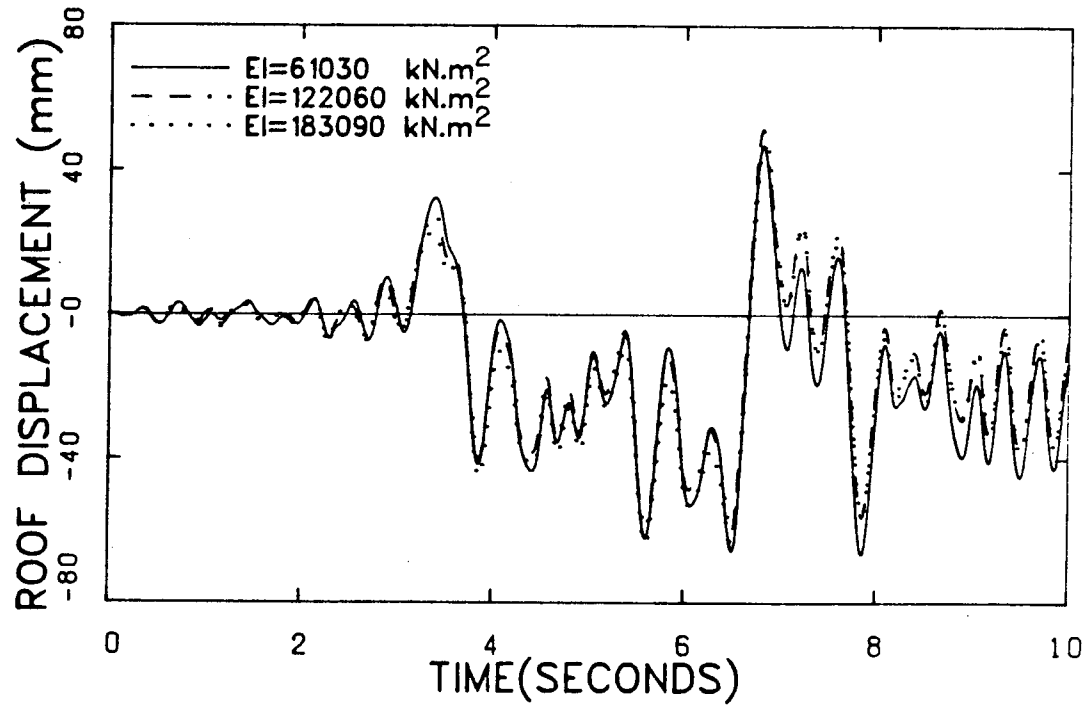

(b)

Figure 6-18 Displacement-Time History Response Showing the Effect of Beam Stiffness (Slender Beams, P.T.)

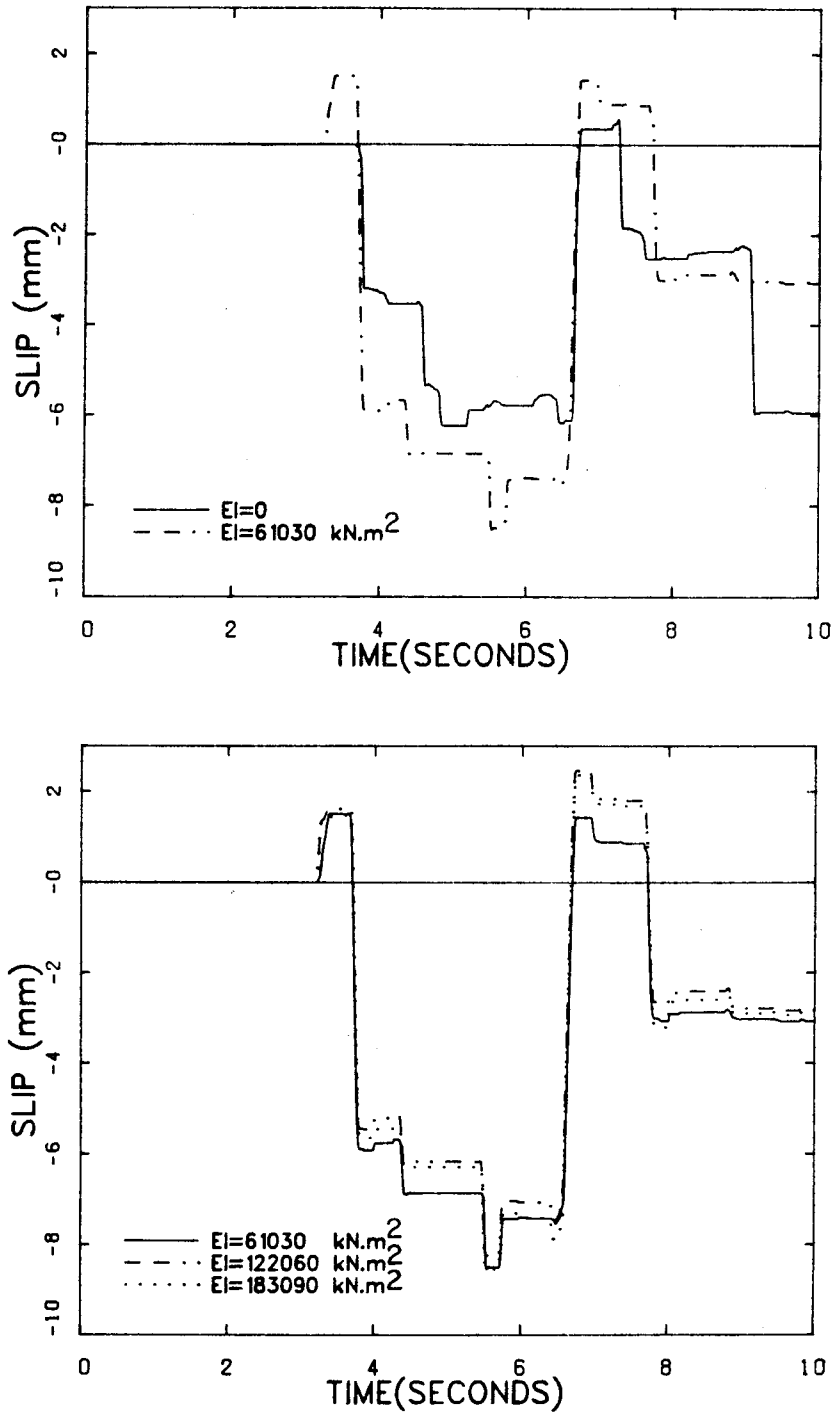

Figure 6-19 Slip-Time History Response Showing the Effect of Beam Stiffness (Slender Beams, P.T.)

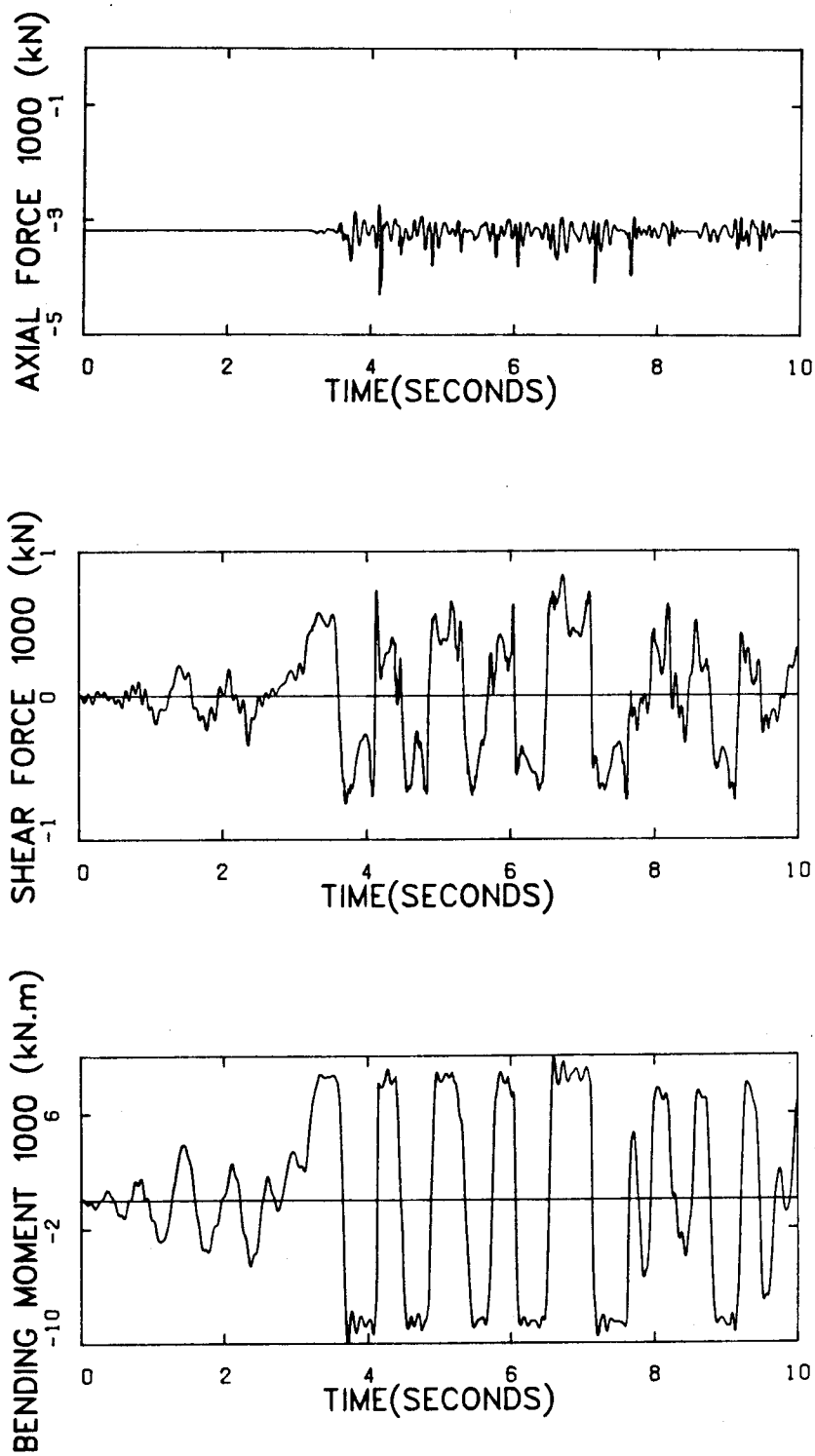

Figure 6-20 Time History Response of Base Forces for a Simple Wall (P.T.)

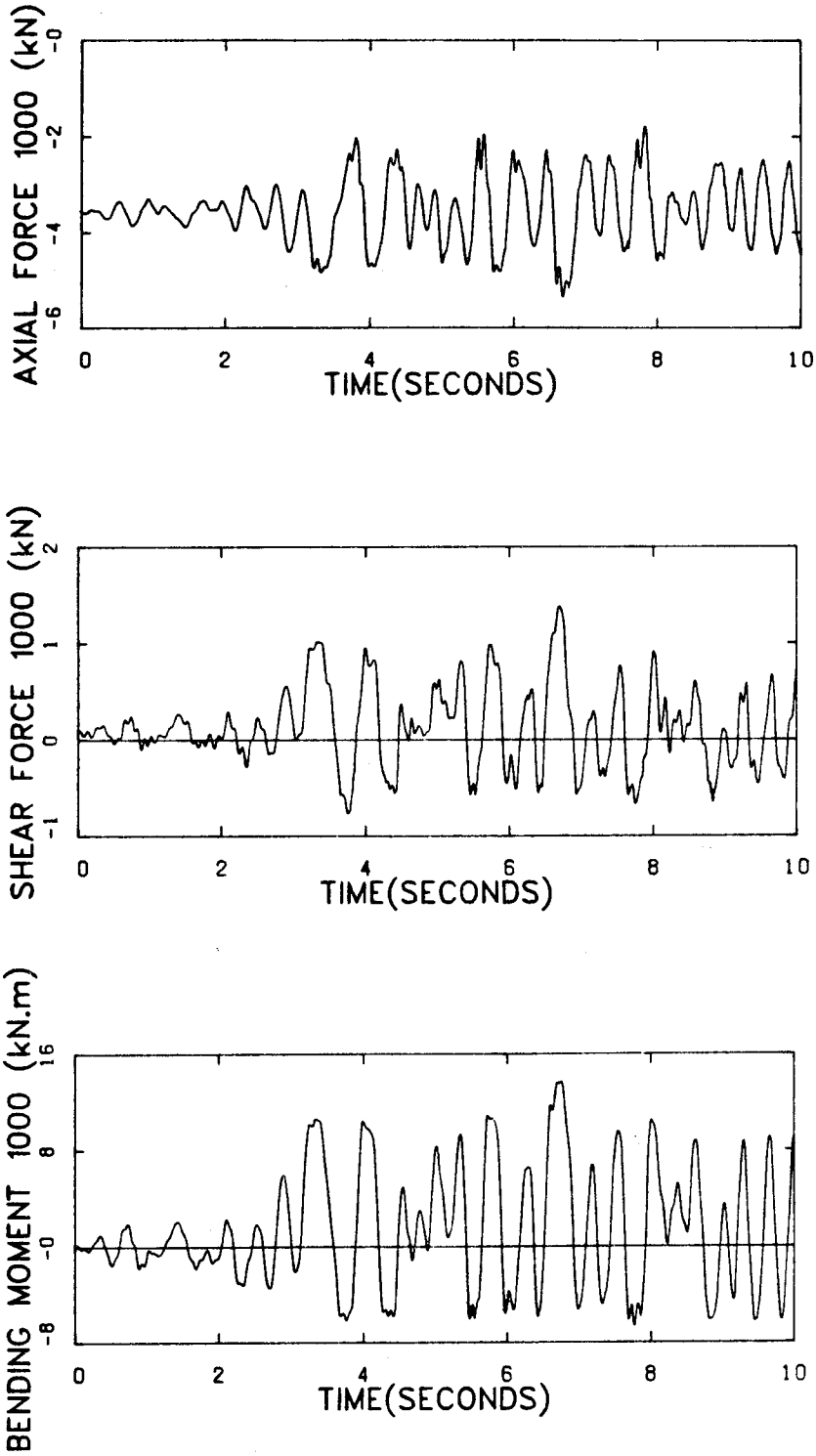

Figure 6-21 Time History Response of Base Forces for a Coupled Wall (P.T.)

history response of structures with other coupling beam stiffness values are shown in Appendix C.

The effects of coupling beam stiffness on the dynamic response of the structures with post-tensioning for vertical continuity can be summarized as follows.

1. As the coupling beam stiffness was increased, the maximum horizontal displacements decreased except one case in which maximum displacement increased.
2. As the coupling beam stiffness was increased, the maximum slip at the base of the structure remained unchanged, but slip at upper levels increased. The simple wall showed the least amount of slip.
3. The amount of gap opening at the base of the wall decreased slightly as the coupling beam stiffness increased. The wall with no coupling beam showed the largest amount of gap opening. However the maximum crack length along the connections remained unchanged.
4. The maximum beam moments and beam ductility factor increased at all levels as the coupling beam stiffness was increased.
5. The axial force, shear force and bending moment at the base of the structure increased slightly as the coupling beam stiffness was increased. The simple wall showed lower forces than the coupled walls.

6.3.2 Response of Deep Coupling Beams

The effect of the stiffness of deep coupling beams on the behaviour of coupled shear walls was studied using different values of length/depth ratios of coupling beams. The selected values of length/depth ratio for this purpose are 1, 1.4 and 1.8. As discussed in Chapter 3, deep coupling beams are modeled as inelastic truss elements. The selected properties of deep coupling beams are listed in Table 5-8.

Figures 6-22(a) and (b) show the envelopes of maximum displacement and slip at each story level, respectively. These results show a reduction in maximum displacements as the length/depth ratio of the coupling beams is increased. An increase in length/depth ratio means a decrease in stiffness of the coupling beams. A comparison between a simple wall and coupled walls show that for length/depth ratios of 1.8, 1.4 and 1.0, the maximum displacements are 58%, 45%, and 40% respectively of the maximum displacements for a simple wall. The increase in beam stiffness also shows a reduction in maximum slip. However, the amount of slip is less for simple walls than the coupled wall structure.

Figure 6-23 shows the effect of beam stiffness on gap opening at each story level and maximum strain distribution at the base of the walls. The effect of an increase in beam stiffness in this case is to reduce the gap opening and consequently reduce the maximum strain distribution. Walls

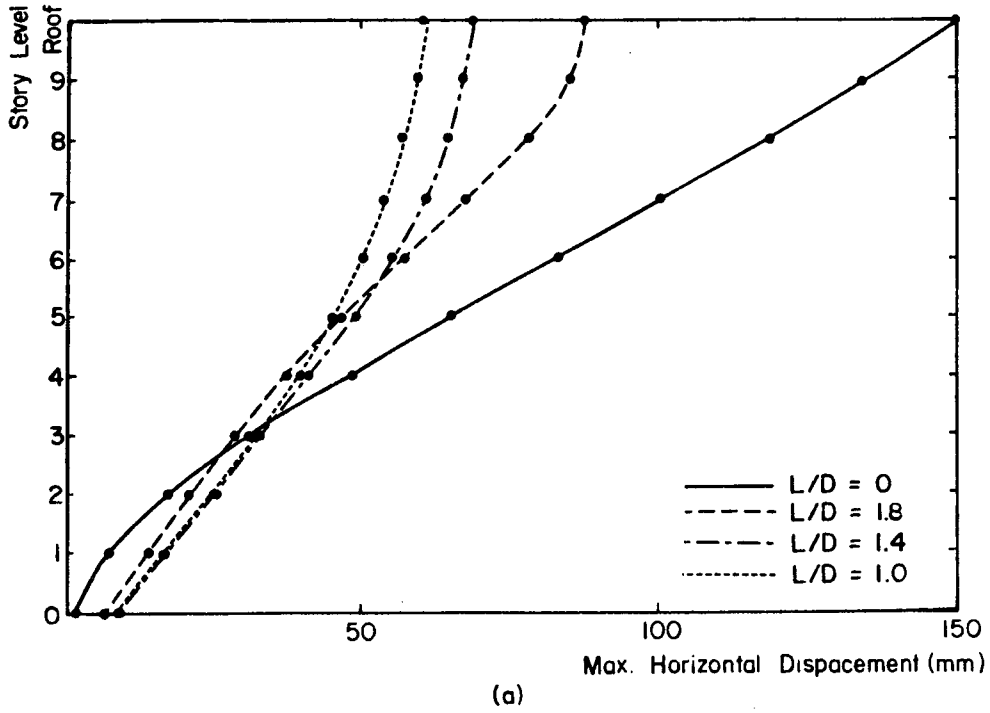

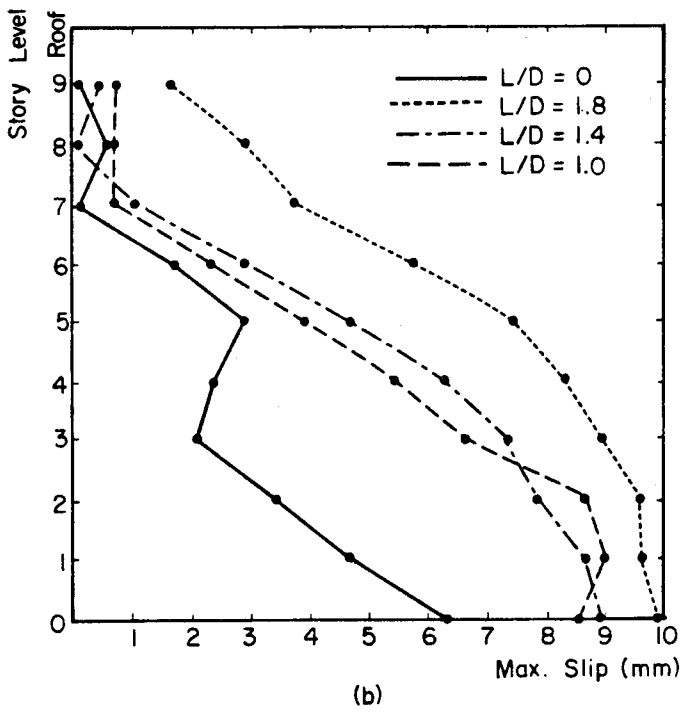

Figure 6-22 Displacement and Shear Slip Envelopes Showing the Effect of Beam Stiffness (Deep Beams, P.T.)

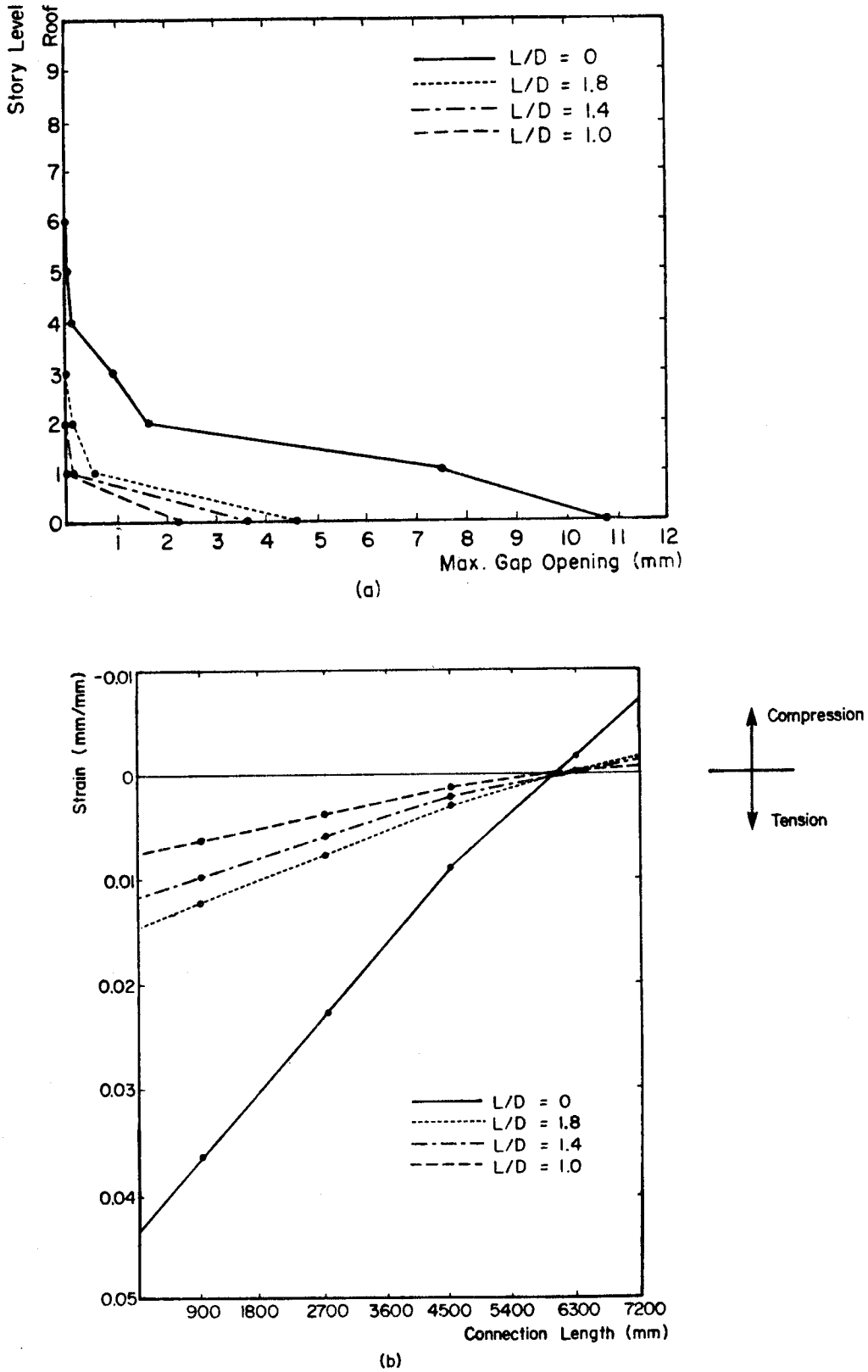

Figure 6-23 Gap Opening and Strain Distribution Showing the Effect of Beam Stiffness (Deep Beams, P.T.)

coupled with coupling beams with length/depth ratios of 1.8, 1.4 and 1.0 reduced the gap openings by 57%, 67%, and 79% respectively, compared to the simple wall. However, the maximum amount of crack length in all cases was similar and found to be about 85% of the total connection length.

Figure 6-24(a) shows the maximum bar forces in the coupling beams and Figure 6-24(b) shows the maximum bar ductility factor at each story level. As the length/depth ratio decreases the bar ductility factor and the maximum bar forces increase. In most cases, yielding takes place in all the bars. The bar ductility factor here is defined as the ratio of the maximum extension divided by extension at yield level.

Table 6-4 shows the maximum forces at the base of the walls for different coupling beam span to depth ratios. Figure 6-25 and 6-26 show a series of plots of maximum response values versus the stiffness of coupling beams. The stiffness of coupling beams is defined as the depth/span ratio. These results show that the response of coupled walls with deep coupling beams is similar to the response of those with slender beams.

Figure 6-27 shows the time history response of roof displacements for different span/depth ratios. These results show that the effect of an increase in beam stiffness is to reduce the maximum displacements. As the coupling beam stiffness is increased, there is a shift in vibration of displacements towards the neutral position in

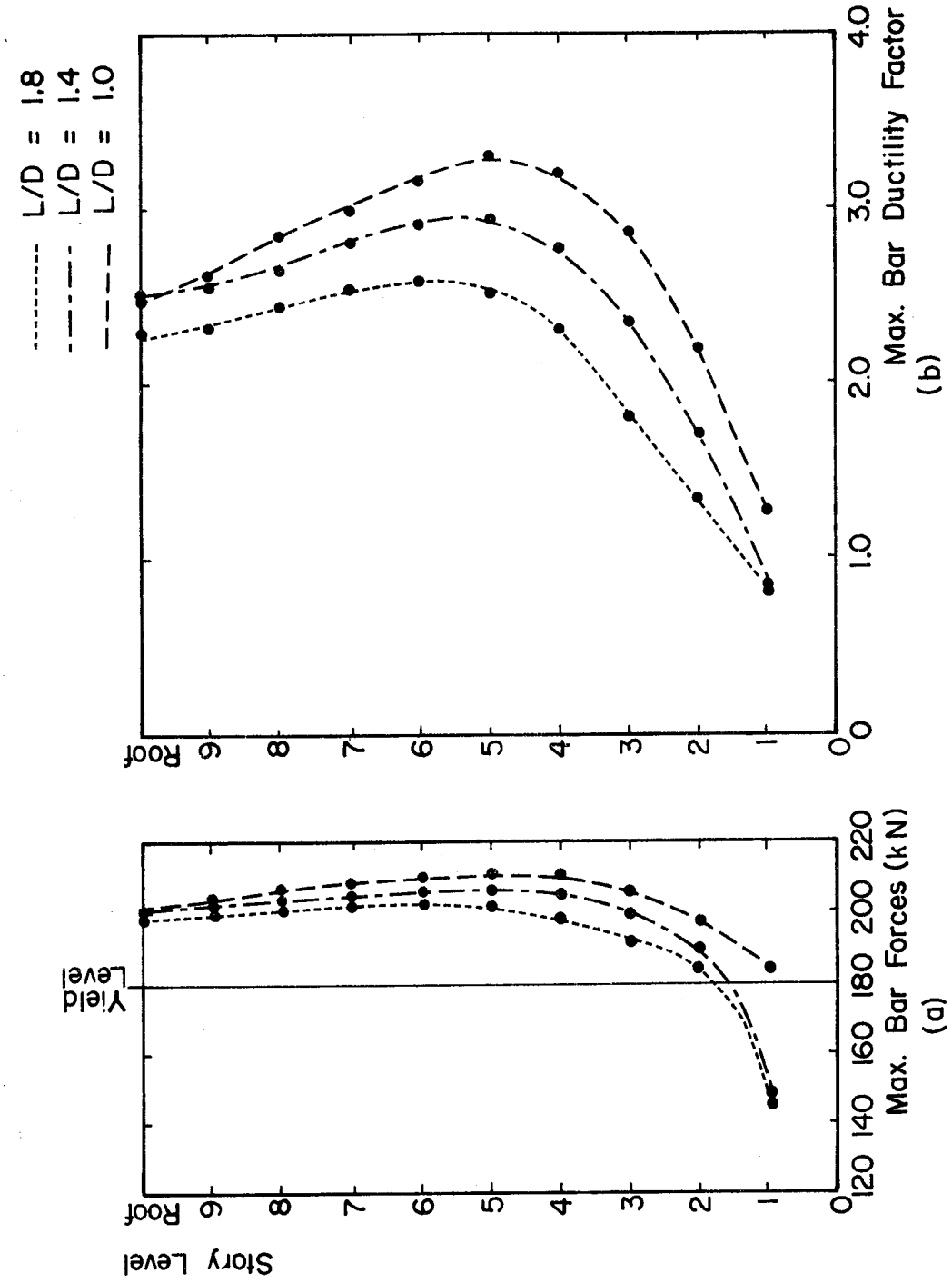

Figure 6-24 Maximum Beam Forces and Maximum Beam Ductility Factor Showing the Effect of Beam Stiffness (Deep Beams, P.T.)

Table 6-4 Maximum Base Forces for Different Values of Beam Stiffness (Deep Beams, P.T.)

L/D	Axial Force (kN)	Shear Force (kN)	Bending Moment (kNm)
0	4252	839	9967
1.8	4995	1364	13853
1.4	5000	1441	14293
1.0	6060	1588	14628

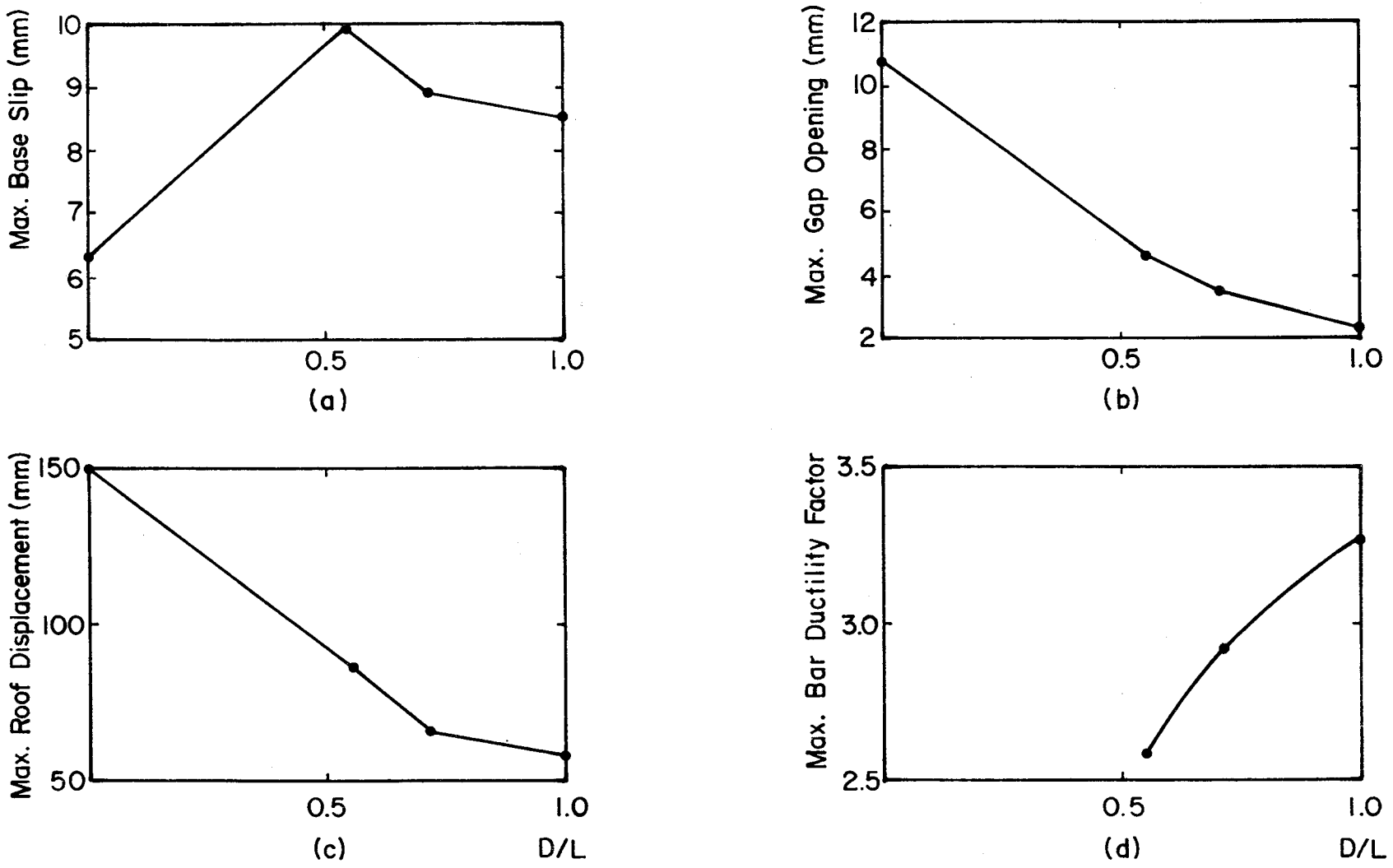

Figure 6-25 Effect of Beam Stiffness on Maximum Response (Deep Beams, P.T.)

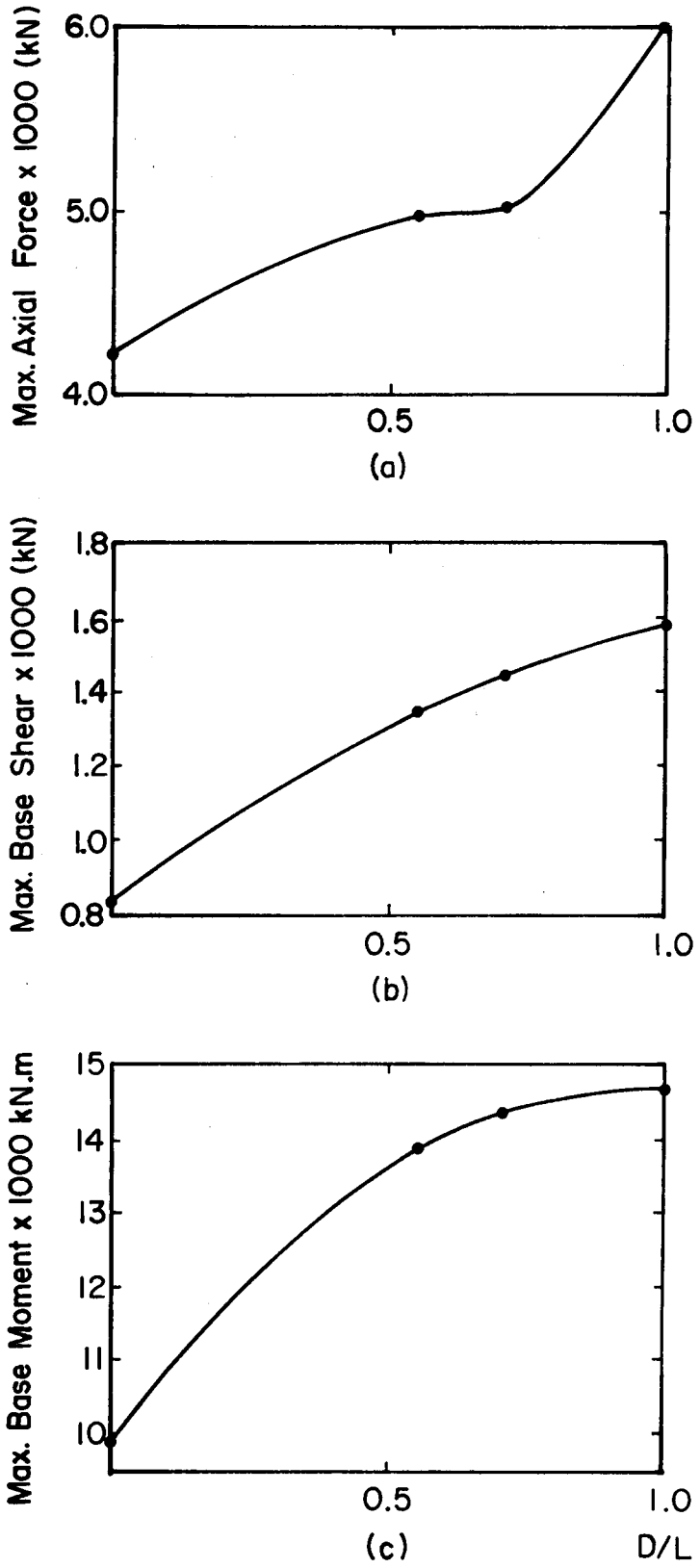

Figure 6-26 Effect of Beam Stiffness on Maximum Base Forces (Deep Beams, P.T.)

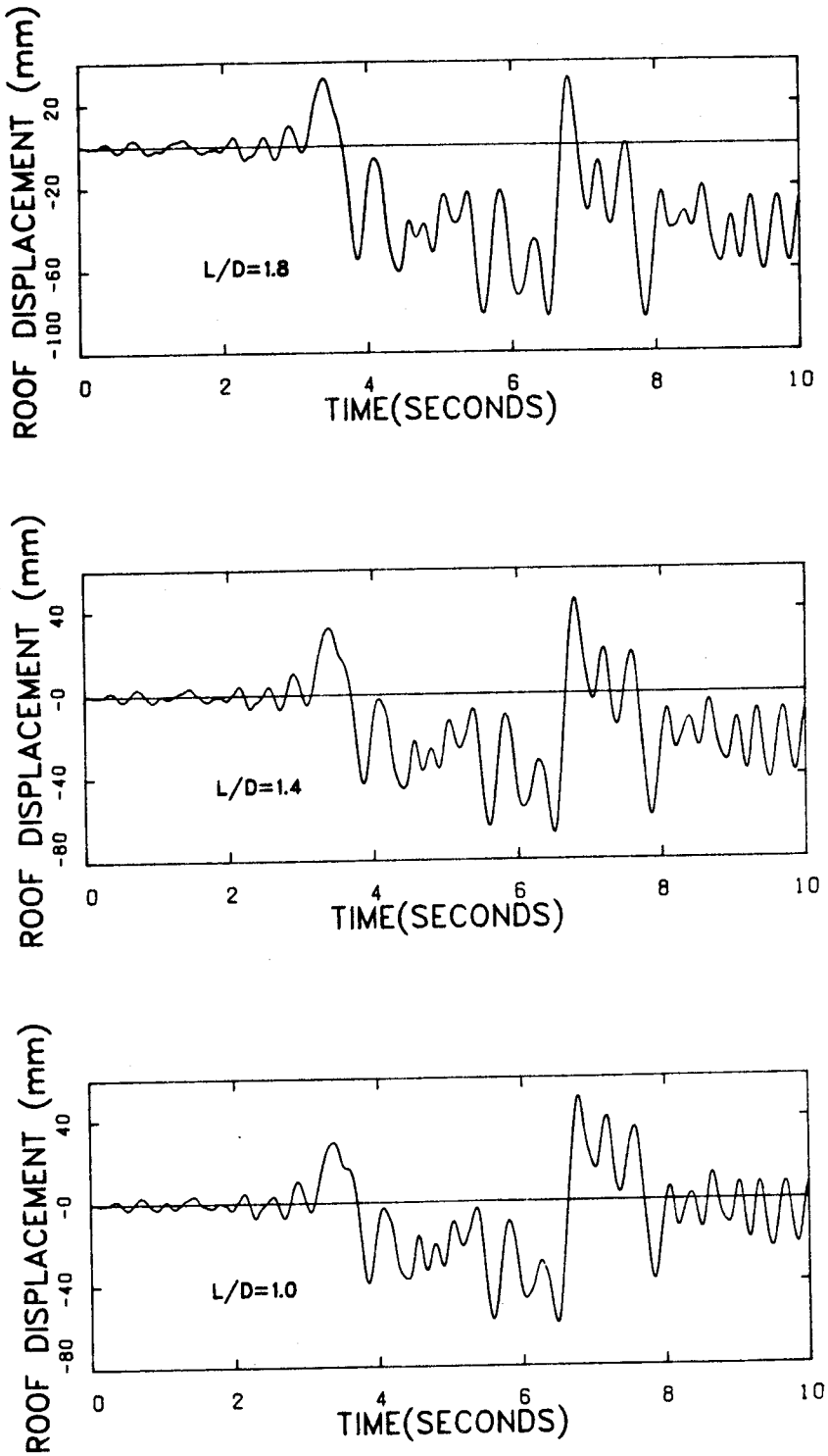

Figure 6-27 Displacement-Time History Response Showing the Effect of Beam Stiffness (Deep Beams, P.T.)

the end of the analysis. However, the period of vibration for all cases is similar. Figure 6-28 shows the time history response of base slip. Coupling beams with length/depth ratio of 1.8 show greater slip than the other two cases.

The time history response of axial force, shear force and bending moment at the base of the structure has the same trend as those with slender coupling beams. These results are shown in Appendix C. The effect of deep coupling beams on the behaviour of coupled wall structures can be summarised as follows.

1. The increase in coupling beam stiffness reduced the maximum slip at each story level and reduced the maximum horizontal displacement. The simple wall showed the lowest amount of slip compared to coupled walls.
2. The increase in beam stiffness reduced the maximum gap opening.
3. The maximum force and maximum ductility factor in the diagonal reinforcing bars increased as the stiffness of the coupling beams increased.
4. The maximum base axial force, base shear force and base bending moments increased as the coupling beam stiffness increased.

6.4 Discussion of Results

In the previous section, the results of analyses

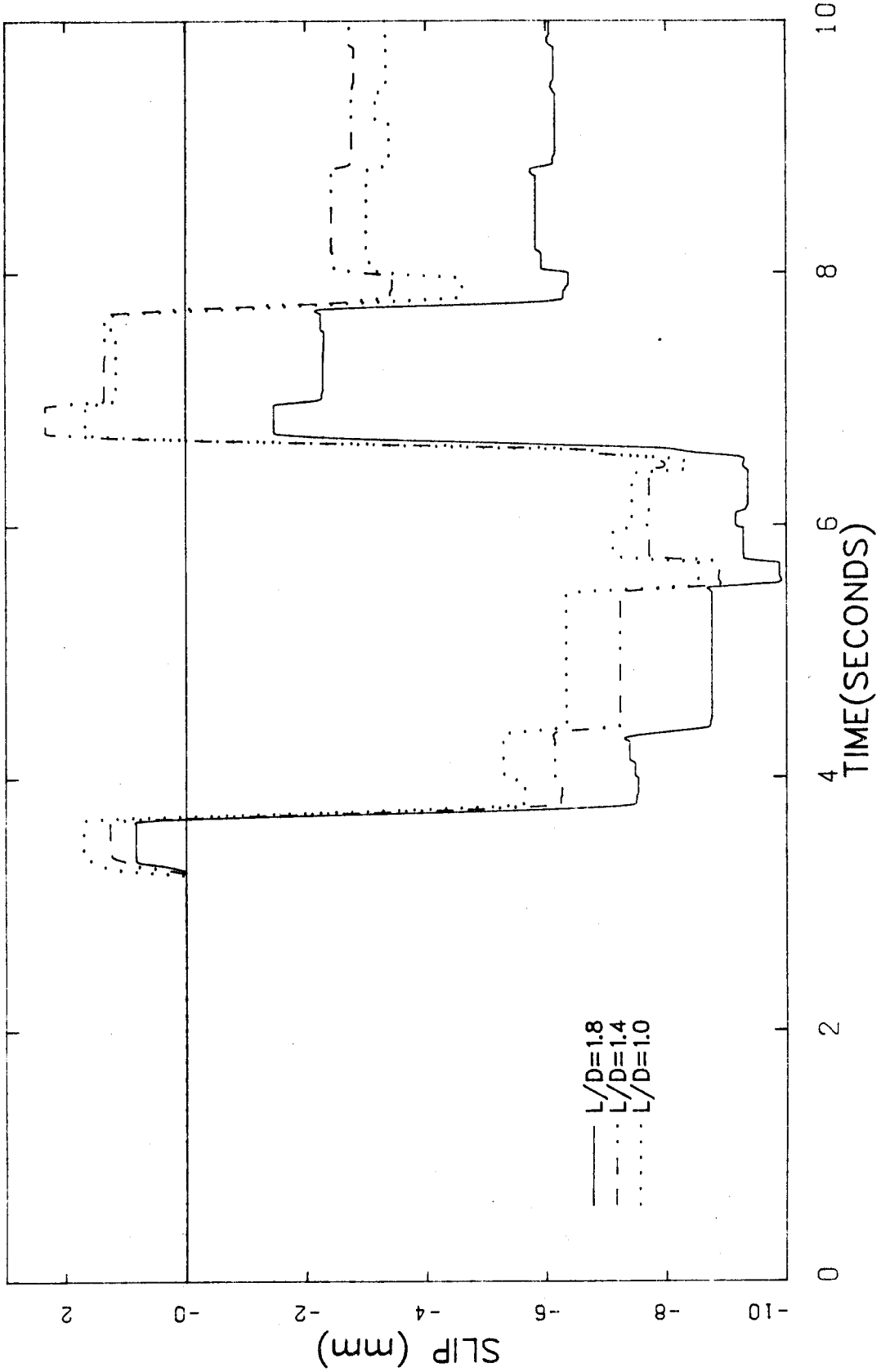

Figure 6-28 Slip-Time History Response Showing the Effect of Beam Stiffness (Deep Beams, P.T.)

carried out on structural precast walls were presented. In this section the most important behavioural aspects of such walls are discussed. First, a comparison is made between the results for simple walls obtained in this investigation with results reported by other researchers. Significant aspects of the behaviour of coupled walls are then discussed in light of the results of the parameter study. Special attention will be focussed on the effect of inelastic coupling beams on dynamic response of these walls. The effect of the method of vertical continuity across the connections will also be discussed.

6.4.1 Comparison of the Response of Simple Walls with Previous Analyses

The inelastic seismic response of simple walls has been analytically studied by Schricker and Powell (1980) and Llorente and Becker (1981). They analysed a 10-story single bay structure with horizontal connections. Their analytical results are compared here with present values obtained from parametric study. The reason for such comparison is to highlight the response of simple walls and also to evaluate the main parameters that may affect the response of these structures.

Schricker and Powell considered two cases with coefficient of friction of 0.2 and 0.6. The total height to the width ratio of their 10-story building model was 3.75. In their analyses, they considered four different

accelerograms with four different intensities of EC = 0.32 g, PD = 0.94 g, AA = 0.39 g and AB = 0.43 g. The maximum slip and maximum gap opening at the connections are shown in Table 6-5 for two different cases of vertical loading a) gravity and b) gravity and post-tensioning respectively. The results show that for small value of coefficient of friction (μ), small gap opening and large slip occur. For higher value of μ, results show large gap opening with small amount of slip. It should be mentioned that their analyses were made assuming zero strain-hardening in the shear-slip model.

Llorente and Becker analysed a 10-story simple wall of height to width ratio of 2.61. The structure was subjected to an artificial ground-motion with two different levels of intensity. The results of their analyses obtained from their published figures are tabulated in Tables 6-6(a) and (b) for maximum peak accelerations of 30% g and 35% g respectively. Their results show that the effect of increase in acceleration intensity is to increase the maximum slip, however, the maximum gap opening is not affected significantly. Similar results can be seen from the structure analysed by Schricker and Powell when vertical loading is provided by gravity and post-tensioning. Table 6-6(b) shows that for μ = 0.4, the effect of providing mild reinforcement as opposed to post-tensioning across the connections is to reduce the maximum gap opening and the maximum slip. Similar behaviour can be seen from the

Table 6-5 Response of 10-Story Simple Walls (Schricker and Powell, 1980)

a) Gravity

	μ = 0.2				μ = 0.6			
	EC	PD	AA	AB	EC	PD	AA	AB
Max. Slip (mm)	10.5	29	25	52	8	6.3	4	6.8
Max. Gap (mm)	0	0.1	0.02	0	17	88	19	26

b) Gravity + Post-tensioning

	μ = 0.2				μ = 0.6			
	EC	PD	AA	AB	EC	PD	AA	AB
Max. Slip (mm)	9.3	36	20	17	0.4	0.4	3.0	0.3
Max. Gap (mm)	1.4	1.6	3.4	0.7	17	17	17.4	21

Note: EC = 1940 El Centro N.S.
PD = 1971 Pacoima Dam S16E
AA = Artificial acceleration
AB = Artificial acceleration

Table 6-6 Response of 10-Story Simple Walls (Llorente and Becker, 1981)

a) 30% g

	P.T. $\mu = 0.2$	P.T. $\mu = 0.4$	R.C. $\mu = 0.4$*	R.C. $\mu = 0.4$
Max. Slip (mm)	4.9	0	7.6	0
Max. Gap (mm)	0.4	0.8	2.0	0.2

* Shear reinforcement only

a) 35% g

	P.T. $\mu = 0.2$	P.T. $\mu = 0.4$	R.C. $\mu = 0.4$
Max. Slip (mm)	11.7	5.0	0.4
Max. Gap (mm)	0.6	1.6	0.2

Table 6-7 Response of 10-Story Simple Walls (Present Study)

	P.T., $\mu = 0.2$	R.C., $\mu = 0.2$
Max. Slip (mm)	6.3	1.48
Max. Gap (mm)	10.8	7.5

present study as shown in Table 6-7, however the magnitudes are different. The reason for this is mainly due to the different accelerograms with different intensities and different values of wall height to width ratios. The 10-story building model selected for the present study had a total height to width ratio of 4.51. The amount of mass and the amount of post-tensioning is also considered to have some effects on the maximum slip and maximum gap opening.

6.4.2 Comparison Between Behaviour of Simple Walls and Coupled Walls

The analytical results presented in previous sections demonstrate that the presence of coupling beams can have a significant effect on the behaviour of structural walls. The response is also significantly affected by the method of providing vertical continuity across the connections.

Table 6-8(a) shows the maximum response values when post-tensioning bars are provided for vertical continuity. The maximum slip in the horizontal connections is higher for coupled walls than for the simple walls. However, the maximum gap opening in coupled walls are considerably lower than those in the simple wall. The magnitude of forces at the base of the coupled walls are higher than those in the simple wall.

Table 6-8(b) shows the maximum response values when reinforcing bars are provided for vertical continuity. The maximum forces at the base of the walls are found to be

Table 6-8 Maximum Response Values Showing the Effect of Coupling on Structural Walls

a) Post-tensioning for vertical continuity

Condition	Maximum Response					
	Max. Base Slip (mm)	Max. Gap (mm)	Max. Base Axial (kN)	Max. Base Shear (kN)	Max. Base Moment (kNm)	Max. Roof Displ. (mm)
Slender Beams M_y = 180 kNm EI = 122060 kNm^2	8.3	3.66	5422	1422	14007	60.1
Deep Beams F_y = 180 kN L/D = 1.0	8.5	2.3	6060	1588	14628	59.5
Simple Wall	6.3	10.8	4252	839	9967	150.1

b) mild reinforcement for vertical continuity

Condition	Maximum Response					
	Max. Base Slip (mm)	Max. Gap (mm)	Max. Base Axial (kN)	Max. Base Shear (kN)	Max. Base Moment (kNm)	Max. Roof Displ. (mm)
Slender Beams M_y = 180kNm EI = 122060 kNm^2	0.7	7.47	5767	2089	19737	86.7
Deep Beams F_y = 180 kN L/D = 1.0	1.67	12.78	7260	1880	18515	103.4
Simple Walls	1.48	7.5	4984	1370	15101	98.4

smaller for simple walls than those for coupled walls.

From the above discussion, it can be concluded that coupling in post-tensioned walls improves the seismic behaviour of large panel walls by reducing the amount of inelastic action concentrated in the horizontal connections, and consequently the danger of serious degradation of the connections. However, the results indicate that for coupled walls, attention should be paid to minimizing the amount of slip occuring during a major earthquake since the significant reduction in gap opening produced by coupling is accompanied by an increase in slip at the connections.

When mild reinforcing bars are provided across the connections, both simple walls and coupled walls do not provide satisfactory response. Large inelastic actions accompanied by large gap opening concentrate at the base of the walls.

6.4.3 Effect of Strength of Coupling Beams on Response

The effect of strength of coupling beams on dynamic response of walls was studied considering two methods for providing vertical continuity across horizontal connections. In the first method, vertical continuity is developed by the use of mild reinforcing steel while the second method uses post-tensioning bars to develop vertical continuity.

Results of dynamic analyses using post-tensioning as vertical continuity showed that the strength of coupling

beams is one of the controlling parameters of inelastic structural behaviour. Coupling beams with different capacities presented different behaviour on dynamic response. Of particular interest was the reduction in gap opening as the coupling beam strength increased; this is shown in Figure 6-9. Gap opening reduced from 5.51 mm for M_y = 90 kNm to 1.29 mm for M_y = 270 kNm. However, the maximum slip for all cases was about 8.30 mm at the base of the walls. This type of behaviour shows the beneficial effect of coupling in structural precast walls. Coupling beams are capable of dissipating some energy and reduce the gap opening across the horizontal connections. It should be noted that the number of analyses carried out with different beam strengths was limited. It is expected that the maximum gap opening would increase for coupling beams of higher strength, especially in the elastic range. This type of behaviour was observed in Section 5.4.2 of the previous chapter when the effect of different earthquakes was studied using a zero-tension material model for the connections and linear-elastic coupling beams. Strong coupling beams may introduce excessive tension in walls which may increase gap opening.

Results of dynamic analyses using post-tensioning for vertical continuity also showed that as the degree of coupling beam strength was decreased, the degree of coupling became less effective and walls started to behave similar to the behaviour of simple walls. Coupling beams of low

strength showed early yielding and for this reason, the ductility requirements increased. Rotational ductility demands as high as 46 were observed for coupling beams with strengths of 90 kNm. Such high ductility requirements are impossible to achieve in practice.

Coupled walls with slender beams and mild reinforcing steel for vertical continuity across the connections showed different response than discussed above. Because of large strain hardening inherent in the shear friction model, walls with varying degree of beam strengths experienced small amounts of slip compared to post-tensioned walls. It was revealed that the amount of slip has a significant effect on the amount of gap opening that may occur. Since the shear friction mechanism has a tendency to reduce slip at the connections, coupled walls showed large gap opening as shown in Figure 6-2. Gap opening increased as the coupling beam strength increased. Associated with the large gap openings, the compressive strains at the base of the walls exceeded the maximum concrete compressive strain capacity. These walls showed large ductility demands in the coupling beams ranging from 37 to 120. These large ductility demands are far beyond the practical limits. For the case of elastic beams for which the yield moment is effectively infinity, complete gap opening occured across the connections at the base of one wall. The very high elastic moments in the coupling beams also cannot be developed in actual practice.

It was expected that the improvement in the vertical

continuity across the horizontal connections may reduce the gap opening and reduce the ductility demand in the coupling beams. For this reason, a structure with post-tensioning in addition to the mild reinforcing was analyzed. In this case, the ductility demands of the coupling beams and the maximum gap opening at the base of the walls did not change significantly. However, the addition of post-tensioning reduced the maximum gap opening slightly at other floor levels as shown in Figure 6-7. Further analysis was carried out on walls with deep beams and mild reinforcing bars for vertical continuity. The results of the analysis were similar to those described above. Complete gap opening occurred at the base of the wall in the coupled wall system. Further analysis with varying beam yield strengths was not carried out as it was expected to produce similar results to those described above.

The above analyses show that the coupled walls with mild reinforcing for vertical continuity are not capable of sustaining this level of earthquake intensity. In some cases, large gap opening introduced net tensile force in one wall and large compressive force in the adjacent wall which led to the failure of the connection material. Large ductility demands were also observed in the coupling beams.

6.4.4 Effect of Stiffness of Coupling beams on Response

Analyses carried out on coupled walls with slender coupling beams and with post-tensioning for vertical

continuity showed that the effect of variation of initial elastic stiffness of coupling beams on dynamic response was not very significant within the range considered. As the degree of coupling varied, the response of the structure changed only slightly. The increase in beam stiffness increased the maximum forces at the base of the walls as illustrated in Table 6-3 and reduced the maximum gap opening. For all cases, the amount of slip at lower connection levels was similar, but increased at upper levels as the beam stiffness increased. The amount of slip was largest at the base of the walls and decreased from one level to the next up to the top floor. This type of behaviour shows that slip is a force isolating mechanism; that is, once the base starts slipping, it limits the amount of slip that may occur at other levels.

The effect of variation of beam stiffness on maximum horizontal displacement was shown in Figure 6-13(a). This figure shows that the maximum displacement is higher for the structure with coupling beam stiffness of 183090 kNm^2 than for the beam with lower initial stiffness. This apparent anomaly can be explained by two facts. Firstly, a portion of the maximum deflection is due to slip at the horizontal connections, which increases with increasing beam stiffness. Also, as inelastic behaviour takes place, the overall stiffness changes, causing movement along the response spectrum for the earthquake record considered. This in turn may lead to an increase or decrease in

response.

The effect of coupling beam stiffness on maximum beam ductility requirements was shown in Figure 6-15(b). Coupling beams with flexural stiffness of 183090 kNm^2 showed large ductility requirements as high as 18.5 which may exceed the available limits. The available ductility of slender coupling beams can be estimated from reported experimental results. Coupling beams with lower stiffness showed ductility demands as low as 7.0.

The effect of stiffness of deep coupling beams on dynamic response of walls was found to be similar to the response of walls with slender beams. However, the effect of variation in beam stiffness was more significant. The results of the analysis showed that as the length/depth ratios of coupling beams increased, the degree of coupling decreased and behaviour approached that of simple walls.

Deep coupling beams showed higher ductility demands and higher bar forces as the depth/length ratios of these beams increased. The maximum ductility demands in the coupling beams were in the range of 2.6 to 3.1.

A comparison of the behaviour of walls coupled with slender beams and those with deep beams showed that walls with deep beams and small length/depth ratios had better structural response. As the length/depth ratios of deep coupling beams increased, the truss action became less efficient and the diagonals became less effective in carrying the applied shear. Coupling beams with smaller

length/depth ratio showed smaller gap openings at the base of the walls and lower ductility ratio compared to walls with slender beams. However, the amount of maximum slip and maximum roof displacement were found to be of the same order of magnitude for both types of walls.

The amount of reinforcement for deep coupling beams was found to be considerably less than the amount used for slender beams. It was found that the required amount of steel for deep beams was 50% lower than those used for slender beams. The maximum forces at the base of walls with deep coupling beams are shown in Table 6-4. These values were slightly higher than those with slender beams.

6.4.5 Effect of Vertical Continuity on Response

To illustrate the effect of different arrangements of vertical continuity across the horizontal connections, the response of two identical structures with similar properties, but one post-tensioned (P.T.) and the other reinforced (R.C.) are compared. Coupling beams of slender type and strength of 90 kNm are chosen for this purpose.

Results of the dynamic analyses reported in Section 6.2 indicate that the response of coupled walls is strongly affected by the method of providing vertical continuity. Figure 6-29 compares the maximum slip at each story level for the two cases mentioned above. Because of large strain-hardening and pinching of hysteresis loops associated with the shear friction model, the amount of slip is considerably

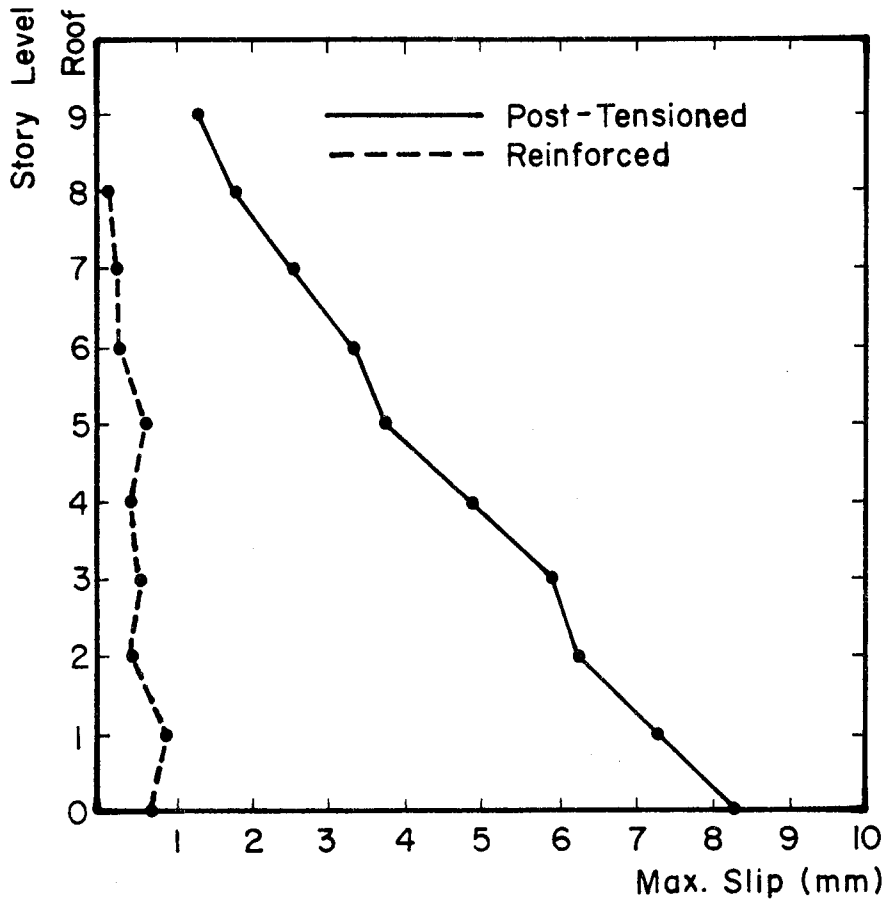

Figure 6-29 Maximum Slip at Each Story Level Showing the Effect of Method of Vertical Continuity

lower for R.C. walls than for P.T. walls. Due to the large slip at the base of the walls, the shear slip model shows a force isolation mechanism which limits the amount of slip that may occur at floors above it. The maximum base shear for R.C. walls is 1.5 times higher than those in P.T. walls which is due to large strain hardening in the shear friction model. It is interesting to note that unlike the P.T. walls, the maximum slip in R.C. walls at every floor level is not with the same phase and they do not occur in the same direction. Figure 6-30(a) and (b) illustrates the time history response of slip and shear at the base of the walls for the two cases. This figure shows that for the R.C. case, once the walls start to slip, the direction of slip is the same and the walls do not return to their original positions. For walls to return to their initial neutral position requires a large force. However, the shear friction model cannot mobilise this force at the base of the walls. This is further illustrated in the time history response of base shear forces shown in Figure 6-30(b). The effect of vertical continuity on maximum gap openings is shown in Figure 6-31(a). Maximum gap opening occurs at the base of the walls where the inelastic action is the greatest. At upper floor levels, the gap opening is considerably smaller in P.T. walls than those in R.C. walls. Gap opening also extend further to the upper levels in R.C. walls.

The maximum ductility factor for P.T. wall and R.C.

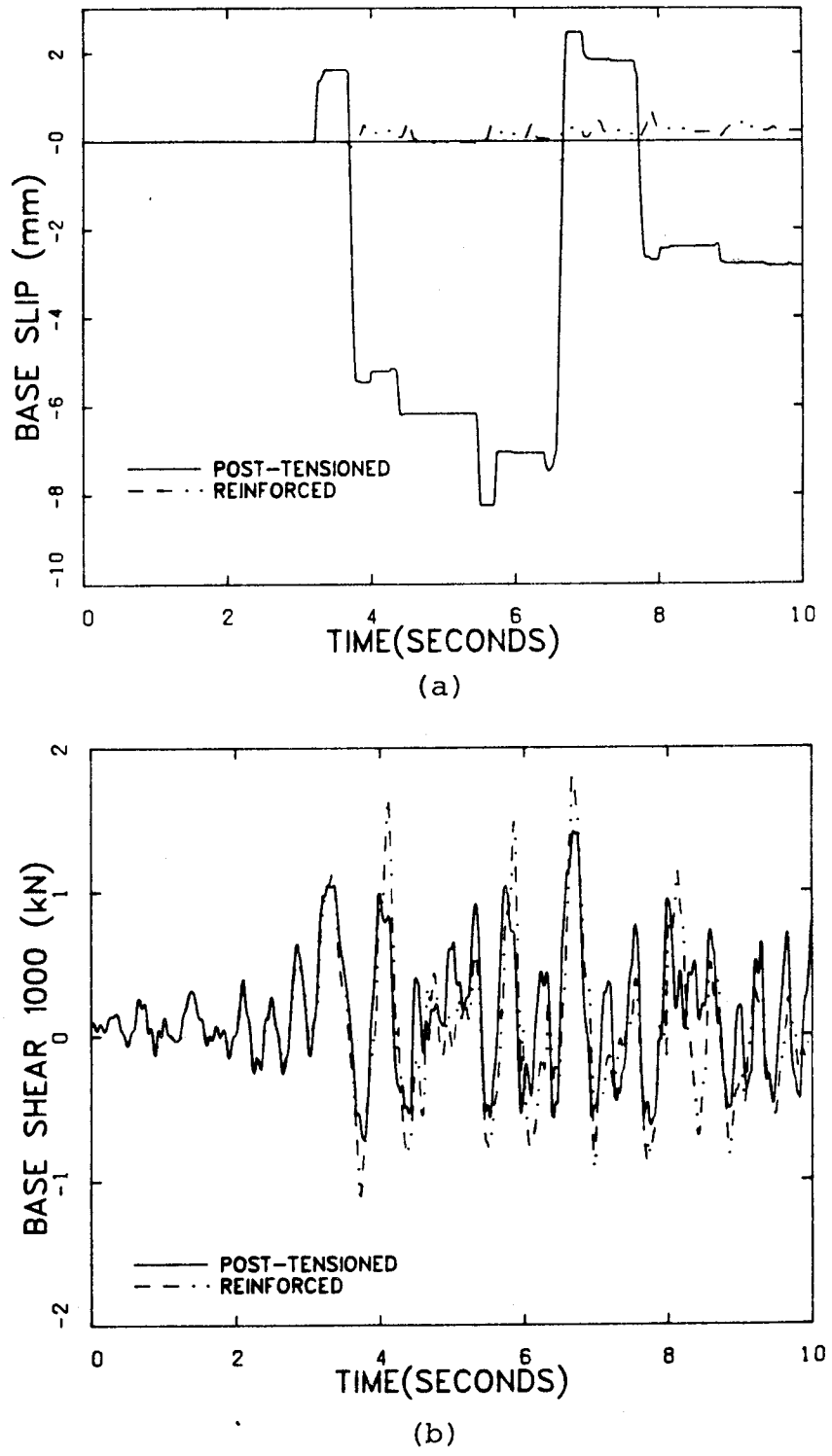

Figure 6-30 Time History Response of Slip and Base Shear Showing the Effect of Method of Vertical Continuity

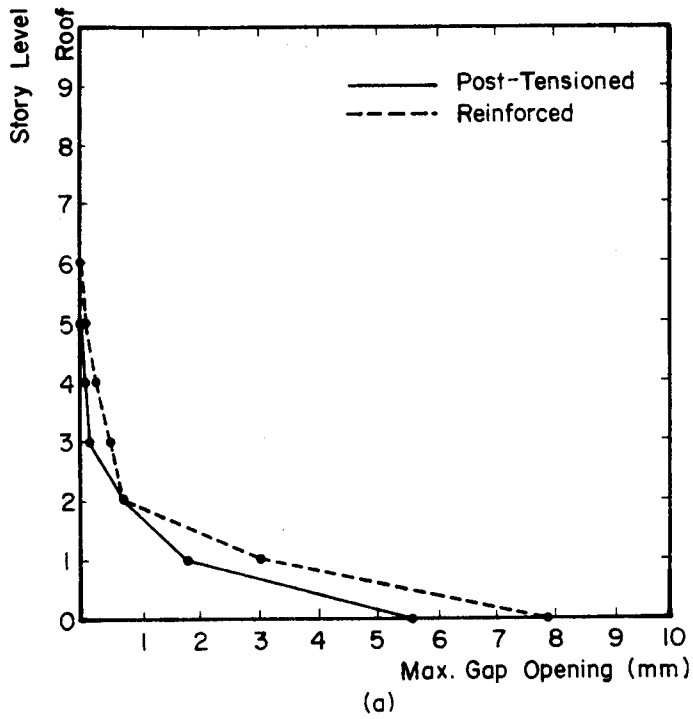

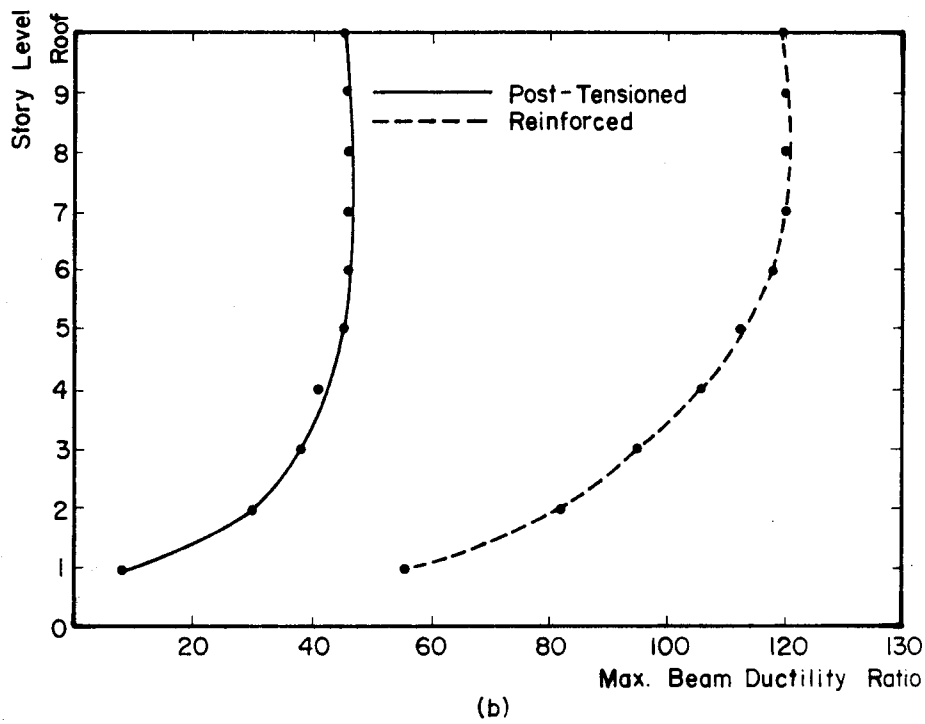

Figure 6-31 Maximum Gap Opening and Maximum Beam Ductility Factor at Each Story Level Showing the Effect of Method of Vertical Continuity

wall are shown in Figure 6-31(b). The maximum ductility factor in R.C. wall is about 2.5 times larger than that in P.T. wall. However the large ductility demands in both walls are not possible to achieve in practice.

6.4.6 Comparison of Analytical Results with ACI (1983) Values

The ultimate moment capacity of the 10-story coupled wall considered for parametric study was calculated using the ACI (1983) procedure. The formulas for the flexural strength of columns were used to calculate the ultimate capacity of walls. The ultimate moments were calculated considering the effect of axial load on the wall capacity. The fluctuations in axial forces due to the earthquake were neglected. Table 6-9 compares the ACI values with the maximum values obtained from the parametric study. For post-tensioned walls, the ACI values are higher than the analytical results. However, for walls with mild reinforcement, the ACI values are very close to the computed values. It should be noted that the analytical results in this case correspond to the walls in which net tension was developed at the base of the walls.

6.5 Conclusion

In this chapter, the effect of various parameters on the inelastic response of a 10 story coupled shear wall was studied. The main objective of the investigation was to

Table 6-9 Comparison of Maximum Wall Moments with Ultimate Values Using the ACI (1983) Procedure

Slender Beams		Deep Beams		Ultimate Moments ACI (1983)	
P.T.	R.C.	P.T.	R.C.	P.T.	R.C.
14007	19737	13853	18515	16705	19761

study the effect of coupling beam parameters on dynamic response of precast wall panels. The strength and stiffness of coupling beams were the two major variables in this investigation. The effect of the method for vertical continuity was also studied.

Analytical studies showed that simple walls behave quite differently from coupled walls. When post-tensioning was provided for vertical continuity, simple walls showed larger gap openings and smaller slip compared to coupled walls. Because of large gap openings, simple walls showed high stress concentrations leading to distress and degradation in the horizontal connections. However, this type of behaviour was not observed in the coupled walls. When mild reinforcing bars were provided for vertical continuity, simple walls showed better response in terms of gap opening and slip than the coupled walls.

Strength of coupling beams played a major role on the behaviour of precast wall panels. When vertical continuity was provided by post-tensioning bars, slender coupling beams with moderate levels of yield strength were found to be most suitable and most effective in precast wall panels. Walls of this type showed small gap opening across the horizontal connections and small ductility demands in the coupling beams. Coupling beams with low levels of yield strength were found to be ineffective. Early yielding in these beams increased their ductility demands and increased gap opening across the connections. Strong coupling beams are also not

effective since they increase tension in the walls which may increase gap opening.

Variation of the initial stiffness of slender coupling beams was found to have little effect on dynamic response. However, beams with high initial stiffness showed large ductility demands. Coupled walls with deep coupling beams of smaller length/depth ratios showed better response than those with larger values in terms of gap opening. The truss action became less effective as the length/depth ratios increased.

The method of providing vertical continuity across the connections had a significant effect on dynamic response of the walls. When vertical continuity was provided by ungrouted post-tensioning bars, the transfer of shear forces across the connections was by Coulomb friction and energy dissipation was mainly through slippage. For this reason, the amount of gap opening was very small for these walls. However, when mild reinforcing bars were used for vertical continuity, the transfer of shear forces across the connections was through shear friction due to clamping action and dowel action of the reinforcement. Because of the pinched shape of the hysteresis loops, the amount of slip was limited and large gap opening occurred which caused stress concentration in the closed portion of the connections and increased the ductility demands of the coupling beams significantly. It was shown that the walls with mild reinforcement were unable to sustain the

earthquake intensity of 1.5 times the intensity of the N-S component of 1940 El-Centro motion whereas walls with post-tensioning showed acceptable behaviour provided that the coupling beams had sufficient strength to avoid large gap opening and avoid large ductility demands in the coupling beams.

Based on the limited study carried out, conclusions can be drawn concerning the general behaviour of precast wall systems as follows.

1) Due to slip mechanism, precast walls have a tendency to move in one direction, and after a major earthquake, they do not return to their original neutral position. This is an unconfined yield mechanism since there is no confining force to return the walls to their original position.

2) Due to the above nature of yield mechanism, it is the strength and stiffness of coupling beams which improve the response of walls rather than the inelastic action in the coupling beams.

3) Level of coupling beam strength is an important parameter in precast wall systems which limits the amount of:

a) tension and compression in the walls

b) gap opening and slip across the connections, and

c) ductility demands in the coupling beams.

4) The response of the walls are controlled mainly by slip when post-tensioning bars are provided for vertical continuity and by gap opening when mild reinforcing bars are

provided.

5) Deep coupling beams are generally more effective than the slender coupling beams due to

a) lower amount of reinforcement required in the beams, and

b) lower ductility demands in the coupling beams.

7. DESIGN CONSIDERATIONS

7.1 General

In this chapter, the results of dynamic analyses obtained from the parametric study are compared with those obtained using the seismic design codes procedure. Some of the important parameters that significantly affect the response of precast wall systems are highlighted. The problems associated with the design of precast wall systems are discussed and the failure modes in these types of structures are identified. A design procedure recommended for precast wall systems is illustrated with a design example.

7.2 Comparison Between Static and Dynamic Forces

There are currently no accepted criteria for the design of precast wall systems for use in seismic regions. The ACI Code (1983), the National Building Code of Canada (NBCC, 1985) and the SEAOC Recommendations (1975) have special provisions for the seismic design of cast-in-place reinforced concrete structures, but do not have provisions for precast concrete buildings.

To study the applicability of the current design method proposed by NBCC (1985) to precast wall systems, the results of the "equivalent static analysis" using NBCC (1985) and discussed in Chapter 5 are compared with those obtained from inelastic dynamic analyses discussed in the previous

chapter. The results are summarised and shown in Table 7-1 and 7-2 for walls with slender beams and deep beams respectively. It was shown in the previous chapter that the response of precast walls is controlled mainly by the strength rather than the stiffness of the coupling beams. For this reason, results of dynamic analyses are shown for various yield strengths. A comparison shows that the maximum base moments and the maximum base shears computed from dynamic analyses are higher and the maximum base axial forces and the coupling beam moments are lower than those obtained from static analyses. The maximum axial forces are approximately 40% higher for those obtained from static analyses than the corresponding forces computed from dynamic analyses. This is mainly due to the effects of live loads and factored loads considered in static analyses and ignored in dynamic analyses. For all cases considered, the maximum base shears are higher for those obtained from dynamic analyses than those computed from static analyses. When shear resistance is provided by mild reinforcing bars across the connections, dynamic analyses show significantly higher base shears than the static analyses.

From the above discussion, it can be concluded that although a large amount of energy has been dissipated through the inelastic connections and the inelastic coupling beams, the maximum forces obtained from dynamic analyses are generally higher than those computed from static analyses. The reason is that the design forces and force distribution

Table 7-1 Response of walls with slender beams

Vertical Continuity	M_y (kNm)	Max. Base Moment (kNm)	Max. Base Shear (kN)	Max. Base Axial (kN)	Max. Beam Moment (kNm)	Max. Beam Ductility Ratio
P.T.	0	9967	839	4252	-	-
	90	13273	1271	4949	155.5	46.4
	180	14007	1422	5422	215.0	7.22
	270	14056	1524	5728	281.0	2.55
R.C.	0	15101	1370	4981	-	
	90	18452	1794	5187	202.7	119.5
	180	19737	2089	5767	285.6	37.2
R.C.+P.T.	180	18071	1578	5367	285	37
Static Analysis (NBCC)	Elastic	10061	1051	10546	413	-

Table 7-2 Response of walls with deep beams

Vertical Continuity	A_s (mm^2)	Max. Base Moment (kNm)	Max. Base Shear (kN)	Max. Base Axial (kN)	Max. Bar Force (kN)	Max. Bar Ducility Ratio
P.T.	0	9967	839	4252	-	-
	600	14293	1441	5000	208	2.9
	1000	13145	1368	6018	299	1.0
R.C.	0	15101	1370	4981	-	-
	600	18515	1880	7260	265	8.4
Static Analysis (NBCC)	600	15781	1083	10152	218	-
	1000	13958	1035	9808	262	-

Note: A_s = cross sectional area of diagonal reinforcing bars
M_y = beam yield moment
P.T. = post-tensioned
R.C. = reinforced

in seismic design codes such as NBCC (1985) are based on flexural ductility which may not be directly applicable to precast wall systems. The building codes take inelasticity into consideration by providing lower design force levels than is actually expected under static conditions. These results also indicate that if a higher ductility factor, k, than the actual value of 1.3 were used, the force distribution in precast wall systems would still be different than the forces resulting from the equivalent static analyses.

7.3 General Behaviour of Large Panel Systems

Studies carried out on the behaviour of simple walls show that these structures are capable of dissipating a large proportion of the input energy in the horizontal connections during a major earthquake. Due to the effects of rocking and slip, the forces at the base of the walls are reduced significantly. However, large slip and gap openings in the horizontal connection is accompanied by concentration of high stresses in the connection regions and large deformation in the structure and consequently the stability and integrity of the building is threatened. For this reason, a design concept that relies on the inelastic energy dissipation of horizontal connections should be avoided.

Vertical coupling elements such as coupling beams are not primary gravity load bearing elements. Therefore the energy dissipation of these elements by yielding does not

threaten the overall stability of the structure, as long as the individual walls have not yet reached their ultimate strength.

Dynamic inelastic analyses carried out on post-tensioned coupled walls showed that the amount of slip experienced along the connections is quite significant. Slip was found to have a tendency to move in one direction. These results showed that it is very unlikely for the walls to return to their original position after a major earthquake. The effect of coupling in post-tensioned walls was shown to have a significant effect in reducing the gap opening across the horizontal connections. The reduced gap opening which eliminates the possibility of the degradation of the horizontal connections is very desirable in precast wall systems. Walls with deep coupling beams of relatively small length/depth ratios and diagonally reinforced or slender coupling beams with moderate level of yield strength were found to be most effective in these types of structures.

Dynamic analyses showed that when mild reinforcing bars are provided for vertical continuity across the connections, the shear friction mechanism reduces the maximum slip significantly. However, the reduced slip was accompanied by large gap opening. Intense rocking motion cause stress concentration in the corners of the connections and wall panels which may lead to degradation, damage, and eventual failure of the structure. In these types of structures,

large gap opening was accompanied by large ductility demands in the coupling beams.

Beam strength also played a major role on the behaviour of precast wall systems. Coupling beams showed large ductility demands when the strength of these beams was relatively low. Coupling beams with high level of yield strength showed net tension in the walls and large gap opening across the connection. Beams with moderate level of yield strength were found to be the most effective in precast wall systems.

7.4 General Design Concepts for Precast Wall Systems

The general design requirements for structures to resist strong ground motions is to have sufficient strength, stiffness, ductile deformation, and energy absorption capability. In precast wall systems, during any damage that may occur, the integrity and stability of the structure must be maintained.

For reasons discussed in the previous chapters, it is undesirable to confine the inelastic energy dissipation to the horizontal connections. Large gap opening must be avoided as it may cause stress concentration in the connections which may lead to degradation and crushing of concrete in the connection region. Consequently, this may pose a threat to the stability and the integrity of the building. Large slip must also be avoided as there are severe reservations towards using this in precast wall

systems. The in-plane slip that occurs in precast wall panels may produce out-of-plane slip and consequently, the stability of the structure is endangered. Therefore, a design concept that relies on slip and gap opening must be avoided.

An alternative design approach which is discussed by Muller (1981) treats precast walls as monolithic walls. The intent of monolithic design is to achieve seismic behaviour similar to that expected in ductile cast-in-place structural walls. The monolithic design concept implies that the connections must be strong enough to resist the forces associated with the formation of plastic hinges at the base of the walls. Since the strength and the stiffness of the horizontal connections are considerably lower than the corresponding wall panels, precast walls require considerable detailing which is very difficult to achieve for reasons of economy and/or construction. It is very likely that plastic hinges will form in the connections at the base of the walls. Therefore a design concept that relies on strong horizontal connection may not be possible to achieve in practice.

The non-load bearing elements such as coupling beams rather than the horizontal connections are the more desirable locations to dissipate energy since the yielding in the coupling beams does not threaten the stability and the integrity of the structure. A design procedure based on such concept is discussed in detail in the following

section. Based on the study discussed in the previous chapter, the choice of vertical continuity across the horizontal connections is an important parameter for design of these walls. When mild reinforcing bars are provided to resist shear forces across the connections, it is more likely that the response is controlled by overturning. In this case, the structure must be examined to ensure there is no sign of distress in the connections or wall panels. The ductility demands in the coupling beams should also be checked to ensure that they are within practical limits. For these structues, coupling beams with lower yield strength is more favorable since coupling beams with higher strength may produce net tension in the walls and produce large gap opening across the connections. When post-tentioning bars are provided for vertical continuity it is more likely that the response is controlled by slip. The maximum slip that usually occurs at the base of the walls or at the first story level should not be excessive. Coupling beams with moderate level of beam strength are most suitable for these types of structures. Coupling beams with low level of beam strength may show excessive ductility demands. Walls of this type may also show excessive gap opening across the connections. Coupling beams with high level of beam strength may produce large tension in the walls which may increase gap opening. When diagonal reinforcing bars are used for vertical coupling, the beams must be relatively deep compared to their span; otherwise,

the coupling becomes less effective to carry the applied shear and large gap opening may occur at the base of the walls similar to those experienced in simple walls.

In coupled wall systems, the coupling beams should be carefully detailed similar to those discussed in Chapter 2 to achieve flexural yielding at the ends of the beams and prevent any premature failure that may occur. Coupling beams must also have sufficient strength and stiffness to avoid excessive tension or compression in the walls and avoid large ductility demands in the beams.

7.5 Proposed Design Procedure

As discussed in Section 7.2, the design forces and the force distribution using the NBCC (1985) based on the "equivalent static analysis" are quite different than the corresponding forces obtained from the inelastic dynamic analyses. Based on the limited results available from dynamic analyses, it is not possible to estimate the forces in precast wall systems using the static analysis used in design codes. A design procedure for precast wall systems which is based on dynamic analysis is proposed and described in the design chart illustrated in Figure 7-1. In this design procedure, the structural properties and dimensions are selected based on the minimum requirements by the codes of practice. The structure is analysed as a frame under factored wind loads using the static analysis proposed by NBCC (1985). The coupling beam section and its properties

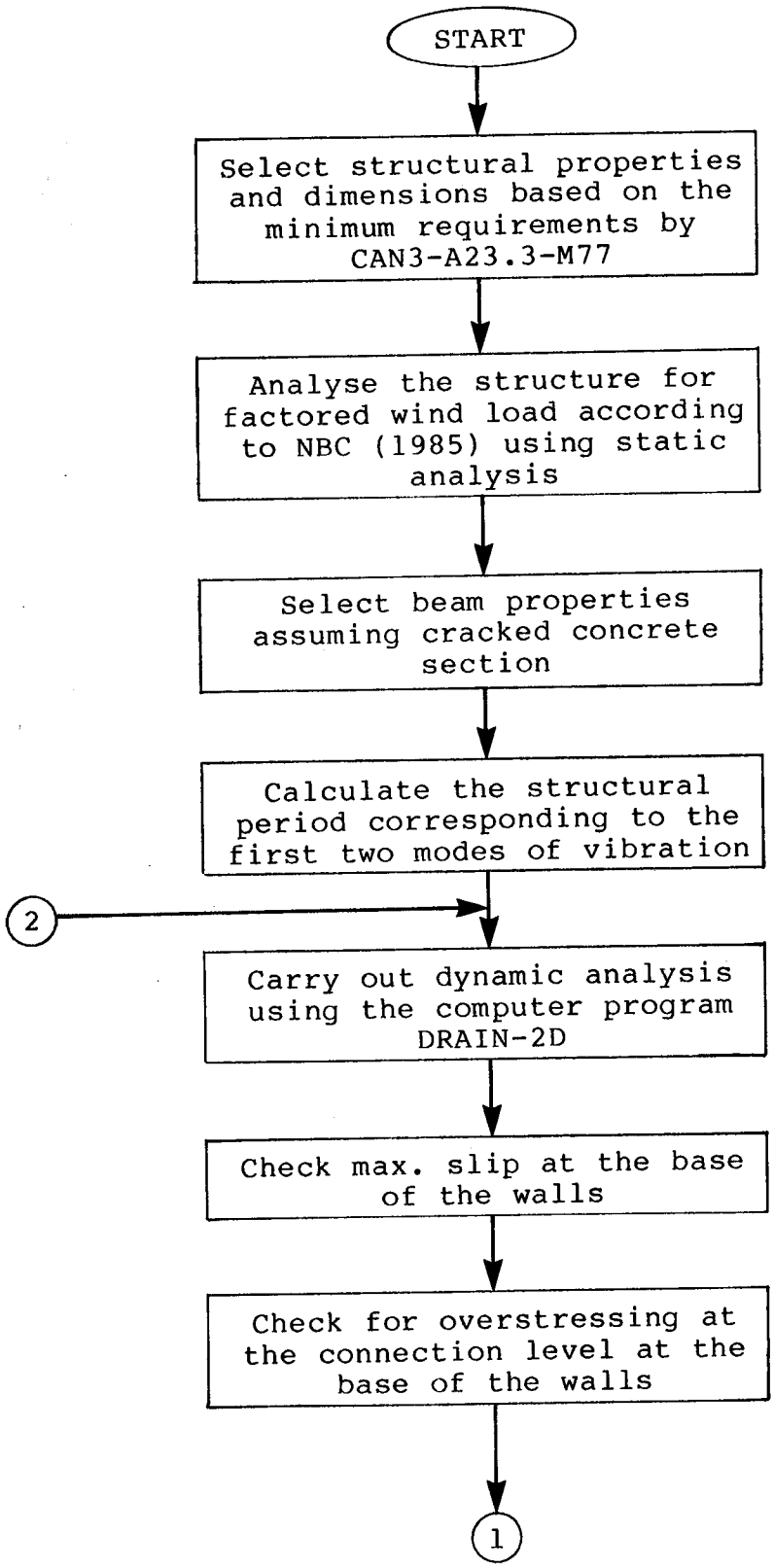
START
Select structural properties and dimensions based on the minimum requirements by CAN3-A23.3-M77
Analyse the structure for factored wind load according to NBC (1985) using static analysis
Select beam properties assuming cracked concrete section
Calculate the structural period corresponding to the first two modes of vibration
2
Carry out dynamic analysis using the computer program DRAIN-2D
Check max. slip at the base of the walls
Check for overstressing at the connection level at the base of the walls
1

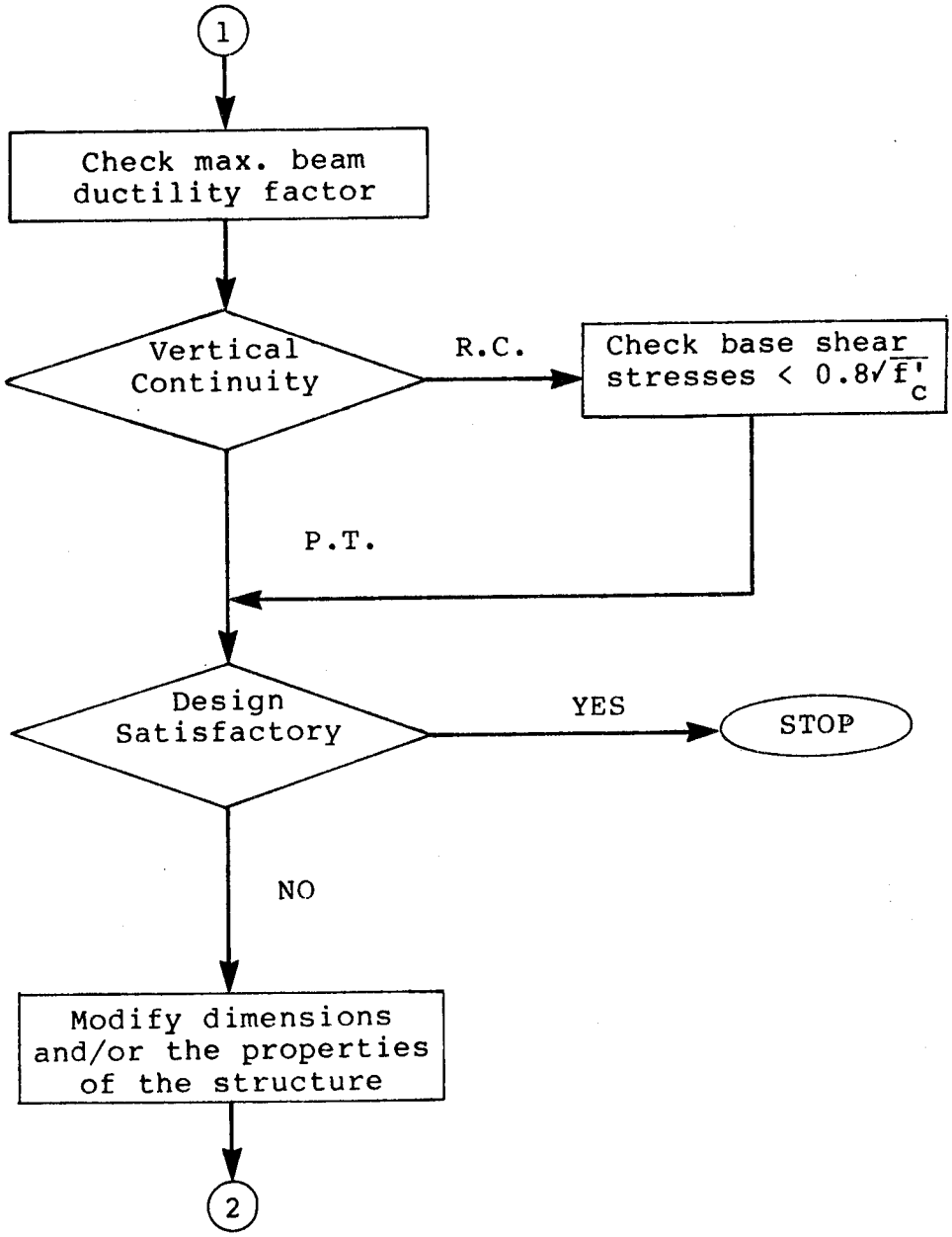

Note: P.T. = Post-tensioned
R.C. = Reinforced

Figure 7-1 Proposed Design Chart for Precast Wall Systems

are selected accordingly, assuming cracked concrete section. Based on a design procedure suggested by Fintel and Ghosh (1981), the level of coupling beam strengths must be selected to ensure elasticity in the beams up to at least the factored design wind loads. To select damping properties, the period of the structure corresponding to the first two modes of vibration should be estimated.

A particular ground motion can be applied to the selected structure using the computer program DRAIN-2D. The results obtained from dynamic analysis must be within the prescribed limits. To satisfy the design requirements, the designer should ensure that:

1) maximum slip at the base of walls is not excessive
2) maximum strains at the corner of the connections are less than the concrete maximum compressive strain at maximum stress level
3) maximum beam ductility factors are within the practical limits, and
4) when mild reinforcing bars are provided for vertical continuity, the maximum shear at the base of the walls satisfy the code requirements.

In any case, if any of the above values exceed the limit, the structural properties and/or dimensions should be modified accordingly and the structure must be reanalysed. This process may be repeated several times until the design is satisfactory.

7.6 Design Example

The 10 story building model selected for parametric study and described in Chapter 5 is used as an example to illustrate the design procedure discussed in the previous section. The design procedure which is based on the design flow-chart shown in Figure 7-1 is as follows.

1) Select structural properties and dimension.

10 story building model with slender coupling beams and post-tensioning bars for vertical continuity. The properties and dimensions of the structure are similar to those described in Chapter 5 except with the post-tensioning force of 352 kN/tendon.

2) Analyse structure under factored wind load.

Reference velocity pressure = 0.55 kN/m^2 (supplement to NBCC 1985)

Specified pressure acting on the wall = 1.14 kN/m^2 (NBCC 1985)

Maximum beam moment under factored wind load using a frame analysis = 60 kNm

3) Select beam properties based on cracked concrete section.

$EI = 122 \times 10^3$ kNm^2

$GA = 403 \times 10^3$ kN

$EA = 403 \times 10^4$ kN

Beam yield moment, M_y = 90 kNm (50% higher than the design

wind moment)

4) Structural period of vibration.

First mode = 0.38 seconds

Second mode = 0.09 seconds

5) Dynamic analysis using the computer program DRAIN-2D.

Assume building is located in zone 6 with zonal velocity ratio of 0.32

Select El Centro 1940, N-S component as the input ground motion with the intensity of 1.0 and maximum peak acceleration of 0.33 g.

Select the integration time step as 0.002 seconds.

6) Analyse results.

Max. slip = 3.8 mm

Max. gap = 1.5 mm

Max. compressive strain at the corner of the connection = 0.0018 mm/mm < 0.002 O.K.

Max. roof displacement = 52 mm

Max. beam ductility factor = 15.7 N.G.

Max. base axial = 4947 kN

Max. base shear = 1053 kN

Max. base moment = 12362 kNm

The above analysis shows that the ductility requirements in the coupling beams are relatively high. The

structure was reanalysed assuming M_y = 180 kNm for the beams. The following results were obtained.

Max. slip = 4.5 mm

Max. gap = 0.7 mm

Max. compressive strain at the corner of the connection = 0.001 mm/mm < 0.002 O.K.

Max. roof displacement = 33 mm

Max. beam ductility factor = 3.2 O.K.

Max. base axial = 5024 kN

Max. base shear = 1212 kN

Max. base moment = 11567 kNm

The above results indicate that the increase in coupling beam strength by a factor of 2.0 reduces the ductility demand by approximately a factor of 5.0.

For design of precast wall systems, a single earthquake record as input may not provide sufficient asssurance that the structure will behave satisfactorily under future earthquakes. For this reason, it is advisable to analyse the structure under a set of earthquake records.

7.7 Summary

It was shown in this chapter that the design forces and the force distribution obtained from the code procedure using the "equivalent static analysis" were significantly different than the corresponding forces obtained from inelastic dynamic analyses. For this reason, a design procedure based on dynamic analysis was recommended. In

this design process, the parameters that the designer should check to ensure the integrity and the stability of the structure were discussed. The application of the proposed design method was illustrated with a design example.

8. SUMMARY, CONCLUSIONS AND RECOMMENDATIONS

8.1 Summary

The inelastic response of precast wall panels with coupling beams was studied under severe earthquake motions. A 10-story building model was used for dynamic analyses. The main aim of the study was to investigate the effect of coupling beams on precast wall systems.

Based on detailed studies of reported experimental test results related to precast wall systems, computer models were developed and incorporated into the computer program DRAIN-2D. It was also possible to use some of the existing elements in the program.

The finite element technique was used to model the precast wall systems. It was assumed that wall panels remain linear-elastic throughout the analysis and that the inelastic action is concentrated in the horizontal connections and the coupling beams. Wall panels were modeled using a 4-node rectangular plane-stress element. For the connections, an element originally developed by Llorente and Becker (1981) for the analysis of simple walls was used. This element takes into consideration the shear slip mechanism and the rocking mechanism which allows for gradual opening and closing of the connections. For the shear behaviour, two elements were used in parallel; contact or interface elements were used to model the shear slip along the connection panel interface and the finite

connection region was used to model joint material deformations.

It was assumed that vertical continuity across the connections is provided by mild reinforcing bars, ungrouted post-tensioning bars or a combination of the two. A linear elastic truss element was used to model post-tensioning bars and an elastic-perfectly plastic model was used to model mild-reinforcing bars. It was assumed that the shear behaviour across the connections is by coulomb friction mechanism in the presence of gravity and/or post-tensioning and by shear friction mechanism in the presence of mild reinforcing bars.

The concrete material model suggested by Darwin and Pecknold (1974) was used to model the axial behaviour of concrete across the connections. However, the ascending branch of the curve was linearized to reduce the computational effort. The descending branch of the curve was also modified to avoid numerical problems.

Experimental test results have shown that the behaviour of deep coupling beams is significantly different from that of slender beams. For this reason, different modeling techniques were used for deep beams and slender beams. Deep beams with main diagonal reinforcing bars were modeled as truss elements and slender beams with longitudinal main reinforcing bars were modeled as beam elements. The inelastic concrete beam element in the computer program DRAIN-2D was used to model the slender coupling beams.

Modifications to the element were made to make it compatible with the plane-stress panel element. Compatibility was assured both in the elastic and the inelastic range.

Verification of the models was accomplished where possible by the use of available experimental or analytical test results. However, in some cases, the hysteretic models were verified by tracing the loops in a step-by-step fashion.

For parametric study, an accelerogram which is relatively strong and likely to cause most damage to the structure was selected. The selected structure was analysed under three available strong ground motions. The effects of coupling beam parameters formed the major part of the parametric study. The strength and stiffness of coupling beams were the major variables in this investigation. The effect of the method of providing vertical continuity across the horizontal connections was also studied. Based on the results of dynamic analyses, a design procedure was recommended for precast wall systems.

8.2 Conclusions

Based on the results of the investigation on precast wall systems, the following conclusions can be made:

1. The method of providing vertical continuity across the horizontal connections has a significant effect on the response of precast wall systems. Although post-

tensioned walls showed good performance, reinforced walls were unable to sustain the earthquake intensity of 1.5 times the N-S component of the 1940 El Centro record.

2. The response of post-tensioned walls and reinforced walls is controlled mainly by slip and gap opening respectively. In precast wall systems, the consequences of large gap opening across the horizontal connections are more significant than those due to large slip.

3. The strength of coupling beams plays a major role in the behaviour of precast wall systems. Coupling beams with a moderate level of beam strength are most suitable for precast walls. Beams with low level of yield strength show large gap opening across the connections and large ductility demands in the coupling beams. Beams with high level of yield strength also show large ductility demands in the beams.

4. The response of coupled wall systems is not significantly affected by the amount of energy dissipated in the coupling beams.

5. The effect of the initial stiffness of coupling beams on the response of precast walls is not very significant. However, slender coupling beams with high level of

stiffness show large ductility demands.

6. Coupled walls with deep beams of low level of span/depth ratio show better structural response than those with high values of span/depth ratios.

7. Coupled walls with deep beams are more suitable than those with slender beams due to:
   (a) lower amount of reinforcement necessary in coupling beams and,
   (b) lower ductility demands in the coupling beams.

8. Coupled walls show better structural response than simple walls in terms of gap opening when post-tensioning bars are provided for vertical continuity across the connections. Coupled walls of this type behave satisfactorily whereas simple walls show signs of distress and degradation in the connection regions.

9. The amount of strain hardening in the shear slip model has a significant effect on the response of precast walls. A small amount of strain hardening can reduce the displacements significantly. For this reason, it is important to select an appropriate value for the amount of strain hardening.

10. The maximum forces and the force distribution using the

"equivalent static analysis" as described by NBCC (1985) are significantly different than those obtained from inelastic dynamic analysis. For this reason, it is not possible to predict the response of precast wall systems using the prescribed static code procedure. Under strong ground motions, the design of precast wall systems should be based on inelastic dynamic analysis.

11. The computer program DRAIN-2D is sensitive to the value selected for integration time step. Care should be taken to select an appropriate value for the integration time step for inelastic dynamic analysis. Time steps of 0.002 seconds or less were found to be sufficient for inelastic dynamic analysis of the structures considered in this study.

8.3 Recommendations

Based on this investigation, recommendations for precast wall systems are presented.

8.3.1 Design Recommendations

A design procedure which is based on inelastic dynamic analysis was discussed in Chapter 7. The main features of the design are as follows.

1. Carry out a preliminary design based on Code minimum requirements.

2. Check that the design is satisfactory under factored wind loads using static analysis. Assume the coupling beams remain elastic under this condition.

3. Carry out dynamic analysis using the computer program DRAIN-2D.

4. Check the strength capacity of reinforcing bars due to shear, concrete crushing, and slip at the base of the walls.

8.3.2 Recommendations for Further Research

Limited parametric study was carried out in this investigation. Further studies can be carried out as follows.

1. Analyse the structure under earthquakes with different intensities. This may provide sufficient information on the level in which precast wall systems with mild reinforcing bars for vertical continuity provide satisfactory response.

2. Analyse walls with varying height/depth ratios and varying number of stories.

3. Analyse walls with different lengths of piers on each

side.

4. Study the effect of variation in the coefficient of friction.

Further extensions can be made to the computer program DRAIN-2D to incorporate:

1. Substructuring of wall panels to reduce the computational effort.

2. A model which considers soil-structure interaction.

3. A model which considers the bonding failure in vertical continuity steel bars and the reinforcing bars in the coupling beams.

4. A model that accounts for the degradation of the coefficent of friction after each cycle.

And most important, experimental tests are needed on both simple walls and coupled wall systems. In recent years, some experiments have been carried out, but the results which have been published are limited. Based on experimental test results, further studies can be carried out to investigate the accuracy of the modeling technique adopted for the present study.

REFERENCES

ACI 318-77. 1977. Building code requirements for reinforced concrete, American Concrete Institute, Detroit, Michigan.

ACI 318-83. 1983. Building code requirements for reinforced concrete, American Concrete Institute, Detroit, Michigan.

ARISTIZABAL-OCHOA, J.D. 1977. Behaviour of ten-story reinforced concrete walls subjected to earthquake motions. Ph.D. Dissertation, Department of Civil Engineering, University of Illinois at Urbana-Champaign, Urbana, Illinois.

BACKLER, A.P. and BAYLIK, M. 1973. Local behaviour of shear transfer and compression transfer joint - The behaviour of large panel structures. CIRIA Report 45, London.

BARNEY, G.B., SHIU, K.N., RABBAT, B.G., FLORATO, A.E., RUSSEL, H.G., and CORLEY, W.G. 1978. Behaviour of coupling beams under load reversals. Portland Cement Association, Research and Development, Construction Technology Laboratories, Skokie, Illinois.

BATHE, K.J., WILSON, E.L., and PETERSON, F.E. 1973. SAPIV, A structural analysis program for static and dynamic response of linear systems, Report No. EERC 73-11, University of California, Berkeley,

California.

BATHE, K.J. and WILSON, E.L. 1976. Numerical Methods in Finite Element Analysis. Prentice-Hall, Inc. 528 pp.

BECKER, J.M. and LLORENTE, C. 1979. The seismic response of simple precast concrete panel walls. Proceedings of U.S. National Conference on Earthquake Engineering, Stanford, CA.

BECKER, J.M. and MULLER, P. 1980. The role of connections in the aseismic design of large panel buildings. Research Conference on Earthquake Engineering, Skopje, Yugoslavia.

BRANKOV, G. and SACHANSKI, S. 1977. Response of large-panel buildings for earthquake excitation in nonelastic state. Sixth World Conference on Earthquake Engineering, New Dehli, India.

BRESLER, B. and PISTER, S. 1964. Strength of concrete under combined stresses. American Concrete Institute Journal, Vol. 61, pp. 321-345.

CAN3-A23.3-M77. 1977. Code for the design of concrete structures for buildings. National Standard of Canada.

CASEY, T.A. 1979. PLOTIT, A Graphics Package (Unpublished Report), University of Alberta, Edmonton, Canada.

CHOLEWICKI, A. 1971. Loadbearing capacity and deformability of vertical joints in structural walls of large panel buildings, Building Science,

Vol. 6, pp. 163-184.

CHU, Y., LIU, Y., CHEN, R., GUAN, Q., and SHOU, G. 1984. Experimental study on the seismic behaviour of multistory precast large panel residential buildings. Proceedings of the Eighth World Conference on Earthquake Engineering, California, U.S.A., Vol. VI, pp. 781-788.

CLOUGH, R.W. and BENUSKA, K.L. 1964. FHA study of seismic design criteria for high-rise buildings. Report HUD TS-3, Federal Housing Administration, Washington, D.C.

COOK, R.D. 1974. Concepts and Applications of Finite Element Analysis. John Wiley and Sons Inc., 402 pp.

COULL, A. and CHOUDHURY, J.R. 1967(a). Analysis of coupled shear walls. Journal of American Concrete Institute, Vol. 64, pp. 587-593.

_____ 1967(b). Stresses and deflections in coupled shear walls. American Concrete Institute, Vol. 64, pp. 587-593.

DARWIN, D. and PECKNOLD, D. 1974. Inelastic model for cyclic biaxial loading of reinforced concrete. SRS No. 409, University of Illinois at Urbana-Champaign, Illinois.

DRENICK, R.F. 1972. Predictions of earthquake resistance of structures. Polytechnic Institute of Brooklyn, New York, Final Report to the National Science

Foundation on Grant GK14550, 128 pp.

EARTHQUAKE ENGINEERING RESEARCH INSTITUTE. 1976. California Institute of Technology, Report No. EERL 76-02, 77 pp.

FINTEL, M. 1977. Performance of precast concrete structures during Romanian earthquake of March 4, 1977, PCI Journal, Vol. 22, No. 2.

FINTEL, M. and GHOSH, S.K. 1981. The seismic design of large panel coupled wall structures. Proceeding of a workshop on design of prefabricated concrete buildings for earthquake. Applied Technology Council, pp. 384-401.

FRANZ, G. 1959. Versuche uber die querkraftaufnahme in fugen von spannbetontragern aus fertigeteileu. Betonund stahlbetonban, 54(6), pp. 137-140.

GALLAGER, R.H. 1975. Finite element analysis. Prentice-Hall Inc.

GASTON, J.R. and KRIZ, L.B. 1964. Connections in precast concrete structures and scarf joints. Journal of Prestresed Concrete Institute, Vol. 9, No. 3, pp. 37-59.

GOELL, S.C. and BERG, G.V. 1968. Inelastic earthquake response of tall steel frames. ASCE Journal of Structural Division, Paper No. 6061, Vol. 94, Part 2, pp. 1907-1934.

HANSON, N.W. 1979. Seismic test of horizontal joints. Design and construction of large panel concrete

structures. Supplemental report C, Prepared for Office of Policy Development and Research, U.S. Department of Housing and Urban Development, Portland Cement Association.

HARRIS, H.G. and ABBOUD, B.E. 1981. Cyclic shear behaviour of horizontal joints in precast concrete large panel buildings. Proceedings of a workshop on design of prefabricated concrete buildings for earthquake loads, Applied Technology Council, pp. 403-438.

HARRIS, H.G. and CACCESE, V. 1984. Seismic behaviour of precast concrete large panel buildings using a small shaking table. Proceedings of the Eighth World Conference on Earthquake Engineering, California, U.S.A., Vol. VI, pp. 757-764.

JONES, L.L. 1959. Shear tests on joints between precast post-tensioned units. Magazine of Concrete Research, Vol. 11, No. 31, pp. 25-30.

KANAAN, A.E., POWELL, G.H. 1975. A General Purpose Computer Program for Inelastic Dynamic Response of Plane Structures. Earthquake Engineering Research Center, Report No. EERC 73-22, University of California, Berkeley, 101 pp.

KARSAN, I.D. and JIRSA, J.O. 1969. Behaviour of concrete under compressive loadings. ASCE Journal of Structural Division, V. 95, No. ST12, pp. 2543-2563.

KUPER, H., HILSDORF, H.K. and RÜSH, H. 1969. Behavior of concrete under biaxial stresses. ACI Journal, V. 66, No. 8, August 1969, pp. 656-666.

KRIPANARAYANAN, K.M. and FINTEL, M. 1976. Design and construction of large-panel concrete structures, Wall panels: analysis and design criteria, Report 3, Portland Cement Association. 78 pp.

LIU, T.C., NILSON, A.H., and SLATE, F.O. 1972. Biaxial stress-strain relations for concrete. ASCE Journal of the Structural Division, V. 98, No. ST5, pp. 1025-1034, Part 2.

LLORENTE, C.A., BECKER, J.M., and KAUSEL, E. 1981. Inelastic behaviour of precast concrete shear walls. Report No. 5. Massachusetts Institutet of Technology. Publication No. R81-25. 309 pp.

MACGREGOR, J.G. 1973. The Shear Strength of Reinforced Concrete Mmembers. ASCE-ACI Task Committee 426 on Shear and Diagonal Tension of the Committee on Masonry and Reinforced Concrete of the Structural Division, ASCE Journal of Structural Division, pp. 1091-1187.

_____ 1985. Private discussion, University of Alberta, Edmonton, Canada.

MACLEOD, I.A. 1969. New rectangular finite element for shear wall analysis. ASCE Journal of Structural Division. Vol. 95, Part 1, pp. 399-409.

MATTOCK, A.H. 1974. The shear transfer behaviour of

cracked monolithic concrete subjected to cyclically reversing shear. Report SM74-4, Department of Civil Engineering, University of Washington, Seattle.

_____ 1976. Shear transfer under monotonic loading across interface between concrete cast at different times. Report SM76-3, Department of Civil Engineering, University of Washington, Seattle.

_____ 1977(a). Shear transfer under cyclically reversing loading across an interface between concrete cast at different times. Report SM 77-1, Department of Civil Engineering, University of Washington, Seattle.

_____ 1977(b). Effect of reinforcing bar size on shear transfer across a crack in concrete. Report SM 77-2, Department of Civil Engineering, University of Washington, Seattle.

_____ 1981. A survey of precast wall systems. Proceedings of a Workshop on Design of Prefabricated Concrete Buildings for Earthquake Loads, Applied Technology Council, pp. 253-276.

MUJAMDAR, V.S. 1977. An approach to earthquake resistant design of precast concrete bearing wall buildings. Proceedings Sixth World Conference on Earthquake Engineering, Vol. II, New Dehli, India, pp. 2093-2095.

MULLER, P. 1981. Behaviour characteristics of precast

walls. Proceedings of a Workshop on Design of Prefabricated Concrete Buildings for Earthquake Loads, Applied Technology Council, pp. 277-308.

MULLER, P. and BECKER, J.M. 1979. Seismic characteristics of composite precast walls. Proceedings, Third Canadian Conference on Earthquake Engineering. Montreal, V. 2, pp. 1169-1199.

_____ 1980. Seismic behaviour of precast walls coupled through vertical connections. Seventh World Conference on Earthquake Engineering, Istanbul, Turkey.

NATIONAL BUILDING CODE OF CANADA. 1985. Issued by the Associate Committee on the National Building Code, National Research Council of Canada, Ottawa.

NILSON, H. 1978. Design of prestressed concrete. John Wiley and Sons.

OLIVA, M.G., and SHAHROOZ, B.M. 1984. Shaking table tests of wet jointed precast panel walls. Proceedings of the Eighth World Conference on Earthquake Engineering, California, U.S.A., Vol. VI, pp. 717-724.

PALL, A.S. and MARSH, C. 1979. Seismic response of large panel structures using limited-slip bolted joints. Third Canadian Conference on Earthquake Engineering, McGill University, Montreal, Vol. 2, pp. 899-916.

PARK, R. and PAULAY, T. 1980. Concrete structures.

Chapter 5 in the Design of Earthquake Resistant Structures. Rosenblueth, E., Editor. John Wiley and Sons, pp.

PAULAY, T. 1971(a). Simulated seismic loading on spandrel beams. ASCE Journal of the Structural Division, Vol. 97, Part 3, pp. 2407-2419.

_____ 1971(b). Coupling beams of reinforced concrete shear walls. ASCE Journal of Structural Division, Vol. 97, Part 1, pp. 843-861.

_____ 1977. Ductility of shear walls. Reinforced concrete structures in seismic zones. American Concrete Institute, Special Publication 53. Detroit, pp. 128-147.

PAULAY, T. and BINNEY, J.R. 1974. Diagonally reinforced coupling beams of shear walls. Shear in reinforced concrete. American Concrete Institute, Special Publication 42. pp. 579-599.

PAULAY, T., PARK, R., and PHILLIPS, M.H. 1974. Horizontal construction joints in cast in place concrete. Shear in reinforced concrete, American Concrete Institute. Special Publication No. SP-42, Detroit.

PAULAY, T. and SANTHAKUMAR, A.R. 1976. Ductile behaviour of coupled shear walls. ASCE Journal of Structural Division, Vol. 102, pp. 93-108.

PEKAU, O.A. 1981. Influence of vertical joints on the earthquake response of precast panel walls. Building and Environment, Vol. 16, No. 2, pp. 153-

162.

POLLNER, E., TSO, W.K. and HERDEBRECHT, A.C. 1975. Analysis of shear walls in large-panel construction. Canadian Journal of Civil Engineers, Vol. 2, pp. 357-367.

RECOMMENDED LATERAL FORCE REQUIREMENTS AND COMMENTARY. 1975. Seismology Committee, Structural Engineers Association of California, San Francisco, 21 pp. plus Commentary and Appendices.

SAATCIOGLU, M. 1981. Inelastic behaviour and design of earthquake resistant coupled walls. Ph.D. thesis, Northwestern University, Illinois.

SCHRICKER, V. and POWELL, G.H. 1980. Inelastic seismic analysis of large panel buildings. Report No. UCB/EERC-80/38 College of Engineering, University of California, Berkely, California.

SPIRA, E. and SOKAL, Y. 1970. Discussion of new rectangular finite element for shear walls analysis. ASCE Journal of the Structural Division Vol. 96, No. ST8, pp. 1799-1802.

TAKAYANAGI, T., SCANLON, A., and CORLEY, W.G. 1981. Earthquake resistant structural walls - Analysis of coupled wall specimens. Portland Cement Association, Skokie, Illinois.

TAKEDA, T., SOZEN, M.A., and NIELSON, N.N. 1970. Reinforced concrete response to simulated earthquakes. ASCE Journal of the Structural

Division, Part 2, Vol. 96, pp. 2557-2573.

THE SUPPLEMENT TO THE NATIONAL BUILDING CODE OF CANADA. 1985. Issued by the Associate Committee on the National Building Code, National Research Council of Canada, Ottawa.

UNEMORI, A.L. 1978. Generalized dynamic behaviour of crosswall building systems. Thesis presented to the Massachusetts Institute of Technology at Cambridge, Massachusetts, in partial fulfillment of the requirements for the degree of Doctor of Science, 331 pp.

VELKOV, M.D. 1977. Earthquake resistant design of twenty-one story prefabricated large panel building. Sixth World Conference on Earthquake Engineering, New Dehli, India.

VELKOV, M., IVKOVISH, M. and PERISHICH, Z. 1984. Experimental and analytical investigation of prefabricated large panel systems to be constructed in seismic regions. Proceedings of the Eighth World Conference on Earthquake Engineering, California, U.S.A., Vol. VI, pp. 773-780.

VELKOV, M.D., GAVRILOVIC, P., and JURUKOVSKI, D. 1978. Seismic stability of an 18-story large panel building constructed in modified "balancy" precast system in Novi Beograd: Analytical and experimental study. Sixth European Conference on Earthquake Engineering, Dubrovnik, Yugoslavia.

VELKOV, M.D., SIMEONOV, B., GAVRILOVIC, P., and JURUKOVSKI, D. 1978. Theoretical and experimental study of the precast large panel structural system "SPUZ". Sixth European Conference on Earthquake Engineering, Dubrovnik, Yugoslavia.

VERBIC, B. 1977. Test of panel joints in "Vranica" type large panel buildings. Institute za Materijale: Konstrukcije, Sarajevo, Yugolavia.

APPENDIX A

Constant Acceleration Method

For solving the equations of dynamic equilibrium in the computer program DRAIN-2D, the step-by-step integration technique with constant acceleration method is used. Details of the procedure are as follows:

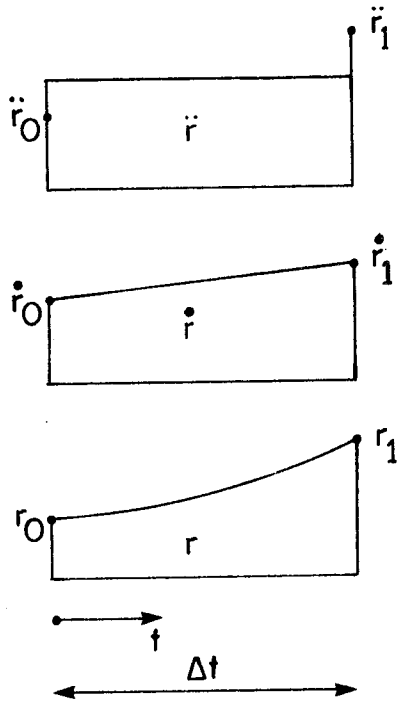

a) Displacement, r_1, as unknown

$$\ddot{r} = \frac{1}{2}\left(\ddot{r}_0 + \ddot{r}_1\right) \qquad \text{(A-1)}$$

$$\dot{r} = \dot{r}_0 + \int_0^t \ddot{r}\, dt \qquad \text{(A-2)}$$

$$\dot{r}_1 = \dot{r}_0 + \ddot{r}_0 \frac{\Delta t}{2} + \ddot{r}_1 \frac{\Delta t}{2} \qquad \text{(A-3)}$$

$$r = r_0 + \int_0^t \dot{r}\, dt \qquad \text{(A-4)}$$

$$r_1 = r_0 + \dot{r}_0 \Delta t + \ddot{r}_0 \frac{\Delta t^2}{4} + \ddot{r}_1 \frac{\Delta t^2}{4} \qquad \text{(A-5)}$$

(b) Rearrange in terms of Δr, where Δr is displacement increment at the end of the time increment Δt.

$$\Delta\dot{r} = -2\dot{r}_0 + \Delta r \frac{1}{\Delta t} \qquad \text{(A-6)}$$

$$\Delta\ddot{r} = -2\ddot{r}_0 - \dot{r}_0 \frac{4}{\Delta t} + \Delta r \frac{4}{\Delta t^2} \qquad \text{(A-7)}$$

(c) Equation of dynamic equilibrium

$$[M]\{\Delta\ddot{r}\} + [C]\{\Delta\dot{r}\} + [K]\{\Delta r\} = \{\Delta P\} \qquad \text{(A-8)}$$

Hence

$$\left[\frac{4}{\Delta t^2}\,[M] + \frac{2}{\Delta t}\,[C] + [K]\right]\{\Delta r\} = \{\Delta P\}$$

$$+\,[M]\left\{2\ddot{r}_0 + \dot{r}_0\,\frac{4}{\Delta t}\right\} + [C]\left\{2\dot{r}_0\right\} \qquad \text{(A-9)}$$

which can be solved for $\{\Delta r\}$.

APPENDIX B

Element Users Guide for the Program DRAIN-2D

In this Appendix, the element users guide for the modified part of the program, DRAIN-2D is presented. The complete users guide for other elements in the program is described in the program manual by Kanaan and Powell (1975).

I. Beam Element Compatible With Plane Stress Element

(a) CONTROL INFORMATION FOR GROUP (8I5) - ONE CARD

Columns

5: Punch 6 (to indicate that group consists of beam elements with degrading stiffness).

6-10: Number of elements in group.

11-15: Number of different element stiffness types (max. = 40).

16-20: Number of different end eccentricity types (max. = 15).

21-25: Number of different yield moment values for cross sections (max. = 40).

26-30: Number of different fixed end force patterns (max. = 34).

31-35: Number of different initial element force patterns (max. = 30).

36-40: Type 1 to indicate compatible with plane stress element.
Type 0 or leave blank otherwise.

(b) Through (h) are identical to Element 6 in the computer program DRAIN-2D (1975).

(i) ELEMENT GENERATION COMMANDS - TWO CARDS FOR EACH GENERATION COMMAND.

Elements must be specified in increasing numerical order. Cards for the first and last elements must be included.

CARD 1: COMMANDS FOR BEAM ELEMENT (12I5, 2F5.0, I5, F5.0)

Columns

1-5: Element number, or number of first element in a sequentially numbered series of elements to be generated by this command.

6-10: Node number at element end i.

11-15: Node number at element end j.

16-20: Node number increment for element generation. If zero or blank, assumed to be equal to 1.

21-25: Stiffness type number.

26-30: End eccentricity type number. Leave blank or punch zero if there is no end eccentricity.

31-35: Yield surface number for element end i.

36-40: Yield surface number for element end j

45: Code for including geometric stiffness. Punch 1 if geometric stiffness is to be included. Leave blank or punch zero if geometric stiffness is to be ignored.

50: Time history output code. If a time history of element results is not required for the element covered by this command, punch zero or leave blank. If a time history printout, at the intervals specified in card D1, is required, punch 1.

51-55: Fixed end force pattern number for static dead loads on element. Leave blank or punch zero if there are no dead loads.

56-60: Fixed end forces pattern number for static live loads on element. Leave blank or punch zero there are no live loads.

61-65: Scale factor to be applied to fixed end forced due to

static dead loads.

66-70: Scale factor to be applied to fixed end forces due to static live loads.

71-75: Initial force pattern number. Leave blank or punch zero if there are no initial forces.

76-80: Scale factor to be applied to initial element forces.

CARD 2: COMMANDS FOR COMPATIBLE PLANE STRESS ELEMENT (2I5)

Columns 1-5: Node number at end K

6-10: Node number at end L

II. PLANE STRESS ELEMENT

(a) CONTROL INFORMATION FOR GROUP (3I5) - ONE CARD

Columns 5: Punch 7 (to indicate that group consists of plane-stress element)

6-10: Number of elements in group

11-15: Number of different element stiffness types (max. 40)

(b) STIFFNESS TYPE (I5, 2F12.0, F6.0, 3F10.0, F10.0) - ONE CARD FOR EACH STIFFNESS TYPE

Columns: 1-5: Stiffness type number in sequence beginning with 1.

6-17: Elastic modulus of concrete.

18-29: Elastic modulus of steel.

30-35: Poisson's ratio for concrete.

36-45: Reinforcement ratio in x-direction.

46-55: Reinforcement ratio in y-direction.

56-65: Element thickness.

(c) ELEMENT GENERATION COMMANDS (7I5) - Elements must be specified in increasing numerical order, cards of the first and last elements must be included.

Columns: 1-5: Element number or number of first element in a sequentially numbered series to be generated by this card.

6-10: Node number i (bottom left).

11-15: Node number J (bottom right).

16-20: Node number K (top right).

21-25: Node number L (top left).

26-30: Node number increment for element generation. If zero or blank, assumed to be equal to 1.

31-35: Stiffness type number.

III. CONNECTION ELEMENT

(a) CONTROL INFORMATION FOR GROUP (3I5) - ONE CARD

Columns: 5: Punch 8 (to indicate that group consists of connection element).

6-10: Number of elements in group.

11-15: Number of different element stiffness types (max. = 40).

(b) STIFFNESS TYPES (I5, 7F12.0, I5) - ONE CARD FOR EACH STIFFNESS TYPE

Columns: 1-5: Stiffness type number in sequence beginning with 1.

6-17: Elastic modulus of concrete.

18-29: Poisson's ratio for concrete.

30-41: Max. compressive strength of concrete.

42-53: Shear modulus of concrete

54-65: Connection thickness.

66-77: Axial reinforcement ratio.

78-89: Shear reinforcement ratio.

90-94: Static code. Punch 1 if static loads are applied. Leave blank or punch

zero otherwise.

(c) MATERIAL PROPERTIES CARD (3F10.0) - ONE CARD

Columns 1-10: Coefficient of friction (μ).

11-20: Elastic modulus of steel.

21-30: Yield stress of steel.

(d) MATERIAL MODEL PROPERTIES CARD (3F8.0, I5) - ONE CARD

Columns 1-8: Strain hardening stiffness parameter for shear slip model (G_s/G_d).

9-16: Strain hardening stiffness parameter for shear friction model (G_s/G_d).

17-24: r Parameter for shear friction model.

25-29: Inelastic Code - Punch 1 for inelastic analysis. Leave blank or punch zero for elastic analysis.

(e) ELEMENT GENERATION COMMANDS (7I5) - Elements must be specified in increasing numerical order, cards of the first and last elements must be included.

Columns: 1-5: Element number or number of first element in a sequentially numbered series to be generated by this card.

6-10: Node number i (bottom left).

11-15: Node number J (bottom right).

16-20: Node number K (top right).

21-25: Node number L (top left).

26-30: Node number increment for element generation. If zero or blank, assumed to be equal to 1.

31-35: Stiffness type number.

APPENDIX C

Results of Parametric Study

Time History Response of Base Forces for Precast Wall Systems

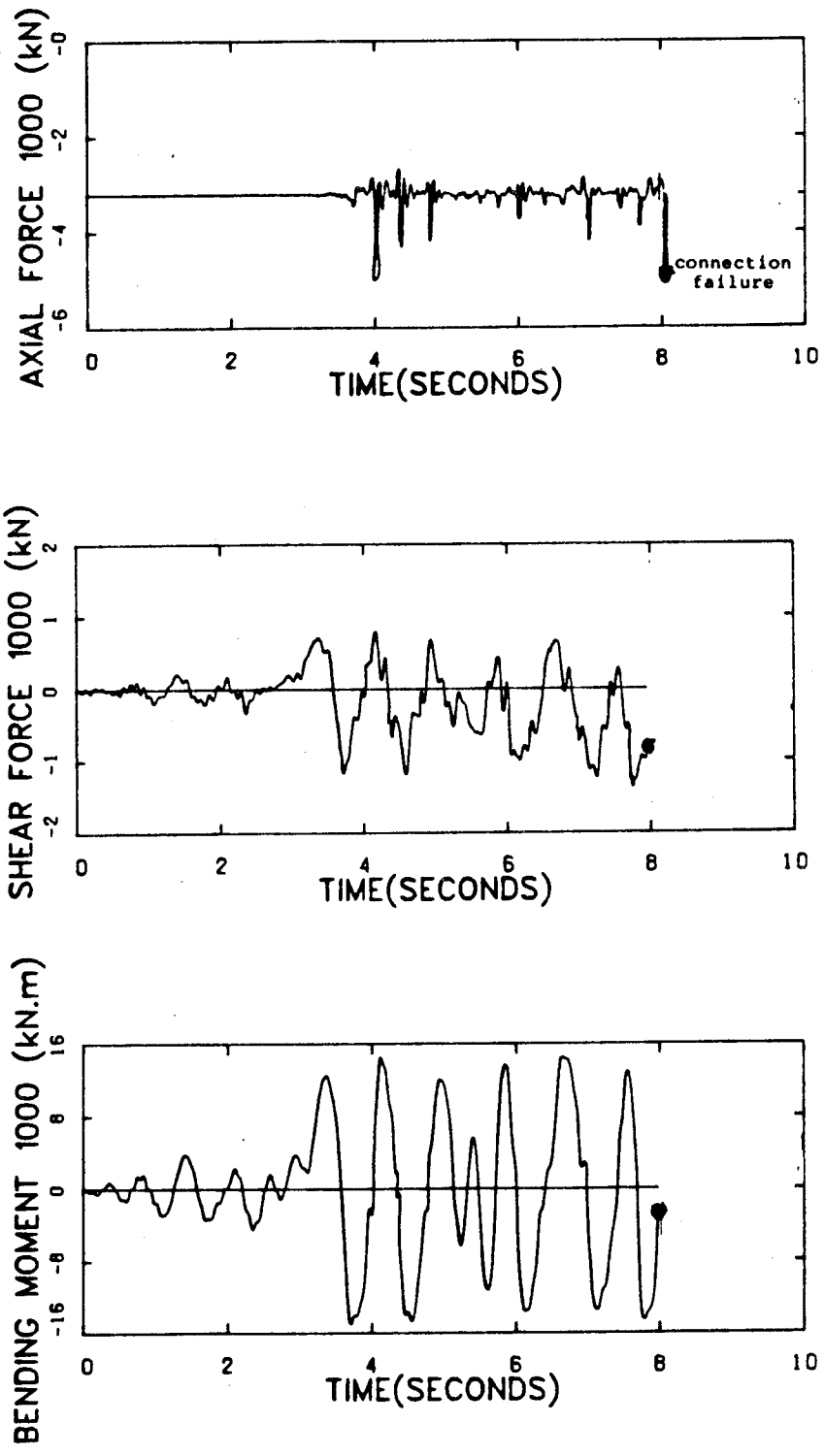

Figure C-1 Simple Wall, R.C.

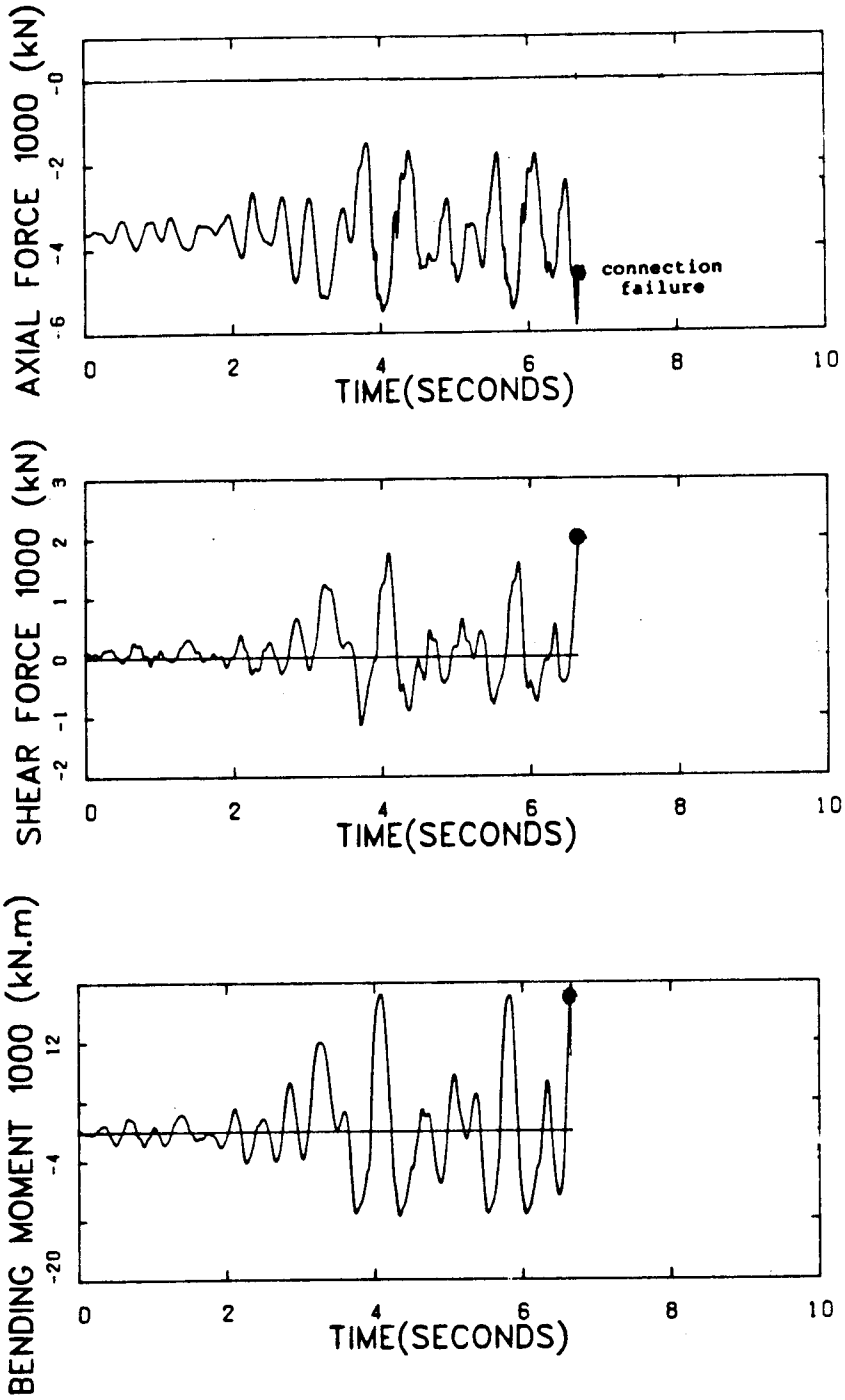

Figure C-2 Slender Beams, R.C., M_y = 180 kNm, EI = 122060 kNm^2

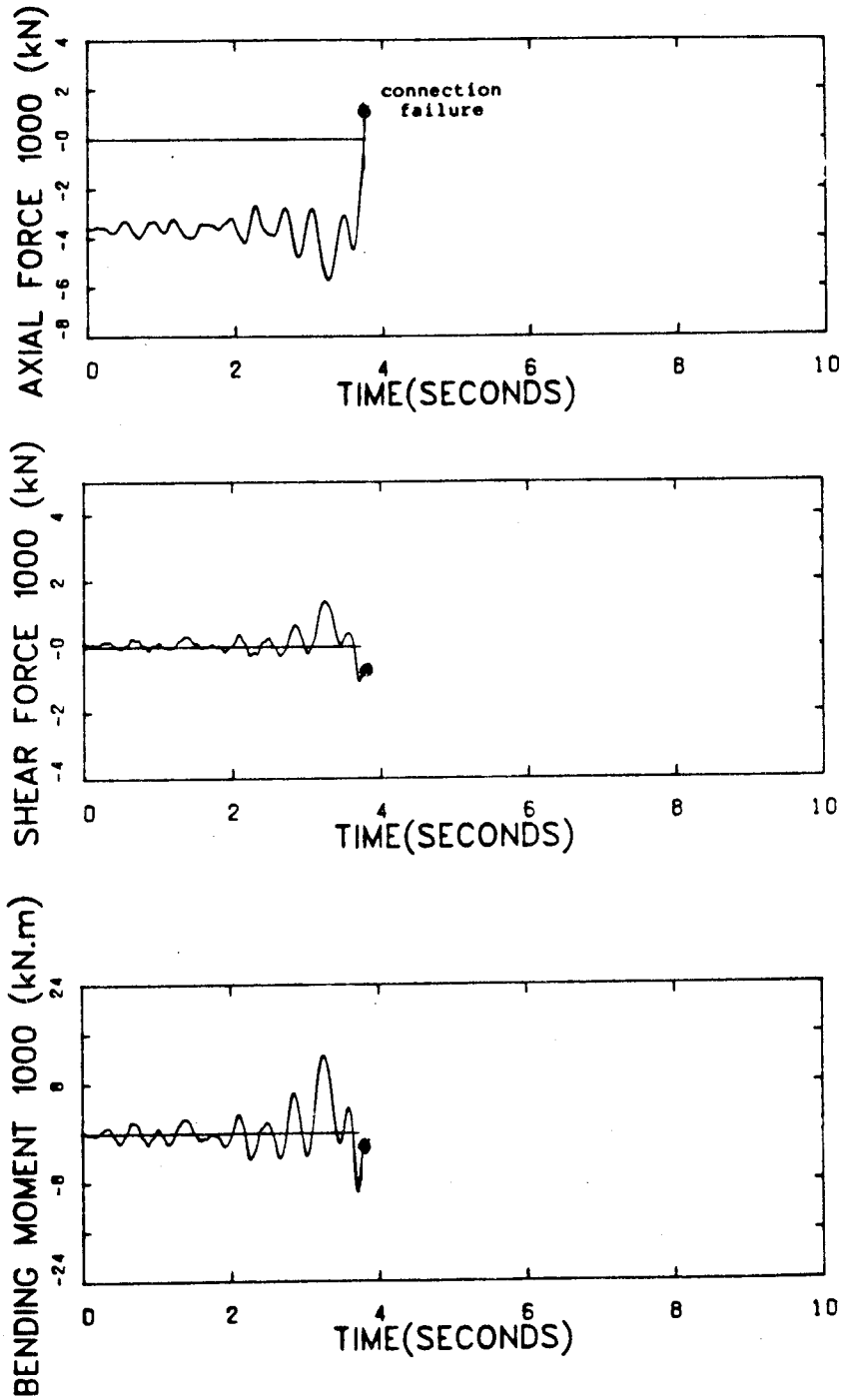

Figure C-3 Slender Beams, R.C., EI = 122060 kNm^2
Elastic Coupling Beams

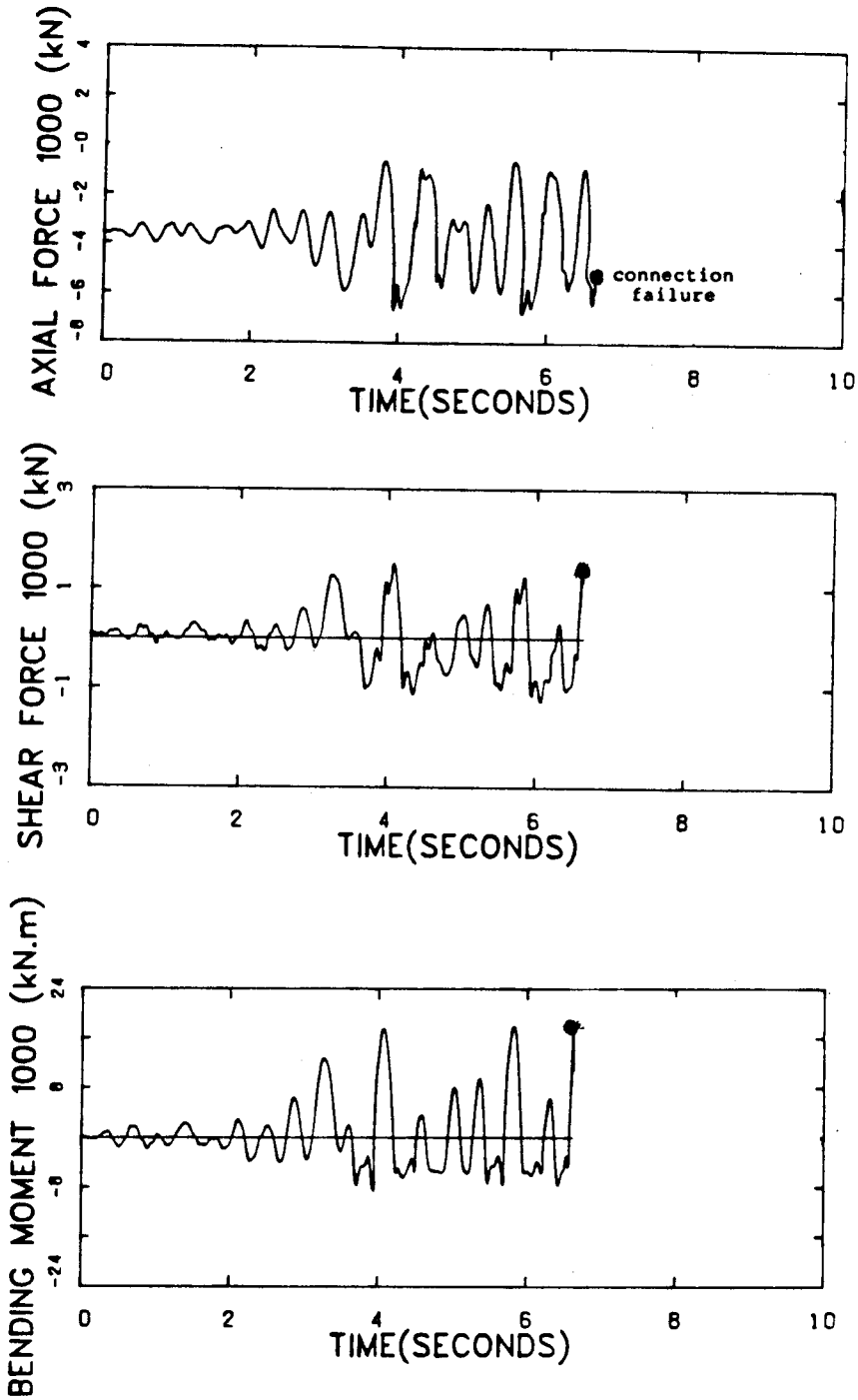

Figure C-4 Deep Beams, R.C., A_s = 600 mm^2, L/D = 1.0

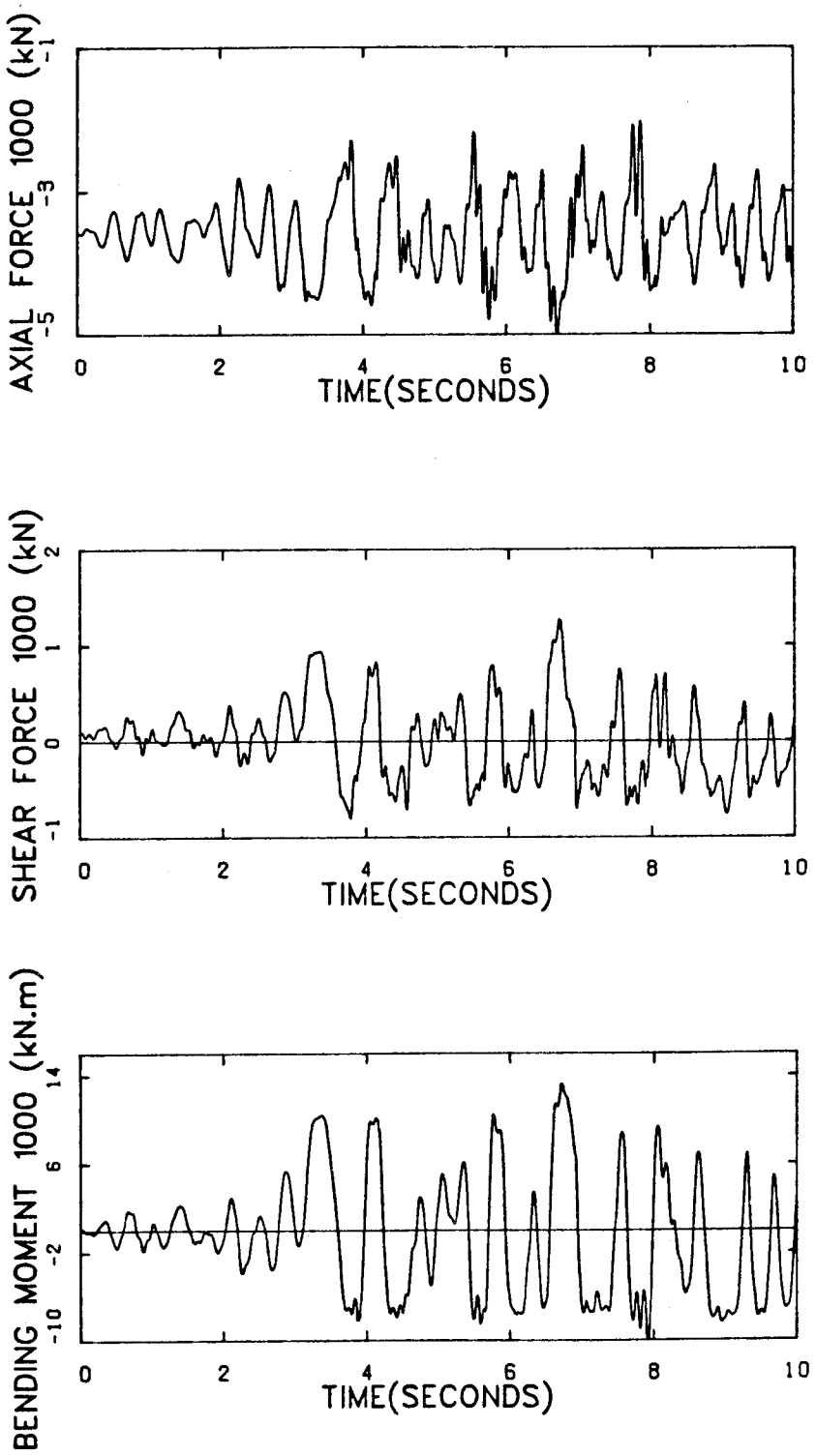

Figure C-5 Slender Beams, P.T., M_y = 90 kNm, EI = 122060 kNm^2

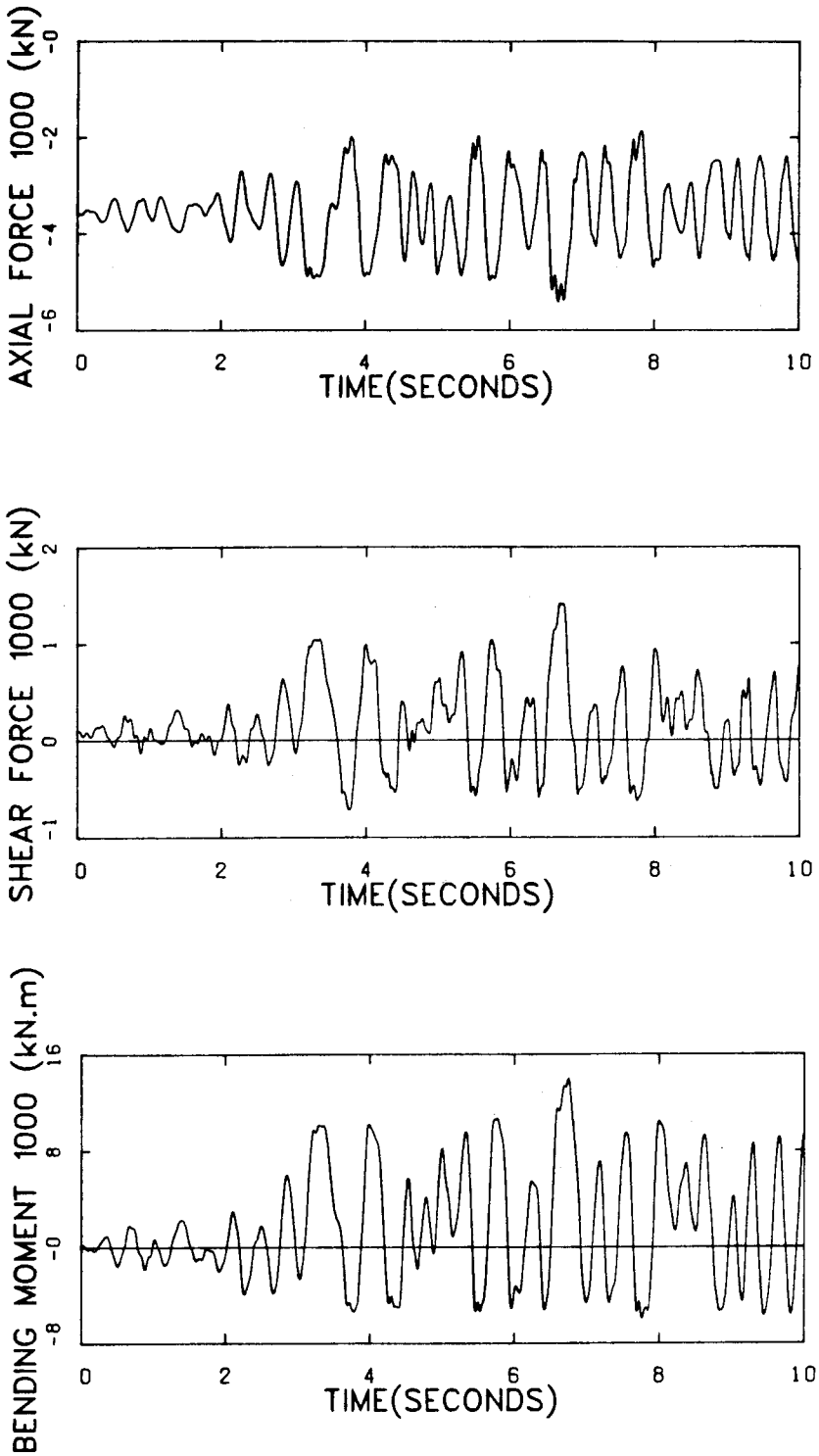

Figure C-6 Slender Beams, P.T., M_y = 180 kNm, EI = 122060 kNm^2

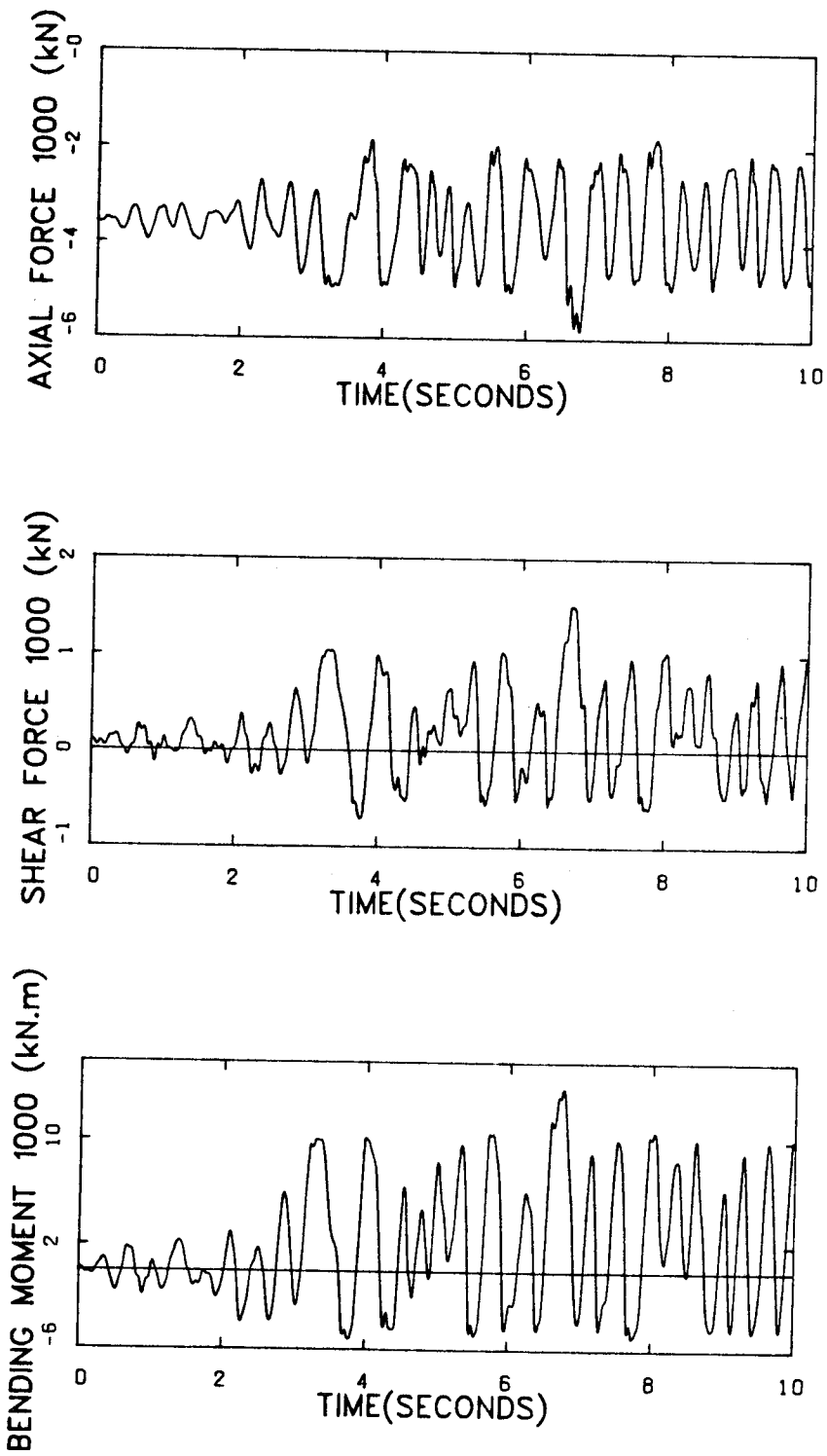

Figure C-7 Slender Beams, P.T., M_y = 270 kNm, EI = 122060 kNm^2

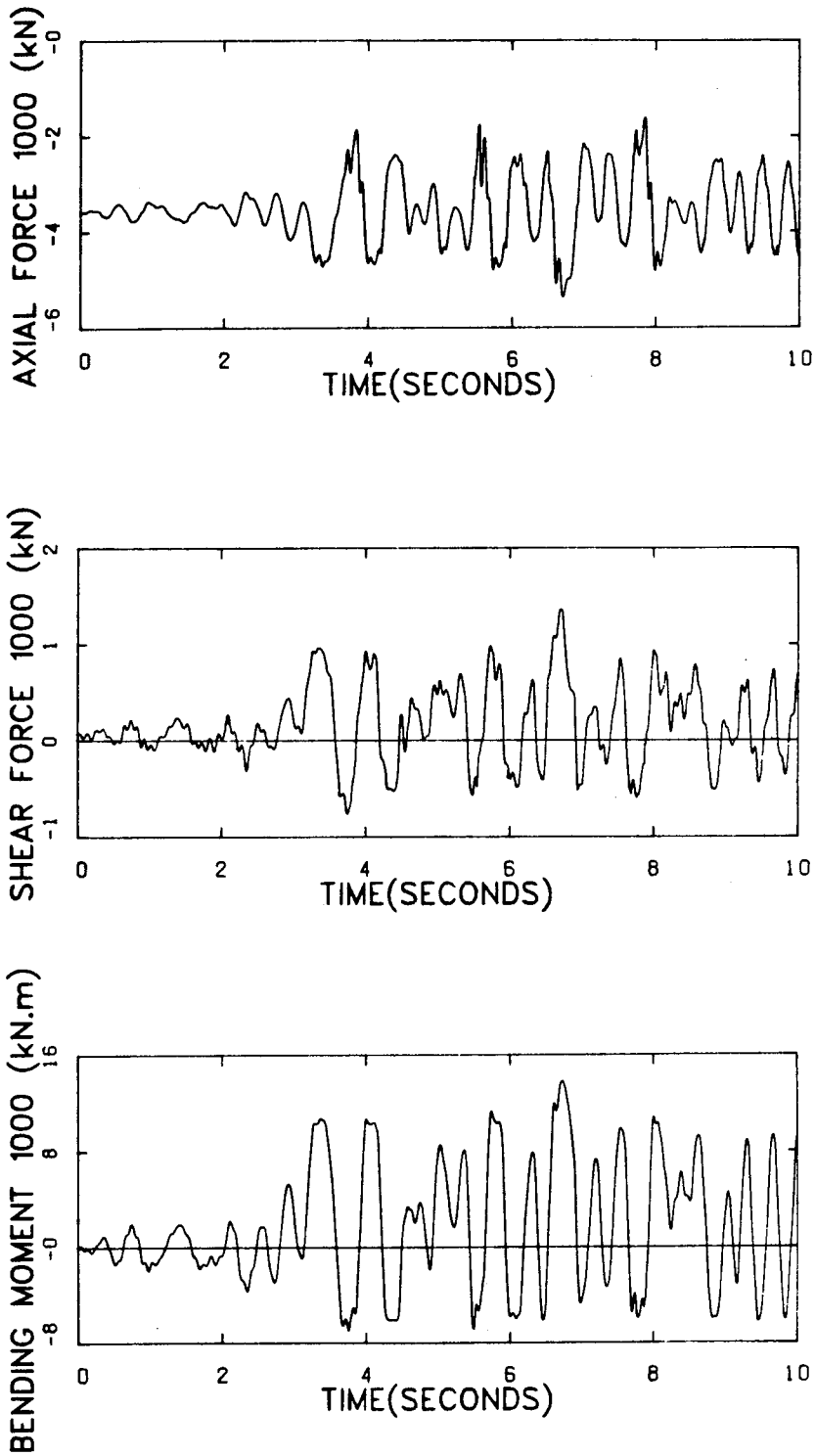

Figure C-8 Deep Beams, P.T., A_s = 600 mm^2, L/D = 1.8

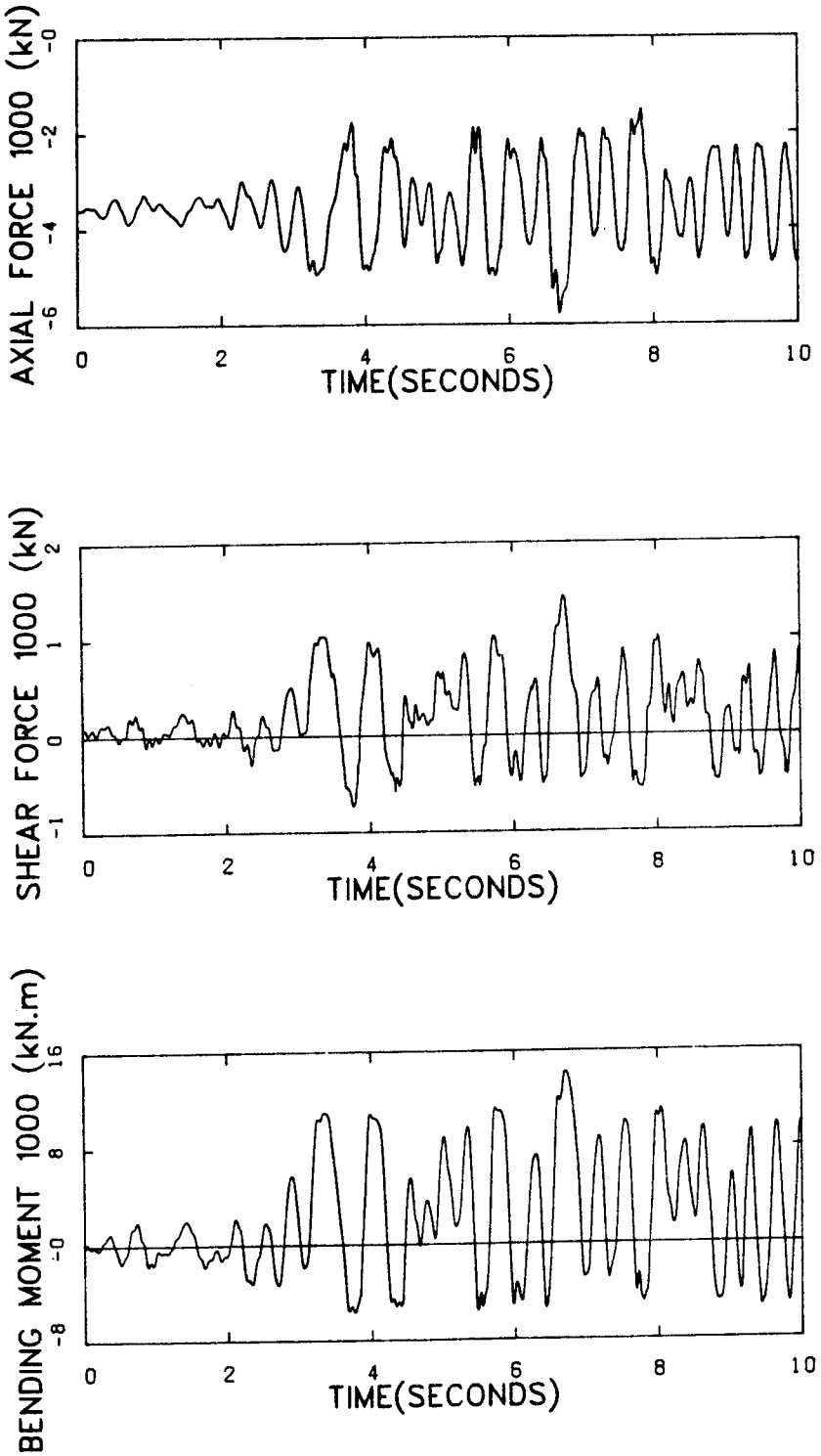

Figure C-9 Deep Beams, P.T., A_s = 600 mm^2, L/D = 1.4

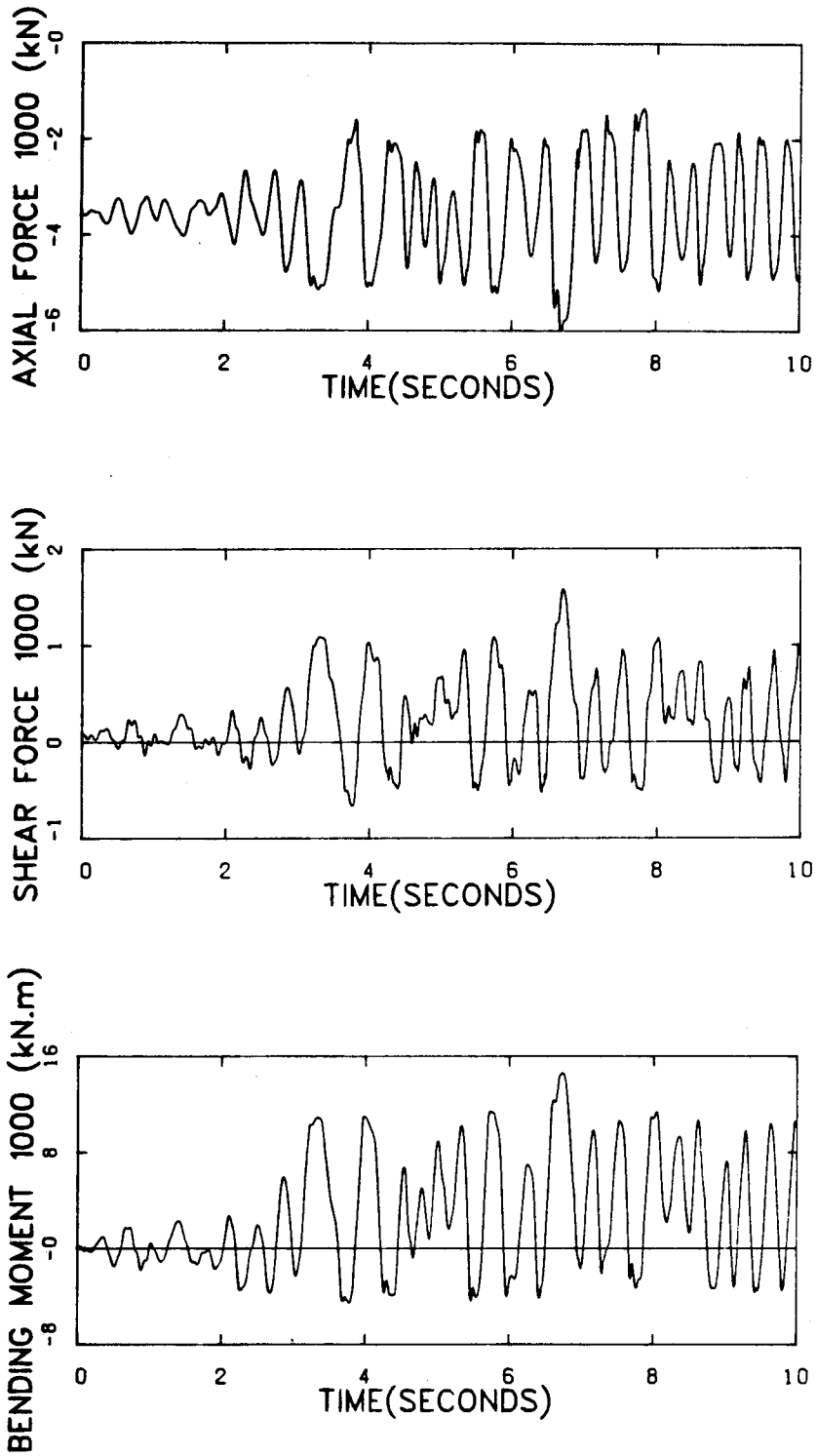

Figure C-10 Deep Beams, P.T., A_s = 600 mm^2, L/D = 1.0